1-7-2008

Binding Studies of Near Infrared Cyanine Dyes with Human Serum Albumin and Poly-L-Lysine Using Optical Spectroscopy Methods

Amy Dawn Watson

BINDING STUDIES OF NEAR INFRARED CYANINE DYES WITH HUMAN SERUM ALBUMIN AND POLY-L-LYSINE USING OPTICAL SPECTROSCOPY METHODS

by

Amy Dawn Watson

Under the Direction of Gabor Patonay, Ph.D.

ABSTRACT

The sensitivity of biological studies performed between 190 and 650 nm is greatly reduced due to the autofluorescence of biomolecules and impurities in this region. Therefore, the enhanced signal-to-noise ratios encountered at longer wavelengths makes biological analysis within the near infrared (NIR) region from 650 nm to 1100 nm far more advantageous. This dissertation describes the noncovalent binding interactions of near-infrared (NIR) carbocyanine dyes with human serum albumin (HSA) and poly-L-lysine (PLL) using UV-Vis/NIR absorption spectroscopy, emission spectroscopy, circular dichroism (CD), and fluorescence detected circular dichroism (FDCD). The optical spectroscopy methods used in this work are described in detail in Chapter 1.

The various applications of NIR dyes in protein analysis are introduced in Chapter 2. In general, the sensitivity of cyanines to the polarity of their local environment makes them quite suitable for protein labeling schemes. In aqueous media, cyanines have a high propensity for self-association. Yet in the hydrophobic binding sites of globular proteins, these aggregates often dissipate. Absorption and emission spectroscopy can be utilized to observe the differential spectral properties of monomer, intra-molecular and intermolecular aggregates. In Chapter 3, the photophysical properties of bis-cyanine NIR dyes containing di-, tri-, and tetra(ethylene glycol) linkers were each examined in the presence of HSA are discussed. Variations in chain length as well as probe flexibility were demonstrated through distinct differences in absorption and emission spectra. The observed changes in the spectral properties of the NIR dyes in the presence and absence of HSA were correlated to the physical parameters of the probes' local environment (i.e., protein binding sites and self-association). All three bis-cyanines examined exhibited enhanced fluorescence in the presence of HSA. The bis-cyanine dye containing the tri(ethylene glycol) spacer allowed for a complete overlap of the benzene rings, to form π-π interactions which were observed as intra-molecular H-aggregate bands. The dye exhibited no fluorescence in buffer, owing to the H-aggregation observed in the absorption data. In the presence of HSA, the intra-molecular dimers were disrupted and fluorescence was then detected. The "cut-on" fluorescence displayed by the dye in the presence of HSA made it ideal for noncovalent labeling applications.

The utility of several NIR dyes for use as secondary structural probes was investigated in Chapter 4. NIR dyes were screened thoroughly using UV-Vis/NIR absorption spectroscopy dyes with spectral properties which were sensitive to protein

secondary structure models of such as PLL in basic solution. Two NIR dyes were found to be quite sensitive to the structural features of uncharged α- and β-PLL. The chiral discrimination of these probes for basic protein secondary structures was also evaluated through CD measurements within the NIR probes' absorption bands.

INDEX WORDS: Circular dichroism (CD), fluorescence detected circular dichroism (FDCD), near infrared (NIR), cyanine dyes, poly-L-lysine, albumin, noncovalent labeling

BINDING STUDIES OF NEAR INFRARED CYANINE DYES WITH HUMAN SERUM ALBUMIN AND POLY-L-LYSINE USING OPTICAL SPECTROSCOPY METHODS

by

Amy Dawn Watson

A Dissertation Submitted in Partial Fulfillment of the Requirements for the Degree of

Doctor of Philosophy

in the

College of Arts and Sciences

Georgia State University

2007

BINDING STUDIES OF NEAR INFRARED CYANINE DYES WITH HUMAN SERUM ALBUMIN AND POLY-L-LYSINE USING OPTICAL SPECTROSCOPY METHODS

by

Amy Dawn Watson

Committee Chair: Dr. Gabor Patonay

Committtee: Dr. Zhen Huang
Dr. Alfons Baumstark

Electronic Version Approved:

Office of Graduate Studies
College of Arts and Sciences
Georgia State University
December 2007

Acknowledgements

Thanks first and foremost to my Lord and Savior Jesus Christ for bringing me so far. His grace and mercy overwhelms me, for I could not have accomplished any of this without Him carrying me in the sand the whole way. Throughout any trials I have faced, my Heavenly Father has always maintained my strength and perseverance. "Let patience have its perfect work."

Thanks to my father, Robert D. Watson, who was first to share his love of science with me. Thanks to my mother, Linda G. Watson, who has always been a shining example of what it means to be a strong, intelligent black woman. Thank you for being a praying mother. Thanks to my brother, Roderick D. Watson. Only you and I know what we truly lost when our father died.

Thanks to my advisor, Dr. Gabor Patonay, for giving me the incredible opportunity to learn and grow as a scientist and to think for myself. When I tried to quit, thank you for reminding me that there were worse obstacles a person could face. Thanks to Jozef Salon and Maghed Henary for all your helpful assistance. Thanks to Jun Seok Kim for all the encouragement and intellectual support you gave to me.

I would also like to thank the Department of Chemistry and the GAANN Fellowship program for their financial support. Thanks, in particular, to Dr. Alfons Baumstark for his financial and emotional support. You stuck by me every step of the way and I'll always be grateful to you for that.

Thanks also to all my friends in the Chemistry Department. There is no possible way a person can successfully complete this process without the intellectual and emotional support of their friends and colleagues. In no particular order, because you all mean so much to me, I want to thank each of you. Lisa M. Jones, you and I are like war buddies; we've been through a lot together and we're still here to tell the story. Thank you so much for listening to me cry, and then yelling at me to get myself together and get back to work! I really needed all those "snap out of it" pep talks. Alpa Patel, thank you for always being there to listen and to advise, and to even cry with me. Subrata Mishra, you have truly been one of my best friends. Thank you for always encouraging me to be the best scientist I can be. The high standard that I hold for myself can be directly attributed to you. Your hard work ethic has always been my inspiration. Thank you for "Amy, you started it, and now you should see it through to the end." Please know that you'll always have a friend for life with me. Pamela Leggett-Robinson, thank you for "But, Amy, once you're done, this will all be such a powerful testimony". Charmita Burch, thank you for all the text messages of encouragement, for praying for me so diligently, and for giving me a sermon on tape at a very low point in my life. Sandra Craig, thanks for also being a spiritual touchstone in my life. I really enjoyed all of our talks together. Jennifer Brown Barber, Brian Crow, and Rucks Winklejohn, thank you for your friendship and encouragement as well. A special thanks to Fred Meadows. Fred, you came along and set me on the path to some really good project ideas. You were truly a Godsend.

Thanks to my dear sister-friends outside the Chemistry Department as well. Alexia E. Guthrie, my very best friend, I thank God for you daily. You were the first person that wasn't a relative to really love me for me! I love you, Lex! Tanya L. Richburg, I will never forget all the notes saying "you can do it, girl" you left on the kitchen counter. Thanks Tanster, you truly are my sister.

Jason Victor Jackson, thank you so much for all the emotional support and unconditional love. Thank you for letting me cry and cry and cry some more. You are truly my great love.

Dedication

In loving memory of

Robert Douglas Watson, my father

Table of Contents

List of Tables

List of Figures

List of Abbreviations

ACE	=	affinity capillary electrophoresis
ANS	=	1-anilinonaphthalene-8-sulfonic acid
BSA	=	bovine serum albumin
BHmC	=	bis(heptamethine cyanine)
CCD	=	charge coupled device
CD	=	circular dichroism
CE	=	Cotton effects
CE-LIF	=	capillary electrophoresis-laser induced fluorescence
CP	=	circularly polarized
CPL	=	circularly polarized light
CSA	=	(+)-camphorsulfonic acid
CTAB	=	cetyltrimethyl-ammonium bromide
DAAC	=	4’-dimethyl amino azo benzene-4-carboxylic acid
DiI	=	1,1’-dioctadecyl-3,3,3’,3’-tetramethylindocarbocyanine perchlorate
DCDSTCY	=	5,5’-dicarboxy-1,1’-disulfobutyl-3,3,3’,3’-tetramethylindotricarbocyanine
DOS	=	degree of substitution
DTTCI	=	3,3’-diethylthiadicarbocyanine iodide
DSTCY	=	1,1’-disulfobutyl-3,3,3’,3’-tetramethylindotricarbocyanine
EM	=	electromagnetic radiation
FDCD	=	fluorescence detected circular dichroism

FDCD	=	fluorescence detected circular dichroism
FFOI	=	fluorescent fiber-optic immunosensor
HOMO	=	highest occupied molecular orbital
HSA	=	human serum albumin
HPLC	=	high performance liquid chromatography
HT	=	high tension
ICD	=	induced circular dichroism
ICG	=	indocyanine green
ITCC	=	indotricarbocyanine
LOD	=	limit of detection
LUMO	=	lowest unoccupied molecular orbital
MO	=	methyl orange
MS	=	mass spectrometry
NHS	=	hydroxysuccinimidyl
NIR	=	near infrared
NMR	=	nuclear magnetic resonance
PBS	=	phosphate buffered saline
PEG	=	poly(ethylene glycol)
PLG	=	poly-L-glutamate
PLL	=	poly-L-lysine
PMT	=	photomultiplier tube
QD	=	quantum dots
R/D	=	residue to dye

SCN	=	isothiocyanate
SLN	=	sentinel lymph node
TPPS	=	porphine-meso-tetra(4-benzene-sulfonic acid)
UV/Vis	=	ultra-violet/visible

CHAPTER I

Optical Spectroscopy

Fluorescence Spectroscopy

Spectroscopy refers to the analytical methods which are based on measuring the amount of electromagnetic radiation produced or absorbed by a molecular or atomic species of interest. Electromagnetic (EM) radiation is a form of energy that is transmitted as either light or radiant heat through space at massive velocities. EM radiation is characterized by its both its particle and wave-like properties. The wave properties of EM radiation can be characterized by the parameters wavelength, frequency, velocity, and amplitude. Unlike most waves, EM radiation requires no medium to propagate and may be transmitted through a vacuum (e.g. space). Discrete packets of energy, photons, are used to describe the particle functions of EM radiation. The Einstein-Planck equation relates the energy of a photon to its wavelength and frequency as followed

$$E = h\nu \tag{1.1}$$

where h is Planck's constant and ν is the frequency of the wave. And frequency is related to wavelength, λ, and the speed of light, c, in equation 2:

$$\lambda = \frac{c}{\nu} \tag{1.2}$$

Herein, the term optical spectroscopy will be used to describe all analytical methods that are based on the absorption or emission of EM radiation by matter within the UV (200-400 nm), visible (400-650 nm), and near infrared (650-1100 nm) regions of the electromagnetic spectrum. Absorption and emission processes are commonly illustrated by the Jablonski diagram shown in **Figure 1.1**.[1] In the diagram, S_0, S_1, and S_2 correspond to the ground, first, and second electronic singlet states respectively. T_1 is used to denote the first excited triplet state. Each electronic energy level is further divided into vibrational energy levels. The absorption processes, and subsequent deactivation processes of excited states are described in detail below.

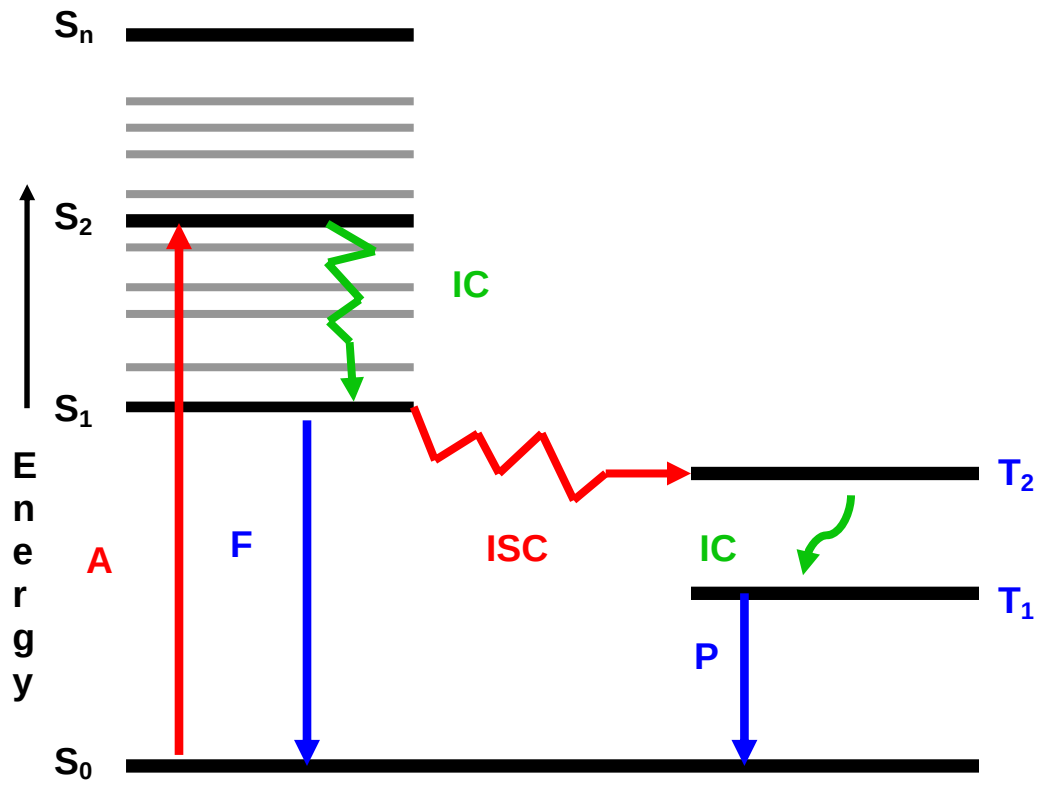

Figure 1.1. Illustration of the Jablonski Diagram.

Absorption. The absorption of light results in an electronic transition in an atom or molecule. Electrons are excited from the ground state, S_0, to some higher vibrational level of either S_1 or S_2 when a photon of light is absorbed. The energy of the absorbed photon of light corresponds to the energy difference between the excited and ground states. In molecules, an electron is promoted from the highest occupied molecular orbital (HOMO) to the lowest unoccupied molecular orbital (LUMO). The absorption process occurs very rapidly (10^{-15} sec) to form excited state, allowing no time for significant displacement of the nuclei; each atom has nearly the same position and momentum before and after an electron transition (Frank Condon principle). Therefore, the absorption spectrum only provides information about the average ground state of the absorbing species, along with its immediate surrounding solvent molecules.

Vibrational Relaxation. The absorption of a photon by a molecule is usually to a vibrational level above the 'zeroth' vibrational level of the excited singlet state.[2] Vibrational relaxation is a nonradiative process that follows the deactivation of a molecule from a higher vibrational level within the same electronic excited state. This process generally occurs within 10^{-12} sec or less. In solution, the molecule quickly loses the excess vibrational energy (heat) through collisions with solvent molecules.

Internal Conversion. Internal conversion describes the nonradiative transition which occurs between two electronic states of the same multiplicity; i.e., when an excited molecule in the S_2 state deactivates to the S_1 state. In this process, the excess energy is again dissipated in the form of heat. Moreover, molecules interacting with each other and the solvent may cause this transition as well.

Intersystem Crossing and Phosphorescence. Intersystem crossing occurs when a molecule transitions from an excited singlet state to the first excited triplet state. As a molecule enters a triplet state, its electron spin becomes reversed. Thus, one of the electrons undergoes a spin inversion from either $+\frac{1}{2}$ to $-\frac{1}{2}$ or vice versa. Phosphorescence is the emission of a photon during a transition between states with different spin quantum numbers.

Fluorescence Emission. The radiational transition from S_1 to S_0 causes the emission of a photon of light energy is called fluorescence. The molecule can return to one of several vibrational energy levels of the ground state. The amount of energy emitted in this process corresponds to the energy difference between $S_1(0)$ and a particular vibrational level of S_1. Just as absorption of light occurs between the lowest vibrational state of S_0 (0) and one of several vibrational levels of S_1, the radiative process of fluorescence place from $S_1(0)$ to any of the vibrational levels of S_0.

Luminescence. Fluorescence and phosphorescence are both examples of luminescence, the emission of light from any excited state in a molecule. Luminescence methods are inherently more sensitive than absorption measurements due to the elimination of background interference in luminescence measurements. Chemiluminescence is produced when a chemical reaction yields an electronically excited molecule, which emits light as it returns to the ground state.[3] When this chemical reaction occurs in biological systems, it is called bioluminescence.

Although both transitions emit photons of light, fluorescence should not be confused phosphorescence. In the case of phosphorescence, the interconversion from a singlet to triplet state is not allowed, and does not occur readily.[4] The result is that

phosphorescence generally takes place in milliseconds or longer. Many biological systems display phosphorescence, such as marine plant and animal life. Because the two processes are merely distinguished by the unpaired spin of the triplet state, examining the magnetic field properties of a biomolecule can confirm the presence of phosphorescence over bioluminescence. Molecules containing heavy atoms such as bromine and iodine are often phosphorescent.[1] The heavy atoms facilitate intersystem crossing, enhancing phosphorescent yields. For the sake of simplicity, only fluorescence emission will be considered for remainder of the discussion.

General Properties of Fluorescence Emission

Compared to the absorption spectra, fluorescence spectra are always bathochromically shifted (i.e., towards longer wavelengths). This is called a Stokes shift. Another general property of fluorescence is that the same emission spectrum is usually observed irrespective of the excitation wavelength. As mentioned previously, fluorescence typically occurs from the lowest vibrational level of an excited state (i.e., Kasha's rule). Upon excitation into higher electronic and vibrational levels, excess energy is quickly dissipated, resulting in relaxation of the excited fluorophore to the lowest vibrational level of S_1. Because this relaxation occurs so rapidly, the emission spectra are usually independent of the excitation wavelength. This phenomenon also results in fluorescence spectra being the mirror image of its absorption spectra.

There are many exceptions to the mirror image rule, particularly seen in cyanine dyes. The shorter wavelength shoulder often observed in cyanine dyes is the result of molecular excitation to the second excited state (S_2) which rapidly relaxes to S_1. Thus,

the mirror image of $S_0 \rightarrow S_1$ absorption is not of the total absorption spectrum. Other exceptions include the spectra of pH-sensitive fluorophores, the formation of excited state complexes, and the formation of excited state dimers (excimers).

Fluorescence Parameters. To understand the quantitative parameters used in fluorescence measurements, the Beer-Lambert law is first examined. According to the Beer-Lambert law, absorbance, A, is defined as

$$A = \varepsilon bc = \log \frac{I_0}{I} \tag{1.3}$$

where ε is the molar extinction coefficient, b is the sample cell pathlength, c is the concentration, I_0 is the intensity of the incident light and I is the intensity of light which passes through the sample. The molar extinction coefficient is a quantitative measurement of a molecule's ability to absorb light, dependent on measured wavelength and not the sample concentration.

Fluorescence can now be written in terms of Equation 1.3.

$$I_A = I_0 - I = I_0(1-10^{-\varepsilon bc}) \tag{1.4}$$

and

$$I_F = I_0(1-10^{-\varepsilon bc})\phi_F \tag{1.5}$$

where the term ϕ_F is the quantum yield of the fluorophore. Thus, the fluorescence signal depends on the incident light intensity, the absorbance of the sample (i.e., sample

concentration) at the wavelength of excitation, λ_{ex}, and ϕ_F. As a result, **Equation 1.5** can be simplified as

$$I_F = 2.303\phi_F I_1 \varepsilon bc \qquad (1.6)$$

In dilute solutions, a linear relationship between the fluorescence intensity and concentration is observed.

Solvent Effects. The wavelength and intensity of fluorescence emission of a fluorophore depend strongly on extrinsic properties such as temperature, viscosity and solvent polarity. In general, emission spectra will weaken and red-shifted with increasing solvent polarity.[1, 5] This phenomenon is attributed to the electron of the fluorophore expanding, thereby increasing the fluorophore's polarizability and lowering the excitation energy. The fluorophore is usually excited to an excited vibrational level within S_1. The excess vibrational energy is rapidly lost to the solvent resulting in the Stokes shift. Solvent effects shift the emission to still lower energy due to stabilization of the excited state by the polar solvent molecules. Typically, the fluorophore has a larger dipole moment in the excited state than in the ground state. Following excitation, the solvent dipoles will reorient around the fluorophore's excited state dipoles, lowering the energy of the excited state. The more polar a fluorophore, the more sensitive it is to solvent polarity. Probe-probe interactions will also affect a fluorophore's emission spectra. The propensity of cyanine dyes to self-associate will discussed in further detail in Chapter 2.

Other Factors Affecting Fluorescence. When performing fluorescence measurements, many factors must be considered. First, all samples will scatter the exciting light to some extent. Two light scattering phenomena to consider during fluorescence measurements are Rayleigh and Raman light scattering. Rayleigh scattering depends on the particle size of the solute or any suspended material.[2] The intensity of Rayleigh scattering is proportional to r^6/λ^4, where r is the particle radius. By monitoring excitation slitwidths and choosing excitation wavelengths on the low energy (red) edge of the absorption spectrum, Rayleigh scattering can be minimized. The second type of scattering, Raman, involves the loss of excitation light energy lessened by vibrational modes of the solvent molecules. When the sample fluorescence is intense, the contribution of the Raman band will be negligible. To test for the contribution of Raman scattering, the measurements can be replicated with the λ_{ex} shifted 10 nm. The Raman band will shift in the same direction.

A great deal of error in fluorescence measurements can be overcome by simply moderating the sample concentration. At high sample concentrations, the solution in the front of the cell is exposed to a higher excitation light intensity than the sample near the opposite side due to sample absorption. This is called the inner filter effect. The inner filter effect can result in a deviation from linearity with respect to **Equation 1.6**. The percent error observed from the inner filter effect is shown in **Table 1.1**. Inner filter error is usually minimized by performing experiments at a concentration at which A at λ_{ex} is <0.1. If experiments must be performed at a certain concentration, then this error may also be minimized by choosing a λ_{ex} at which A is <0.1 on the low energy side of the absorption spectrum.

Table 1.1.[a] Relationship of Fluorescence Error Propagation with Absorbance

Absorbance	Percentage error in I_F
0.01	1.1
0.05	5.5
0.10	10.6
0.20	20.0

[a]Adapted from reference 2.

Circular Dichroism

Circular dichroism is a form of absorption spectroscopy which measures the differential absorption of right- and left-circularly polarized light (CPL). Asymmetric or chiral molecules exhibit CD bands within its absorption spectra because they absorb left- and right-CPL to different extents and therefore considered optically active. CD can only arise within in the spectral region where absorbance occurs. If the absorbance is essentially zero, there cannot be a measurable difference in CPL:

$$\Delta A = A_L - A_R \qquad 1.7$$

Origin of the Ellipse. Linear polarized light can be viewed as a superposition circularly polarized light possessing equal and opposite amplitude and phase (**Figure 1.2**).[6] A projection of the combined amplitudes perpendicular to the propagation direction thus yields a line. When this light passes through an optically active sample with a different absorbance for the two components, the amplitude of the stronger component will be smaller than that of the less absorbed component. The consequence is that a projection of the resulting amplitude yields an ellipse instead of the usual line, while the polarization direction has not changed. This ellipticity is called CD or Cotton Effects (CE). Right and left CPL will be absorbed to different extents at some wavelengths due to differences in extinction coefficients for the two polarized rays. It is important to note that CD will only be observed within the absorption bands of the asymmetric chromophore (intrinsic) or symmetric chromophore in an asymmetric environment (extrinsic CD).

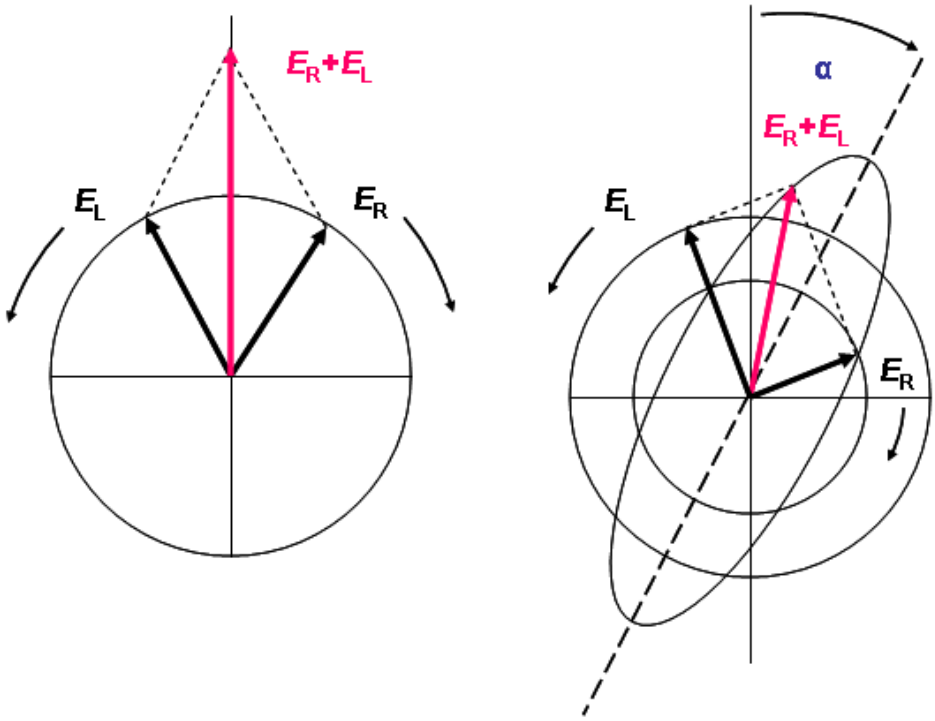

Figure 1.2. Illustration of the origin of an ellipse adapted from reference 6. Linear polarized light can be viewed as a superposition of opposite circular polarized light of equal amplitude and phase. The differential absorption of the left- and right hand polarized component leads to an ellipse (CD band).

CD Instrumentation. CD measurements are performed on a CD spectropolarimeter. The essential elements of spectropolarimeter are shown in **Figure 1.3**. Typically the instrument is equipped with a Xenon Arc lamp excitation light source. However, unlike a traditional spectrophotometer, CD instruments only contain one monochromator (quartz prism or diffraction grating). Linearly polarized light is passed through either a Pockels cell or photoelastic modulator which produces a beam that modulates the beam alternately into left- and right-CPL.[7] Pockels cells or photoelastic modulators are isotropic elements which are rendered anisotropic through the application of external stress. In Pockels cells, stress is created by the application of AC high-voltage to an ammonium dideuterium phosphate crystal. In photoelastic modulators, stress is induced through a piezoelectric effect. The beam then passes through the sample to a photomultiplier tube (PMT). The PMT signal output is converted to voltage and split. One signal contains the alternating current signal proportional to the CD (the differential absorption of one component over the other). The other signal is averaged, and is related to the mean light absorption. The ratio of the two signals varies linearly as a function of the CD amplitude, and is the recorded signal of interest. The detected signal can then be processed as ΔA vs. λ.

The difference in left and right handed absorbance $A_L - A_R$ is very small, usually in the range of 0.0001, corresponding to an ellipticity of a few $1/100^{th}$ of a degree. Ellipticity, θ, is related to ΔA as followed:[8]

$$\theta = \frac{2.303}{4} \cdot (A_L - A_R) \cdot \frac{180}{\pi} \cdot [\text{deg}] \qquad 1.8$$

For most spectropolarimeters, raw data output of ellipticity, θ, is in units of millidegrees.

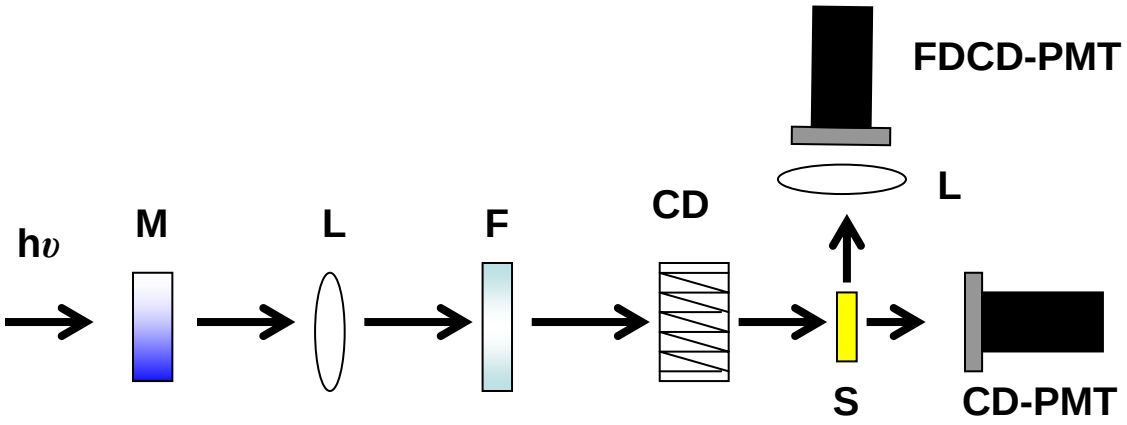

Figure 1.3. Schematic diagram of a spectropolarimeter. hν = light energy; M = monochromator; L = lens; F = filter; CD = CD modulator; S = sample; CD-PMT = CD photomultiplier tube; FDCD-PMT = FDCD photomultiplier tube.

In order to normalize CD data with respect to concentration, C, pathlength, l, CD is often reported in the literature as either molar ellipticity, [θ], or molar CD, $\Delta\varepsilon$:

$$[\theta] = \frac{\theta}{10 \cdot C \cdot l} \quad 1.9$$

$$\Delta\varepsilon = [\theta]/3298 \quad 1.10$$

And protein CD is typically reported in terms of mean residue ellipticity $[\theta]_{MRE}$:

$$[\theta]_{MRE} = \frac{\theta}{10 \cdot C_r \cdot l} \quad 1.11$$

where

$$C_r = \frac{n \cdot 1000 \cdot c_g}{MW} \quad 1.12$$

and n is the number of peptide bonds (residues), c_g is the macromolecule concentration (g/mL), and MW is the molecular weight of the species.

Applications of Circular Dichroism

Far UV Protein Analysis. The major advancements in protein engineering and protein synthesis in the last two decades has brought about a resurgence of interest in protein secondary structure determination using CD techniques. And many detailed reviews have been published dedicated to the use of CD for protein research.[9-17] Protein optical activity is owed to their abundance of L-amino acids and right handed α-helices. The electronic transitions between different residues in a protein also contribute to its overall optical activity. When CD measurements are performed in the far UV (170-250 nm) and UV (250 - 400 nm) region, chromophores from amino acid side chains (asymmetric) and peptide bonds (symmetric) will give important information about protein primary structure.

Protein secondary structure cannot be differentiated using isotropic absorption spectroscopy techniques. The spectral comparisons of far UV spectrophotometry versus far UV CD are presented in **Figure 1.4**. However, using anisotropic CD measurements, protein secondary structure is readily discerned.[18] The orientation differences of the peptide bond chromophore in the three protein secondary structures result in differences in the electronic transitions. These differences translate to three distinct bands for the three basic secondary structures α-helix, β-sheet, and randomly coiled. The lowest energy transition in the peptide bond chromophore is the $n\rightarrow\pi^*$ transition observed at 210-220 nm displaying very weak intensity (ε_{max} ~100). The $n\rightarrow\pi^*$ transition appears in the α-helical polypeptides as a small shoulder near 220 nm. For α-helical polypeptides, a much stronger band is center at 190 nm corresponding to the $\pi\rightarrow\pi^*$ transition. This transition is responsible for the majority of the peptide bond absorbance (ε_{max} ~7000). In using CD over isotropic far-UV absorbance, these transitions are more easily distinguished. Exciton splitting of the $\pi\rightarrow\pi^*$ transitions results in the positive band at 192 nm and the negative band at 208 nm observed in α helical polypeptides. **Table 1.2** displays the three basic protein secondary structures, the corresponding CE bands and the electronic transitions responsible for them. The mean residue ellipticity reported was used in **Chapter 4** to validate CD data collected for poly-L-lysine.

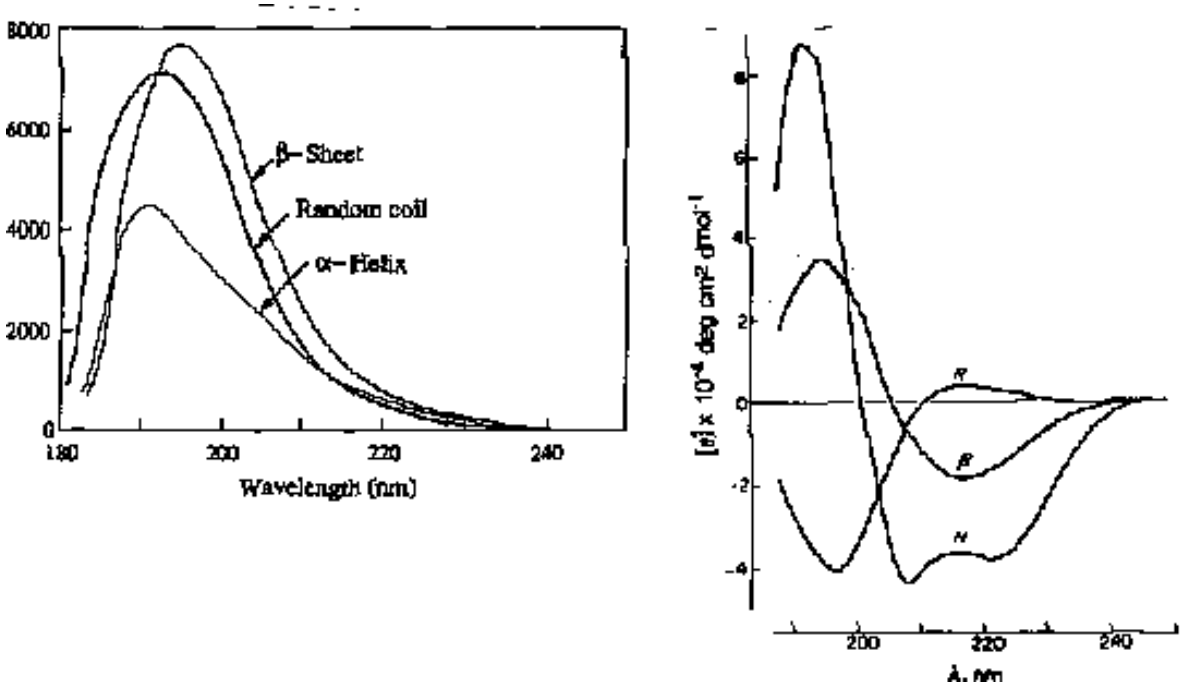

Figure 1.4. Far UV spectral comparison of absorption vs. CD spectroscopy for protein secondary structure identification. The spectra on the left are adapted from reference 17 and the spectra on the right are from reference 18.

Table 1.2 Far UV CD of Proteins

Secondary structure	Cotton Effects (Wavelength)	[θ] (deg cm^2 dmol^{-1})	Electronic Transition
α-helix	+ ~192 nm	60,000 to 80,000	$\pi \rightarrow \pi^*$
	- 208 nm	-36,000	$\pi \rightarrow \pi^*$
	- 222 nm	-36,000	$n \rightarrow \pi^*$
β-sheet	+ 195-200 nm	30,000 to 50,000	$\pi \rightarrow \pi^*$
	- 215-220 nm	-10,000 to -20,000	$n \rightarrow \pi^*$
random coil	- ~200 nm	-20,000	$\pi \rightarrow \pi^*$
	+ 220 nm	---	$n \rightarrow \pi^*$

As with NMR experiments, CD measurements are quite advantageous for the purpose of determining protein secondary structure in its native form (i.e., aqueous solution). Furthermore, CD allows for changes in solvent environment (e.g. pH, denaturants, temperature) to be monitored accurately. And most importantly, CD experiments are non-destructive to protein samples. Yet advantages of CD spectroscopy must also be tempered with the drawbacks met in measuring CD in the far UV region. Specifically, interference from the sample matrix can be quite problematic. To minimize interference, only very dilute non absorbing (i.e., 20mM phosphate, borate, or Tris) buffers are allowed for measurements below 200 nm. Unfortunately, background interference makes CD experimentation subject to a great deal of experimental error; the average accuracy of fits is about +/- 10%.

Induced CD. When an achiral chromophore is bound to a chiral molecule, CD can be observed within the absorption bands of that chromophore. **Figure 1.5** This phenomenon is called induced CD or extrinsic Cotton effects (CE).[19, 20] Although the CD of the chiral inducer may also change upon association, this is not indicative of induced CD. There are two generally accepted modes of inducing CD, induction of a dominating chiral structure of the achiral molecule or induction of a chiral arrangement of the electric dipole transition moments between the relevant chromophores of the achiral (guest) and chiral (host) molecules. Because some chiral inducing molecules such as tartrates can induce substantially different CD bands within different achiral environments, it is important to confirm induced CD of the achiral molecule outside the absorption band of the chiral species.

Induced CD has been quite advantageous to the drug industry by elucidating the binding interactions between achiral drug chromophores and protein binding sites. Induced CD can also be used to describe the absolute configuration of the associating species.[21] Induced CD is also utilized to describe chiral selectivity and recognition. Chiral recognition within protein or enzyme binding sites is often described in terms of a three-point interaction model.[22-26] This model mandates that a chiral selector will only recognize its chiral target if three points of interaction occur. However, this model has come under quite a bit of scrutiny in recent years for being too stringent and quite possibly only relevant to the lock and key mechanisms of enzymology.

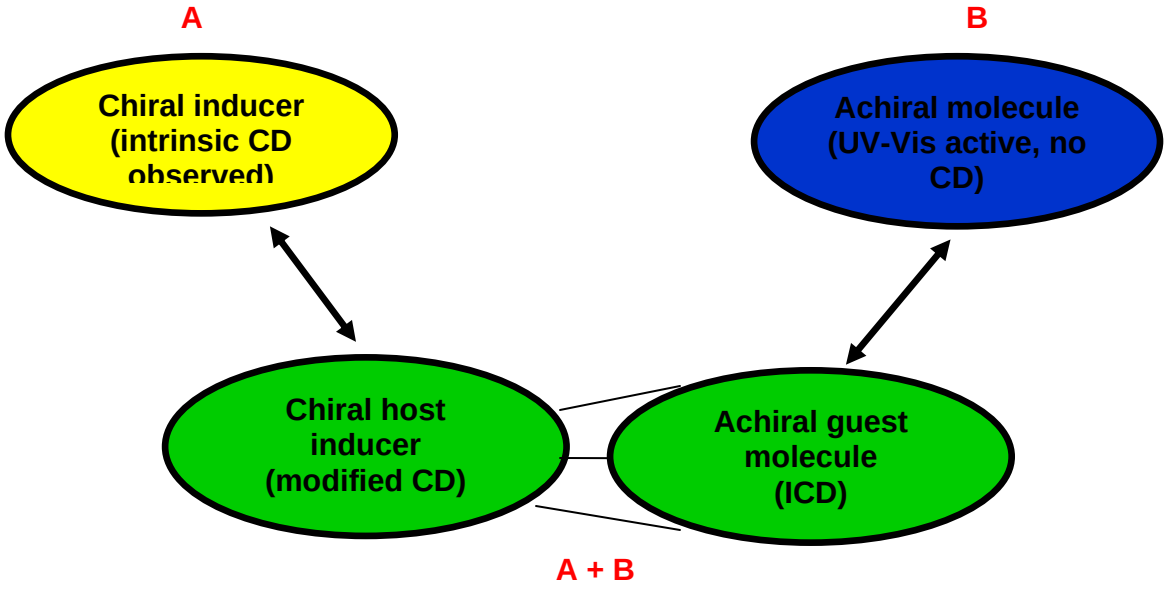

Figure 1.5. Illustration of induced CD.

Exciton Coupling and the Exciton Chirality Method. When two or more chromophores are brought into proximity with each other, even if they are not conjugated, they may interact with each other when one chromophore is excited. This phenomenon is called exciton coupling.[27] Using CD, valuable stereochemical information may be extracted from exciton-coupled spectra. A bisignate CD band is observed when the interacting chromophores form a chiral array of excited dipoles. Even if the two chromophores have no orbital overlap and electron exchange is negligible, two or more chromophores can interact with each. When two chromophores have similar energy levels, the electric dipole transition on one chromophore can interact with that from the other chromophore, and the excitation energy becomes delocalized over the two chromophores. The term exciton refers to the delocalized excitation produced by dipole-dipole coupling of locally excited states. The exciton coupling results in a split of the locally excited states. This splitting is can be observed in absorption spectrophotometry as two distinct bands in the UV-Vis spectrum, one red shifted from the center of the local excitation and one blue shifted from the excitation. Yet, unless the exciton splitting is quite large, one typically sees only a single broad band when both exciton transitions are allowed. When only one transition is allowed, the band may be either red-shifted or blue-shifted. It is important to note that two chromophores may or may not be identical and, moreover, they do not necessarily have to be in the same molecule to interact.[28]

Each exciton band will have a corresponding CD band if the two chromophores are arranged in a chiral configuration. Since exciton coupling always appears as a oppositely signed CD bands, it is usually much easier to detect exciton coupling by CD spectroscopy than with absorption spectroscopy. Both spectrophotometry and CD

spectra depend on the electronic transitions, as well as their distance and orientation with one another. Harada and Nakanishi determined that the sign of the biphasic CD band is directly related to the absolute configuration of the interacting chromophore.[27-31] This observation, termed the exciton chirality rule, is illustrated in **Figure 1.6**. According to the when the induced electric dipoles are oriented in a negative (-) torsion angle (i.e., negative chirality), the longer wavelength component of the associated exciton couplet exhibits a negative CE. Alternately, when dipoles are oriented to form a positive (+) torsion angle (positive chirality), the longer wavelength CE is positive. The distance between the two component CD curves of opposite signs (not the positive and negative extrema of actual curves) is called the Davydov split.

The exciton chirality rule, allows for a simple and versatile approach for establishing absolute configurations and conformations of organic compounds in solution on a microscale. This technique is commonly referred to as the exciton chirality method. The exciton chirality method is quite sensitive. The amount of sample required is of the same order as that for measurements of electronic spectra. Exciton chirality is also quite significant in far UV CD measurements of proteins and peptides. In a polypeptide, the amide chromophore exhibits little orbital overlay or charge transfer.[29] The CD spectrum of the α-helix is dominated by the exciton effect of the 190 nm $\pi \rightarrow \pi^*$ electronic transition. Particularly in the case of short helices, the spectrum is very sensitive to the direction of the $\pi \rightarrow \pi^*$ transition dipole moment.

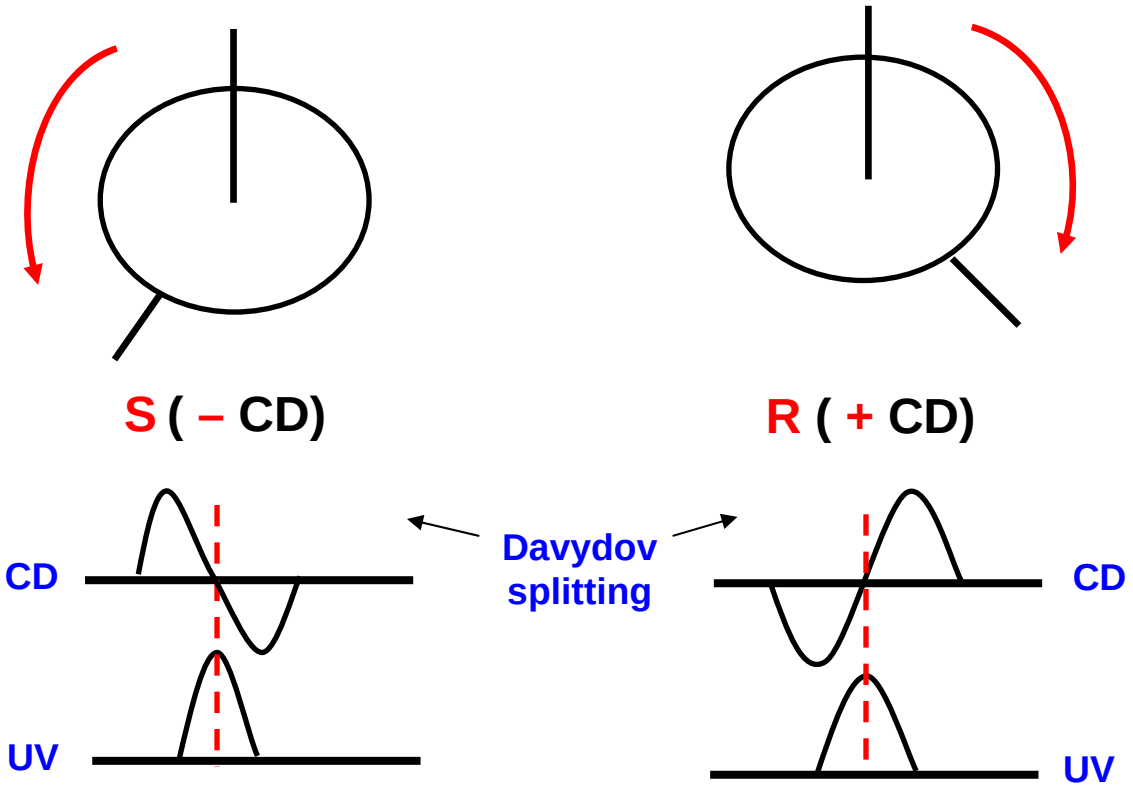

Figure 1.6. The determination of absolute configuration by using the Exciton Chirality Method.

Fluorescence Detected Circular Dichroism

Fluorescence detected circular dichroism (FDCD) is a chiroptical technique first developed by Tinoco and co-workers.[32] In FDCD, the difference in absorption for left and right-CPL is obtained by measuring the difference in fluorescence intensity for left and right circularly polarized excitation. The method is based on the assumption that the excitation spectrum of a fluorophore parallels that of the absorption spectrum. This is usually true for fluorophores in which energy transfer is negligible.

FDCD reports information about the fluorophore in the ground state.[33] The polarization of the fluorescent light is not measured. The method in which the actual polarization of fluorescent light is measured is called circularly polarized (CP) luminescence. In contrast to FDCD, CP luminescence gives information about the excited state of a fluorophore.[34] Although CP luminescence is useful in multichromophoric molecules, the vanishing fluorescence yield renders the technique inapplicable to many monochromophoric systems. This example demonstrates advantage of FDCD over CP luminescence.

As with other fluorescence techniques, the fluorescence detection of FDCD has several advantages over its absorption counterpart. FDCD techniques are more selective and sensitive of the CD measurement for chiral chromophores. First, FDCD allows for zero background interference in measurements, thus allowing for more sensitivity. Experimentally, FDCD measurements have shown up to a 100-fold improvement in sensitivity over CD measurements.[35] In **Figure 1.7** gives a spectral comparison of induced CD and induced FDCD of equimolar concentrations of NIR cyanine dye IR 783 bound to HSA at 0.5 μM. Increased sensitivity allows for minimal analyte concentrations

to be used, thereby eliminating spectral alterations from unwanted intermolecular and intramolecular associations which may alter the CD measurements. In addition, the selectivity gained in FDCD measurements becomes quite useful in systems in which both fluorescent and nonfluorescent chromophores are present. And any spectral changes observed will be as a result of changes in the microenvironment of the fluorophore alone.

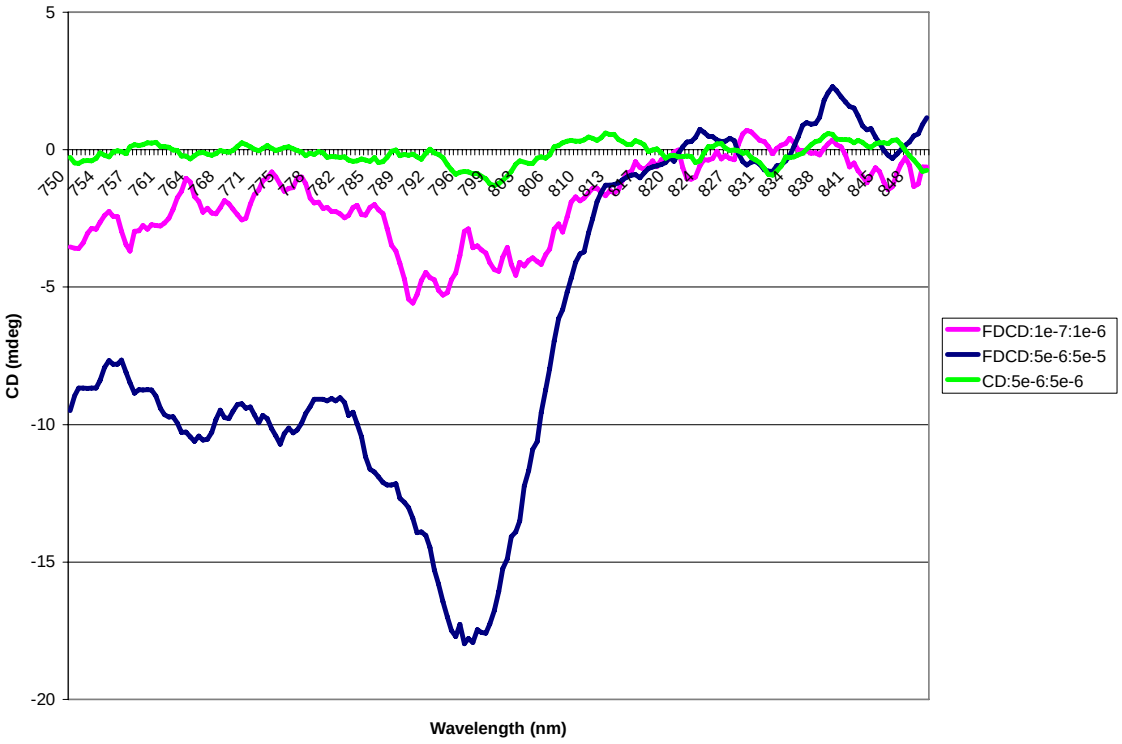

Figure 1.7. Depiction of the sensitivity of FDCD over CD.

The binding interactions of bilirubin to four mammalian serum albumins were reported using multi-dimensional FDCD.[36] The FDCD instrument used by Thomas et al measures the multidimensional FDCD spectrum as a function of excitation and emission wavelengths. For this unique technique, an intensified photodiode array was introduced as the detector. The multidimensional FDCD allowed for even more selectivity over standard FDCD and CD measurements. This modified instrument allowed for separation of mixtures by spectral methods instead of chemical or physical techniques. In order to further separate the contribution of specific chiral fluorophores from sample mixtures, competitive assays using the anticoagulant drug warfarin were also performed. In using multidimensional technique, Thomas and co-workers were able to demonstrate the application of separating chiral fluorophores from an interfering background without the need for exhaustive separation steps prior to FDCD analysis.

In addition, combining quenching techniques with multidimensional FDCD experiments provided a selective monitor for chiral fluorophores.[37] When various quenchers are utilized in a study, fluorescence quenching can provide invaluable information about the specific microenvironment of a fluorophore (e.g. hydrophobicity and electrostatic interactions), thereby allowing for even more selectivity. In this technique, the diminution of FDCD to confirm the quenching of bound ligand to HSA. Combining quenching experiments with multidimensional FDCD is quite useful in systems containing both a chiral and achiral fluorophore. Multidimensional FDCD was also paired with quenching techniques to study Site I and Site II ligand binding in HSA.[38] In using the combined techniques, Thomas et al confirmed that Site I was more hydrophobic than Site II.

Summary

The optical spectroscopy methods discussed herein were each utilized for the investigation of binding interactions of near infrared (NIR) cyanine dyes with proteins and polypeptides. The spectral properties of cyanines are quite sensitive to the probe's microenvironment. Much information can be derived from the distinct spectral changes observed when NIR probes are either bound to protein or exist as aggregates. In this way, the optical spectroscopy methods mentioned allow for binding interactions of biomolecule-ligand (e.g., protein-dye) systems to be detected indirectly. Through these spectral changes, a linear relationship can be derived in which the apparent binding constants can also be obtained. Emission spectroscopy is quite advantageous for the determination of binding constants, since blue-shifted cyanine aggregates exhibit minimal fluorescence and spectra are not complicated by multiple species. The high sensitivity of fluorescence spectroscopy also allows for the use of very low probe concentrations. Low dye concentrations ensure protein structure is not distorted by the labels, thus confirming a more accurate binding model. Furthermore, these methods are also noninvasive, nondestructive, and in many cases very little material is required for analysis. Another advantage of optical spectroscopy methods is that samples can be measured in solution, in contrast to certain techniques such as X-ray crystallography. And finally the information obtained from CD and FDCD measurements when a symmetrical probe is in an asymmetrical environment (e.g. protein binding site) is quite valuable. Induced CD only occurs when the chromophore is bound to protein through at least three points of

interaction. This fact confers a great deal of selectivity in chiroptical measurements. And for all these reasons, optical spectroscopy methods are ideal for binding analysis of biomolecule-dye interactions.

References

1. Lakowicz, J. R., *Principles of Fluorescence Spectroscopy*. 3rd ed.; Springer Science: New York, 2006.

2. Gore, M. G., *Spectrophotometry and Spectrofluorimetry: A Practical Approach*. Oxford University Press: Oxford, 2000.

3. Skoog, D. A.; West, D. M.; Holler, F. J.; Crouch, S. R., *Fundamentals of Analytical Chemistry*. 8th ed.; Brooks/Cole-Thomson Learning: Belmont, 2004.

4. Hammes, G. G., *Spectroscopy for the Biological Sciences*. John Wiley and Sons: Hoboken, 2005.

5. Schmidt, W., *Optical Spectroscopy in Chemistry and Life Sciences: An Introduction*. Wiley-VCH: KGaA, 2005.

6. Snatzke, G.; Woody, R. W., Circular Dichroism: An Introduction. In *Circular Dichroism: Principles and Applications*, 2nd ed.; Berova, N.; Nakanishi, K.; Woody, R. W., Eds. Wiley-VCH: New York, 2000.

7. Brittain, H. G., Techniques of Chiroptical Spectroscopy. *Applied Spectroscopy* **2000,** 35, (3), 175-201.

8. Woody, R. W., Circular dichroism. *Methods in Enzymology* **1995,** 246, 34-71.

9. van Mierlo, C. P. M.; de Jongh, H. H. J.; Visser, A. J. W. G., Circular dichroism of Proteins in Solution and at Interfaces. *Applied Spectroscopy Reviews* **2000,** 35, (4), 277-313.

10. Wu, D.; Xu, G. Y., Study on protein-surfactant interaction by spectroscopic methods. *Acta Physico-Chimica Sinica* **2006,** 22, (2), 254-260.

11. Bulheller, B. M.; Rodger, A.; Hirst, J. D., Circular and linear dichroism of proteins. *Physical Chemistry Chemical Physics* **2007,** 9, (17), 2020-2035.

12. Johnson, W. C., Protein Secondary Structure and Circular Dichroism: A Practical Guide. *Proteins: Structure, Function, and Genetics* **1990,** 7, 205-214.

13. Kelly, S. M.; Price, N. C., The Use of Circular Dichroism in the Investigation of Protein Structure and Function. *Current Protein and Peptide Science* **2000,** 1, 349-384.

14. Kelly, S. M.; Jess, T. J.; Price, N. C., How to study proteins by circular dichroism. *Biochimica Et Biophysica Acta-Proteins and Proteomics* **2005,** 1751, (2), 119-139.

15. Wang, W., Protein aggregation and its inhibition in biopharmaceutics. *International Journal of Pharmaceutics* **2005,** 289, (1-2), 1-30.

16. Greenfield, N. J., Analysis of circular dichroism data. In *Numerical Computer Methods, Pt D*, 2004; Vol. 383, pp 282-317.

17. Cantor, C. R.; Schimmel, P. R., *Biophysical chemistry: Part II: Techniques for the Study of Biological Structure and Function*. W.H. Freeman: New York, 1980.

18. Greenfield, N.; Fasman, G. D., Computed circular dichroism spectra for the evaluation of protein conformation. *Biochemistry* **1969,** 8, (10), 4108-16.

19. Gawronski, J.; Grajewski, J., The significance of induced circular dichroism. *Organic Letters* **2003,** 5, (18), 3301-3303.

20. Hatano, M., Induced circular dichroism in biomolecules. In *Biomolecules*, Nagata, C., Ed. Elsevier: Amsterdam, 1985; pp 181-204.

21. Cheruvallath, V. K.; Riley, C. M.; Narayanan, S. R.; Lindenbaum, S.; Perrin, J. H., A quantitative circular dichroic investigation of the binding of the enantiomers of ibuprofen and naproxen to human serum albumin. *Journal of Pharmaceutical and Biomedical Analysis* **1997,** 15, (11), 1719-1724.

22. Wainer, I. W.; Caldwell, J., The 1996 Chirality debate. *Chirality* **1997,** 9, (2), 95-95.

23. Booth, T. D.; Wahnon, D.; Wainer, I. W., Is chiral recognition a three-point process? *Chirality* **1997,** 9, (2), 96-98.

24. Davankov, V. A., The nature of chiral recognition: is it a three-point interaction? *Chirality* **1997,** 9, 99-102.

25. Pirkle, W. A., On the minimum requirements for chiral recognition. *Chirality* **1997,** 9, 103.

26. Allenmark, S., Induced circular dichroism by chiral molecular interaction. *Chirality* **2003,** 15, (5), 409-22.

27. Lightner, D.; Gurst, J., *Organic Conformational Analysis and Stereochimstry from Circular Dichroism Spectroscopy*. John Wiley & Sons: New York, 2000.

28. Berova, N.; Nakanishi, K., Exciton Chirality Method:Principles and Applications. In *Circular Dichroism: Principles and Applications*, 2nd ed.; Berova, N.; Nakanishi, K.; Woody, R. W., Eds. John Wiley & Sons: New York, 2000.

29. Woody, R. W., The Exciton model and the circular dichroism of polypeptides. *Monatshefte Fur Chemie* **2005,** 136, (3), 347-366.

30. Lightner, D., Determination of absolute configuration by CD. Application of the Octant Rule and the Exciton Chirality Rule. In *Analytical Applications of Circular Dichroism*, Purdie, N.; Brittain, H. G., Eds. Elsevier: Amsterdam, 1994.

31. Kuball, H. G.; Dorr, E.; Hofer, T.; Turk, O., Exciton chirality method. Oriented molecules - Anisotropic phases. *Monatshefte Fur Chemie* **2005,** 136, (3), 289-324.

32. Turner, D. H.; Tinoco Jr., I.; Maestre, M. F., Fluorescence Detected Circular Dichroism. *Journal of the American Chemical Society* **1974,** 96, (13).

33. Turner, D. H., Fluorescence Detected Circular Dichroism *Methods in Enzymology* **1978,** 49, 199-237.

34. Dekkers, H. P. J. M., Circularly Polarized Luminescence: A Probe for Chirality in the Excited State. In *Circular Dichroism: Principles and Applications*, 2nd ed.; Berova, N.; Nakanishi, K.; Woody, R. W., Eds. John Wiley & Sons: New York, 2000; pp 185-215.

35. Meadows, F.; Narayanan, N.; Patonay, G., Determination of protein-dye association by near infrared fluorescence-detected circular dichroism. *Talanta* **2000,** 50, 1149-1155.

36. Thomas, M. P.; Patonay, G.; Warner, I. M., Fluorescence-Detected Circular Dichroism Studies of Serum Albumins. *Analytical Biochemistry* **1987,** 164, 466-473.

37. Thomas, M. P.; Patonay, G.; Warner, I. M., Selective Monitoring of Stern-Volmer Quenching of Chiral Molecules via Fluorescence Detected Circular Dichroism. *Analytical Letters* **1987,** 20, (5), 717-730.

38. Thomas, M. P.; Nelson, G.; Patonay, G.; Warner, I. M., Analysis of drug binding sites on human serum albumin using multidimensional fluorescence measurements. *Spectrochimica Acta* **1988,** 43B, (4), 651-660.

CHAPTER II

Near Infrared Cyanine Dyes and Their Applications

Introduction

The photophysical properties of near infrared (NIR) dyes within various types of media have resulted in their use in a variety of applications such as photodynamic therapy, silver halide sensitizers, laser diodes, and optical data storage to name a few.[1] Cyanine dyes contain two heterocyclic components connected by a polymethine bridge having an odd number of carbons.[2] Varying the nature of the heterocyclic structure or lengthening the bridge results in dye absorption and fluorescence maxima extending into longer wavelengths. NIR dyes are typically characterized by large molar absorptivities and strong fluorescence in aqueous solutions. In biological applications, NIR fluorescence can be particularly advantageous due to the absence of background interference because dye absorption bands are well removed from those most biomacromolecules (**Figure 2.1**). Furthermore, scatter noise (i.e., Raman and Rayleigh) is reduced in NIR spectroscopy since it is related to wavelength of detection by $1/\gamma^4$.[3] In addition, NIR spectroscopy has become advantageous because diode lasers as excitation sources and the avalanche photodiodes as signal transducers are now more readily available at relatively low cost, possessing long operation lifetimes.

Dyes have been used extensively in biological research throughout the last several decades. When examining the published literature, it is important to note that this research has always been dictated by dye availability. Because visible dyes were made available much earlier than their longer wavelength counterparts, a significant part of the

literature focuses only on dyes exhibiting spectral characteristics (absorption and emission) in the visible region of the electromagnetic spectrum. Despite the numerous advantages of using near-infrared (NIR) dyes, the limitations of earlier detection methods made the utilization of the longer wavelength range less attractive. However, with the advent of both semiconductor detectors and laser excitation sources in the 1980s, instruments working within the NIR region began to emerge. The use of the compact and cheap GaAlAs laser diode with its high power output and long lifetime (≥100 000 h) opened up opportunities for researchers that had not previously been available. Since then a large number of research groups have been actively utilizing the NIR spectral region for a broad range of biological applications.

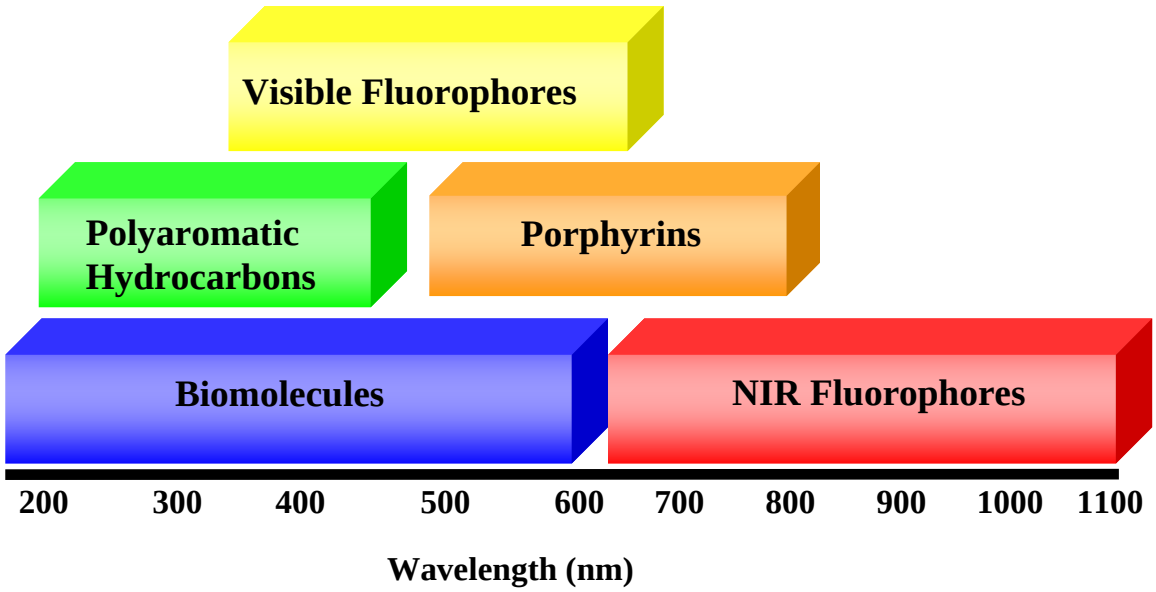

Figure 2.1. The typical absorption range of organic compounds used for the analysis of biomolecules. Revised from reference 11.

Polymethine carbocyanine dyes, possessing varying numbers of conjugated systems commonly absorb in the NIR region. Because NIR carbocyanine dyes readily dissolve in water, they are particularly useful for biological and medical applications. In recent years, NIR dyes have been used to study proteins in solution owing to their absorption regions lying far beyond the absorption of most biomolecules. Although biomolecules such as hemoglobin and cytochromes exhibit NIR absorption, their absorption bands are much weaker than dye in this region. Moreover, few biomolecules undergo any electronic transitions within the NIR region, thus Raman and Rayleigh light scattering is greatly reduced. Consequently, improved signal-to-noise ratios are typically observed in the NIR region. And impurities from other sources or unreacted starting materials need not be considered since such species are not detected in longer wavelengths, particularly when single wavelength detection methods (i.e., some chromatographic techniques) are employed and only pure compound is observed.

As a result of the increasing availability of resources, NIR spectroscopy has become much more specialized as well. This chapter will focus only on a specific segment of this field, i.e., protein-carbocyanine dye interaction. Although at first glance this scope may seem quite narrow, carbocyanine dyes are some of the most valuable probes for protein research because they are water soluble at low concentrations and demonstrate strong affinities for biomolecules. In addition, carbocyanines are relatively easy to synthesize and their properties are readily controlled by subtle structural changes. Although nucleic acids are also an important class of biomolecules, they typically require

dyes with properties uniquely tailored for their characterization. Thus, this chapter will mainly focus on medical and clinical applications using only NIR carbocyanine dyes and protein.

Polymethine Dye Structure

Polymethine and polyene dyes are characterized by a chain of methine groups, i.e., by a system of conjugated double bonds.[4] The carbon atoms of the methine groups may be substituted by groups other than hydrogen, or they may be parts of carbocyclic or heterocyclic ring systems. The chain ends of polyenes are typically alkyl or other groups which do not influence the electronic excitation of the dye. Carotenoids, the most important group of polyene dyes, are naturally occurring in nature and require twenty-two methine groups, or 11 double bonds, to shift the absorption spectrum into the visible region.

In polymethine dyes, an electron donor D and an electron acceptor A terminate the chain of methine groups. The structural backbone of polymethine dyes is depicted in **Figure 2.2**. Polymethines can be classified by the number of methine groups in which n = 0, 1, 2, etc. corresponding to mono-, tri-, penta- (etc)-methines. In addition, polymethines can be further subdivided with respect to the structure of the electron donor-acceptors. For instance, in the largest group of cationic polymethine dyes (i.e., q = +1 in **Figure 2.2**) the donor and acceptor moieties contain nitrogen. And depending on whether or not both or one of the nitrogens are components of a ring moiety, they are named cyanine, hemicyanine, or streptocyanine. The classification of polymethines is illustrated in **Table 2.1**.

Generally, polymethine dyes have an all-trans geometry in their stable form. However, the photoisomerization of these dyes have also been reported.[5-8] Tatikolov et al. report the interaction of meso-substituted anionic thiacarbocyanines with HSA results in cis→trans isomerization and, as a consequence, an appearance and a steep rise of dye fluorescence.

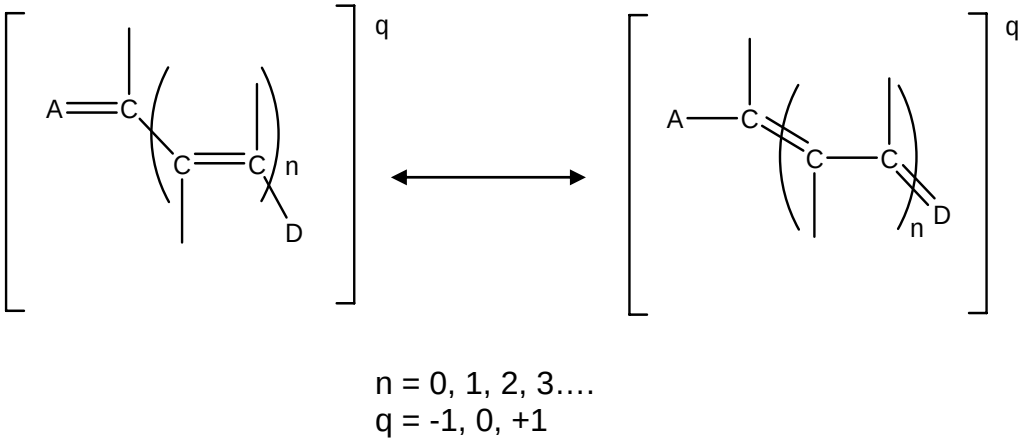

Figure 2.2. Structural backbone of polymethine dyes. Revised from reference 4.

Table 2.1.[a] Classification of polymethine dyes

Group Name	General Formula	Example
Cyanine	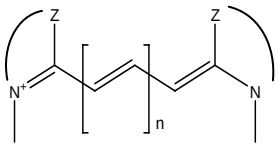	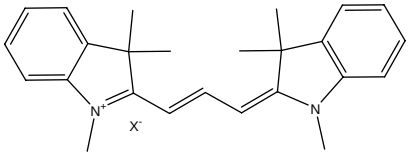
Hemicyanin	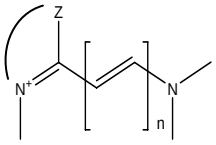	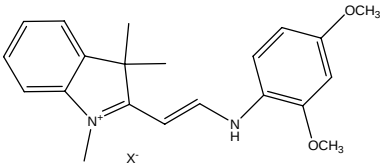
Streptocyanine	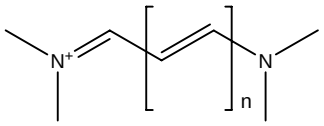	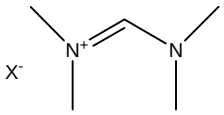
Oxonol	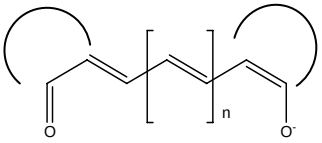	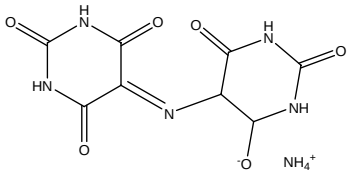

[a]Taken from reference 4.

The Spectra-Dye Structure Relationship

The monomethine cyanines typically show absorption in the visible region, and with each extension of the chromophore by one vinylene moiety (CH=CH) causes a bathochromic shift of about 100 nm.[1, 9-11] Substituents at the chromophore cause additional shifts in absorption. Marked spectral changes are observed with strongly electron donating or strongly electron withdrawing substituents on the chain. Cationic dyes display solvent effects in nucleophilic solvents, but the spectral shifts of the λ_{max} values is generally low for symmetric dyes. For asymmetrical dyes in which two different chromophores are present, their maxima are generally displaced to shorter wavelengths compared to the average values of λ_{max} in the corresponding symmetric dyes.

The extensive conjugation in the dye molecule increases the instability which can result in photobleaching or shorten the shelf life of the label. This instability may be reduced with appropriate dye design such as phthalocyanines or incorporating the polymethine chain into a cyclic structure. The formation of an anti-aromatic ring structure through the cyclization of the polymethine chain leads to deeply colored compounds (i.e., high molar absorptivities). Yet, this structural modification results in small spectral shifts. Patonay and Strekowski's research groups synthesize heptamethine cyanine dyes. In their methodology, two heterocyclic moieties are linked by Vilsmeier-Haack reagent which includes a heptamethine chain and the rigid structure and conjugation of NIR dyes allows high quantum yield (Φ, 0.05-0.5) and absorptivity (ε, 150 000-250 000) and thus facilitating low detection limits.[12] **Figure 2.3** shows the general structures of some indolium substituted heptamethine cyanine dyes. In general,

squarylium dyes are close in wavelength to the cationic dinuclear cyanine dyes.[1] A comparison of croconium and squarylium dyes shows the former to be more bathochromic. Moreover, a considerable bathochromic shift has also been observed if the O^- is replaced by OMe.

Polymethine cyanines are weakly fluorescent owing to its conformational flexibility. In general, the fluorescence quantum yield of cyanine dyes passes through a maximum value with extension of the polymethine bridge. The fluorescence efficiency of some NIR polymethines is enhanced upon immobilization in complexes with biomolecules.

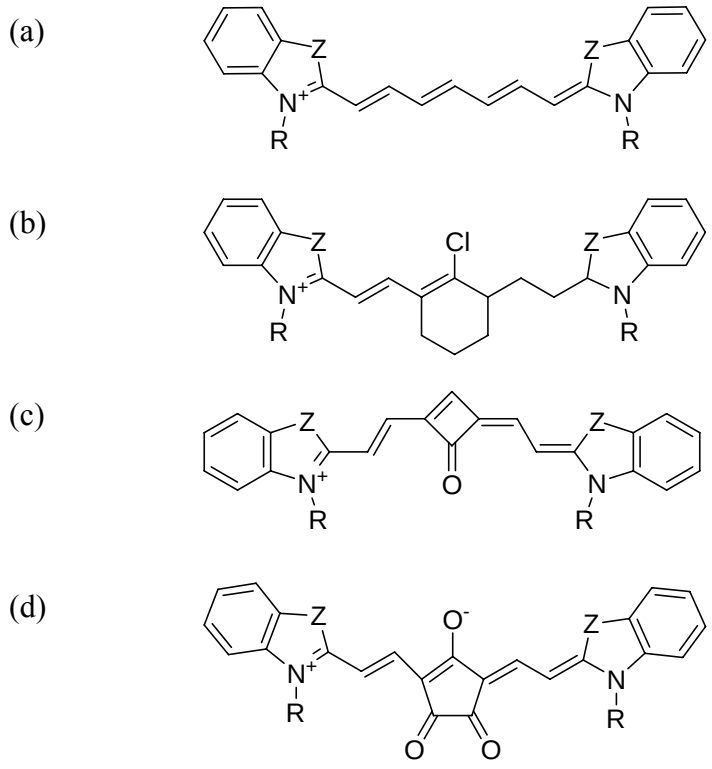

Figure 2.3. General structures of indolium substituted (a) indolenine heptamethine cyanine dye and indolium substituted (b) tricarbocyanine, (c) squarylium, and (d) croconium heptamethine cyanine dyes.

Frontiers in Heptamethine Cyanine Dye Synthesis

The synthesis of sterically rigidized polymethine dyes containing rings within the polymethine backbone typically start with alicyclic ketones, ketals, enamines, or enol ethers.[13] These compounds possess two activated methine or methylene groups, which readily react with Vilsmeier's reagent to form the initial cyanine whose polymethine chain can then be lengthened by nucleophilic reaction with other heterocyclic methylene bases leading to tricarbocyanines similar to the one pictured in **Figure 2.3**. This synthetic pathway is used extensively by both the Patonay[14] and Strekowski[9, 15] groups. Many of the dyes synthesized and characterized by the Patonay and Strekowski groups contain chlorine atoms at the meso position of the cyclic polymethine backbone which are ideal for facile displacement reactions in the presence of nucleophiles. This novel approach to the derivatization of cyanines was used for the synthesis of an isothiocyanato derivative of a tricarbocyanine heptamethine dye for covalent protein labeling schemes.[16]

Most cyanine dyes have traditionally been synthesized by a condensation reaction between a heterocyclic base containing an activated methyl group and an unsaturated bis-aldehyde or its equivalent, usually as Schiff base in the presence of a catalyst.[17] The catalyst most often used has been sodium acetate. Narayanan and Patonay reported a novel method for the uncatalyzed synthesis of heptamethine cyanine dyes. The potential of these dyes as precursors for making functionalized near-infrared biomolecular labels was also reported. The reaction involves heating a mixture of *N*-alkyl-substituted quarternary salts derived from 2,3,3-trimethylindole or 2,3,3-trimethylbenzindole and 2-chloro-1-formyl-3-(hydroxymethylene)cyclohex-1-ene to reflux in a mixture of 1-butanol and benzene as solvent. An important feature of this method is that the slower rate of the

reaction allows one to prepare asymmetric dyes derived from two different heterocycles in a single pot with fairly good yield. Thus, allowing for more uniquely tailored spectral characteristics of the NIR labels. These dyes can be readily derivatized for various covalent protein labeling and DNA sequencing applications.

Cyanine Dye Aggregation

Cyanine dyes quite readily aggregate in aqueous solution. These aggregates exhibit absorption bands quite different from the monomeric species.[10] Aggregate bands which are bathochromically shifted in relation to monomeric band are called J-aggregates, after E.E. Jelley.[18-21] Bands which are blue shifted relative to the monomeric peak are attributed to the H-aggregates. **Figure 2.4** illustrates the typical absorption spectra of H- and J-aggregates in aqueous solutions. The tendency of dye molecules to aggregate depends on the structure of the dye as well as the environment.[10] Dye aggregation is mainly promoted by hydrogen bonding and/or strong van der Waals interactions. The delocalized positive charge of the cyanine dye structure promotes strong stacking by van der Waals interactions. Flat ring moieties such as benzene rings also readily aggregate. Environmental factors of aggregation include micellar, pH, ionic strength, concentration, solvent polarity, and temperature.

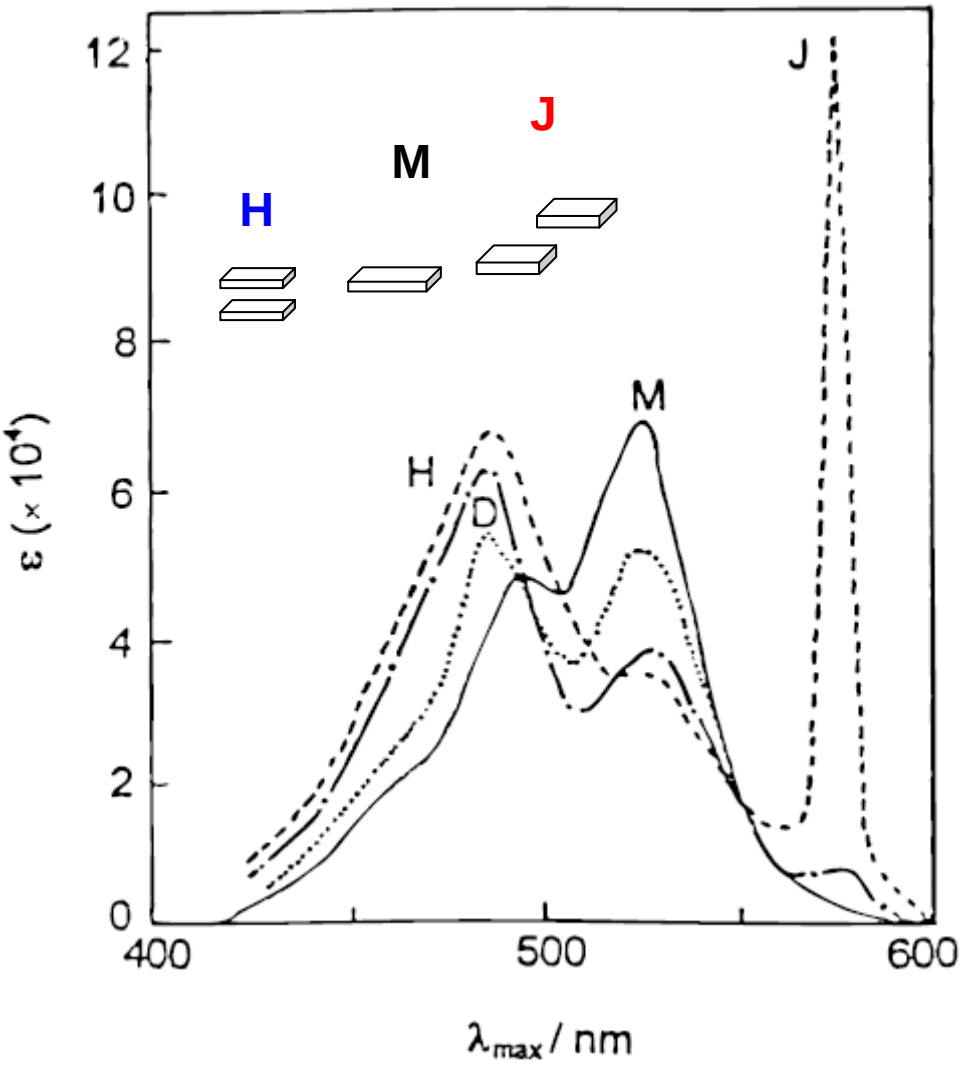

Figure 2.4. Absorption spectra of cyanine dye aggregation. Revised from reference 10.

Cyanine dye aggregation has been described by the exciton coupling model (**Figure 2.5**).[10] Both H- and J-aggregates are composed of parallel dye molecules stacked plane to plane and end to end to produce a two-dimensional dye crystal structure. According to this model, the dye molecule is described as a point dipole and the excitonic state of the dye aggregate splits into two levels through the interaction of transition dipoles. The molecules may aggregate in a parallel way (plane to plane stacking) or in a head to tail (end to end) arrangement to form H- and J-aggregates respectively. The angle between the line of centers of a column of dye molecules and the long axis of any one of the parallel molecules is called the angle of slippage, α. The bathochromic shift exhibited by J-aggregates is the result of a large molecular slippage ($\alpha < \sim 32°$). Likewise, the small slippage angle ($\alpha > \sim 32°$) results in the hypsochromic shift of H-aggregates.

H-aggregates are described to be in a brickwork formation, whereas J-aggregates are believed to be more of a staircase conformation. In the brickwork formation, dipoles are completely coupled and are promoted to higher energy excited states (shorter wavelengths). Yet, in the staircase conformation, J-aggregate dipoles are only partially coupled and are only excited to the lowest energy excited states (longer wavelengths). Only J-aggregates are capable of producing fluorescence with a large quantum yield.[22] Since fluorescence only occurs from the lowest energy excited state (Kasha's rule), only J-aggregates will fluoresce. H-aggregates typically posses low molar extinction coefficients and quantum yields compared to their monomeric absorption bands.[14, 23, 24]

H-aggregation is mainly encountered in bioorganic systems, whereas J-aggregation is generally applied in to photographic light harvesting, optical recording media, and laser technology. The orientation of dye molecules related to the angle of slippage is depicted in **Figure 2.6**.

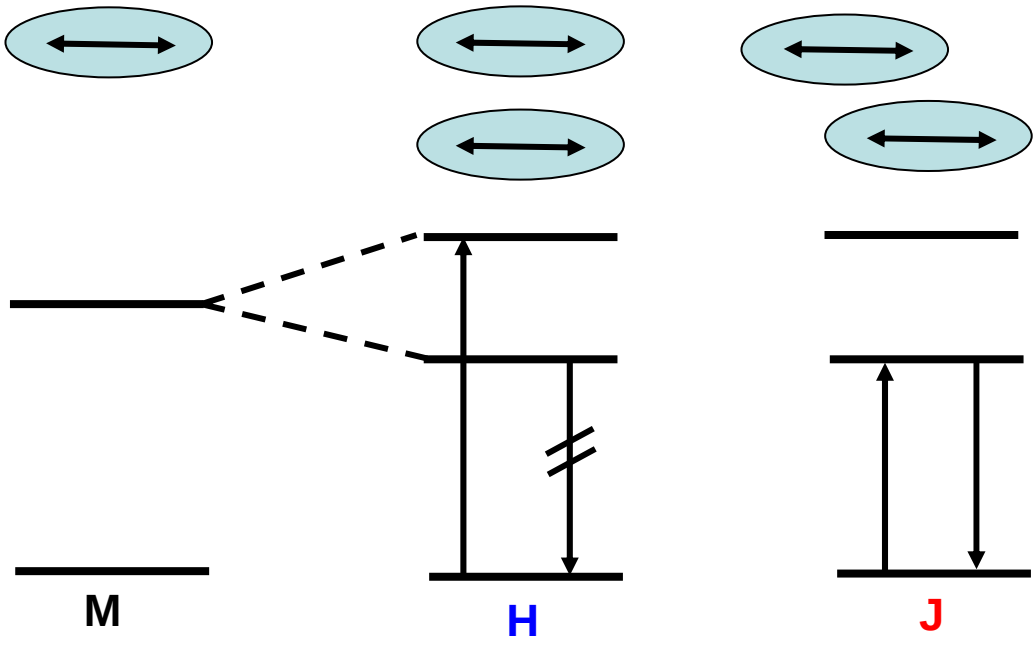

Figure 2.5. Exciton coupling model of carbocyanine aggregation. After reference 10.

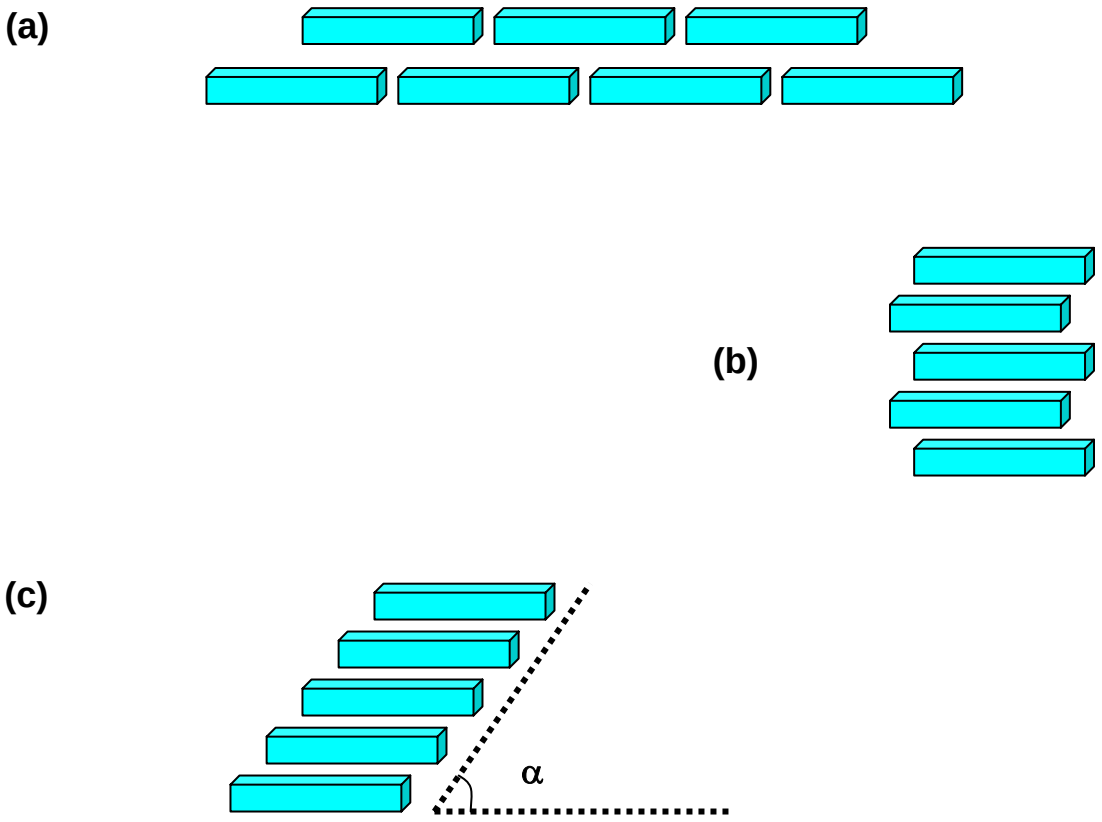

Figure 2.6. Representative models of cyanine dye aggregates in solution: dye aggregates with brickwork (a); ladder (b); and staircase (c) molecular arrays; α is the angle of slippage. After reference 10.

Understanding Protein-Ligand Interactions Through Dye Aggregation Spectra

The propensity of cyanines to aggregate in aqueous solution can be quite useful for noncovalent protein labeling studies. Important information about protein binding sites can be derived from the spectral changes observed when the polarity of a probe's microenvironment is altered. For instance, when cyanines form H-aggregates in aqueous solution, no or minimal fluorescence is observed. Yet, when dye is bound inside hydrophobic binding sites, the H-aggregates are dissipated and monomeric fluorescence is observed. This phenomenon is often referred to "cut-on fluorescence" and is often exploited in noncovalent labeling studies. Cut-on fluorescence will be discussed in further detail in the section to follow. Cut-on fluorescence was also detected for one of the bis-cyanine dyes introduced in Chapter 3 as well.

A portion of the work presented in this dissertation involves evaluating near infrared probes for the detection of protein secondary structures in proteins and polypeptides (Chapter 4). Amino acids in proteins and polypeptides orient themselves into ordered repeating units stabilized by hydrogen bonds between amide and carboxyl groups of the protein backbone. Similarly, cyanine dye aggregates also form ordered, repeating structures which are stabilized by noncovalent interactions. Dye aggregates can sometimes utilize the ordered structures of proteins and polypeptides to form a scaffold through which supramolecular structures are formed. And depending of the orientation of the self-associated chromophores, these superstructures may chiral in nature, exhibiting CD within the absorption bands of the dye aggregates. For this reason,

cyanine dye aggregates are quite ideal for the application of protein secondary structure sensors. The spectroscopic properties of cyanine aggregates templated by proteins and polypeptides are described in further detail in the sections to follow.

Intramolecular H-aggregation. The nature of dye aggregation is also quite dependent upon its interaction with a protein binding site. Jun et al. reported that bis-heptamethine cyanine (BHmC) dyes are comparable to its monomeric counterpart (RK780) in CE-LIF analysis.[14] The monomeric dye, RK780, exhibits a noisy chromatogram due to electrostatic interactions with the charged capillary wall. However, the BHmCs reduces the noises and increases the LOD which is attributed to the strong internal π-π interactions of the two monomeric chromophores.[14, 25] The intramolecular-H-type dimerization causes a reduction in spectrum response even though there may be an interaction between positive dye and negative capillary wall. The addition of a protein grabs and opens the stacked internal dimer and resulting in a high fluorescence response.

Another application for H-aggregation is in measuring hydrophobicity. In this particular technique, the hydrophobicity of a dye can be applied relative to a variety of solvent systems. Therefore, a dye in highly polar solvent exhibits essentially non-fluorescence and changing relative polarity with various organic alcohols increases the quantum yield.

J-aggregates using a protein scaffold. Tatikolov and Panova [26] found that an anionic carbocyanine dye (K4) containing sulfonate groups produced J-aggregates both alone in aqueous solution and in the presence of the structural proteins collagen type I and type III. In aqueous solution, K4 exists primarily in the dimeric state with a λ_{max} =

535 nm and the monomeric shoulder λ_{max} ~ 570 nm. And at higher concentrations (~10^{-4} mol L^{-1}), J-aggregates appear at λ_{max} = 657-660 nm. Tatikolov and Panova report the stimulation of J-aggregate formation when collagen is added to dilute solutions of K4 whereby aggregates were previously absent. The initial λmax of the absorption spectrum (535 nm) drops at the expense of a growing J-aggregate band between 642 and 648 nm for both collagen types. The J-aggregates detected in the presence of collagens have different spectral characteristics compared to those observed for K4 alone aqueous solution and in the presence of other additives such as gelatin; the J-aggregates formed by using collagen as a template were considered broader and at shorter wavelengths. Yet as with most J-aggregates, fluorescence emission was detected for J-aggregates formed by collagen. In addition, fluorescence excitation corresponded to the absorption spectrum observed for the aggregates. Tatikolov and Panova consider the broader bands of the collagen J-aggregates to be indicative of less homogenous binding sites present on collagen compared to gelatin. Furthermore, J-aggregates formed by different collagen also appeared different from one another in λmax, bandwidth, and molar absorptivity. The unique characteristics observed by K4 in the presence of different collagens make it a useful probe for the application of determining the presence and type of collagens present in a biochemical system.[26, 27]

Chiral J-aggregates using a HSA scaffold. The propensity of cyanine dyes to form aggregates in polar solution has been extensively reported.[28-31] The types of aggregate states formed is dependent upon several factors such as dye structure, concentration solvent polarity, pH, ionic strength, and temperature.[32] The phenomenon of achiral cyanine dyes spontaneously forming chiral J-aggregates has gained much

attention in recent years for its potential to increase spectral sensitivity of photographic emulsions.[33-37] The formation of J-aggregates has recently extended to using biomolecules such as proteins.[8, 26, 38] and DNA[39, 40] as templates for aggregate formation. For instance, Zhang and co-workers formed chiral J-aggregates using the achiral cyanine dye PTC {3,3'-di(3-sulfopropyl)-4,5,4',5'-dibenzo-9-phenyl-thiacarbocyanine triethylammonium salt] templated by HSA. The research group used a phosphate buffered saline (PBS) solution to form J-aggregates (λ_{max} = 686 nm) which were red-shifted and significantly narrowed compared to the monomeric band. Upon the addition of HSA, a gradual decrease of the absorbance of the aggregate band accompanied the appearance of a new peak at 615 nm, the monomeric band for PTC. Thus, HSA effects the J-aggregates formed in PBS solution. This can be explained by the stronger interactions of hydrophobic and electrostatic interactions between the HSA and PTC as compared to the weaker van der Waals forces involved in PTC self-association.

No CD signal was detected for J-aggregates alone in PBS. However, when HSA was bound to PTC, a bisignate CD was observed. A positive band at longer wavelengths (694 nm) and a negative band at shorter wavelengths (676 nm) are indicative of positive chirality within J-aggregate absorption bands (686 nm). No CD was detected corresponding with monomeric dye molecules bound to HSA. Zhang and coworkers propose that the induced CD observed was brought about by the conformational changes due to local distortion when HSA and PTC aggregates, which are both oppositely charged and hydrophobic in nature, interact with each. Furthermore, as the concentration of HSA increases, a CD signal reversion from positive to negative chirality is observed.

This reversion in chirality was presumed to be related to preferential binding between different protein secondary structures. HSA predominantly consists of both α-helix and randomly coiled structures. To test this assumption, the polypeptide poly-L-glutamate (PLG) was used. At pH 4.5 and above pH 8, PLG adopts the α-helix and randomly coiled conformations respectively. Apart from a slight decrease in the maximum absorbance of J-aggregates bound to PLG, increasing the pH from 1.42 to 9.00 had little effect on the overall appearance of the absorbance spectrum. However, α-helix PLG induced a positive CD signal for PTC aggregates. In addition, at pH 8 randomly coiled PLG showed a lower negative CD signal. The lower CD signal was attributed to the fact that as HSA concentration increases, the J-aggregates begin to dissociate and monomer PTC molecules are predominantly present.

At low HSA to PTC ratios (aggregates in excess), Zhang and co-workers consider dye aggregates bind to both α-helix and randomly coiled structures. But because α-helix structures are the predominant secondary structures in HSA, only positive chirality is observed. However, when HSA is in excess of PTC aggregates (high HSA concentrations) the aggregates appear to bind preferentially to randomly coiled structures. Zhang and coworkers believe this may be due to higher repulsive forces between the neighboring molecules when J-aggregates are bound to α-helix structures, leading to lower stability of these bound J-aggregates. Thus, as the HSA concentration increases, only the aggregates bound to randomly coiled structures remain intact and visible by CD. This conclusion was confirmed by titrating J-aggregates with more PTC. As predicted, as the concentration of PTC increased at constant HSA concentration, the CD signal passed from a negative to a positive CD signal.

In addition, the reversion of chirality is also observed by varying the solution pH. Under acidic and basic conditions, the J-aggregates exhibit negative chirality, while positive chirality is observed under neutral conditions. These observations were attributed to the conformation changes of HSA at different pH values as well. This idea was confirmed by determining the % α-helix content of HSA at various concentrations using far UV CD. At pH 7 to 8, HSA adopts a predominantly alpha-helical structure, thus the CD of signal of J aggregates show a positive CD band under similar conditions. Furthermore, the presence of J-aggregate and monomer HSA bound dye is also dependent on pH. At neutral and weakly basic pH values, most of the J-aggregates dissociate to for monomers. Therefore, spectral changes can be explained by changes in the conformation of HSA at different pH values. Thus, Zhang and coworkers were able to show the presence of chiral J aggregates formed by using protein secondary structures as scaffolds.

Protein labeling

Protein labeling with cyanine dyes is based on the relatively low fluorescence of H-aggregates in aqueous solution. The fluorescence intensity of the dye is typically enhanced in the presence of proteins as dye interaction with large biomolecules disrupts the aggregates. The most advantageous feature of these noncovalent interactions is that enhancement of the probes quantum yield, facilitating detection of biomolecules. However, qualitative and quantitative studies of proteins are not the only useful applications of protein labeling. Understanding the noncovalent binding mechanisms biomolecules is invaluable to protein structure-function work in which protein-dye interactions can be correlated to protein drug interactions. Yet, there is a great deal of

difficulty in studying the physical parameters of noncovalent interactions. Spectroscopic studies of noncovalent protein labeling further the understanding of protein-ligand interactions. Binding parameters such as the binding constant and stoichiometry of protein-dye complexes can be derived simply by measuring the emission of bound dye relative to free dye. This very important application of protein labeling was utilized and discussed in detail for the bis-cyanine-HSA studies presented in Chapter 3. Protein labeling and the various advantages and disadvantages of both covalent and noncovalent labeling are discussed in the sections to follow.

Protein characterization methods can be categorized as either qualitative or quantitative analysis. Mass spectroscopy (MS), nuclear magnetic resonance (NMR) and X-ray crystallography are the techniques commonly employed for qualitative studies.[41-47] While these techniques are quite accurate, as with many complicated techniques, expensive instrumentation and laborious sample preparations are often required. In quantitative protein studies, sensitivity is often an issue, particularly in determining the protein primary structure. And for those detection methods that utilize intrinsic protein properties such as tryptophan fluorescence, sample size may also be an inhibiting factor. Hence, there has been a need for an alternative way to identify and quantify proteins that is simple and efficient as well as sensitive. Protein labeling techniques have been most advantageous in this way. And a wide variety of dyes have been intensively researched for labeling techonology.[9, 48-50]

Labeling or probe technology involves the attachment of a chromophore to a biomolecule either covalently or noncovalently. Labeling allows for much higher sensitivity and better detection limits because the detection of the extrinsic chromophore

has a much higher molar absorptivity than the protein's intrinsic chromophore. As previously mentioned, greater sensitivity is also achieved when studies are performed in the more advantageous NIR region of the electromagnetic spectrum. For both qualitative and quantitative analysis either covalent labeling or noncovalent labeling techniques can be employed.[9, 14, 49-51]

Covalent labeling. Many near-infrared dyes containing reactive groups are commercially; yet, the majority of covalent labels are synthesized for specific biological applications. Reactive moieties on the protein (e.g. primary amines and side chain functional groups) are targeted by dyes for conjugation.[52] Reactive amino acid functional groups such as amines, thiols, phenols, and carboxylic acids are targeted by dyes for covalent substitution. Dye functional groups such as isothiocyanates (SCN) and N-hydroxysuccinimidyl (NHS) esters, aldehydes, and sulfonyl halides are often used to target either lysine or α-amines. In addition, dyes derivatized with iodoacetamides and maleimides have been synthesized to react with protein thiols. Whereas, hydrazide or amine groups on dyes have been used for carboxylic acid side chain substitution. **Figure 2.7** shows the reactive pathways of some common labeling reagents.

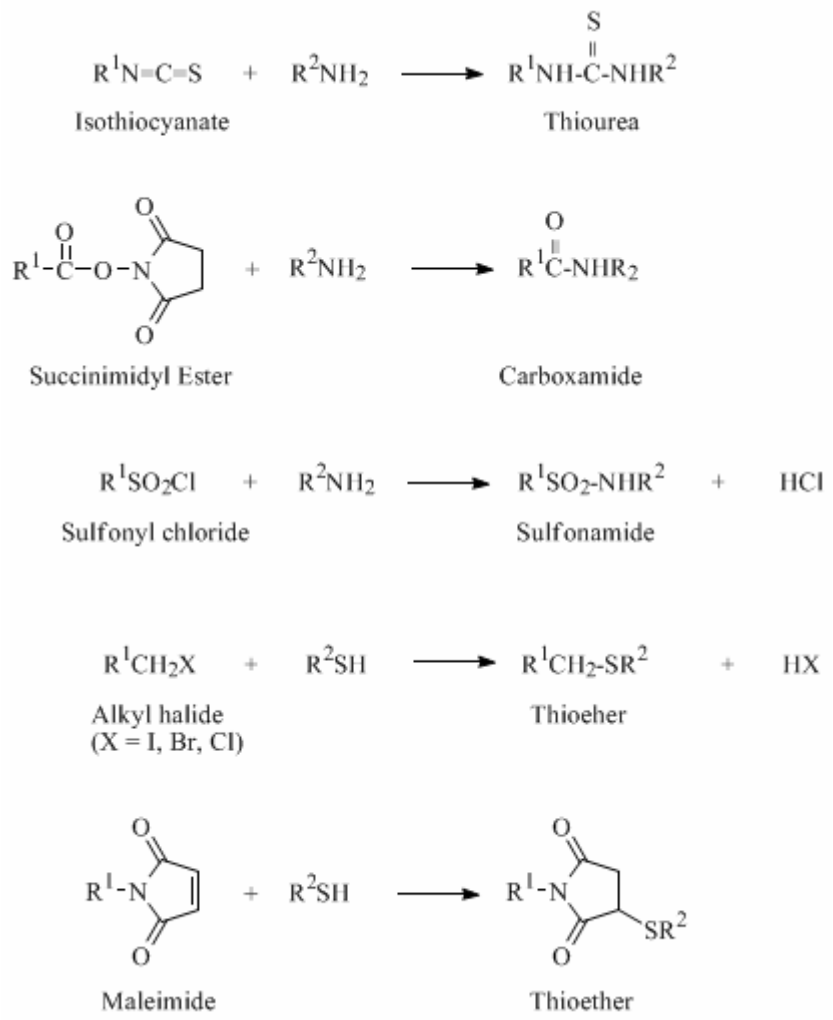

Figure 2.7. Covalent labeling schemes of amine and thiol groups of proteins and peptides.

In choosing a dye for a particular application, the stability of the covalent bond must also be considered. Certain chemical reactions are only achievable depending upon the location and quantity of reactive amino acid functional groups. Steric hindrance and hydrophobicity make some locations of the protein undesirable. Thus, labeling efficiency is often affected by dye specificity. For instance, Ernst and coworkers report needing at least four reactive sites per antibody molecule in order for a covalently attached cyanine dye to produce significant fluorescence signal for analysis.[53] Yet labeling efficiency is rarely an issue if the appropriate amino acids are targeted. Amino acid side chains susceptible to nucleophilic attack are abundant in most proteins. Because of their hydrophilic nature, amino acids such as lysine are typically found on the surface of globular proteins. Thus, dyes with functional specific for amines are often used in covalent labeling assays. Reactions involving lysine occur easily and cleanly with a variety of commercially available reagents. In addition, α- and ε-amine groups are readily distinguished by exploiting the differences in pKa.

There are quite a few advantages of covalent labeling over noncovalent methods. Covalently labeled complexes are much more stable and the opportunity for nonspecific interactions is greatly minimized. And fluorescent covalent labels in particular, exhibit good photostability, water solubility, and favorable photophysical properties. Due to the specificity which can be achieved with covalent labeling, it is often the labeling method of choice in quantitative analysis. In quantitative analysis studies, the specific dye attached to the protein can provide the number of reactive sites or at least the degree of

substitution (DOS).[54] This particular feature of covalent labeling is useful in determining the number of functional groups (e.g., amines) present on a protein of interest. Other advantages and applications of covalent labeling will be discussed in further detail later.

Noncovalent labeling. Some of the drawbacks of covalent labeling are either eliminated or minimized in noncovalent labeling techniques. Covalent labeling schemes can be quite time consuming and require laborious purification steps. Oftentimes, covalent labeling reactions also require harsh, sometimes denaturant, conditions such has elevated pH.[52] In addition, Craig and Dovichi [55] reported band broadening in chromatographic applications as a result of analyte:dye heterogeneity. Alternately, noncovalent labeling is fast with little or no pH dependence. Also, noncovalent labels affect the functional activity of labeled protein to a lesser extent than covalent labels.[56]

Covalent probes simply substitute a specific functional group of an amino acid with a dye's reactive moiety. In contrast, noncovalent labels are affected by a series of neighboring subunits in the protein binding site. Thus, before any binding studies are performed, one needs to consider the protein-dye binding equilibria (i.e., stoichiometry, association constants and cooperativity). Both homogenous and heterogeneous ligand binding can be affected by cooperative binding effects.[57] Therefore, cooperativity must be investigated if more than 1:1 stoichiometry is determined. And although noncovalent labeling minimizes this concern, the affects of ligand binding on structure and function must also be closely monitored. Experimentally, circular dichroism (CD) and X-ray crystallography are commonly used for this purpose.[57-59] In the sections that follow, the methods for the determination of stoichiometry and binding equilibria will be discussed further.

When used in conjunction with capillary electrophoresis-laser induced fluorescence (CE-LIF) increased LOD is also another important advantage of noncovalent labeling over covalent labeling schemes as well. Benito et al. studied the noncovalent labeling of N-arylaminonaphthalene sulfonates, bis-ANS and 2,6-TNS, with whey proteins.[60] By using CE-LIF, the LOD was increased twice that of UV detection measurements. In addition, Colyer and coworkers has also studied noncovalent labeling using capillary electrophoresis with laser-induced fluorescence detection (CE-LIF) extensively.[49, 61, 62] Using symmetric NN127, asymmetric SQ-3 and indocyanine green (ICG) protein were covalently labeled. These dyes exhibit negligible fluorescence in aqueous solution and enhanced fluorescence upon binding to proteins. Using the aforementioned dyes, Colyer and co-workers successfully separated human serum albumin (HSA), bovine serum albumin (BSA), β-lactoglobulin A, and trypsinogen. In addition, symmetric dyes also strongly interact with HSA.[49, 62, 63] A covalently labeled NN382 shows attomole-range detection limit and noncovalently labeled RK780 provides femtomole-range detection limit.[12, 25]

Applications of NIR Carbocyanine Dyes

Carbocyanines are so ideal for the study of biomolecules because their binding properties can be uniquely tailored for specific binding sites and their spectral properties are readily manipulated through structural changes. Fluorescent NIR dyes, in particular, have been used more and more in protein assays as an alternative to the hazardous radioactive labels used historically. Many researchers have utilized these NIR dyes with strong binding specificity for biomolecules as valuable tools for investigating the structure and function of proteins. In this section we will review some of the countless techniques which use NIR carbocyanine dyes to study proteins through both covalent and noncovalent labeling methods. NIR dyes have been studied over a vast range of disciplines using a wide variety of instrumental methods. Because of the numerous advantages of noncovalent over covalent labeling methods, covalent labeling techniques are used a lot less often in chromatographic analysis. Moreover, since a large number of medicines bind to proteins noncovalently in the human body, noncovalent labeling is particularly useful in the pharmaceutical industry for the purpose of understanding protein-ligand binding interactions. The information gained in noncovalently labeled spectroscopy will also be discussed in the sections to follow. Yet, NIR dye conjugation still plays a vital role in the optical imaging and immunoassay techniques.

John et al. has also recently reported on the potential medical applications of NIR dyes.[64] In this study, the invisible NIR light and lowered photon absorption and light scattering allowed the light source to penetrate deeper tissue than other non-NIR probes. Near-infrared fluorescence techniques utilize relatively inexpensive instrumentation, improved resolution, and high sensitivity for fluorescence imaging in mammalian tissues

at centimeter depths.[65, 66] However, there are some requirements for using NIR probes in medical applications. For covalent labeling, these probes should be highly water soluble so that they exhibit high absorptivity and quantum yield. In addition, photobleaching and dye aggregation may case problems experimentally. And, naturally, these probes must be nontoxic. Yet, until recently, the only NIR probe approved by FDA was indocyanine green (ICG) due to the aforementioned issues.[67, 68] Generally, low absorptivity, low quantum yield and dye aggregation are caused by the long polymethine chain that shifts carbocyanine dyes to NIR absorption. However, these limitations have recently been overcome by designing the appropriate substituents.

Contrast Agents for Optical Imaging. The differentiation and characterization of biological tissues with light from the near-infrared region have recently led to the development of a wide range of contrast agents for use in biomedical imaging.[69-77] Particularly in the field of mammography, NIR optical imaging techniques could overcome the limitations of conventional X-ray mammography, such as breast tissue density, or patients with scars or implants.[70] Optical imaging in the near infrared region using the intrinsic absorption of tissue is limited by light scattering, particularly in differentiation between benign and malignant tissue. Indocyanine green (ICG; cardiogreen) has already been utilized extensively in other medical applications such as angiography, as just one of many examples. The chemical structure of ICG is illustrated in **Figure 2.8**. The inherent hydrophilic nature of cyanine dyes makes their use in biological applications particularly advantageous. Yet, stability and fluorescence efficiency issues in aqueous media, as well as strong plasma protein binding interactions,

have created a great deal of interest in the development of NIR cyanines with more uniquely tailored characteristics allowing for better stability, quantum yield and specificity to tumor cells.

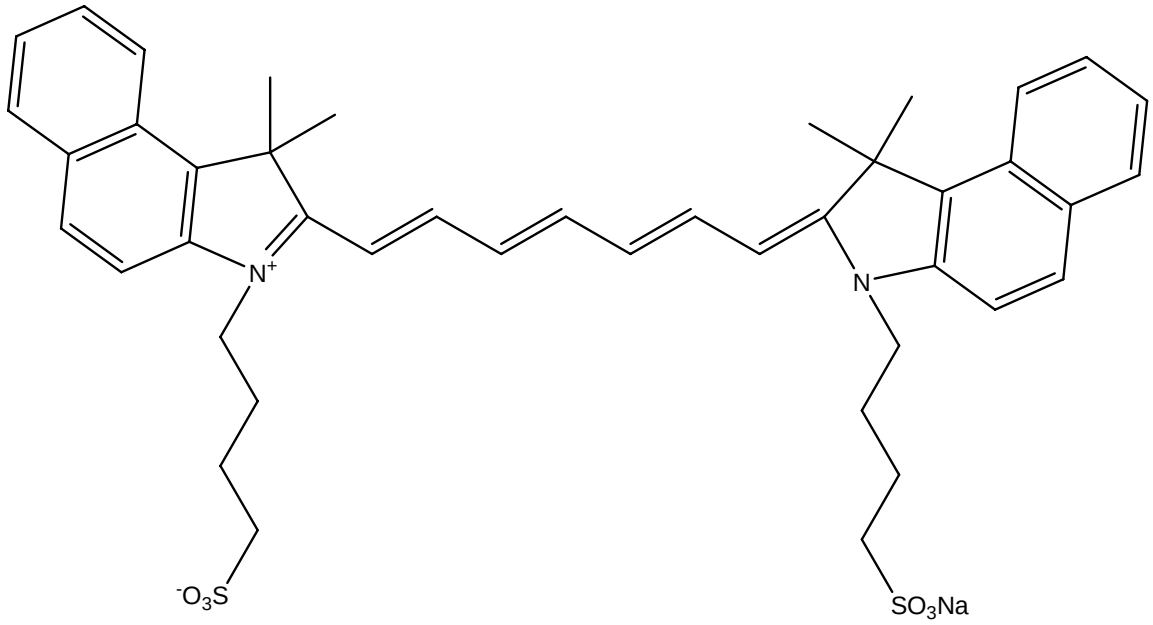

Figure 2.8. Chemical structure of Indocyanine Green (ICG).

The conjugates of macromolecular carriers bound to NIR carbocyanine dyes are now commercially available which may provide a new class of contrast agents for optical imaging. Becker et al. examined the utility of using an indotricarbocyanine (ITCC) dye derivative similar to ICG conjugated to the carrier proteins HSA and transferrin.[77] The serum proteins transferring and HSA are commonly used as macromolecular carriers for targeting tumors with anticancer drugs, photosensitizers and contrast-enhancing materials. The ITCC labeled proteins were evaluated for their binding ability to tumor cells and also tested *in vivo* for their potential as contrast agents in tumors. Receptor mediated-uptake by human colon cancer cells was observed *in vitro* with transferrin-labeled ITCC, but not with HSA conjugates. Yet in mice models, both ITCC-labeled proteins exhibited increased fluorescence contrast of tumors *in vivo*. After 24 hours, the transferrin-labeled ITCC exhibited higher contrast between malignant and benign tissue. Overall, Becker and co-workers reported that ITCC-labeled proteins had utility as macromolecular contrast agents for optical imaging of tumors, with transferrin-ITCC conjugates displaying higher quantum efficiency.

Somatostatin, an inhibitory hormone secreted from various parts of the digestive system, is the subject of countless pharmacological research.[78] Octreotide a synthetic octapeptide which mimics somatostatin pharmacologically. Licha and co-workers have reported the synthesis and characterization of covalently labeled ITCC-octapeptides targeted to somatostatin cell receptors.[71] This work demonstrated that NIR dyes can be conjugated to site specific peptides to enhance the specificity of fluorescent contrast agents *in vivo*. The contrast potential of these NIR dye-labeled peptides is quite impressive. Becker et al report that tumor fluorescence rapidly increases and is more

than three-fold higher than normal tissue from 3 to 24 hours after application.[76] Tumor imaging using cyanine dye-peptide conjugates, such as those reported in the aforementioned studies, can be applied to the detection of superficial lesions, especially with endoscopic techniques.

Frangioni's research group has studied intraoperative NIR fluorescence imaging systems for small animal surgery. In this study, HSA was covalently labeled with IRDye78 (HSA-78) as a fluorescent lymph tracer.[65, 79] This tracer is adequate for use in the intraoperative NIR fluorescence imaging study since it is non-toxic and the excitation light source is safe for animals. Furthermore, the tracer exhibits clearly resolved images.

Intraoperative NIR fluorescence imaging has been used for real-time image guidance during surgical procedures in cancer patients.[80] Molecules with a hydrodynamic diameter less than approximately 10 nm have the potential to travel beyond the sentinel lymph node, molecules with a 50-100 nm hydrodynamic diameter require up to 3 hours to label the lymph node, and very large molecules (>200 nm) require up to 24 hours to achieve lymph node labeling. Due to the potential toxicity of QDs, Onishi and co-workers compared the utility of NIR probes with that of quantum dots (QDs) for use in lymph node mapping procedures. Organic heptamethine cyanine dyes are typically small in size (HD; ~7 nm for both covalently and noncovalently dye-HSA labels) and are non-toxic. Covalently labeled HSA (HSA800) showed a much higher quantum yield *in vivo* than noncovalently labeled indocyanine green (ICG). Thus, HSA800 was reported to be quite useful for in lymph node mapping techniques.

Licha and co-workers synthesized a new group of glucamine and glucosamine-substituted ICG derivatives for tumor imaging applications.[70] These dyes boasted increased hydrophilicity and less plasma protein binding (<50%), than the ICG analogue. The dyes also, exhibited a 7-15% increase in fluorescence yield in a physiological environment over ICG. The most hydrophilic derivative in the study (SIDAG) showed enhanced tissue-efflux half-life, a two-fold higher initial tissue absorption coefficient over ICG, and an increased tumor-to-tissue concentration gradient after injection. Therefore, contrast agents suitable for optical tumor imaging can be designed by simply increasing the hydrophilicity of NIR carbocyanines. Ebert et al. reported that SIDAG was enriched in a mammary tumor of a rat model up to a ratio of 6:1 and no significant fluorescence originated from the surrounding tissue.[75] In addition, improved contrast was obtained by calculating the ratio of fluorescence and transmittance images, with transmittance taken at the wavelength of the laser excitation source.

The potential use of NIR cyanine dye-poly(ethylene glycol) conjugates as optical imaging contrast agents has also been investigated.[69, 72] It has been reported that the derivatization of drugs and contrast agents with poly(ethylene glycol) (PEG) substituents have enhanced retention in tumor tissue, owing to increasing hydrophilicity. Licha and co-workers[69] investigated the differential tumor to tissue fluorescence signal contrast observed by systematically changing the molecular weight of the (PEG) residues. The general chemical structure of the PEG substituted dyes is show in **Figure 2.9**. The group's overall objective was to increase the plasma half-life of the NIR dyes. This would in turn adjust the time window of fluorescence imaging to earlier time points after intravenous injection by attaching fluorophores to defined macromolecules of different

molecular weights. Using a PEG backbone is particularly advantageous for this purpose since low *in vivo* toxicity and defined binding sites have already been reported. The molecular weights for the cyanine dye-PEG conjugates used in the study ranged from 2000 to 40000 g/mol. However, it was determined that the molecular weight modification of the PEG residues had no influence on the photophysical properties (i.e., absorption and fluorescence maxima, molar extinction coefficient, and quantum yield in physiological media and bovine plasma).

The pharmacokinetic properties of the PEG-conjugated dyes were investigated by Riefke et al.[72] The group reported that the pharmacokinetic properties of the dye conjugates were readily controlled by the varying the PEG chain length. Specifically, the plasma half-life of the dyes increased with increasing molecular weight and the distribution volume, the distribution of a sample throughout the body after dosing, decreased. Increased retention in tumor environment and improved tumor contrast is observed at later times for dye conjugates over 6000 g/mol molecular weight. This work the useful application of NIR carbocyanine-PEG conjugates as contrast agents for tumor imaging.

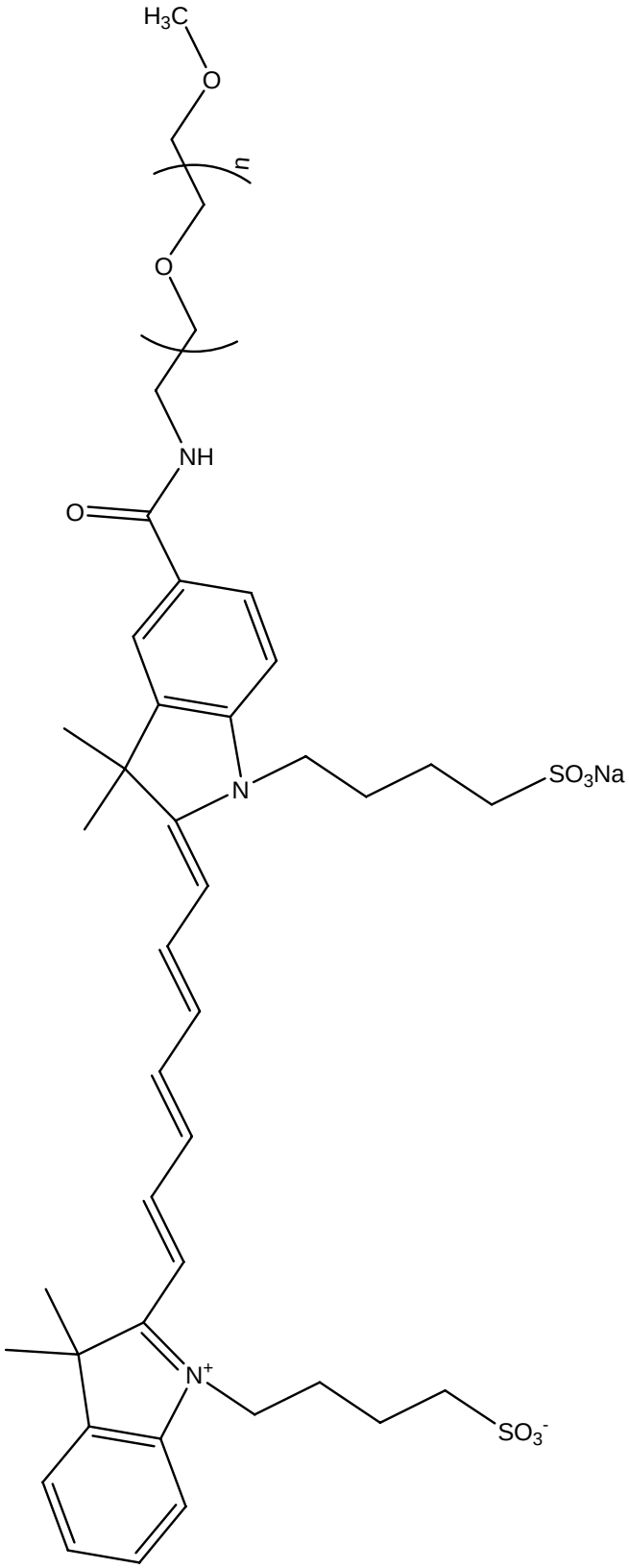

Figure 2.9. General chemistry structure of a NIR PEG substituted dye.

The commercially available lipophilic dye 1,1'-dioctadecyl-3,3,3',3'-tetramethylindocarbocyanine perchlorate (DiI) has been used extensively in optical imaging research.[81-83] The chemical structure of DiI is listed in **Figure 2.10**. DiI was initially introduced as a neuroanatomical tracer for labeling neurons in living tissue and later applied to aldehyde fixed tissue. The hydrophilic head of the label lies above the plasma membrane and two lipophilic hydrocarbon side chains insert into the hydrophobic plasma membrane. As a neuronal tracer, the dye diffuses along the lipid bilayer of membranes and sometimes moves transcellularly. Bruce et al used this property to identify the first contacts between a growing axon and its targets by the appearance of transneuronally labeled target cells.

Noninvasive *in vivo* imaging of targeted cells is a promising field for studying cell behavior and movement in animal models.[84] The iodide derivative, DiR, has been used to safely and directly label the membranes of human leukemic cell lines as well as primary murine lymphocytes and erythrocytes. DiR has absorption and fluorescence maxima at 750 and 782 nm, respectively. Kalchenko and co-workers used a charge-coupled device (CCD)-based imager for noninvasive whole-body imaging of DiR-labeled cell homing in intact animals. The resolving power of the imager coupled with the lipophilic NIR dye demonstrated the potential application of visualizing any cell type without use of specific antibodies conjugated with fluorescent tags or loading cells with transporter-delivered NIR fluorophores.

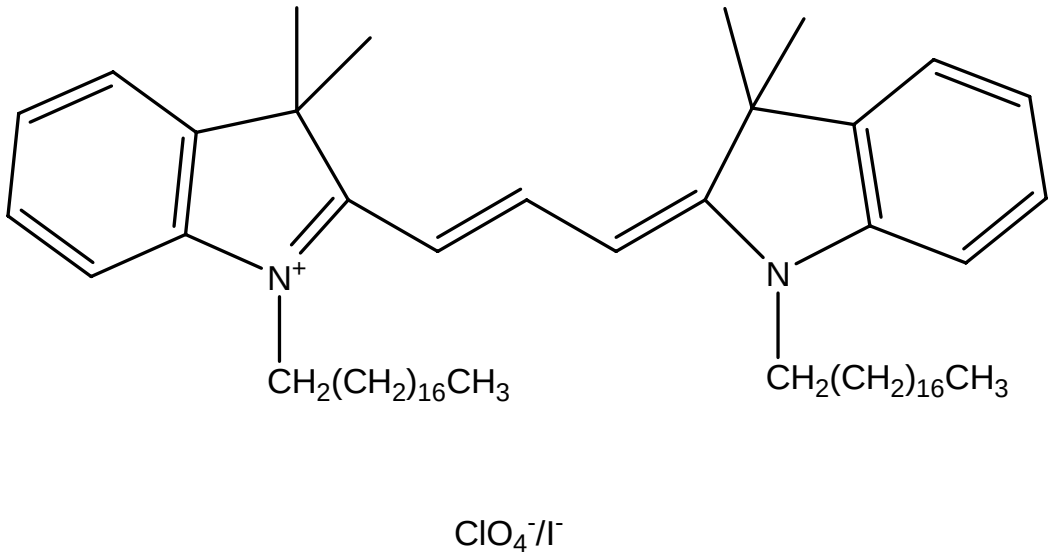

Figure 2.10. Chemical structure DiI.

Immunoassays. The most attractive feature of covalent labeling is that very low limits of detection (LOD) can be achieved by CE with laser-induced fluorescence (LIF) detection.[12] Less than attomole range can be achieved when NIR dyes are used with this technique. In conjunction with immunoassays, CE-LIF is particularly beneficial.[85] An antibody labeled with NIR dye reduces the LOD for an antigen. The role of antibodies is important in that the antibody has a specific binding site and this specificity allows for only a particular antigen. The combination of the selectivity of immunoassays with the sensitivity of NIR detection, makes combining the two techniques quite desirable for protein analysis.[85] Note that the relationship of antibody and antigen is a type of ligand-receptor relationship; thus, it is another type of noncovalent interaction. Furthermore, the use of immunoassays in CE analysis is a type of affinity capillary electrophoresis (ACE), since the mobility of unbound fluorescence tagged antibody is quite different than that of the antigen-bound covalently labeled antibody.[86]

Patonay investigated the detection of biomolecules with a fluorescent fiber-optic immunosensor (FFOI).[87] In this analysis, anti-IgG was immobilized on the tip of FFOI so that the antigen-antibody complex was formed. Then, NIR dye-labeled secondary antibody was introduced to generate a fluorescence signal. This type of immunoassay is called a sandwich assay.

Qualitative Analysis of Protein Binding Sites. Much information about protein binding sites can be derived by introducing a NIR label through noncovalent interactions. The binding site microenvironments of several mammalian and egg albumins was investigated by Andrews-Wilberforce et al [88] using both dicarbocyanine and

tricarbocyanine dyes from the thia- and oxa- classes. Upon complexation with HSA, only the thiatricarbocyanine dye, 3,3'-diethylthiadicarbocyanine iodide (DTTCI), exhibited a meaningful spectral variation, thus indicating a change in the probe's electronic transition. Andrews-Wilberforce reports that a 5:1 binding ratio of the dye with HSA. In order for perturbations in the electronic transitions to occur, the dye must be located in a binding site where strong specific interactions are possible between the NIR dye and HSA. When DTTCI is bound to HSA, a significant blue shift was observed (745 to 566 nm) with a concomitant decrease in absorptivity. Blue shift is typically indicative of dimer or higher order aggregate formation. This phenomenon is often observed with cyanine dyes in water. However, for dimer formation to occur, dye concentrations are typically at least 1000 times higher than those reported in this study. Andrews-Wilberforce attributed the spectral changes observed to extensive delocalization in the dye's polymethine chain limited by noncovalent interactions of the dye with HSA binding sites resulting in a shift to lower wavelengths and lower molar absorptivity. In a competitive assay with 1-propanol, DTTCI competed with the organic solvent for the same binding site, indicating the role of hydrophobic interactions. Yet only DTTCI exhibited appreciable interactions when bound to HSA. The four dyes examined by Andrews-Wilberforce only differed by polymethine chain length and heteroatoms present. Thus, interactions which are more specific than hydrophobicity must also be responsible for DTTCI-HSA binding.

Quantitative Protein Analysis. In noncovalent labeling studies, binding sites can be either directly or indirectly characterized through changes in the probe's spectrum. For example, if the composition of one of the active sites of a protein molecule is

changed by substituting an amino acid, the magnitude of the dye's association constant will also change. Spectral changes can be observed as result of changes in binding interactions and thereby further elucidating the role of specific amino acids inside specific binding sites.

The binding properties of NIR dye 1,1'-disulfobuyl-3,3,3',3'-tetramethylindotricarbocyanine (DSTCY) and serum albumins were observed using spectrophotometry by Wang and co-workers. [89] The chemical structure of DSTCY and its dicarboxylated derivative DCDSTCY are listed in **Figure 2.11**. Under acidic conditions (pH 1.7), the molar absorptivities of DSTCY bound to both bovine serum albumin (BSA) and human serum albumin (HSA) were 3.73 x 10^6 and 3.45 x 10^6 L $mol^{-1}cm^{-1}$ at 814 nm, respectively. Detection limits for DSTCY in BSA and HSA are 20 and 30 ng mL^{-1}, respectively. Because the absorption maximum is 78 nm removed from unbound absorption bands (736 nm), minimal background interference from unbound dye was observed. Interference from coexisting substances such as glucose, DNA, Cu2+, Fe2+, Mg2+, Ca2+, cetyltrimethyl-ammonium bromide (CTAB), and various amino acids was also evaluated. Except for Fe^{2+}, Cu^{2+}, phenylalanine, and cetyltrimethyl-ammonium bromide were the only coexisting substances to show assay interference. The abundance of Fe^{2+} and Cu^{2+} in body fluids is much less abundant than protein in the serum. Additionally, given that serum samples are typically diluted 500-fold in practical cases, the ion interference is considered negligible. Compared to more traditional protein assays such as Bradford, Bromocresol green, and Lowry to name a few, the DSTCY assay was longest to avoid interference from coexisting biomolecules in the matrix. When this assay was applied to human serum and urine samples, the results were

comparable to those of the biuret assay. The dicarboxylated derivative of DSTCY, 5,5'-dicarboxy-1,1'-disulfobutyl-3,3,3',3'-tetramethylindotricarbocyanine (DCDSTCY) was also used to determine total protein in serum.[90] Using the molar ratio method, the binding number for DSTCY and DCDSTCY bound to BSA was 100 and 133 respectively.[89, 90] Thus, the addition of carboxyl groups increased the binding affinity of the NIR dye to albumins.

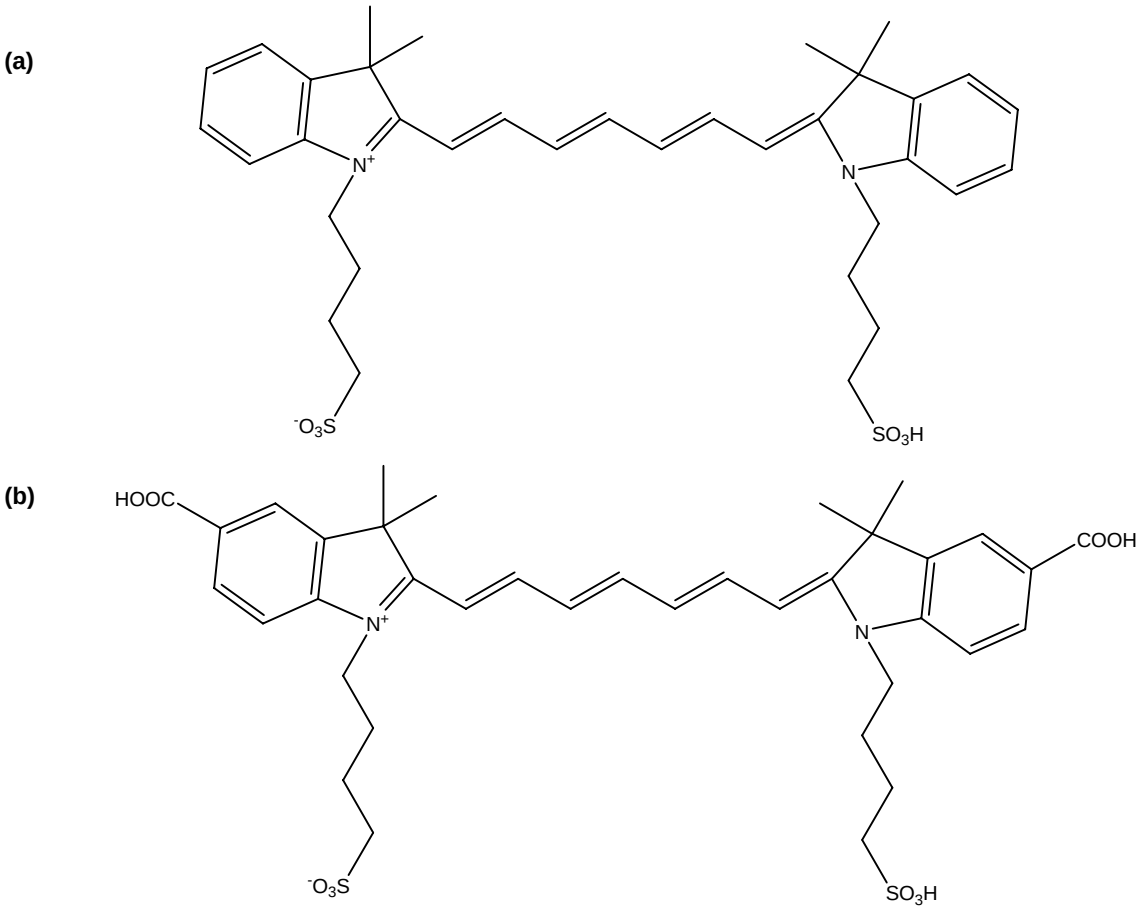

Figure 2.11. Chemical structures of (a) DTCY and (b) DCDSTCY.

Zheng and co-workers have reported using the cationic surfactant CTAB and an anionic NIR dye, the total protein in human serum has been determined by the fluorescence recovery method.[91] The fluorescence intensity of the dye is quenched to a minimum in the presence of CTAB. When protein is introduced into the system, the fluorescence of the NIR dye is recovered. The recovered fluorescence intensity is proportional to the amount of protein present in solution. When total protein concentration in human serum was evaluated using this method, values were again comparable to the values determined by the biuret method (up to 2.01% RSD).

Oswald and co-workers also determined protein concentration using fluorescence spectroscopy.[92] The group compared the fluorescent properties of squaraine carbocyanine dye Sq635-b-NHS-ester with the commonly used noncovalent protein label Cy5. Quantum yield values for Cy5 were reported to decrease considerably in the presence of protein. Sq635-b-NHS-ester exhibited a low quantum yield in water (φ = 0.15) and high quantum yields (φ = 0.6-0.7) when bound to protein. The molar absorptivities for Cy5 and Sq635-b-NHS-ester were reported to be 250000 and 140000 L mol-1 cm-1 respectively. Due to the high extinction coefficient and quantum yield of the squaraine dye, detection limits in whole blood were twice as low as Cy5.

Hydrophobicity Probe. Patonay investigated the potential of NIR dyes as hydrophobic probes.[93] The dyes used in the study exhibited significant spectral changes in the presence of solvents varying in polarity. The hydrophobicity of dye solvent is the

major determining factor in the process of dimer formation. NIR probe I displayed well separated bands of the monomeric and dimeric forms, thereby making the dye potentially useful as a probe for determining the hydrophobicity of soluble proteins.

Fluorescent probes such as 1-anilinonaphthalene-8-sulfonic acid (ANS) have previously been used to determine the hydrophobicity of BSA.[94] However, fluorescence decay times decrease as the number of ANS molecules bound increases. Thus, fluorescence techniques are considered less desirable for hydrophobicity determination studies. NIR probes are ideal for overcoming the problems inherent to fluorescence measurements. The potential of NIR probe I (**Figure 2.12**) as a hydrophobic probe in several mammalian serum albumins was investigated by Antoine and co-workers.[95] The high molar absorptivities observed for most NIR dyes allow for very small amounts to be employed without using emission spectroscopy. Lower probe concentrations are particularly important in avoiding protein denaturation. Furthermore, the cyanine moiety allows such dyes to remain more soluble in water than hydrophobic probes commercially available at present. The primary objective in hydrophobicity studies is to minimize the effect of nonspecific binding which may result in incorrect hydrophobicity values. Since the absorbance of NIR dyes is far removed from that of most biomolecules, binding specificity can be inferred by spectral changes in the probe. Antoine et al. reported pronounced spectral changes in the NIR absorption spectra of NIR dye I. Protein hydrophobicity was calculated from the peak ratios of the dye's spectra. Thus proving that NIR dyes can be quite useful as hydrophobicity probes in proteins.

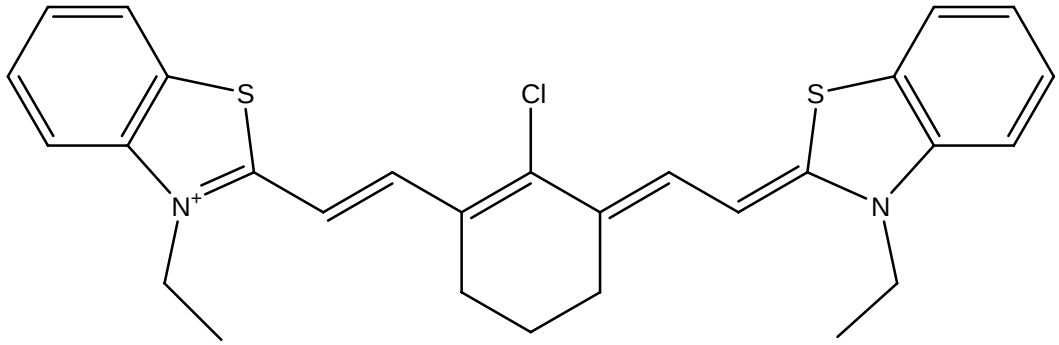

Figure 2.12. Chemical structure NIR probe I.

Chemical Ion Sensors. Noninvasive monitoring of clinically relevant species and physiological parameters is one important potential application of fluorescence biosensors.[96, 97] Perhaps in the distant future, a portable, noninvasive device will measure the clinical values of interest then store, and/or transmit, them to the physician. The concept of rapid point-of-care clinical diagnostics is driving the rapid development of numerous biosensors. A biosensor can be generally defined as a device that consists of a biological recognition system, or bioreceptor, and a transducer. The general principles of biosensing technology are outlined in **Figure 2.13**. The interaction of the analyte with the bioreceptor is designed to produce an effect measured by the transducer, which converts the information into a measurable effect such as an electrical signal. A bioreceptor is a molecular species (e.g., an antibody, an enzyme, a protein, or a nucleic acid) or a living biological system (e.g., cells, tissue, or whole organisms) that utilizes a biochemical mechanism for recognition. Transduction can be accomplished via a great variety of methods. Three very broad classes of transducers include: 1) optical detection methods (e.g., absorption or fluorescence spectroscopy), 2) electrochemical detection methods (e.g., voltammetry) and 3) mass detection methods (e.g., piezoelectric crystal devices). The third class is the newest class and is capable of Angstrom level measurements.

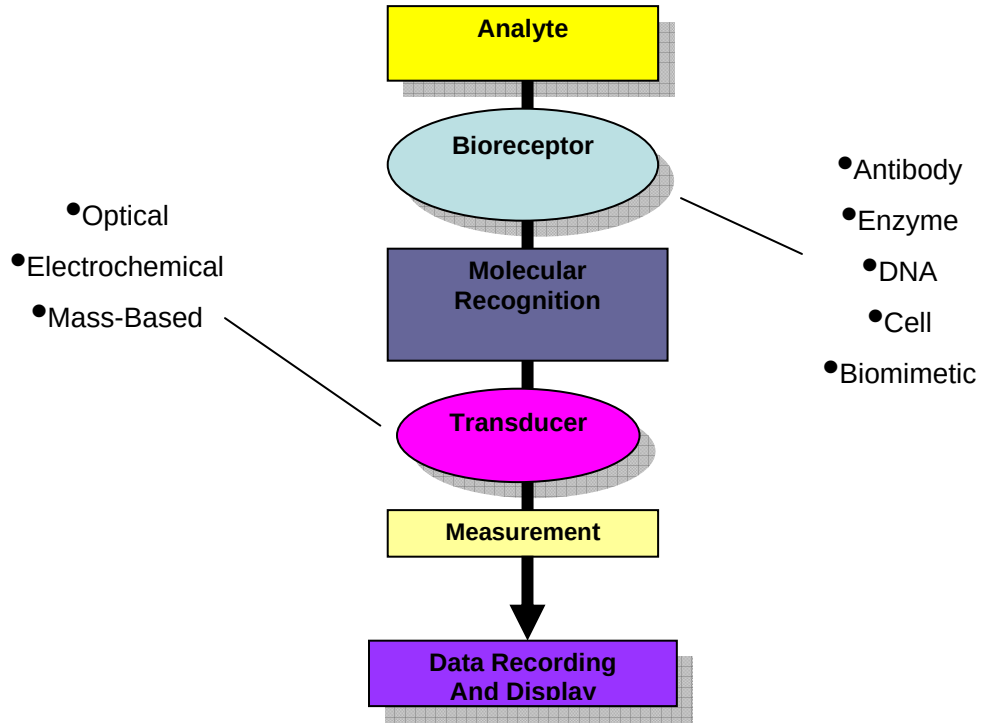

Figure 2.13. Principles of biosensing technology. Revised from reference 97.

At this point we will consider the potential of NIR dyes for sensing applications. The ability to monitor the influx of metal ions and subsequent concentrations inside the cell would greatly facilitate the treatment of diseases related to the overabundance or deficiency of metals such as calcium in cells.[98] The introduction of a metal binding dye into cells allows for an analysis of metal concentrations which would possibly aid in diagnosis of metal-related diseases. And ideal dye for such applications would enable researchers to identify the stimuli which cause a flux in metal ion concentrations of diseased cells. To date, the accurate measurement of intracellular calcium concentrations, especially with penetration to multiple layers of cell tissue and high sensitivity, has not yet been developed. Therefore, numerous research is currently aimed towards this objective.

Ellis et al. reported the characterization of a newly synthesized calcium sensitive carbocyanine dye exciting in the NIR region, 15C5-774. The dye structure contained a metal binding benzo-15-crown-5 moiety (15C5) linked at the meso position to a heptamethine cyanine (**Figure 2.14**). The dye exhibited good solubility in aqueous buffer. In addition, the metal binding affinities of 15C5-774 are in micromolar range for all metals tested and follow the order $Ca^{2+} > Mg^{2+} > Sr^{2+} \approx K^{+} \approx Na^{+} > Zn^{2+} > Li^{+}$. Although binding affinities were only slightly affected by pH, the absorption spectrum for 15C5-774 was in fact sensitive to pH changes. Therefore, the dye also shows good potential as a monitor for pH flux changes.

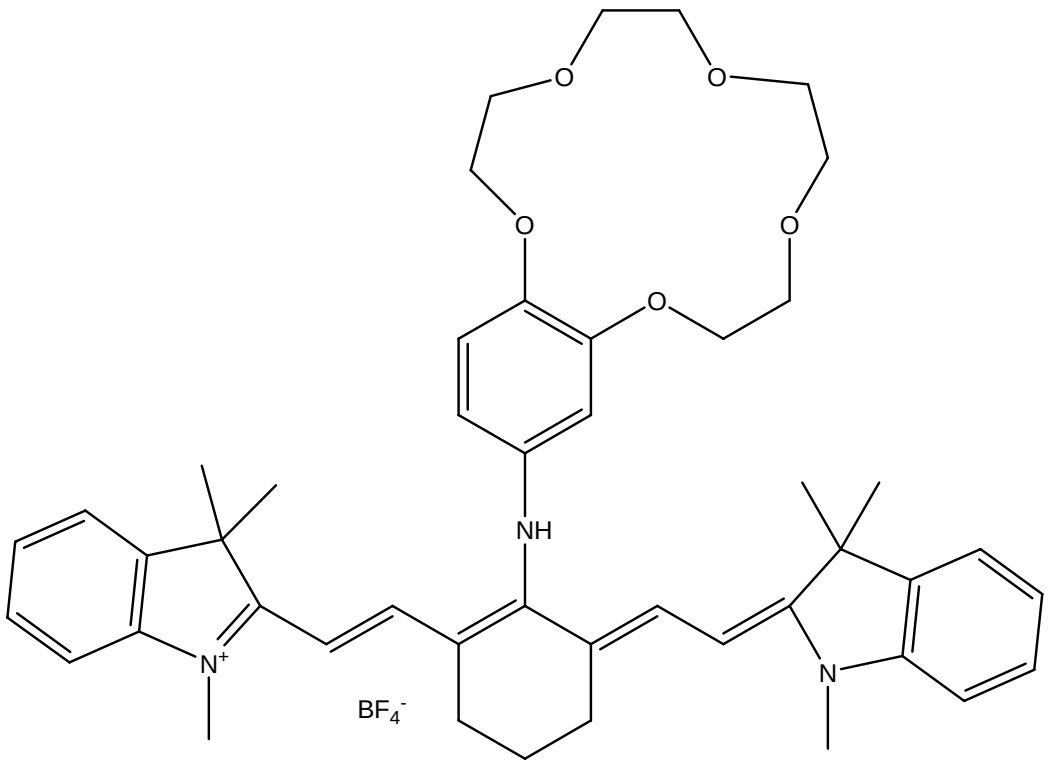

Figure 2.14. Chemical structure of 15C5-774.

Pharmacological Research. Sowell et al have studied HSA drug binding by utilizing a competitive assay and a NIR probe.[48] In this study, the hydrophobic sites of HSA that provide high affinity to drugs were also the target binding site for the carbocyanine dye. The drugs compete with a noncovalently labeled NIR dye in the same binding site and the dye, possessing a lower binding affinity, will be replaced with drugs. By using this method, the affinity constants of individual site-specific drugs were indirectly calculated. The most advantageous feature of this technique is that we can simply anticipate the binding site of unknown drugs without further experimentation.

Cut on/cut off technology. A squaraine dye (SQ1) absorbing in the NIR region was reported to selectively bound, with a high association constant ($1.4 \pm 0.1 \times 10^6$ M^{-1}) owing to the multiple hydroxyl groups of its structure.[99] The chemical structure of SQ1 was given **Figure 2.15**. Binding was exhibited by dual modes recognition as a visible color change and "cut on" fluorescence. The dye exhibited an initial decrease in absorbance when BSA was added up to a 1:2 protein:dye ratio. When the BSA concentration was increased further, a bathochromic shift from 584 to 610 nm in the absorption spectrum was confirmed by a visible color change from pink to blue. Half – reciprocal plot analysis of the absorption spectrum showed a 1:1 binding stoichiometry for the complex between SQ1 and BSA. Similarly, a bathochromic shift from 600 to 620 nm in the emission spectrum as well. As more than twice the molar concentration of BSA is introduced the dye's fluorescence intensity increases approximately 80-fold. This "cut-on" fluorescence mechanism was also visibly apparent. The complex formation of SQ1 and BSA was further confirmed by CD, cyclic voltammetry (CV), and 1H NMR techniques. The corresponding induced CD signal at 610 nm, the decrease in current

intensity, and the upfield shift of protons all confirmed the formation of a stable SQ1-BSA complex. Competitive binding assays involving fluorescence lifetime measurements and two ligands with Site I and Site II specificity showed 40% displacement at Site I and 60% displacement for SQ1. At low BSA concentrations (up to 1:2 protein:dye ratio), the decrease in absorbance with increasing protein is attributed to a tightly bound complex of SQ1 inside the relatively small cavity (2.53 Å) of Site I. In addition, the presence of a single tryptophan residue promotes binding through π-stacking and hydrophobic interactions, resulting in a longer lifetime (1.5 ns) at this site. At concentration ratios above 1:2, the increase in absorbance and fluorescence is credited to a more loosely bound SQ1 inside the relatively larger cavity (2.6 Å) through hydrophobic, hydrogen bonding, and electrostatic interactions. This loose association is also confirmed by the shorter lifetime (0.5 ns) of SQ1 at Site II. Furthermore, with the absence of tryptophan residues and the relatively loose protein-dye complex a bathochromic shift in both absorption and emission spectra was observed. Thus, binding of SQ1 at Site II allows for dual mode visible recognition of albumin through both a visible color change and "turn on" fluorescence.

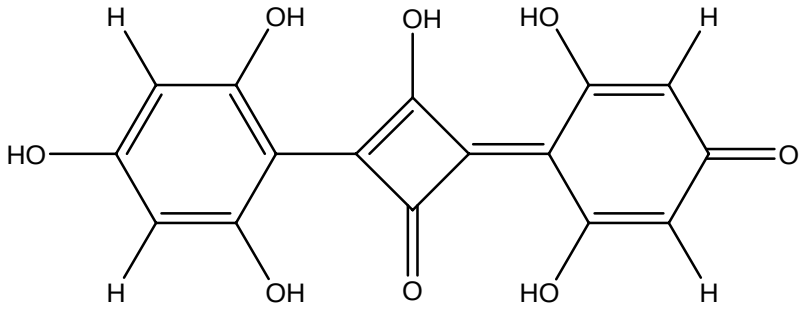

Figure 2.15. Chemical structure of SQ1.

Summary

Herein, the basic structure, synthesis, and spectral characteristics of NIR cyanine dyes have been described. The broad range of techniques and their applications for the purpose of protein identification and quantification have also been discussed. The most advantageous aspect of covalent labeling methods is that a series of identical amino acid side chains in a protein can be tagged with a probe, thereby causing a protein of interest to display different spectral responses in spectroscopic analysis and different retention times or mobilities in chromatographic analysis. However, the drawback to this technique is that the experimental labeling environment needs to be controlled. In contrast, the relatively simple methodology of noncovalent labeling can also be used for the investigation of specific protein binding sites, although the analysis the system's binding parameters can be quite tedious and complex. However, the information obtained from noncovalent dye-protein binding studies can be applied to analogous systems such as the noncovalent interactions of proteins with drugs in pharmacological studies. Therefore, the advantages of noncovalent labeling methods far outweigh the drawback.

The application of using cyanine probes to further the understanding of protein-ligand interactions, far surpasses the general qualitative and quantitative applications already discussed herein. The bis-cyanine dyes discussed in Chapter 3 have the ability to exhibit both intra-molecular and inter-molecular H-aggregates. Their utility for noncovalent protein labeling was investigated using absorption, emission, and FDCD spectroscopic techniques.

References

1. Fabian, J.; Nakazumi, H.; Matsuoka, M., Near-Infrared Absorbing Dyes. *Chemical Reviews* **1992,** 92, (6), 1197-1226.

2. Hannah, K. C.; Armitage, B. A., DNA-templated assembly of helical cyanine dye aggregates: A supramolecular chain polymerization. *Accounts of Chemical Research* **2004,** 37, (11), 845-853.

3. Baars, M. J.; Patonay, G., Ultrasensitive detection of closely related angiotensin I peptides doing capillary electrophoresis with near-infrared laser-induced fluorescence detection. *Analytical Chemistry* **1999,** 71, (3), 667-671.

4. Zollinger, H., *Color Chemistry: Syntheses, Properties, and Applications of Organic Dyes and Pigments*. 2nd ed.; VCH Publishers: New York, 1991.

5. Khimenko, V.; Chibisov, A.; Gorner, H., Effects of alkyl substiutents in the polymethine chain on the photoprocesses in thiacarbocyanine dyes. *J Phys Chem A* **1997,** 101, 7304-7310.

6. Tatikolov, A. S.; Costa, S. M. B., Effects of normal and reverse micellar environment on the spectral properties, isomerization and aggregation of a hydrophilic cyanine dye. *Chemical Physics Letters* **2001,** 346, (3-4), 233-240.

7. Tatikolov, A. S.; Costa, S. M. B., Photophysics and photochemistry of hydrophilic cyanine dyes in normal and reverse micelles. *Photochemical & Photobiological Sciences* **2002,** 1, (3), 211-218.

8. Tatikolov, A. S.; Costa, S. M. B., Complexation of polymethine dyes with human serum albumin: a spectroscopic study. *Biophysical Chemistry* **2004,** 107, (1), 33-49.

9. Patonay, G.; Salon, J.; Sowell, J.; Strekowski, L., Noncovalent labeling of biomolecules with red and near-infrared dyes. *Molecules* **2004,** 9, (3), 40-49.

10. Mishra, A.; Behera, R. K.; Behera, P. K.; Mishra, B. K.; Behera, G. B., Cyanines during the 1990s: A review. *Chemical Reviews* **2000,** 100, (6), 1973-2011.

11. Patonay, G.; Antoine, M. D., Near-Infrared Fluorogenic Labels: New Approach to an Old Problem. *Analytical Chemistry* **1991,** 63, (6), 321A-327A.

12. Baars, M.; Patonay, G., Ultrasensitive detection of closely related angiotensin I peptides using capillary electrophoresis with near-infrared laser-induced fluorescence detection. *Anal Chem* **1999,** 71, (3), 667-71.

13. Stoyanov, S., *Probes: Dyes Fluorescing in the NIR Region*. Marcel Dekker, Inc.: New York, 2001.

14. Kim, J. S.; Kodagahally, R.; Strekowski, L.; Patonay, G., A study of intramolecular H-complexes of novel bis(heptamethine cyanine) dyes. *Talanta* **2005,** 67, (5), 947-954.

15. Patonay, G.; Kim, J. S.; Kodagahally, R.; Strekowski, L., Spectroscopic study of a novel bis(heptamethine cyanine) dye and its interaction with human serum albumin. *Applied Spectroscopy* **2005,** 59, (5), 682-690.

16. Strekowski, L.; Lipowska, M.; Patonay, G., Substitution Reactions of a Nucleofugal Group in Heptamethine Cyanine Dyes. Synthesis of an Isothiocyanato Derivative for Labeling of Proteins with a Near-Infrared Chromophore. *Journal of Organic Chemistry* **1992,** 57, (17), 4578-4580.

17. Narayanan, N.; Patonay, G., A New Method for the Synthesis of Heptamethine Cyanine Dyes. *Journal of Organic Chemistry* **1995,** 60, (8), 2391-2395.

18. Jelley, E. E., Spectral absorption and fluorescence of dyes in the molecular state. *Nature (London, United Kingdom)* **1936,** 138, 1009-10.

19. Jelley, E. E., Molecular, nematic and crystal states of 1,1'-diethyl-y-cyanine chloride. *Nature (London, United Kingdom)* **1937,** 139, 631-2.

20. Scheibe, G., Variability of the absorption spectra of some sensitizing dyes and its cause. *Angew. Chem.* **1936,** 49, 563.

21. Scheibe, G., The variation of absorption spectra in solutions and the side valences as its cause. *Angew. Chem.* **1937,** 50, 212-19.

22. Yao, H.; Domoto, K.; Isohashi, T.; Kimura, K., In situ detection of birefringent mesoscopic H and J aggregates of thiacarbocyanine dye in solution. *Langmuir* **2005,** 21, (3), 1067-1073.

23. Yarmoluk, S. M.; Lukashov, S. S.; Ogul'Chansky, T. Y.; Losytskyy, M. Y.; Kornyushyna, O. S., Interaction of cyanine dyes with nucleic acids. XXI. Arguments for half-intercalation model of interaction. *Biopolymers* **2001,** 62, (4), 219-27.

24. Ogul'chansky, T.; Losytskyy, M.; Kovalska, V. B.; Yashchuk, V. M.; Yarmoluk, S. M., Interactions of cyanine dyes with nucleic acids. XXIV. Aggregation of monomethine cyanine dyes in presence of DNA and its manifestation in absorption and fluorescence spectra. *Spectrochim Acta A Mol Biomol Spectrosc* **2001,** 57, (7), 1525-32.

25. Patonay, G.; Strekowski, L.; Kim, J. S.; Henary, M., The increasing role of NIR fluorescence spectroscopy in bioanalytical chemistry *NIR news* **2007,** 18, (3), 7-9.

26. Tatikolov, A. S.; Panova, I. G., A spectroscopic study on the interaction of polymethine dyes with collagens. *High Energy Chemistry* **2005,** 39, (4), 232-236.

27. Panova, I. G.; Sharova, N. P.; Dmitrieva, S. B.; Poltavtseva, R. A.; Sukhikh, G. T.; Tatikolov, A. S., Use of a cyanine dye as a probe for albumin and collagen in the extracellular matrix. *Analytical Biochemistry* **2007,** 361, (2), 183-189.

28. Min, H.; Park, J.; Yu, J.; Kim, D., The Spectroscopic Studies on the Agregation Behavior of Cyanine Dyes. *Bulletin of the Korean Chemical Society* **1998,** 19, (6), 650-654.

29. West, W.; Pearce, S., The Dimeric State of Cyanine Dyes. *The Journal of Physical Chemistry* **1965,** 69, (6), 1894-1903.

30. Green, M. D.; Patonay, G.; Ndou, T.; Warner, I. M., Spectroscopic Effects of Organized Media on a Cyanine Dye Pyrene Derivative. *Journal of Inclusion Phenomena and Molecular Recognition in Chemistry* **1992,** 13, (2), 181-193.

31. Mishra, A.; Behera, R. K.; Behera, P. K.; Mishra, B. K.; Behera, G. B., Cyanines During the 1990s: A Review. *Chemical Reviews* **2000,** 100, (6), 1973-2011.

32. Herz, A., Aggregation of sensitizing dyes in solution and their adsorption onto silver halides. *Advances in Colloid and Interface Science* **1977,** 8, (4), 237-298.

33. Kirstein, S.; von Berlepsch, H.; Bottcher, C.; Burger, C.; Ouart, A.; Reck, G.; Dahne, S., Chiral J-aggregates formed by achiral cyanine dyes. *Chemphyschem* **2000,** 1, (3), 146-+.

34. Spitz, C.; Dahne, S.; Ouart, A.; Abraham, H. W., Proof of chirality of J-aggregates spontaneously and enantioselectively generated from achiral dyes. *Journal of Physical Chemistry B* **2000,** 104, (36), 8664-8669.

35. Saeva, F.; Olin, G.; Turner, S.; Yanus, J.; Sandman, D., Circular dichroism spectropolarimetric characterization of J-aggregates species of some pyrylium dyes. *Photographic Science and Engineering* **1978,** 22, (3), 129-132.

36. Honda, C.; Hada, H., Spectroscopic study on the J-aggregate of cyanine dyes. II. Circular dichroism of J-aggregates. *Photographic Science and Engineering* **1977,** 21, (2), 91-96.

37. Neumann, B.; Pollmann, P., Investigation of spectral shifts of monomeric and J-aggregated cyanine dyes at high pressure by UV/Vis spectroscopy. *Physical Chemistry Chemical Physics* **2001,** 3, (6), 943-951.

38. Zhang, Y. Z.; Xiang, J. F.; Tang, Y. L.; Xu, G. Z.; Yan, W. P., Chiral transformation of achiral J-aggregates of a cyanine dye templated by human serum albumin. *Chemphyschem* **2007,** 8, (2), 224-226.

39. Seifert, J. L.; Connor, R. E.; Kushon, S. A.; Wang, M.; Armitage, B. A., Spontaneous assembly of helical cyanine dye aggregates on DNA nanotemplates. *Journal of the American Chemical Society* **1999,** 121, (13), 2987-2995.

40. Ogul'chansky, T. Y.; Losytskyy, M. Y.; Kovalska, V. B.; Lukashov, S. S.; Yashchuk, V. M.; Yarmoluk, S. M., Interaction of cyanine dyes with nucleic acids. XVIII. Formation of the carbocyanine dye J-aggregates in nucleic acid grooves. *Spectrochimica Acta Part a-Molecular and Biomolecular Spectroscopy* **2001,** 57, (13), 2705-2715.

41. Hardouin, J., Protein sequence information by matrix-assisted laser desorption/ionization in-source decay mass spectrometry. *Mass Spectrom Rev* **2007,** 26, (5), 672-682.

42. Srebalus Barnes, C. A.; Lim, A., Applications of mass spectrometry for the structural characterization of recombinant protein pharmaceuticals. *Mass Spectrom Rev* **2007,** 26, (3), 370-88.

43. Craik, D. J.; Daly, N. L., NMR as a tool for elucidating the structures of circular and knotted proteins. *Mol Biosyst* **2007,** 3, (4), 257-65.

44. Foster, M. P.; McElroy, C. A.; Amero, C. D., Solution NMR of large molecules and assemblies. *Biochemistry* **2007,** 46, (2), 331-40.

45. Rosano, C.; Zuccotti, S.; Bolognesi, M., The three-dimensional structure of beta2 microglobulin: results from X-ray crystallography. *Biochim Biophys Acta* **2005,** 1753, (1), 85-91.

46. Carlomagno, T., Ligand-target interactions: what can we learn from NMR? *Annu Rev Biophys Biomol Struct* **2005,** 34, 245-66.

47. Lecomte, C.; Guillot, B.; Muzet, N.; Pichon-Pesme, V.; Jelsch, C., Ultra-high-resolution X-ray structure of proteins. *Cell Mol Life Sci* **2004,** 61, (7-8), 774-82.

48. Sowell, J.; Mason, J. C.; Strekowski, L.; Patonay, G., Binding constant determination of drugs toward subdomain IIIA of human serum albumin by near-infrared dye-displacement capillary electrophoresis. *Electrophoresis* **2001,** 22, (12), 2512-2517.

49. Welder, F.; Paul, B.; Nakazumi, H.; Yagi, S.; Colyer, C. L., Symmetric and asymmetric squarylium dyes as noncovalent protein labels: a study by fluorimetry and capillary electrophoresis. *J Chromatogr B Analyt Technol Biomed Life Sci* **2003,** 793, (1), 93-105.

50. Fukushima, T.; Usui, N.; Santa, T.; Imai, K., Recent progress in derivatization methods for LC and CE analysis. *J Pharm Biomed Anal* **2003,** 30, (6), 1655-87.

51. Patonay, G.; Kim, J. S.; Kodagahally, R.; Strekowski, L., Spectroscopic study of a novel bis(heptamethine cyanine) dye and its interaction with human serum albumin. *Appl Spectrosc* **2005,** 59, (5), 682-90.

52. Garman, A., *Non-radioactive labelling: a practical introduction*. Academic Press: San Diego, 1997.

53. Ernst, L.; Gupta, R.; Mujumdar, R.; Waggoner, A., Cyanine dye labeling reagents for sulfhydryl groups. *Cytometry* **1989,** 10, (6), 3-10.

54. Jacobsen, C., Trinitrophenylation of the bilirubin binding site of human serum albumin. *Int J Pept Protein Res* **1975,** 7, (2), 161-5.

55. Craig, D. B.; Dovichi, N. J., Multiple labeling of proteins. *Analytical Chemistry* **1998,** 70, (13), 2493-2494.

56. Williams, R. J.; Lipowska, M.; Patonay, G.; Strekowski, L., Comparison of Covalent and Noncovalent Labeling with near-Infrared Dyes for the High-Performance Liquid-Chromatographic Determination of Human Serum-Albumin. *Analytical Chemistry* **1993,** 65, (5), 601-605.

57. Holde, K. E. v.; Johnson, W. C.; Ho, P. S., *Principles of Physical Biochemistry*. 2nd ed. ed.; Pearson Education, Inc.: New Jersey, 2006; p 605 pp.

58. Drenth, J., *Principles of Protein X-Ray Crystallography*. 3rd ed. ed.; Springer Science New York, 2007.

59. Bulheller, B. M.; Rodger, A.; Hirst, J. D., Circular and linear dichroism of proteins. *Phys Chem Chem Phys* **2007,** 9, (17), 2020-35.

60. Benito, I.; Marina, M. L.; Saz, J. M.; Diez-Masa, J. C., Detection of bovine whey proteins by on-column derivatization capillary electrophoresis with laser-induced fluorescence monitoring. *J Chromatogr A* **1999,** 841, (1), 105-14.

61. Yan, W.; Colyer, C. L., Investigating noncovalent squarylium dye-protein interactions by capillary electrophoresis-frontal analysis. *Journal of Chromatography, A* **2006,** 1135, (1), 115-121.

62. McCorquodale, E. M.; Colyer, C. L., Indocyanine green as a noncovalent, pseudofluorogenic label for protein determination by capillary electrophoresis. *Electrophoresis* **2001,** 22, (12), 2403-2408.

63. Moody, E. D.; Viskari, P. J.; Colyer, C. L., Non-covalent labeling of human serum albumin with indocyanine green: a study by capillary electrophoresis with diode laser-induced fluorescence detection. *Journal of Chromatography, B: Biomedical Sciences and Applications* **1999,** 729, (1 + 2), 55-64.

64. Flaumenhaft, R.; Tanaka, E.; Graham Gwenda, J.; De Grand Alec, M.; Laurence Rita, G.; Hoshino, K.; Hajjar Roger, J.; Frangioni John, V., Localization and quantification of platelet-rich thrombi in large blood vessels with near-infrared fluorescence imaging. *Circulation FIELD Full Journal Title:Circulation* **2007,** 115, (1), 84-93.

65. Parungo, C. P.; Ohnishi, S.; De Grand, A. M.; Laurence, R. G.; Soltesz, E. G.; Colson, Y. L.; Kang, P. M.; Mihaljevic, T.; Cohn, L. H.; Frangioni, J. V., In vivo optical imaging of pleural space drainage to lymph nodes of prognostic significance. *Ann Surg Oncol* **2004,** 11, (12), 1085-92.

66. Kim, S.; Lim, Y. T.; Soltesz, E. G.; De Grand, A. M.; Lee, J.; Nakayama, A.; Parker, J. A.; Mihaljevic, T.; Laurence, R. G.; Dor, D. M.; Cohn, L. H.; Bawendi, M. G.; Frangioni, J. V., Near-infrared fluorescent type II quantum dots for sentinel lymph node mapping. *Nat Biotechnol* **2004,** 22, (1), 93-7.

67. Ballou, B.; Fisher, G. W.; Hakala, T. R.; Farkas, D. L., Tumor detection and visualization using cyanine fluorochrome-labeled antibodies. *Biotechnol Prog* **1997,** 13, (5), 649-58.

68. Ballou, B.; Ernst, L. A.; Waggoner, A. S., Fluorescence imaging of tumors in vivo. *Curr Med Chem* **2005,** 12, (7), 795-805.

69. Licha, K.; Riefke, B.; Semmler, W., Synthesis and characterization of cyanine dye - Poly(ethylene glycol) conjugates as contrast agents for in vivo fluorescence imaging. *Proceedings of SPIE* **1998,** 3196, 98-102.

70. Licha, K.; Riefke, B.; Ntziachristos, V.; Becker, A.; Chance, B.; Semmler, W., Hydrophilic cyanine dyes as contrast agents for near-infrared tumor imaging: Synthesis, photophysical properties and spectroscopic in vivo characterization. *Photochemistry and Photobiology* **2000,** 72, (3), 392-398.

71. Licha, K.; Hessenius, C.; Becker, A.; Henklein, P.; Bauer, M.; Wisniewski, S.; Wiedenmann, B.; Semmler, W., Synthesis, characterization, and biological properties of cyanine-labeled somatostatin analogues as receptor-targeted fluorescent probes. *Bioconjugate Chemistry* **2001,** 12, (1), 44-50.

72. Riefke, B.; Licha, K.; Nolte, D.; Ebert, B.; Rinneberg, H.; Semmler, W., Tumor detection with cyanine dye - poly(ethylene glycol) conjugates as contrast agents for near infrared imaging. *Proceedings of SPIE* **1998,** 3196, 103-110.

73. Riefke, B.; Licha, K.; Semmler, W., Contrast agents for optical mammography. *Radiologe* **1997,** 37, (9), 749-755.

74. Minet, O.; Beuthan, J.; Licha, K.; Mahnke, C., The Medical Use of Rescaling Procedures in Optical Biopsy and Optical Molecular Imaging. *Journal of Fluorescence* **2002,** 12, (2), 201-204.

75. Ebert, B.; Sukowski, U.; Grosenick, D.; Wabnitz, H.; Moesta, K. T.; Licha, K.; Becker, A.; Semmler, W.; Schlag, P. M.; Rinneberg, H., Near-infrared fluorescent dyes for enhanced contrast in optical mammography: phantom experiments. *Journal of Biomedical Optics* **2001,** 6, (2), 134-140.

76. Becker, A.; Hessenius, C.; Licha, K.; Ebert, B.; Sukowski, U.; Semmler, W.; Wiedenmann, B.; Grotzinger, C., Receptor-targeted optical imaging of tumors with near-infrared fluorescent ligands. *Nature Biotechnology* **2001,** 19, (4), 327-331.

77. Becker, A.; Riefke, B.; Ebert, B.; Sukowski, U.; Rinneberg, H.; Semmler, W.; Licha, K., Macromolecular Contrast Agents for Optical Imaging of Tumors: Comparison of Indotricarbocyanine-labeled Human Serum Albumin and Transferrin. *Photochemistry and Photobiology* **2000,** 72, (2), 234-241.

78. Broglio, F.; Papotti, M.; Muccioli, G.; Ghigo, E., Brain-gut communication: cortistatin, somatostatin and ghrelin. *Trends in Endocrinology and Metabolism* **2007,** 18, (6), 246-251.

79. Nakayama, A.; del Monte, F.; Hajjar Roger, J.; Frangioni John, V., Functional near-infrared fluorescence imaging for cardiac surgery and targeted gene therapy. *Mol Imaging FIELD Full Journal Title:Molecular imaging : official journal of the Society for Molecular Imaging* **2002,** 1, (4), 365-77.

80. Ohnishi, S.; Lomnes, S. J.; Laurence, R. G.; Gogbashian, A.; Mariani, G.; Frangioni, J. V., Organic alternatives to quantum dots for intraoperative near-infrared fluorescent sentinel lymph node mapping. *Mol Imaging* **2005,** 4, (3), 172-81.

81. Bruce, L. L.; Christensen, M. A.; Fritzsch, B., Electron microscopic differentiation of directly and transneuronally transported DiI and applications for studies of synaptogenesis. *Journal of Neuroscience Methods* **1997,** 73, 107-112.

82. Woodhams, P. L.; Terashima, T., Aberrant trajectory of entorhino-denate axons in the mutant Shaking Rat Kawasaki: a DiI-labelling study. *European Journal of Neuroscience* **2000,** 12, 2707-2720.

83. Anadon, R.; Manso, M.; Rodriguez-Moldes, I.; Becerra, M., Neurons of the olfactory organ projecting to the caudal telencephalon and hypothalamus: a carbocyanine-dye labelling study in the brown trout (Teleostei). *Neuroscience Letters* **1995,** 191, 157-160.

84. Kalchenko, V.; Shivtiel, S.; Malina, V.; Lapid, K.; Haramati, S.; Lapidot, T.; Brill, A.; Harmelin, A., Use of lipophilic near-infrared dye in whole-body optical imaging of hematopoietic cell homing. *Journal of biomedical optics* **2006,** 11, (5).

85. Sowell, J.; Parihar, R.; Patonay, G., Capillary electrophoresis-based immunoassay for insulin antibodies with near-infrared laser induced fluorescence detection. *J Chromatogr B Biomed Sci Appl* **2001,** 752, (1), 1-8.

86. Schou, C.; Heegaard, N. H., Recent applications of affinity interactions in capillary electrophoresis. *Electrophoresis* **2006,** 27, (1), 44-59.

87. Daneshvar, M. I.; Peralta, J. M.; Casay, G. A.; Narayanan, N.; Evans, L., III; Patonay, G., Detection of biomolecules in the near-infrared spectral region via a fiber-optic immunosensor. *J. Immunol. Methods FIELD Full Journal Title:Journal of Immunological Methods* **1999,** 226, (1-2), 119-128.

88. Andrews-Wilberforce, D.; Patonay, G., Investigation of near-infrared laser dye albumin complexes. *Spectrochimica Acta Part A-Molecular and Biomolecular Spectroscopy* **1990,** 46A, (8), 1153-1162.

89. Li, W. R.; Wang, H.; Yang, T. X.; Zhang, H. S., Direct spectrometric determination of proteins in body fluids using a near-infrared cyanine dye. *Analytical and Bioanalytical Chemistry* **2003,** 377, (2), 350-355.

90. Wang, H.; Li, W. R.; Guo, X. F.; Zhang, H. S., Spectrophotometric determination of total protein in serum using a novel near-infrared cyanine dye, 5,5 '-dicarboxy-1,1 '-disulfobutyl-3,3,3 ',3 '-tetramethylindotricarbocyanine. *Analytical and Bioanalytical Chemistry* **2007,** 387, (8), 2857-2862.

91. Zheng, H.; Zhu, C. Q.; Li, D. H.; Chen, Q. Y.; Yang, H. H.; Chen, X. L.; Xu, J. G., A novel method for the determination of total protein in human serum by near infrared fluorescence recovery. *Fresenius J Anal Chem* **2000,** 368, (5), 511-5.

92. Oswald, B.; Patsenker, L.; Duschl, J.; Szmacinski, H.; Wolfbeis, O. S.; Terpetschnig, E., Synthesis, spectral properties, and detection limits of reactive squaraine dyes, a new class of diode laser compatible fluorescent protein labels. *Bioconjug Chem* **1999,** 10, (6), 925-31.

93. Patonay, G.; Antoine, M. D.; Devanathan, S.; Strekowski, L., Near-Infrared Probe for Determination of Solvent Hydrophobicity. *Applied Spectroscopy* **1991,** 45, (3), 457-461.

94. Lakowicz, J. R., Fluorophores. In *Principles of Fluorescence Spectroscopy*, 2nd ed.; Kluwer Academic/Plenum New York, 1999; pp 63-93.

95. Antoine, M. D.; Devanathan, S.; Patonay, G., Determination of hydrophobicity of albumins and other proteins using a near-infrared probe. *Spectrochimica Acta Part A-Molecular and Biomolecular Spectroscopy* **1991,** 47A, (3/4), 501-508.

96. Lakowicz, J. R., *Principles of Fluorescence Spectroscopy*. 3rd ed.; Springer Science: New York, 2006.

97. Vo-Dinh, T.; Cullum, B., Biosensors and biochips: advances in biological and medical diagnostics. *Fresenius J Anal Chem* **2000,** 366, 540-551.

98. Ellis, A. L.; Mason, J. C.; Lee, H. W.; Strekowski, L.; Patonay, G.; Choi, H.; Yang, J. J., Design, synthesis, and characterization of a calcium-sensitive near infrared dye. *Talanta* **2002,** 56, (6), 1099-1107.

99. Jisha, V. S.; Arun, K. T.; Hariharan, M.; Ramaiah, D., Site-selective binding and dual mode recognition of serum albumin by a squaraine dye. *Journal of the American Chemical Society* **2006,** 128, (18), 6024-6025.

CHAPTER III

Noncovalent Binding Interactions of Bis-cyanine Dyes and Human Serum Albumin

Human Serum Albumin

Serum albumin is one of the most abundant carrier proteins, responsible for the transport and disposition of both endogenous (e.g., fatty and amino acids, bilirubin) and exogenous (e.g., drugs, dyes) ligands present in the body.[1, 2] Owing to its physiological importance, this protein has been extensively studied for its numerous clinical and medical applications.[3-7] Given that its ability to effectively transport molecules is related to its binding affinity, the various ligand binding sites and corresponding association constants have been the specific aim of many spectroscopic studies such as absorption,[8, 9] fluorescence,[2, 10] capillary electrophoresis (CE),[6, 11, 12] high performance liquid chromatography (HPLC), circular dichroism (CD),[13] and fluorescence detected circular dichroism (FDCD).[14]

The crystal structure of human serum albumin (HSA) shown in **Figure 3.1**.[15] He and Carter were first to report the three dimensional structure of human serum albumin crystallographically to a resolution of 2.8 Å.[16] The protein's tertiary structure is comprised of three homologous domains which assemble to form a heart-shaped molecule. Each domain consists of two subdomains possessing common structural motifs. The majority of all ligand binding is contained in the hydrophobic pockets of subdomains IIA and IIIA, also known as Sudlow site I and II respectively.[16-18] Binding in Site I occurs mainly through hydrophobic interactions.[19] Alternately, a combination of hydrophobic, hydrogen bonding, and electrostatic interactions typically occurs in Site II.

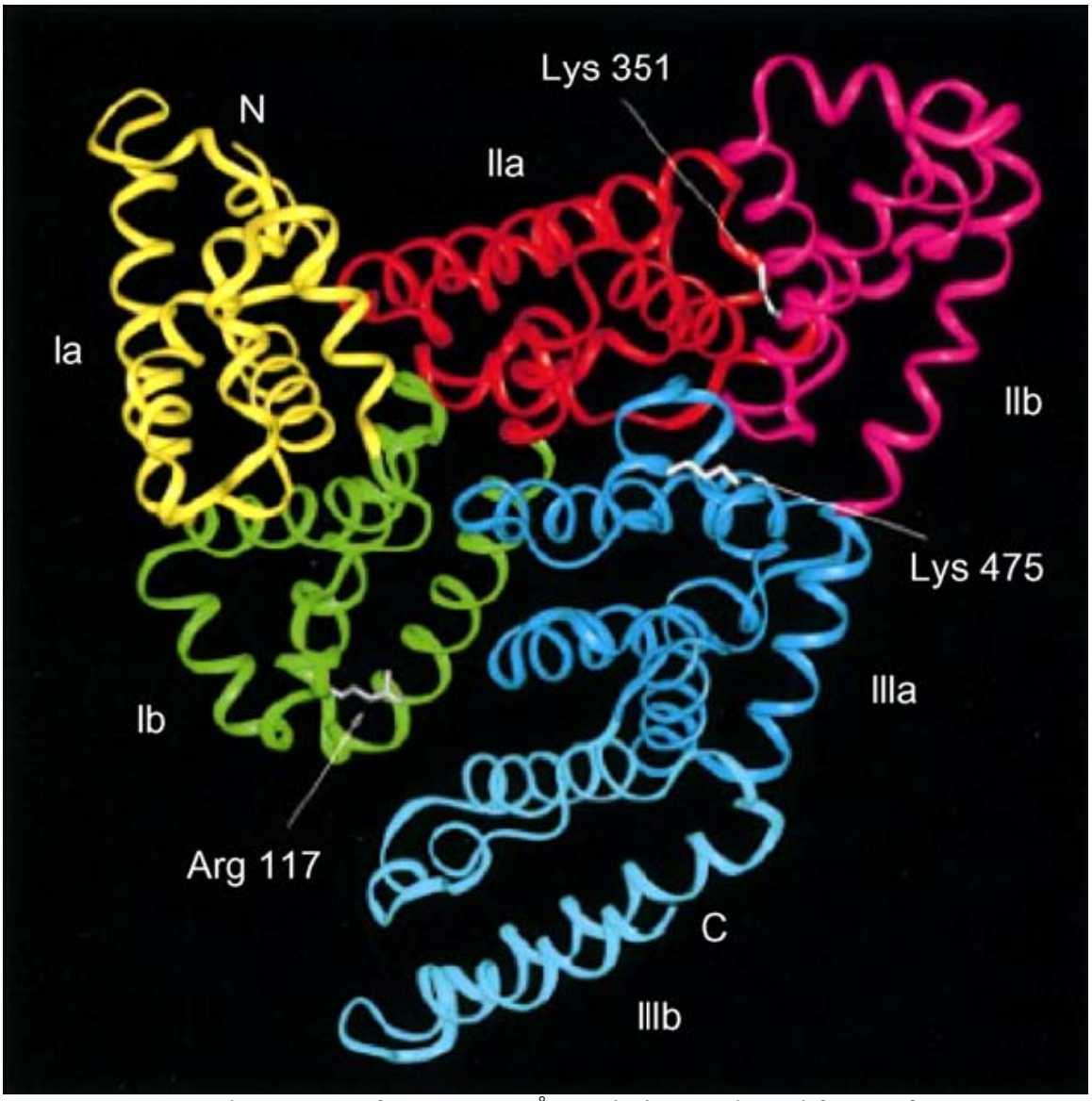

Figure 3.1. Crystal structure of HSA at 2.5 Å resolution. Adapted from reference 15.

Noncovalent labeling of HSA

Noncovalent intermolecular forces (e.g., electrostatic, van der Waals, hydrogen binding, and the hydrophobic effect) play a critical role in many biological receptor-ligand processes such as enzyme-substrate, antibody-antigen, and drug-receptor interactions. The noncovalent interactions of biomolecules with NIR dyes can be particularly useful in further understanding structure-function relationships. A number of fluorogenic, hydrophobic probes (e.g., 1-anilinonophthalene-8-sulfonate, ANS) have been reported which provide information about protein conformation.[20] By observing the spectral changes which occur when NIR labels are noncovalently bound, information can be derived about the dye's microenvironment in a protein of interest.

Noncovalent Interactions of Bis-squaraine Dyes with HSA. Nakazumi et al reported on a series of bis-squaraine dyes which may be useful in noncovalent protein labeling technology.[21] The dyes consisted of two squaraine units linked by multiple thiophene or pyrene spacers. Molar absorptivities for monothiophene derivatives were $1.4 \times 10^5 - 2.4 \times 10^5$ $M^{-1}cm^{-1}$ in chlorophorm and $7 \times 10^4 - 9 \times 10^4$ in DMSO. Dyes containing dithiophene and terthiophene linkers exhibited band broadening and were blue shifted (by 14-50 nm) compared to the monothiophene derivative. Nakazumi considered the significant blue shift was due to planar π-conjugated chromophores inhibited by torsion amongst multiple thiophene rings. Monothiophene or pyrene spacer derivatives containing carboxylic groups at various positions were further investigated for their potential as fluorophores in aqueous buffer. Although the monothiophene derivatives showed decreased absorptivity values in aqueous buffer compared to chloroform, the absorption maxima were also blue shifted by 65-75 nm in buffer, suggesting aggregate

formation in aqueous solution. For one of the monothiphenes, a new peak bathochromically shifted by 47 nm with respect to the λ_{max} in buffer was observed when HSA was added. The large shift in λ_{max} is a feature which is most favorable for high sensitivity analytical techniques. The pyrene spacer derivatives also exhibited a decrease in absorption in buffer, yet the red shifted λ_{max} accompanying dye-protein complex formation was relatively small. Fluorescence intensities were also determined for titration of HSA in buffer using monothiophene and pyrene bis-squaraine derivatives containing carboxylic substituents. As expected, the monothiophene dyes exhibited an enhancement in fluorescence with increasing HSA concentration. Monothiphene dyes alone in aqueous solution exhibited low quantum yields which were thereby increased with when HSA was bound. Job's plot analysis reported a 1:1 stoichiometry between monothiophene derivatives and HSA. By using techniques reported by Tarazi et al,[22] the stability constant Ks of one monothiophene dye was approximately $1.26 \times 10^6 - 1.40 \times 10^6$ M^{-1}, thus indicating strong interactions between dye and protein.[21] Although the pyrene spacer derivatives also exhibited enhanced fluorescence with increasing protein concentration, the absolute fluorescence values were lower than the monothiophene derivatives overall. Job's plot analysis also predicted a 1:1 stoichiometry for pyrene linked bis-squaraine dyes bound to HSA and Ks was between $1.0 \times 10^6 - 4.7 \times 10^6$ M^{-1}. The significant increase in quantum yield observed in pyrene derivatives bound to HSA was attributed to the significant Stokes' shift observed. Therefore, the significant changes exhibited by the aforementioned bis-squaraine derivatives in both absorbance and fluorescence applications make them great candidates for noncovalent protein labeling applications.

Noncovelant Interactions of Cationic Bis-cyanine Dyes. It is particularly important to understand dye aggregation in noncovalent labeling techniques because the same noncovalent interactions that affect dye binding to protein also govern dye self-association as well. And although proteins also exhibit self-association, this aggregation is homogenous in nature. Therefore, we can assume that protein aggregation does not play an important role in quantitative and qualitative studies in which a dye or a ligand is used since these studies are only performed within the dye's absorption bands. Consequently, only when a protein alone is studied, should the biomolecular aggregation be considered.

Although NIR cyanine dyes are advantageous over UV/Vis dyes, the use of dyes in the NIR region may not always be an answer to improving method detection limits since, in some cases, dyes may exhibit fluorescence in the absence of protein. In a recent report from the Patonay group, this problem has been solved by using NIR bis-cyanine dyes.[23-25] The group used bis-heptamethine cyanines which contained monomeric subunits, analogous to the commercially available label IR780 (Sigma, St. Louis, MO), that were linked by flexible alky bridges of varying lengths. The structural orientations of the dyes used are shown in **Figures 3.2-3.5**. The flexibility of the alky linkers contained in these dyes was the key feature in their utility as a probe for protein studies. These bis-cyanines were the first reported which contained its own cut-on/cut-off fluorescence switch facilitated by the "clam-shell" orientation of the intramolecular aggregates in the absence of protein (cut-off) and the more planar conformation of the dyes when bound to HSA binding sites (cut-on). These dyes exhibited intramolecular H-aggregates which were independent of concentration. That particular attribute is quite

important for systems in which protein stability and quaternary structure is sensitive to ligand binding. Furthermore, low dye concentrations could mean that intermolecular aggregation of protein-bound dye can either be avoided or perhaps eliminated completely.

The varying number of carbons contained within the bis-cyanine linkers allowed for marked differences in intra-molecular aggregate formation and dye-HSA interactions.[23] The fluorescence spectral comparisons of BHmCs and its monomeric analogue IR 780 are given in **Figure 3.6** and the fluorescence spectral comparisons of BHmCs in the presence of HSA are given in **Figure 3.7**. In buffer alone, BHmC-6 (shown in **Figure 3.3**) exhibits the stronger H-aggregate bands with respect to IR780, and displays the lowest fluorescence intensity compared to the other BHmCs examined. Similarly, BHmC-8 (shown in **Figure 3.4**) also exhibits strong intramolecular complexes in phosphate buffer. The shorter carbon spacer in BHmC-4 (shown in **Figure 3.2**) exhibits higher monomeric character (less intramolecular H-aggregation) and displays the highest amount of fluorescence intensity compared to other bis-cyanines in the studies.

In the presence of HSA, the weaker intramolecular associations of BHmC-4 easily dissociate in the presence of HSA and exhibit markedly higher fluorescence than the other BHmCs analyzed. Jun et al. report that BHmC-6 has a conformationally rigid structure owing to its strong intramolecular H-dimer and emits relatively low fluorescence in the presence of HSA. The Patonay group presumes that the binding sites of the rigid cationic BHmC-6 dimers are contained within hydrophobic cavities of the protein and the negatively charged surface of HSA (pI 4.8). And although BHmC-8, with it long carbon-8 spacer is more flexible and easily opens up in methanol, it remains

strongly associated in buffer and aggregates are not readily disrupted in the presence of HSA. The spectral response of BHmC-10 (shown in **Figure 3.5**) is still even more perceptible.[25] This dye forms both inter- and intra-molecular aggregates alone in polar solvents. Upon the addition of HSA, the H and D bands are decreased and the monomeric band is increased with a concomitant increase in fluorescence intensity, suggesting that the "clam-shell" disrupted by HSA binding. Patonay et al report the binding stoichiometry for this dye is 1:1.

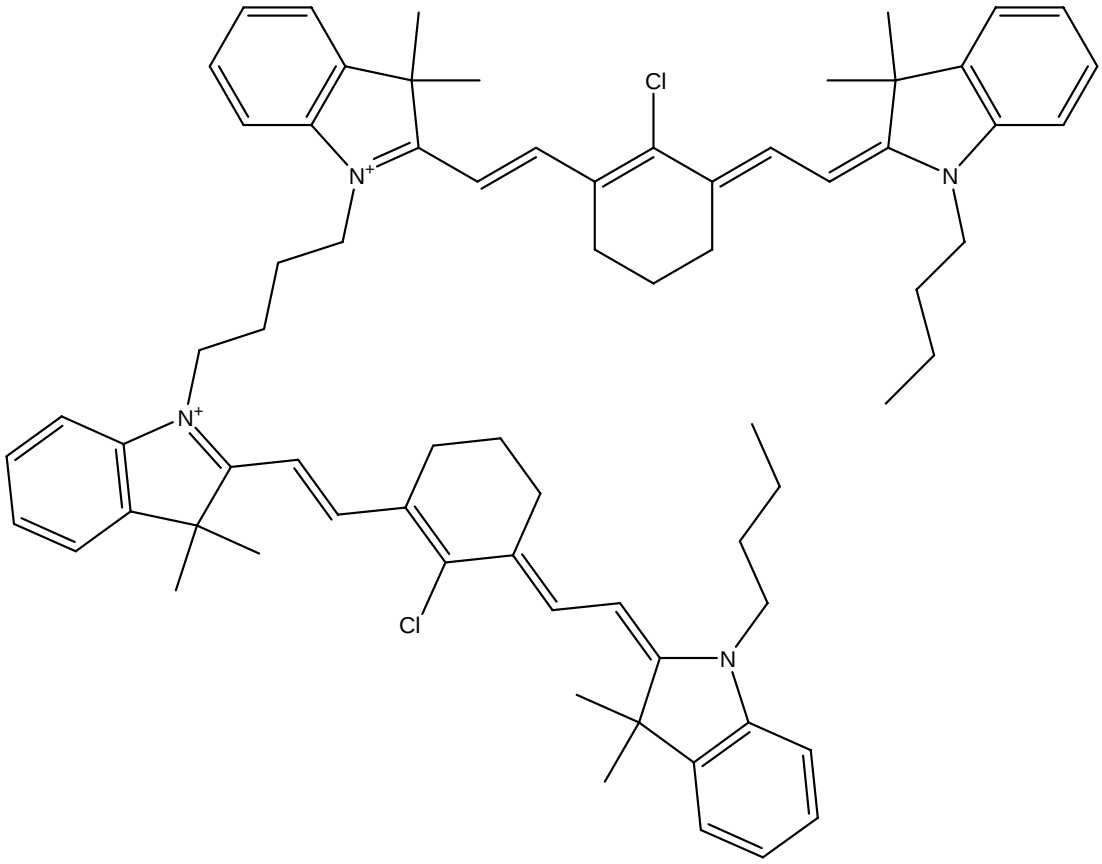

Figure 3.2. Structural simulation of bis-cyanine dye BHmC-4 using ChemDraw® Ultra 8.0 Software.

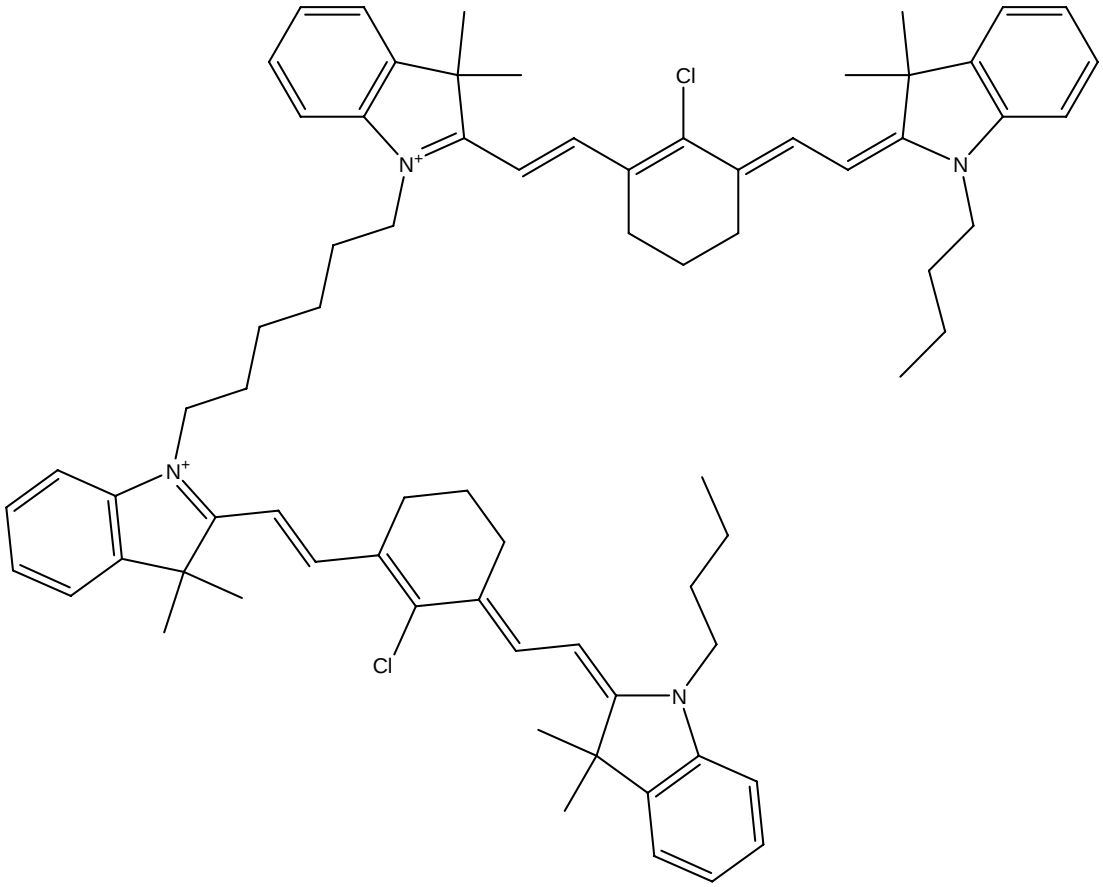

Figure 3.3. Structural simulation of bis-cyanine dye BHmC-6 using ChemDraw® Ultra 8.0 Software.

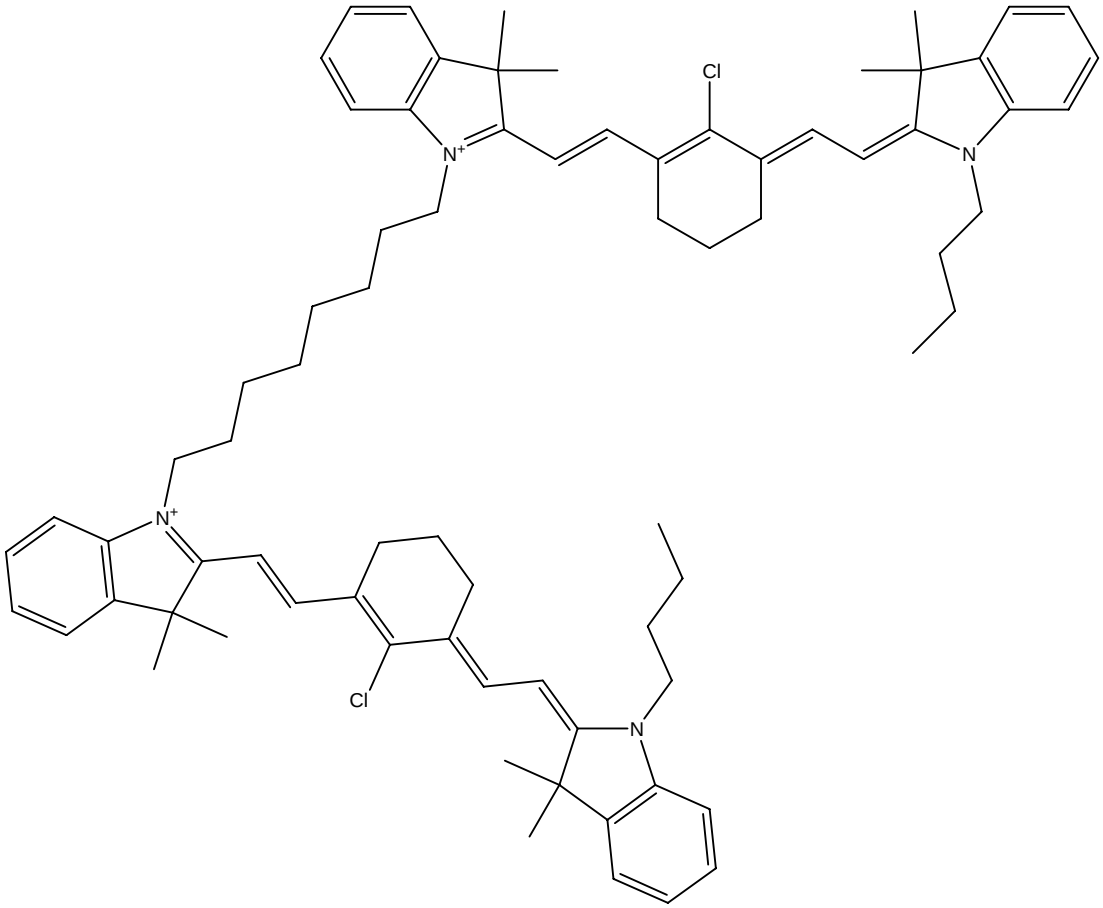

Figure 3.4. Structural simulation of bis-cyanine dye BHmC-8 using ChemDraw® Ultra 8.0 Software.

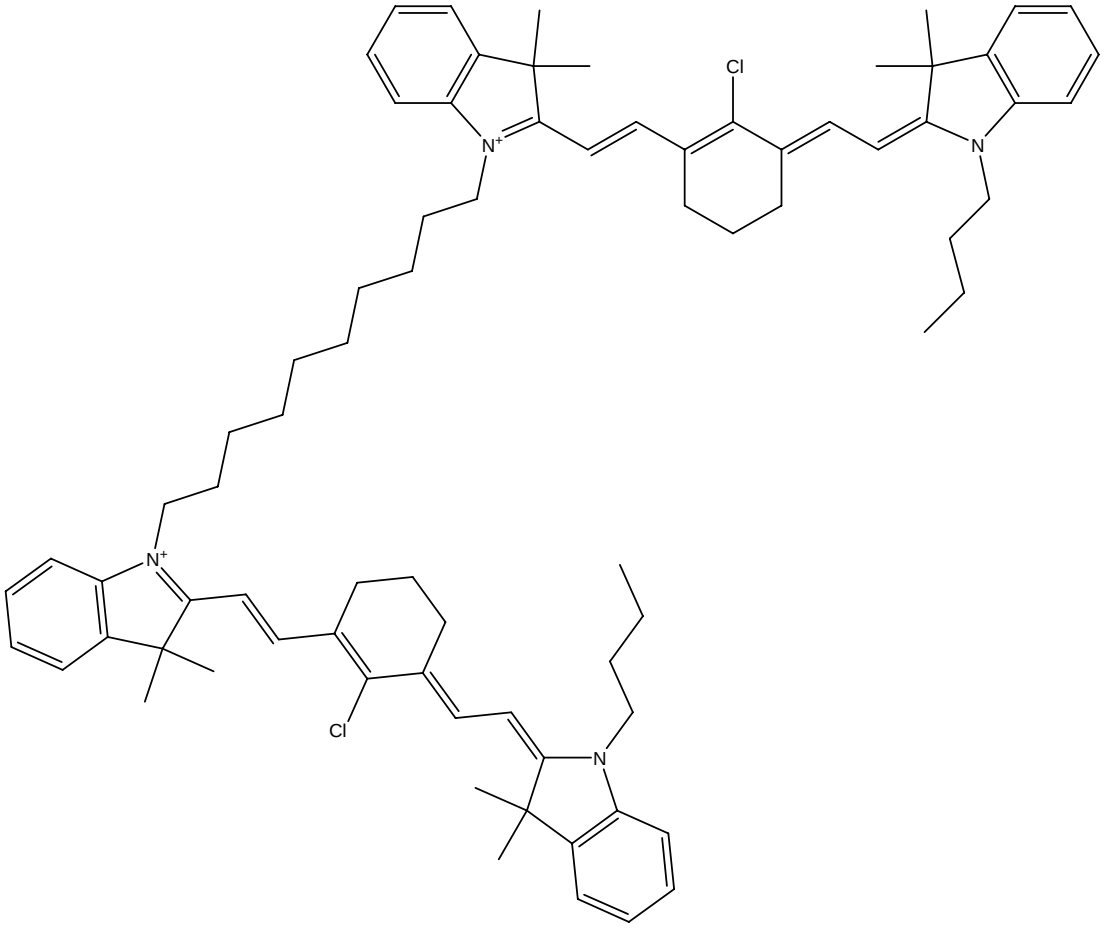

Figure 3.5. Structural simulation of bis-cyanine dye BHmC-10 using ChemDraw® Ultra 8.0 Software.

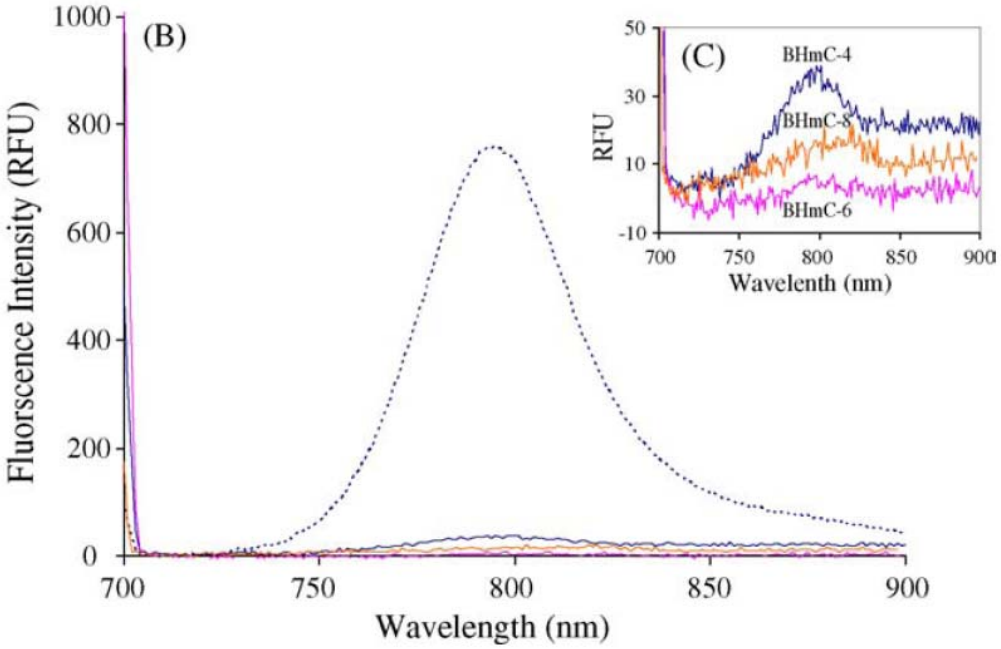

Figure 3.6. Fluorescence spectra of 10 μM IR780 and its bis-cyanine analogs in buffer alone. Adapted from reference 23.

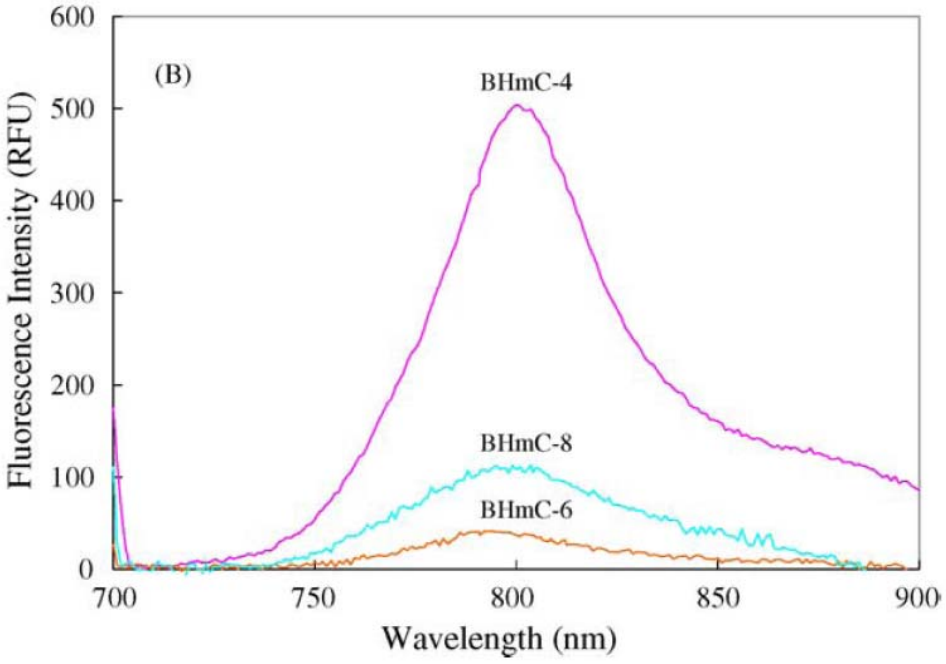

Figure 3.7. Fluorescence spectra of 10 μM IR780 and its bis-cyanine analogs with equimolar concentrations of HSA. Adapted from reference 23.

Project Aims

NIR Dyes Containing Ethylene Glycol. The properties of heptamethine carbocyanines are readily controlled by modest alterations to dye structure. For instance, poly(ethylene glycol) (PEG) substituents have been used to design hydrophilic chemical ion sensors.[26] Herein, bis(heptamethine cyanine) dyes containing poly(ethylene glycol) (PEG) spacers are evaluated for their potential as noncovalent labels. Noncovalently labeled protein complexes are typically less robust than their covalently labeled counterparts.[20] And the relative weakness of these complexes precludes their analysis by some separation methods such as HPLC or gas chromatography. Optical spectroscopy methods are an ideal alternative for the determination of HSA-NIR dye binding parameters. By using absorption, fluorescence, and fluorescence detected circular dichroism (FDCD) techniques, the binding interactions between three bis(heptamethines) and HSA are studied. The commercially available monomeric analogue, IR 783 is also examined. All dye structures used for this study are given in **Figures 3.8-3.11**

Naturally, the ethylene glycol linker allows for higher dye solubility in aqueous solution. Therefore, the appearance of dye intramolecular aggregation previously reported[23] is expected to be minimal. Furthermore the cationic BHmCs previously were believed to bind inside either hydrophobic binding cavities or on the negative surface of the globular protein surface. Contrastly, the use of anionic labels such as IR783 have been well reported in the literature.[1, 5, 9, 11, 12, 19, 27-30] These labels bind through electrostatic interaction in Site II. For this reason, the bis-cyanine OxoDyes could possibly have higher affinity for HSA than the cationic BHmCs previously reported. In addition, the hydrophobicity of the various linkers is not the only structural difference

between OxoDyes and BHmCs, the distance between chromophoric subunits is quite different as well. For BHmCs C-4, C-6, C-8, and C-10, the monomers are separated by 4, 6, 8, and 10 carbons respectively. Whereas, OxoDyes 1, 2, and 3 are separated by 5, 8, and 11 atoms, respectively.

The conformational flexibility of bis(heptamethines) makes chiroptical measurements ideal. Yet the same disadvantages observed in other absorption spectroscopy techniques, such as spectral overlap of biomolecules in the visible region, increased background interference, and larger analyte concentrations, are also encountered with absorption CD. As previously mentioned, it is imperative to closely monitor dye concentrations given the propensity of cyanines to aggregate in aqueous media. And although the PEG linkers should minimize intramolecular aggregation, the potential of these dyes to form intermolecular aggregates still remains. Therefore, FDCD is the more appropriate technique for detecting induced CD of cyanine fluorophores.

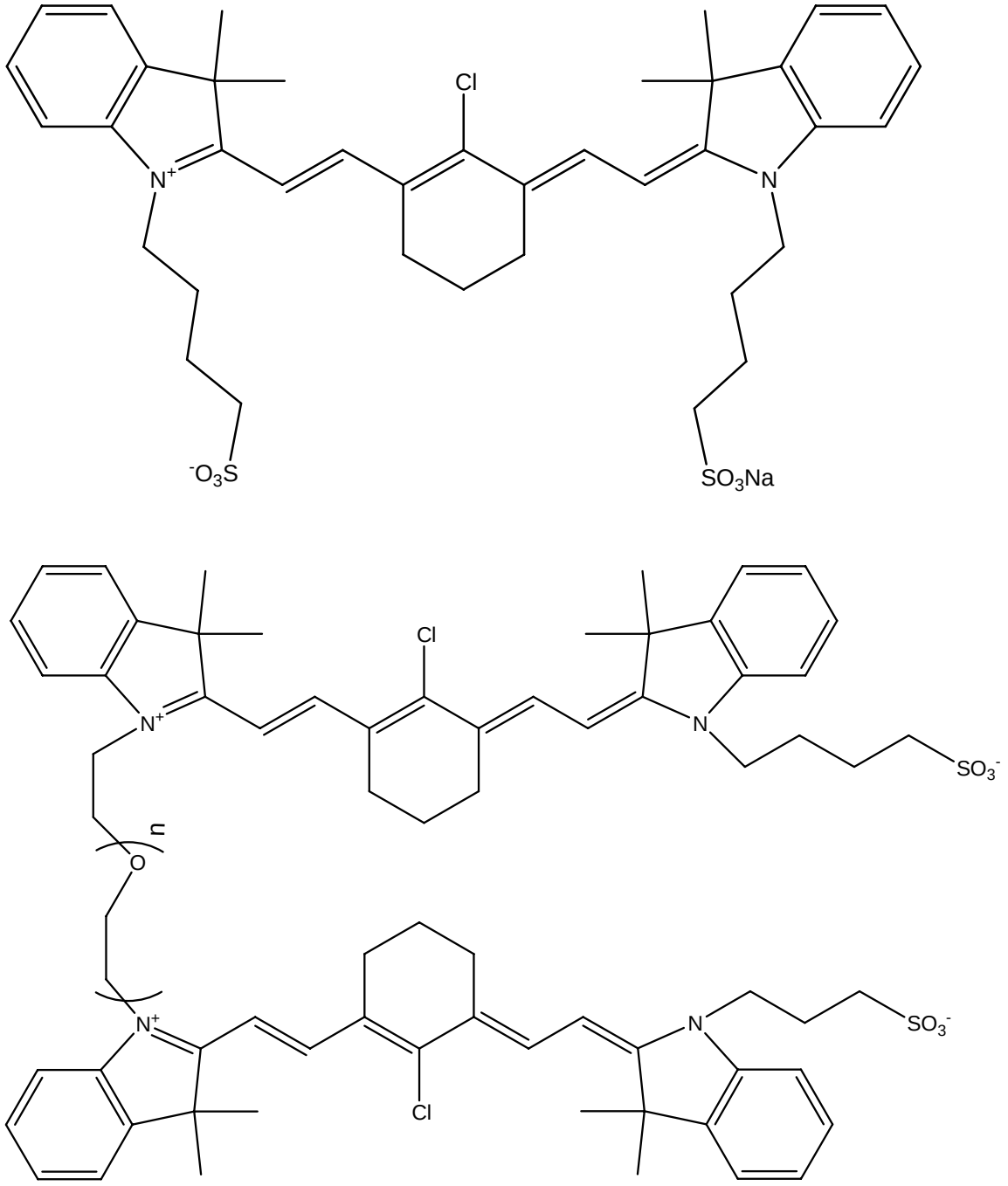

OxoDye1: n = 1; di(ethylene glycol)
OxoDye2: n = 2; tri(ethylene glycol)
OxoDye3: n = 3; tetra(ethylene glycol)

Figure 3.8. Chemical structure of 2-[2-[2-chloro-3-[2-[1,3-dihydro-3,3-dimethyl-1-(4-sulfobutyl)-2*H*-indol-2-ylidene]-ethylidene]-1-cyclohexen-1-yl]-ethenyl]-3,3-dimethyl-1-(4-sulfobutyl)-3*H*-indolium hydroxide, inner salt sodium salt (IR 783) and its bis analogs.

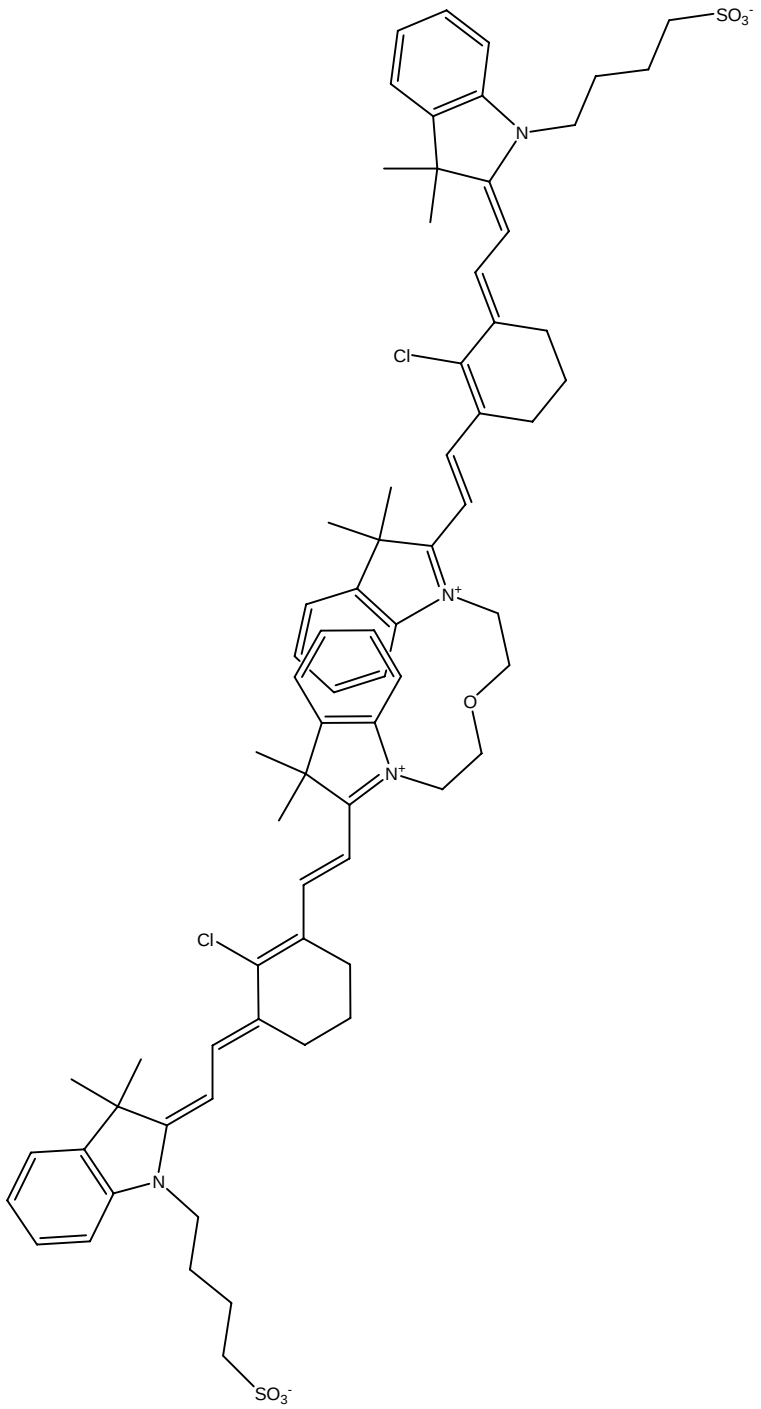

Figure 3.9. Structural simulation of di(ethylene glycol)[bis[2-[2-[2-chloro-3-[2-[1,3-dihydro-3,3-dimethyl-1-(4-sulfobutyl)-2*H*-indol-2-ylidene]-ethylidene]-1-cyclohexen-1-yl]-ethenyl]-3,3-dimethyl-1-(4-sulfobutyl)-3*H*-indolium hydroxide, inner salt (OxoDye1) using ChemDraw® Ultra 8.0 Software.

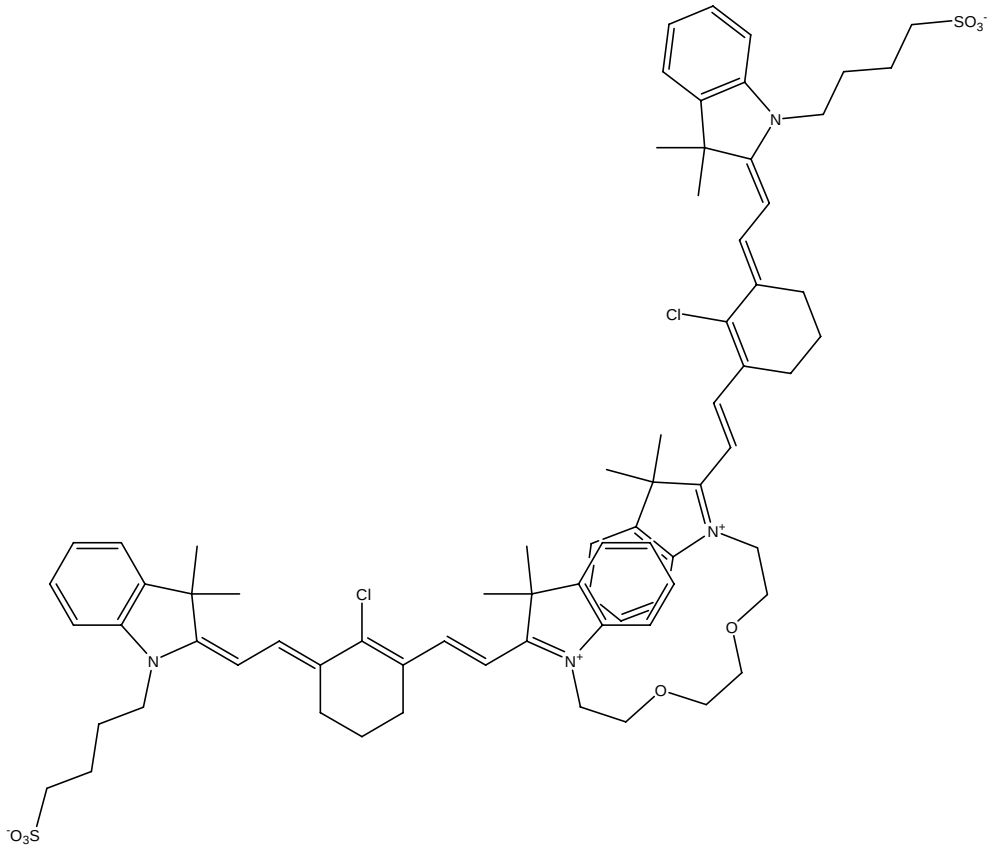

Figure 3.10. Structural simulation of tri(ethylene glycol)[bis[2-[2-[2-chloro-3-[2-[1,3-dihydro-3,3-dimethyl-1-(4-sulfobutyl)-2*H*-indol-2-ylidene]-ethylidene]-1-cyclohexen-1-yl]-ethenyl]-3,3-dimethyl-1-(4-sulfobutyl)-3*H*-indolium hydroxide, inner salt (OxoDye2) using ChemDraw® Ultra 8.0 Software.

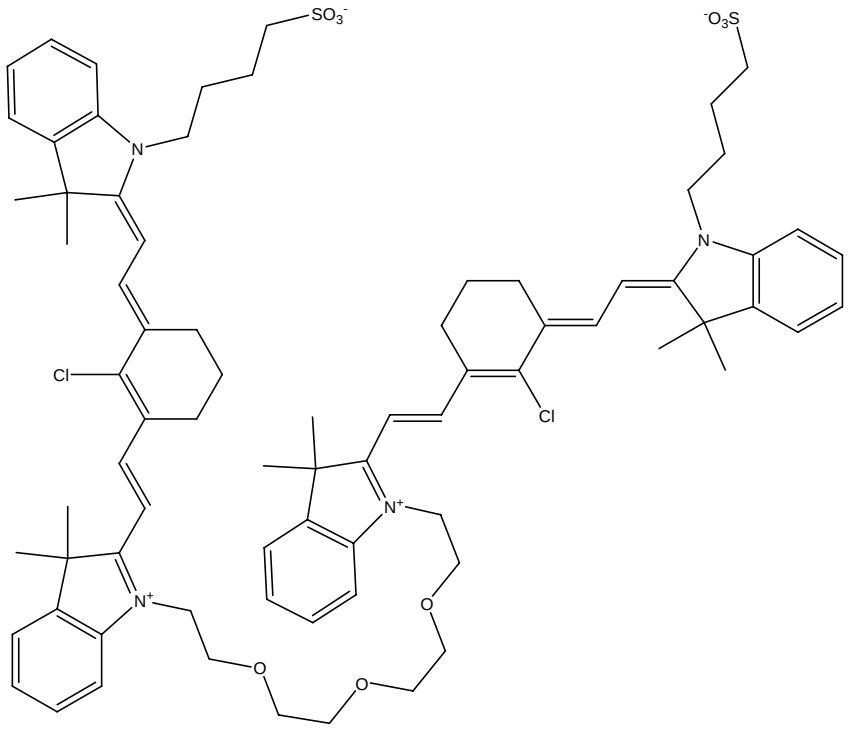

Figure 3.11. Structural simulation of (tetraethylene glycol)[bis[2-[2-[2-chloro-3-[2-[1,3-dihydro-3,3-dimethyl-1-(4-sulfobutyl)-2*H*-indol-2-ylidene]-ethylidene]-1-cyclohexen-1-yl]-ethenyl]-3,3-dimethyl-1-(4-sulfobutyl)-3*H*-indolium hydroxide, inner salt (OxoDye3) using ChemDraw® Ultra 8.0 Software.

Experimental

Instrumentation. Circular dichroism (CD) experiments were performed using a Jasco 710 spectropolarimeter (Easton, MD). The instrument was equipped with a 450 W Xenon Arc lamp, a 50 kHz piezo-elastic modulator, and a double prism monochromator. Fluorescence detected circular dichroism measurements were obtained using a model 309 FDCD attachment and a long wavelength (600 – 1100 nm) Hamamatsu R375 photomultiplier tube (PMT) positioned perpendicular to the excitation beam. CD measurements were performed with a short wavelength (200 – 800 nm) Hamamatsu R375 PMT positioned directly in front of the excitation beam. All CD and FDCD studies were performed in rectangular quartz cells containing 1 cm path lengths. The instrument was calibrated in the UV region using (+)-camphorsulfonic acid (CSA) as described in the literature.[31] Prior to the measurement of protein spectra, the CSA standard was scanned in a 1 cm quartz cell and the instrument's high tension (HT) voltage was adjusted to 190.4 ± 1 mdeg at 290.5 nm. Any subsequent far UV CD measurements for protein alone were done in the 200 to 300 nm region. Fluorescence detected circular dichroism (FDCD) measurements were performed only after the instrument was calibrated in the near infrared region (NIR). FDCD calibrations were performed as described by Konno using nickel sulfate.[32] The HT voltage was adjusted until molar CD values were approximately -101.2 ± at 718 nm and -100.7 ± 1 at 777 nm respectively. CSA was also used as a short wavelength standard for FDCD.[33] Absorption measurements were performed on the Perkin Elmer UV-Vis/NIR spectrophotometer (Norwalk, CT). The instrument was calibrated prior to measurement by using a quartz cell containing phosphate buffer as a blank. The blank was scanned in the 600 to 900 nm

region with a 1 nm step resolution. Baselines were recorded as the optically inactive fluorophores in CD cuvettes. Fluorescence measurements were performed on an ISS K2 Multifrequency Phase Fluorometer (Champaign, IL). The slit widths were 2 mm and the integration time was 3 sec. Step resolution between 0.2 and 0.5 nm/sec was used. All samples were excited with a commercial GaAlAs laser diode (Laser Max, Rochester, NY) at 690 nm, to avoid the potential inner filter effects of the high quantum yield of the dyes studied. All absorption and fluorescence measurements were taken with a 1 cm cuvette.

Materials. Human serum albumin (HSA) was provided as ≥ 96% fatty acid free from Sigma (St. Louis, MO). (+)-10-Ammonium camphorsulfonic acid was acquired from Jasco. Nickel sulfate hexahydrate and potassium sodium tartrate were purchased from Sigma. HPLC grade methanol was purchased from Fisher Scientific (Pittsburgh, PA). All other reagents were purchased from Sigma. Water was obtained from a Barnstead NANOpure Ultrapure Water System (Van Nuys, CA). Filtering was performed using Anotop® 25 Disposable Syringe Filters manufactured by Whatman (Clifton, NJ).

Sample Preparation. Buffer solutions of sodium dibasic phosphate were prepared at pH 7.4 in water at a concentration of 10 mM. Sodium phosphate buffer pH was adjusted using concentrated phosphoric acid. Stock solutions of HSA solutions were prepared at varying concentrations in sodium phosphate buffer. Protein concentrations were obtained by using UV-Vis spectroscopy. The absorbance of 1 mg/mL of HSA in buffer was 0.545 at 280 nm.[34] The molar absorption coefficient for human serum albumin at 280 nm was 3.63×10^4 $M^{-1}cm^{-1}$. NIR dyes were first solubilized in minimum

concentrations of methanol. Dyes were then further diluted to appropriate concentration with buffer. In most cases, the final total volume of methanol was not more than 3%. Varying concentrations of albumin were prepared in phosphate buffer. Protein and dye solutions were prepared by using equal volumes of both. Protein concentrations were varied using phosphate buffer. For the binding studies, the dye concentration was held constant and albumin concentrations were varied. Dye and protein solutions were prepared and allowed to incubate at room temperature for one hour. A 0.06% (w/v) stock solution of ammonium (+)-10-camphorsulfonate was prepared in water.[31] Stock solutions of nickel (II) sulfate (solution A) and potassium sodium tartrate (solution B) were prepared in water at 0.240 M and 0.360 M concentrations, respectively. The nickel (II) sulfate solution was prepared by mixing equal volumes of solutions A and B immediately preceding FDCD calibration.

Binding Data Analysis. The Scatchard model[35] for ligand binding was used to determine binding stoichiometry. Equation 1 describes the Scatchard plot relationship:

$$K_a = \frac{[PD]}{[P][D]} \tag{3.1}$$

K_a represents the association constant, [P] is the concentration of unoccupied binding sites, [D] represents the concentration of unbound dye, and [PD] is the concentration of the protein-dye complex or the concentration of binding sites occupied by the dye on protein. The total concentration of protein binding sites will be $[P]_T$ and will be related as followed

$$\nu = \frac{[PD]}{[P]_T} \tag{3.2}$$

where ν is the fraction of available binding sites of protein that are occupied.

Equation 2 is related to Equation 1 as followed,

$$\nu = \frac{nK_a[D]}{(1 + K_a[D])} \tag{3.3}$$

Alternately, Equations 2 and 3 can be related to the total dye concentration $[D]_T$ as followed

$$\nu' = \frac{[PD]}{[D]_T} = \frac{nK_a[P]}{(1 + K_a[P])} \tag{3.4}$$

Equation 4 is then written as its double reciprocal:

$$\frac{1}{\nu'} = \frac{1 + K_a[P]}{nK_a[P]} = \frac{1}{nK_a[P]} + 1 \tag{3.5}$$

When equation 4 is plotted, a binding stoichiometry of 1:1 protein to dye ratio is indicated by a straight line. Therefore, when $n \leq 1$, 1 or more dye molecules are bound to protein.

In this work, K_a values were calculated according to fluorescence data by using the modified equation: [28, 36]

$$\frac{1}{F_x - F_0} = \frac{1}{F_\infty - F_0} + \frac{1}{K_a[P]} \times \frac{1}{F_\infty - F_0} \tag{3.6}$$

where F_o, F_x, and F_∞ are the fluorescence intensities of monomeric dye molecules in the absence of HSA, in the presence of intermediate concentrations of HSA, and at a concentration of complete interaction, respectively. Rearranging Equation 6:

$$\frac{F_\infty - F_0}{F_x - F_0} = 1 + \frac{1}{K_a[P]} \tag{3.7}$$

And the binding constant is calculated from the plot of F_∞-F_0/F_x-F_0 against [P].

In addition, the use of an alternate equation has been reported for the determination of K_a from fluorescence intensity data:[21, 37-39]

$$\frac{1}{F} = \frac{1}{k[D]} + \frac{1}{k[D]K_a} \cdot \frac{1}{[P]} \quad (3.8)$$

which also takes into consideration the dye concentration, [D], and the constant, k, which is dependent on the instrument and quantum efficiency of the process. Both equations 3.7 and 3.8 were used to determine and compared the apparent binding constants of the bis(cyanines) bound to HSA.

Results and Discussion

ChemDraw® Simulations of Bis-cyanine OxoDyes

The structural simulations of the bis-cyanine OxoDyes were determined by ChemDraw® Ultra 8.0 Software (**Figure 3.9-3.11**). For OxoDye 1 (**Figure 3.9**), the benzene rings of the two monomeric subunits will only partially overlap. And it should be noted that the two benzene rings do not form π-π interactions due to the steric hindrance of the di(ethylene glycol) spacer. However, in the case of OxoDye2 (**Figure 3.10**), the tetra(ethylene glycol) linker allowed for a complete overlap of the benzene rings, to form π-π interactions which should exhibit intra-molecular H-aggregation bands. And the tetra(ethylene glycol) spacer should of OxoDye3 (**Figure 3.11**) displays no aggregation since the energy minimization of this long linker allows for no chromophoric overlap. It is also important to note that, according to the structural simulations of both the BHmCs and the bis-cyanine OxoDyes, the whole chromophoric units of the BHmCs will interact with each other. Yet, the poly(ethylene glycol) only allows for partial interactions of the chromophores.

Bis-cyanine OxoDyes in Buffer

As predicted by the ChemDraw® simulations, the monomeric IR 783 exhibits both dimeric and higher order aggregates (H-bands) in aqueous buffer caused by plane to plane stacking of the chromophoric rings (**Figure 3.12.**). Both OxoDye1 and OxoDye3 show no sign of either intramolecular or intermolecular aggregation in buffer. For OxoDye1, this is most likely due to the steric hindrance of the short di(ethylene glycol) bridge preventing complete "head to head" contact of the monomeric units. And although the tetra(ethylene glycol) spacer is longer, the orientation of its oxygens make intramolecular interactions unfavorable in OxoDye3 as well. In contrast, OxoDye2 exhibits H-aggregation bands similar to that of the monomeric analogue. These aggregation bands were attributed to intramolecular H-aggregation, or essentially, dimeric aggregates. Moreover, the monomeric band in OxoDye2 has less absorptivity in comparison to IR783; i.e., bis-OxoDye2 exists primarily as dimeric chromophores interacting with one another. Based on the orientation of the tri(ethylene glycol) linkage, the chromophoric units in OxoDye2 will have "head to head" interactions of an aromatic ring on each monomeric subunit, thus confirming intramolecular H-aggregation.

HSA Interactions of Bis-cyanine OxoDyes

Absorption Spectra. The absorbance consistently increased with increasing HSA concentration (**Figures 3.13**) for all three dimeric dyes and IR783. Specifically, the monomeric components of all four dyes appeared to have the most interaction with protein, exhibiting increased absorptivity in the presence of HSA. In the case of IR 783 (**Figure 3.14**), the H-aggregation band completely dissipates at high protein

concentrations. And according to the absorbance saturation curve (**Figure 3.15**), absorption for IR783 follows Beer's law up to HSA concentrations higher than 1:10 (5 x 10^{-6} M); i.e., IR783 is completely bound to HSA at this concentration.

Out of the three dyes studied, OxoDye1 appears to be the only dye exhibiting any aggregate bands in the visible region (**Figure 3.16**). The peak observed at 413 nm is attributed to intermolecular H-aggregates, since a band having decreased intensity with respect to the monomeric band is typically indicative of intermolecular H-aggregation.[40] So, although the monomeric subunits of bis-OxoDye1 never appear to come in contact with each other, whole bis-cyanine molecules interact with each other inside of HSA binding sites. Most notably, OxoDye1 exhibited a spectral shift with increasing protein concentration. This observation points to the appearance of a possible J-aggregate band.[27] A possible equilibrium of the dye at high HSA concentrations is given as followed:

$$\text{Dye-HSA} + \text{Dye} \leftrightarrow \text{Dye}_2\text{-HSA}$$

$$\text{Dye}_2\text{-HSA} + \text{Dye} \leftrightarrow \text{Dye}_3\text{-HSA}$$

etc.

$$\text{Dye}_{m-1}\text{–HSA} + \text{Dye} \leftrightarrow \text{Dye}_m\text{-HSA} \qquad (3.9)$$

Tatikolov and Costa reported a thiamonomethine dye which also formed J-aggregates while bound to HSA.[27]

In buffer alone and at 1:1 dye protein ratios, bis-OxoDye2 appears to behave similar to its monomeric counterpart IR 783 (**Figure 3.13**). However, at higher HSA concentrations, the intramolecular aggregation bands of the bis-cyanine seem quite different (**Figure 3.17**). At first, monomeric OxoDye2 interacting with HSA appears to

be the principal species present. Yet as dye:protein ratios increase, a distinct H-aggregate or dimeric band emerges and other aggregate-protein interactions become more evident. When examining **Figure 3.17**, it appears that OxoDye2 displayed not only intramolecular H-dimers, but also intermolecular H aggregates which were disrupted in the presence of increasing HSA. At high concentrations of protein, the dimeric band of OxoDye2 along with its monomeric band, meaning that the intramolecular interactions of the bis-cyanine are quite strong and not readily disrupted by HSA binding. It is quite possible that HSA binding will not disrupt the dye's intramolecular interactions, since HSA most likely interacts only electrostatically with a butyl substituent of the dye. In addition, Furthermore, the overall large size of the bis molecule makes it unable to fit in any known HSA binding sites.[1] And if hydrophobic interactions were the primary binding mode for the bis-dyes, dye self-association would be sterically hindered.

As mentioned previously, OxoDye3 exhibits no aggregation in buffer. Therefore, the monomeric subunits will interact solely with HSA and not with each other (**Figure 3.18**). When the dye-protein ratio reached 1:10, the monomeric band blue shifted from 780 to 791 nm. These types of spectral changes at high protein concentrations have been studied for their potential as protein aggregation sensors.[41, 42] In addition, at high dye:protein ratios, HSA appears to induce a small amount of H-aggregation in the visible region.

Fluorescence Spectra. The emission spectrum of IR 783 and bis-dyes in buffer is shown in **Figure 3.19**. Due to its high propensity to form hypsochromically shifted aggregates in solution, IR 783 has minimal fluorescence at low concentrations. Similarly, OxoDye2, the only bis-OxoDye exhibiting H-aggregation, also had relatively

low fluorescence. As previously mentioned, H-aggregates do not typically fluoresce because only transitions to the higher energy exciton state is allowed. Most notably, OxoDyes 1 and 3 exhibit strong fluorescence at 0.5 μM concentrations alone in buffer. The bis-dyes previously reported, containing flexible alkyl spacers, exhibited virtually little or no fluorescence in buffer alone at concentrations up to 10 μM due to the strong intramolecular H-aggregation exhibited by the dyes.[23] Thus, the high fluorescence intensity of OxoDye1 and OxoDye3 at such low concentrations further confirms the absence of either intramolecular or intermolecular H-aggregation in buffer alone.

The λ_{max} for all four dyes in buffer was approximately 800 nm. Alternately, when the dyes bind to 0.5 μM HSA, the λ_{max} shifts to 805 nm for IR 783 and OxoDyes 2 and 3 and 801 nm for OxoDye1 (**Figure 3.20**). As mentioned previously, OxoDye1 exhibits a H-aggregation band in the visible region, thereby causing the spectral shift. When bound to protein, OxoDye2 exhibits decreased fluorescence compared to IR 783, owing to the strong intramolecular interactions of HSA-bound OxoDye2.

The emission spectrum and corresponding saturation plot for IR783 is shown in **Figures 3.21 and 3.22** respectively. As was predicted by the absorbance saturation plot in **Figure 3.16,** IR 783 is completely bound in 5 μM HSA. Using Equations 3.7 and 3.8, the binding curve for IR 783 was also calculated (**Figure 3.23**) and the apparent association constant was determined to be between 1 and 2 x 10^5 M^{-1}. The binding constants of several anionic labels are reported in **Table 3.1**, including the value our laboratory derived from CE-LIF experimental data.[12] The emission spectra of OxoDye 1, OxoDye2, and OxoDye 3 in increasing concentrations of albumin are given in **Figures 3.24-3.26**. The increasing fluorescence with increasing protein concentration exhibited

by IR783 and OxoDye2 can further be attributed to the disruption of weakly associated intra- and intermolecular aggregates when bound to HSA. Most notably, the spectral shifts observed for OxoDyes1 and 3 in for the absorption spectra, are also observed in the fluorescence spectra. Since J-aggregation is often characterized by its fluorescence spectra, the broad fluorescence bands observed for these dyes could potentially be the product of the combined spectra of monomeric, as well as J-aggregate bands.

The concentration at which the OxoDyes are completely bound to HSA was not clearly defined by saturation plots. But F_{max} was approximated at protein concentrations at which Beer's law deviates. This concentration was similarly 5 x 10^{-6} M HSA for all three OxoDyes. Further increases in fluorescence may be attributed to binding modes higher than 1:1 dye to protein such as a protein binding to intermolecular dye aggregates. It has been reported that the biomolecular marker indocyanine green has a binding stoichiometry with HSA of ~1.5:1 dye:protein ratio.[5] Job's plot analysis should be performed on these dyes to confirm binding stoichiometry.

K_a values for IR 783 and its bis-cyanine analogues are listed in **Table 3.2**. Two different binding equations which make use of fluorescence data, Equations 3.7 and 3.8, were used to validate the reported data. The apparent results were quite interesting. As previously mentioned, the spectral properties of IR783 and OxoDye2 were analogous. This was also true for OxoDyes 1 and 3. For the monomeric analogue, IR 783, the results determined from the two binding equations were in rather good agreement. However, yet in the case of OxoDye 2, Equation 3.8 reports a binding constant which is weaker by an order of magnitude. Conversely, Equation 3.8 reported K_a values for OxoDyes 1 and 3 which were an order of magnitude higher in strength. This phenomenon can be explained

by the dye aggregation already observed. First, both equations are only valid in systems in which 1:1 binding is present. Therefore, if dyes are binding to more than one binding site, or if one protein- bound dye molecule also self-associates, the equations will not be accurate. The overall conformations of the OxoDyes are quite large and expansive compared to the BHmCs, therefore monomeric subunits remain quite capable of self-association outside of the HSA binding site. In addition, polymethine cyanine J-aggregates templated by HSA has also been reported.[43, 44] The spectral properties of IR783 and Although OxoDyes 1 and 3 do not appear to form intra-molecular aggregates, the appearance of a monomeric shift with increasing HSA concentration points to possible J-aggregation of protein-bound dyes. In the case of OxoDye2, binding data irregularities are explained by the strong intramolecular H-aggregates observed in **Figure 3.17**.

FDCD Measurements of HSA-OxoDyes Binding

Fluorescence detected CD was observed for the monomeric IR 783 and OxoDyes within the corresponding absorption bands (**Figures 3.27, 3.28**). **Figure 3.28** shows the titration of the monomeric IR 783 with increasing HSA concentration. Because induced CD requires three point interactions, the CD spectra confirm specific binding of the dyes within HSA binding sites, rather than nonspecific surface interactions. Likewise, the relatively large binding constants observed in **Table 3.2** are corroborated by the three-point binding of induced CD interactions. The FDCD band exhibited by the cyanine dyes were in good agreement with the spectral characteristics observed in the emission spectra. That is, OxoDye3 exhibited the largest induced fluorescence CD and IR 783 and OxoDye2 showed similar fluorescence CD bands in HSA. The H-dimer observed for

OxoDye2 bound to HSA appeared to have no effect of the binding interactions or induced CD. However, the small induced CD band observed for OxoDye1 may be related to the protein-dye aggregate complex detected in the visible region. Neither absorption CD nor FDCD measurements were performed in this region because H-aggregates do not typically fluorescence nor exhibit chirality for the reasons already mentioned. But visible absorption CD measurements should be carried out in the future to confirm this.

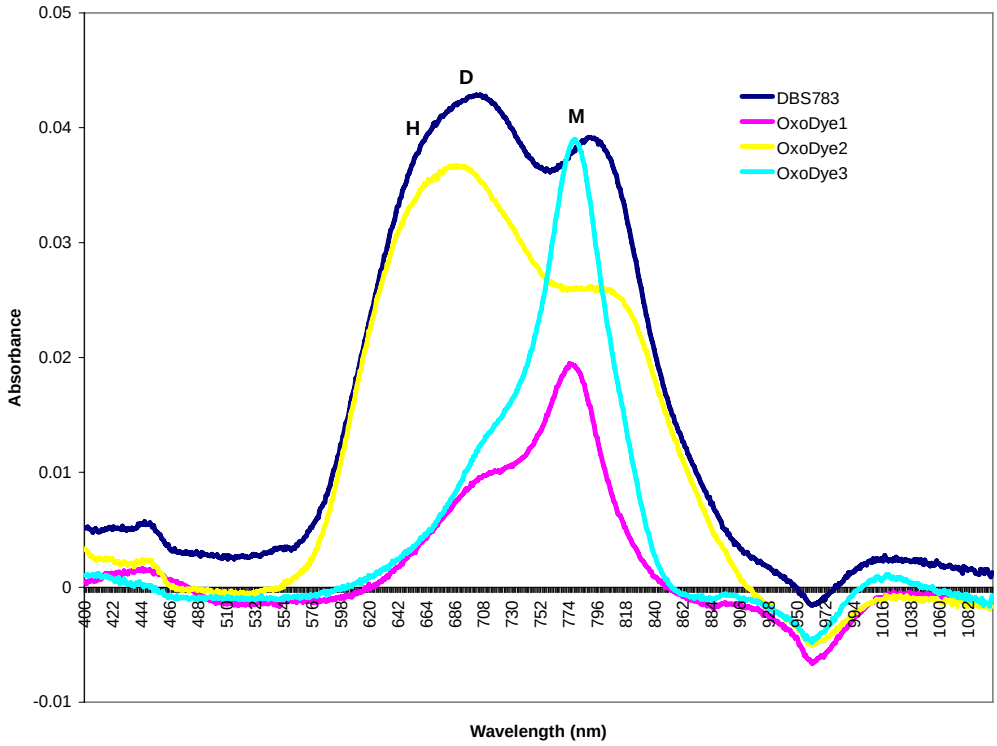

Figure 3.12. Absorption spectra of 0.5 μM IR 783, OxoDye1, OxoDye2, and OxoDye 3 in buffer.

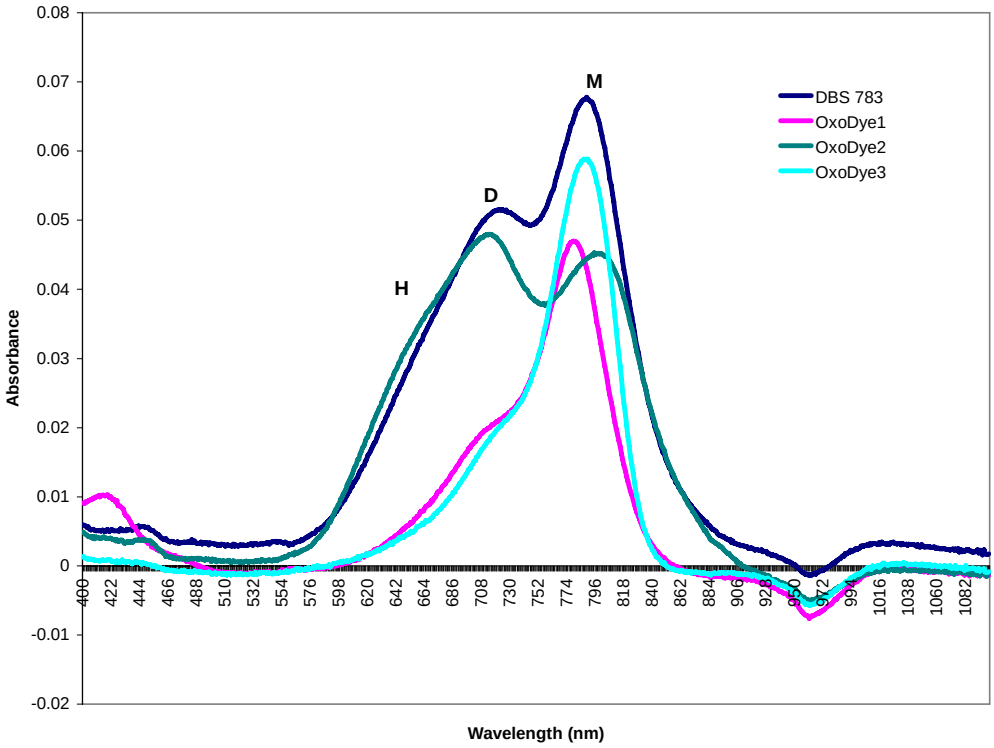

Figure 3.13. Absorption spectra of 0.5 μM IR 783, OxoDye1, OxoDye2, and OxoDye 3 in 0.5 μM HSA.

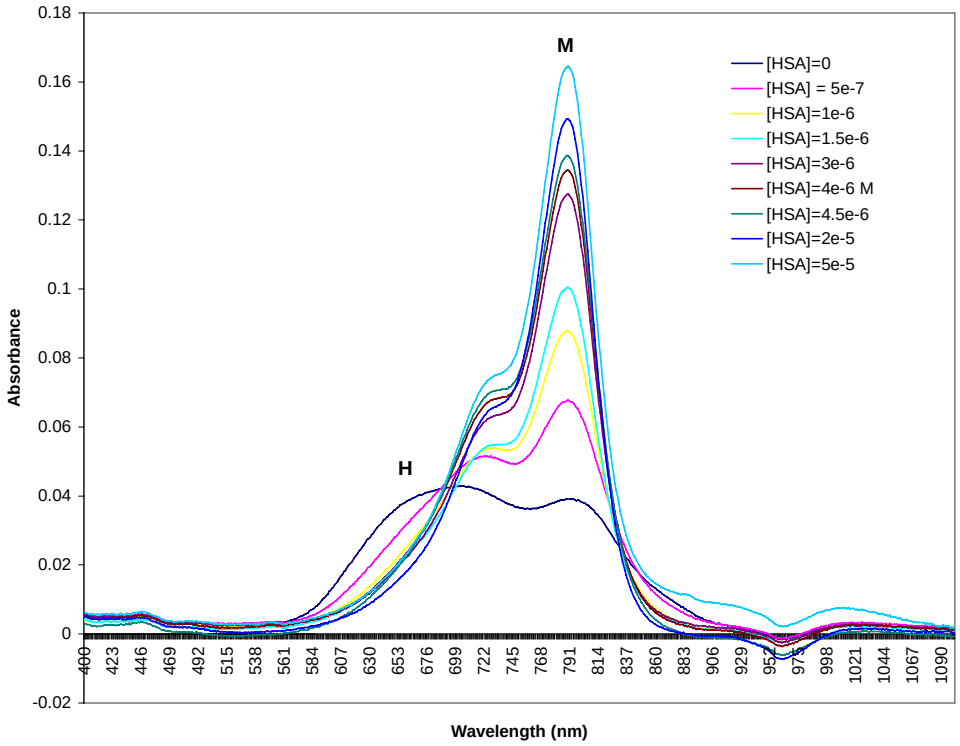

Figure 3.14. Absorption spectra of 0.5 μM IR 783 with various concentrations of HSA.

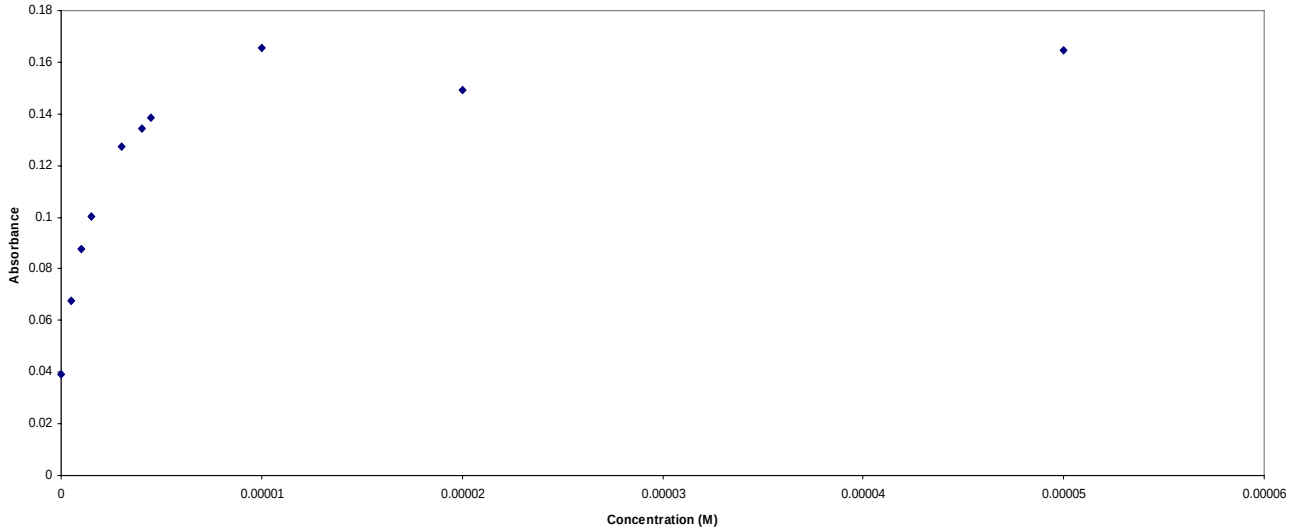

Figure 3.15. Absorption plot of 0.5 μM IR 783 with various concentrations of HSA.

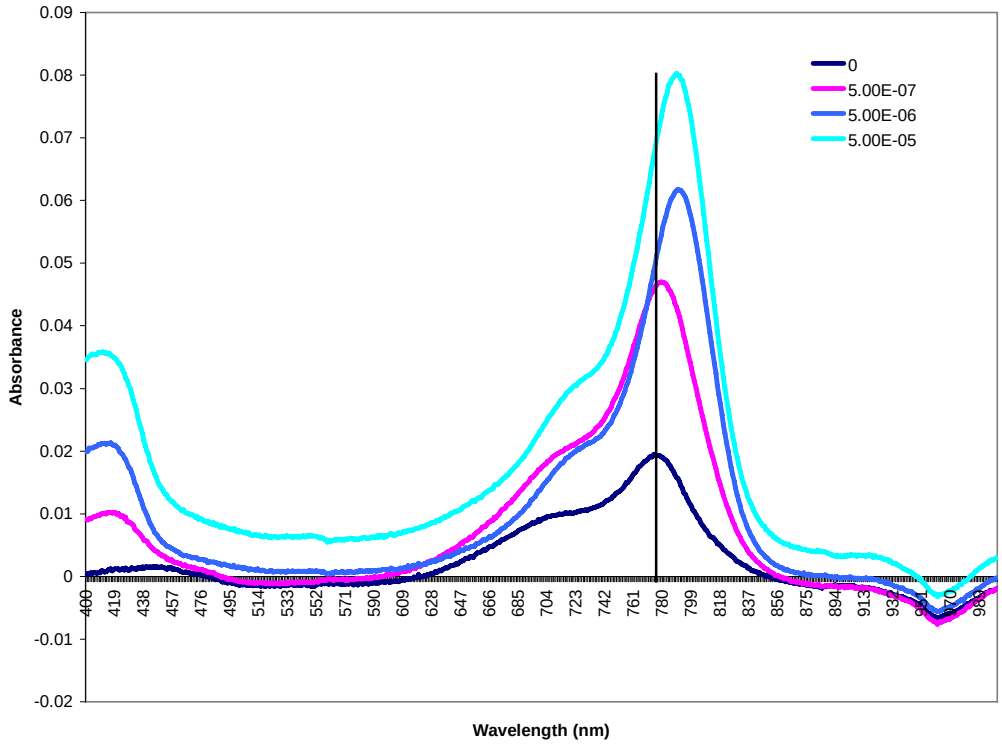

Figure 3.16. Absorption spectra of 0.5 μM OxoDye1 in 0, 0.5, 5, and 50 μM HSA.

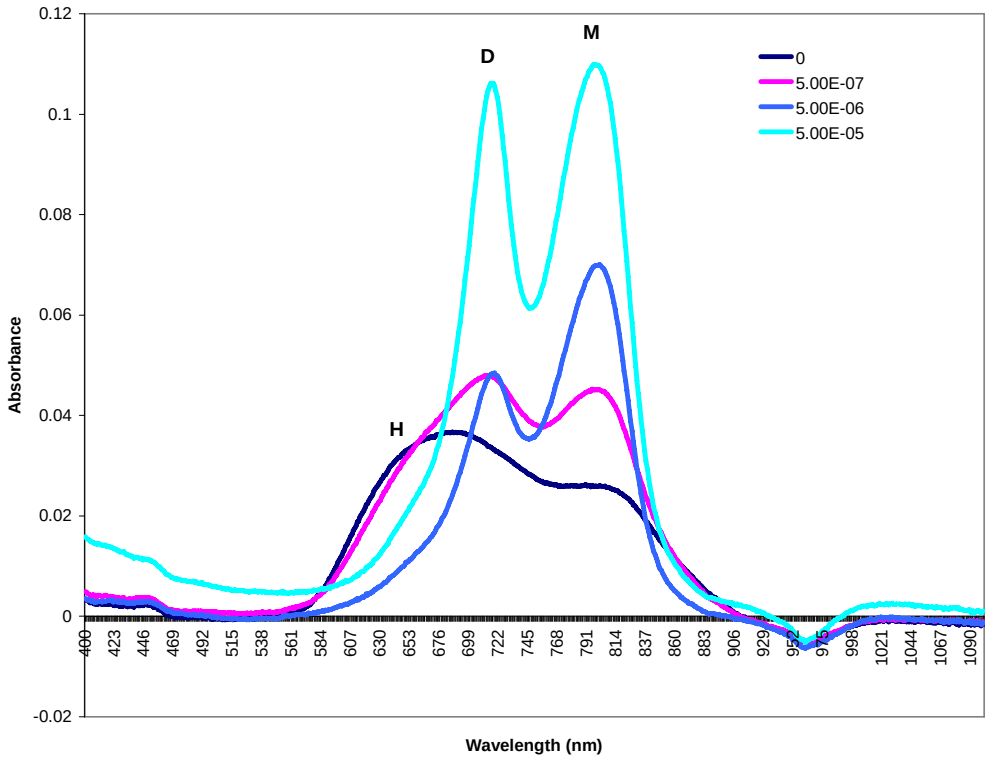

Figure 3.17. Absorption spectra of 0.5 μM OxoDye2 in 0, 0.5, 5, and 50 µM HSA.

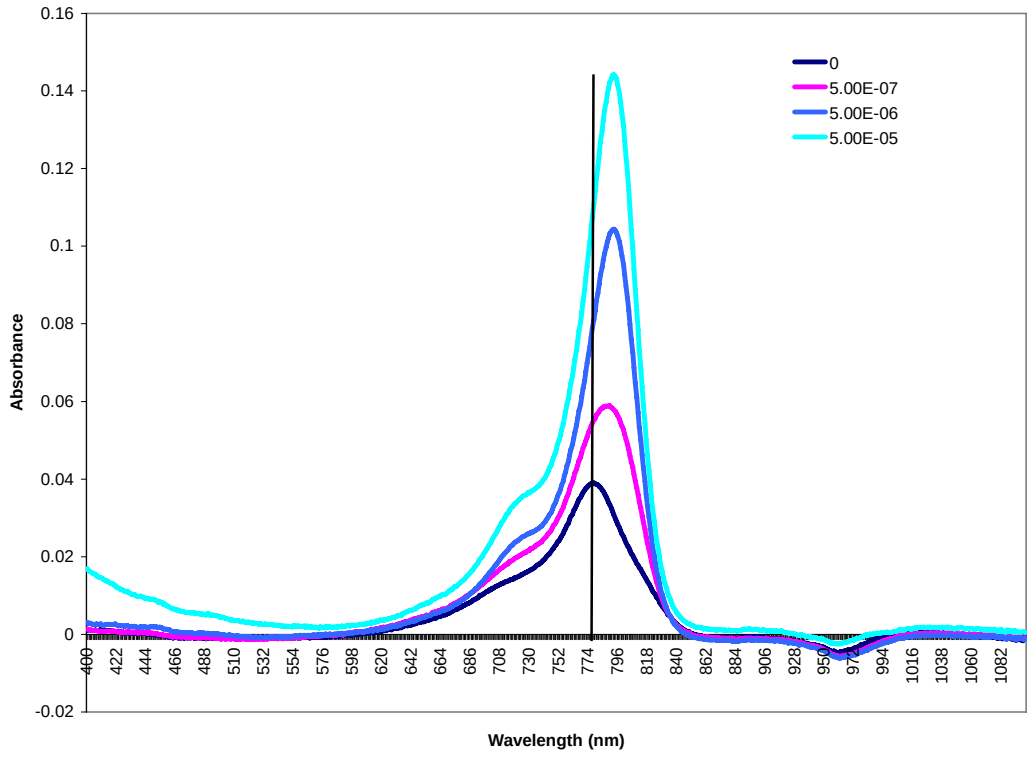

Figure 3.18. Absorption spectra of 0.5 μM OxoDye 3 in 0, 0.5, 5, and 50 µM HSA.

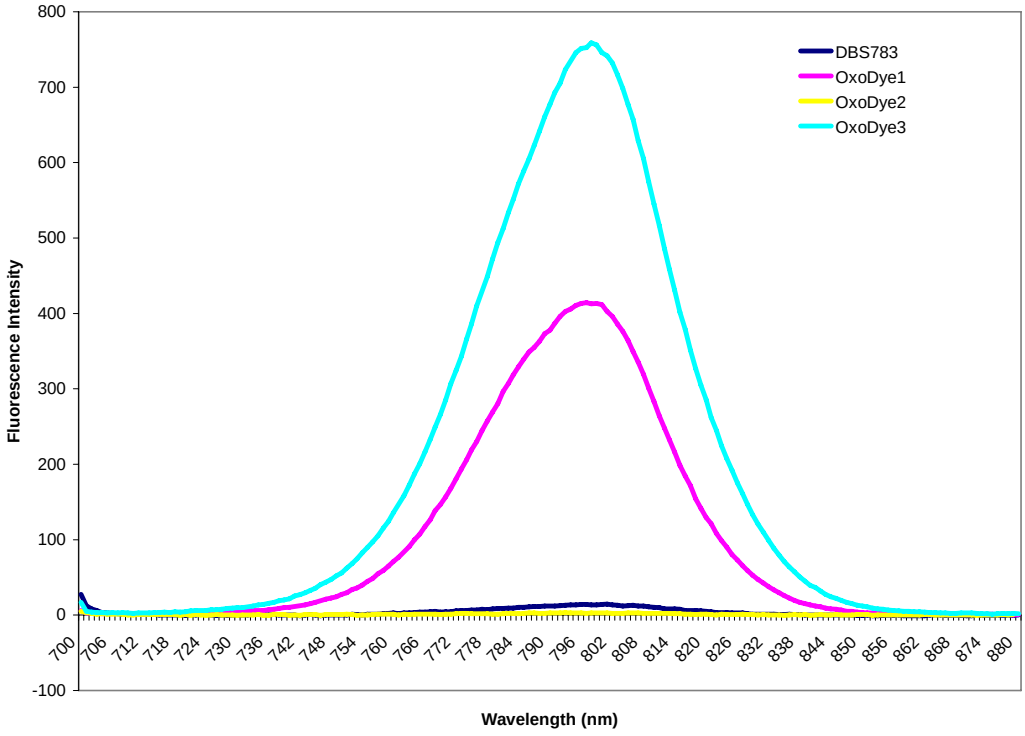

Figure 3.19. Fluorescence spectra of IR783, OxoDye1, OxoDye2, and OxoDye3 in 10mM phosphate buffer at 0.5 μM concentration.

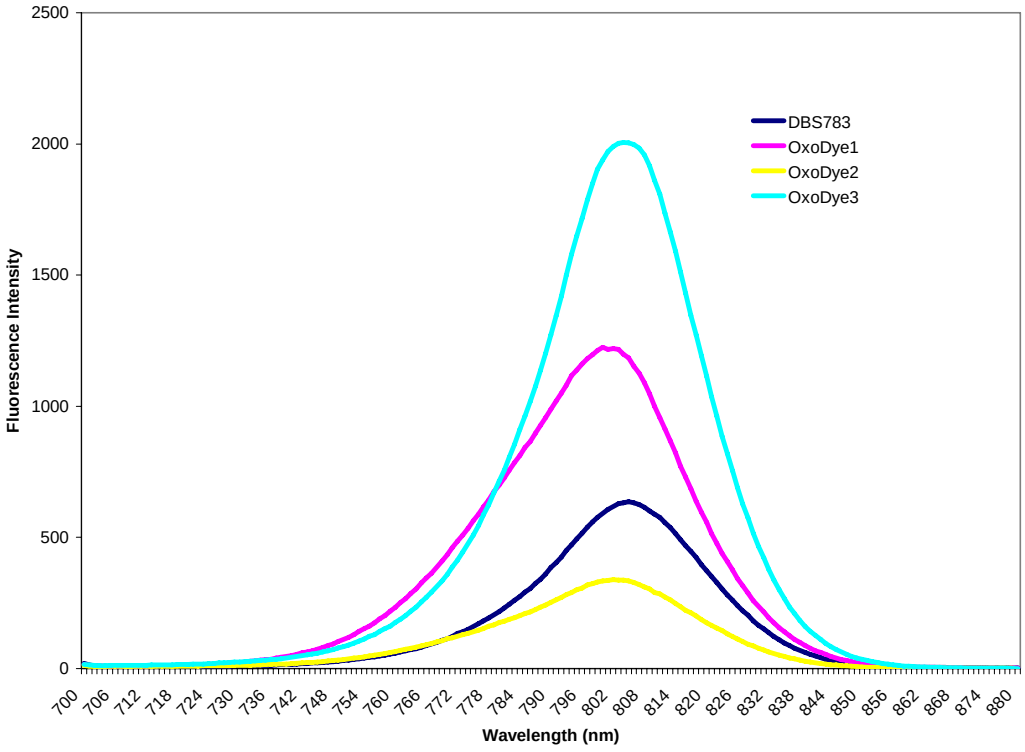

Figure 3.20. Fluorescence spectra of 0.5 μM IR 783, OxoDye1, OxoDye2, and OxoDye 3 in 0.5 μM HSA.

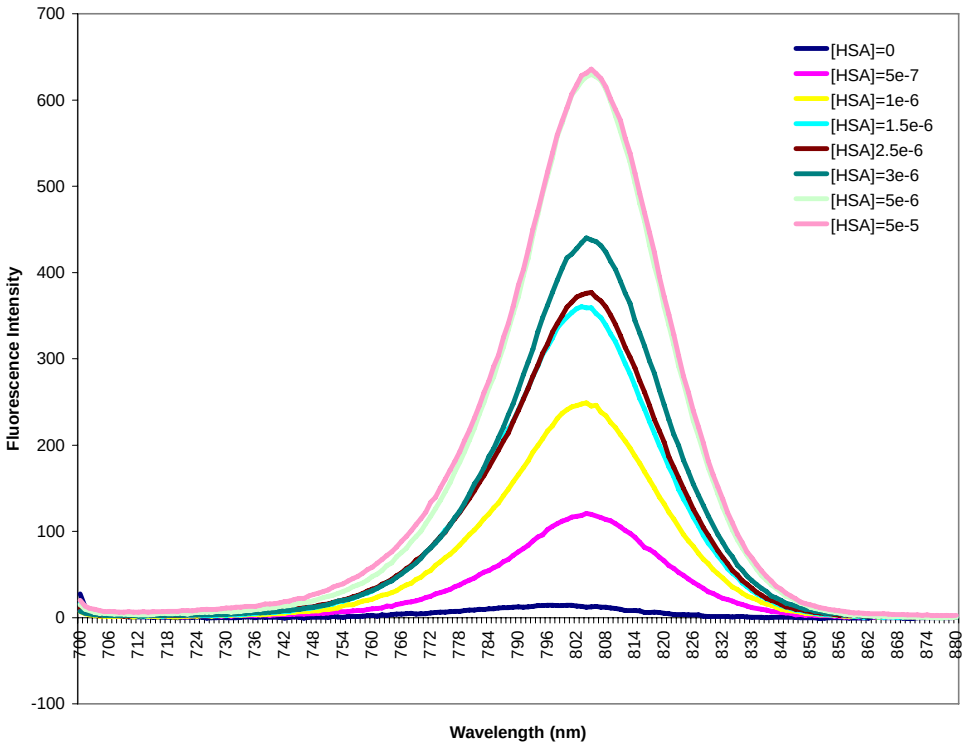

Figure 3.21. Fluorescence spectra of 0.5 μM IR783 in various HSA concentrations.

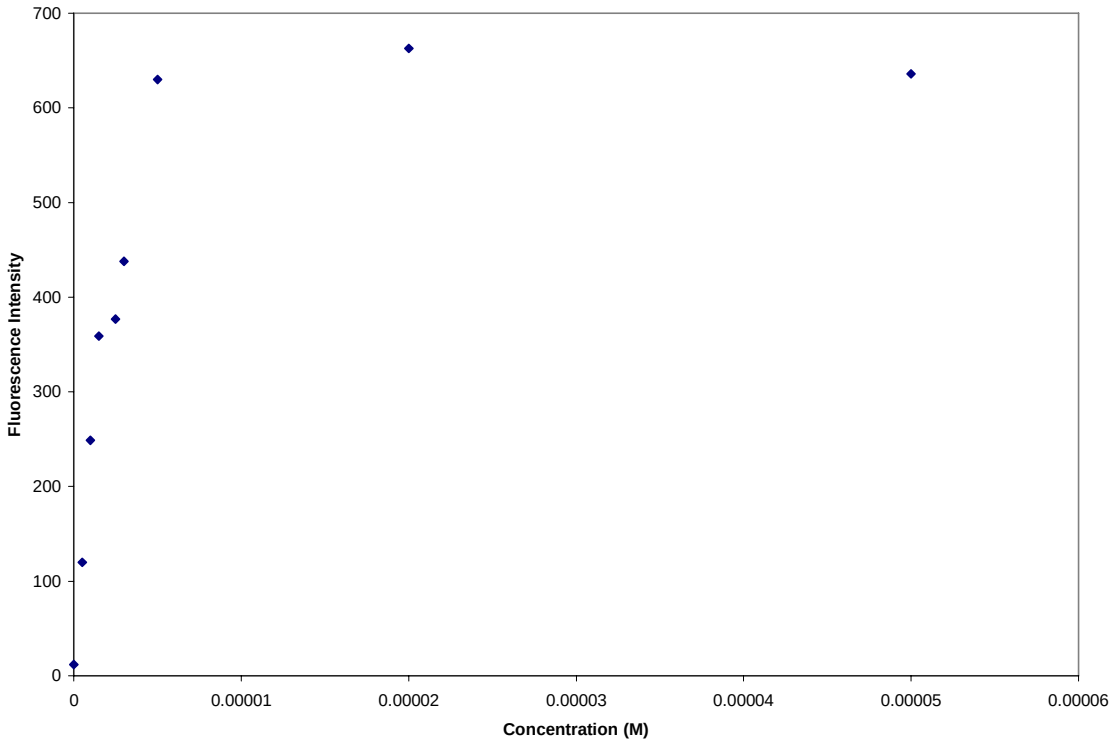

Figure 3.22. Fluorescence saturation curve 0.5 μM IR 783 in various HSA concentrations.

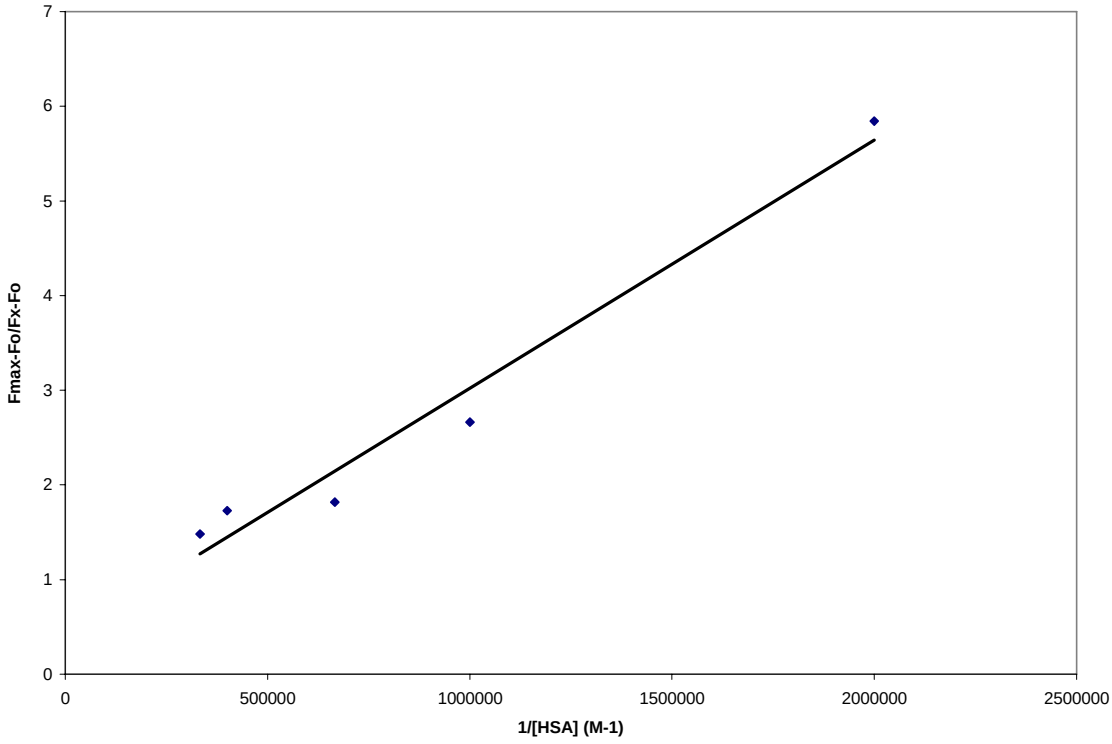

Figure 3.23. Fluorescence binding curve of 0.5 μM IR 783 in various HSA concentrations.

Table 3.1. Binding of HSA to Anionic Dyes

Compound	Association Constant, K (M^{-1})	n	Reference
Phenol red	2.8×10^4	1	Peters (1996)
Bromocresol green	7×10^5	3	Peters (1996)
Bromophenol blue	1.5×10^6	3	Peters (1996)
Methyl orange	2.2×10^3	---	Peters (1996)
Methyl red	2.2×10^5	---	Peters (1996)
Evans blue	4.0×10^5	14	Peters (1996)
Thiacarbocyanines	$8 \times 10^4 – 5 \times 10^7$	0.03-1.0	Tatikolov (2004)
Thiacarbocyanines	$7.7 \times 10^4 – 2.04 \times 10^5$	---	Zhang (2007)
Tetrasulfonated aluminum phthalocyanine	1.2×10^7	---	Filyasova (2001)
SQ1	1.4×10^6	---	Jisha (2006)
IR783	6.5×10^6	---	Sowell (2001)

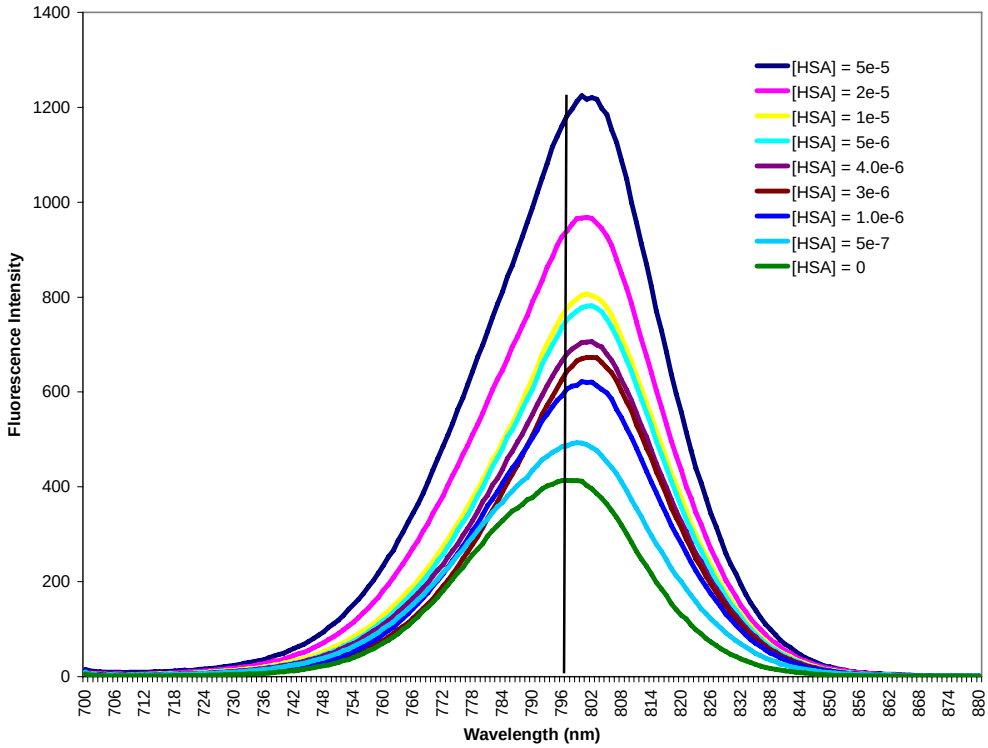

Figure 3.24. Emission spectrum of 0.5 μM OxoDye 1 in various HSA concentrations.

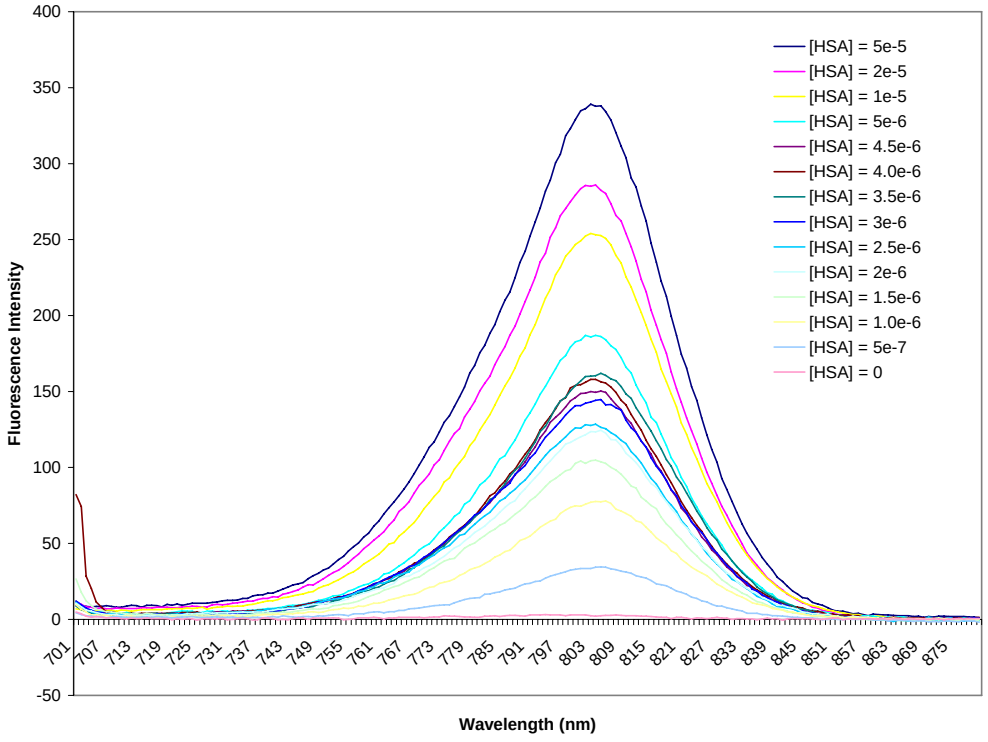

Figure 3.25. Emission spectrum of 0.5 μM OxoDye 2 in various HSA concentrations.

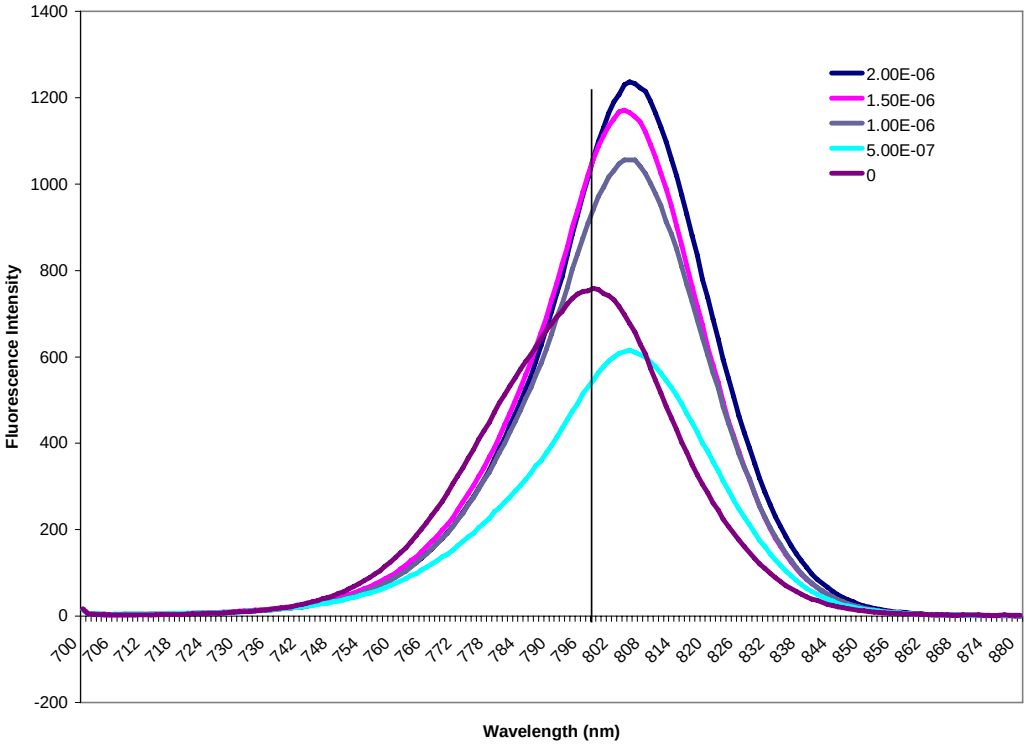

Figure 3.26. Emission spectrum of 0.5 μM OxoDye 3 in various HSA concentrations.

Table 3.2. Association constants of dimeric dyes

Dye[a]	Fluorescence		
	λ_{max}	K_a (M^{-1}) Eq.3.7	K_a (M^{-1}) Eq. 3.8
IR 783	805	1×10^5	2×10^5
OxoDye 1	801	3×10^5	3×10^6
OxoDye 2	805	6×10^5	6×10^4
OxoDye 3	805	7×10^5	2×10^6

[a] 0.5μM Dye in varying concentrations of HSA up to 5 μM.

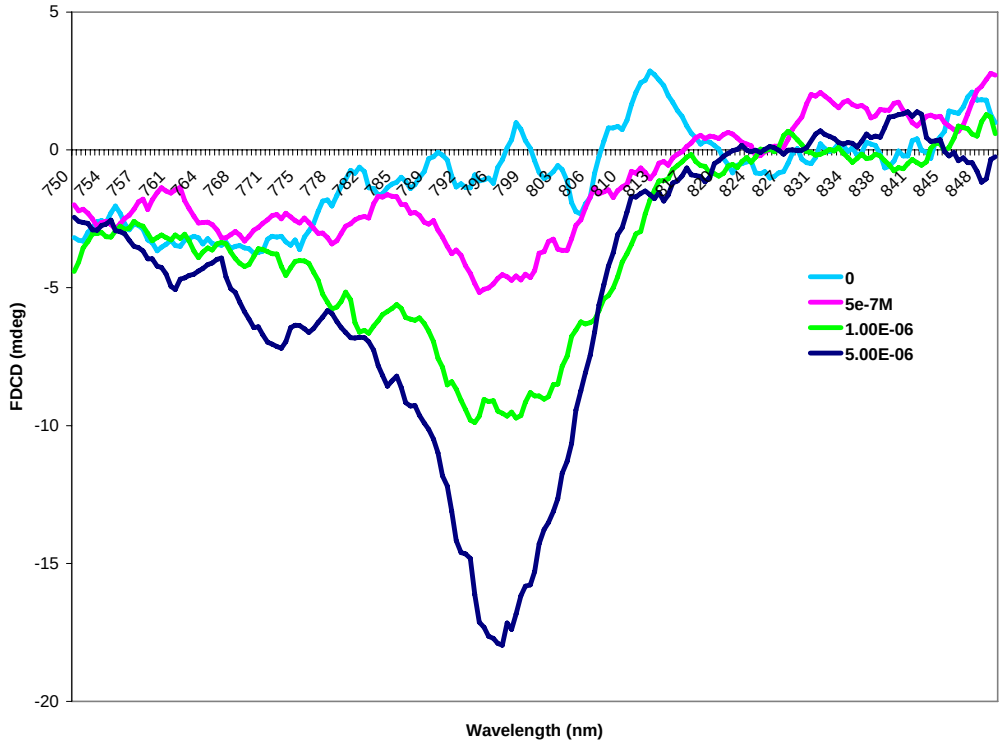

Figure 3.27. FDCD of 5 μM IR 783 in varying concentrations of HSA.

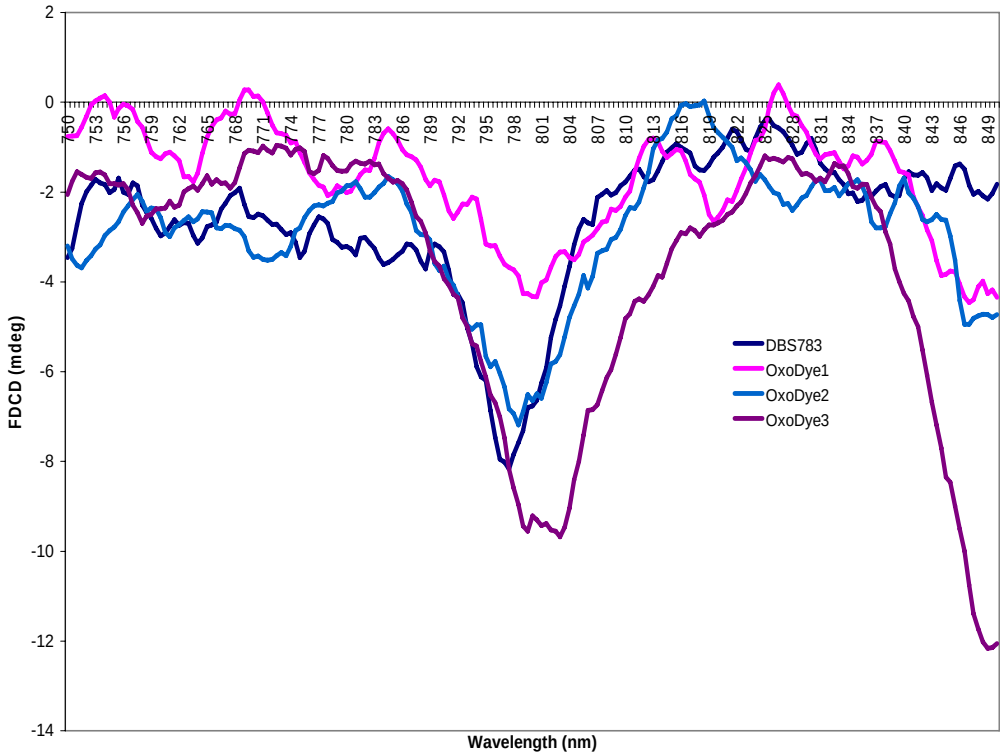

Figure 3.28. FDCD of 2 μM OxoDyes in 2 μM HSA.

Conclusions

The spectroscopic properties of three bis(heptamethine cyanine) dyes tethered by poly(ethylene glycol) linkers were investigated. Blue-shifted bands relative to the monomeric band were detected for both IR783 and OxoDye2 alone in 10 mM phosphate buffer in the near infrared region. These bands were attributed to both intramolecular (OxoDye2) and intermolecular H-aggregates (IR783 and OxoDye2). This assignment was further confirmed by the absence of fluorescence within these bands. In the presence of HSA, the aggregate bands of IR 783 dissipated. The intermolecular H-aggregation bands exhibited by OxoDye2 also decreased with increasing HSA concentration, and a very distinct intramolecular dimer H-band also appeared as well. Thus, monomeric IR 783 and bis-cyanine dimers both predominantly interact with HSA binding sites.

No aggregation was detected with OxoDyes1 and 3 alone in 10 mM phosphate and both exhibited fluorescence alone in aqueous. However, in the presence of HSA, OxoDye1 monomeric NIR bands, as well as a newly formed visible H-aggregate band, increased in absorptivity with increasing HSA concentration, owing to protein complex formation. Monomeric subunits bound to HSA appeared to be the primary binding modality for OxoDye3.

All four dyes exhibited enhanced fluorescence in the presence of HSA. And the dyes appeared to be completely bound at HSA concentrations of 5 μM. However, it should be noted that OxoDyes1 and 3 may not be useful as noncovalent labels, since they exhibit such high fluorescence alone in solution, making it potentially difficult to distinguish protein bound dye from unbound dye in solution. Yet, when the labels are used in conjunction with chiroptical methods such as FDCD or circularly polarized

luminescence (CPL), specific binding of the biomarkers inside protein binding sites can be confirmed. Induced FDCD of protein bound NIR labels was detected for all four labels.

Using fluorescence data, binding constants were determined to be between 1 and 7 x 10^5 M^{-1} for the bis(heptamethine) dyes and the monomeric analogue. However, additional calculations must be conducted to verify that the appropriate binding equation was used. Furthermore, Scatchard and Hill analysis using FDCD measurements could potentially be useful in validating binding association values. However, it is important to also note that CD and FDCD measurements provide a single, overall average of the optical activity of a probe. The dye molecule could be bound to multiple sites on a macromolecule and information about individual local binding sites cannot be determined. Yet, these limitations are typically overcome by performing lifetime-resolved FDCD, quenching, denaturation, or competitive binding studies.[14, 45-47]

In future work, competitive assays involving known Site I and Site II ligands, such as dansylamide[19] and dansylproline respectively, should be performed to confirm the specific binding sites of the OxoDyes. Moreover, OxoDyes should also be investigated for their potential as ion or pH sensors.[26, 48] The hydrophilic nature of the PEG spacer will likely be spectroscopically sensitive to changes in polarity, ionic strength, or pH. Changes in these parameters may also cause the dyes to exhibit intrinsic CD. Tanaka et al has reported intrinsic Cotton effects for (1R,2R)-trans-cyclohexanediol bis(6-methoxy-2-naphthoate) in both CD and FDCD measurements owing to the intramolecular interactions oxygen lone pairs.[49]

References

1. Peters Jr., T., *All About Albumin: Biochemistry, Genetics, and Medical Applications*. Academic: San Diego, 1996.

2. Shang, L.; Jiang, X.; Dong, S., In vitro study on the binding of neutral red to bovine serum albumin by molecular spectroscopy. *Journal of Photochemistry and Photobiology A: Chemistry* **2006,** 184, 93-97.

3. Desmettre, T.; Mordon, S.; Devoisselle, J. M.; Soulie, S.; Mitchell, V., Indocyanine Green-Dye (Icg) Enhanced Laser-Absorption - Role of Albumin on Selectivity and Reproducibility of Photocoagulation. *Investigative Ophthalmology & Visual Science* **1995,** 36, (4), S244-S244.

4. Haller, M.; Brechtelsbauer, H.; Finsterer, U.; Forst, H.; Bein, T.; Briegel, J.; Peter, K., Determination of Plasma-Volume with Indocyanine Green in Humans. *Anaesthesist* **1992,** 41, (3), 115-120.

5. Moody, E. D.; Viskari, P. J.; Colyer, C. L., Non-covalent labeling of human serum albumin with indocyanine green: a study by capillary electrophoresis with diode laser-induced fluorescence detection. *Journal of Chromatography B* **1999,** 729, (1-2), 55-64.

6. McCorquodale, E. M.; Colyer, C. L., Indocyanine green as a noncovalent, pseudofluorogenic label for protein determination by capillary electrophoresis. *Electrophoresis* **2001,** 22, (12), 2403-2408.

7. Orth, V. H.; Rehm, M.; Haller, M.; Thiel, M.; Finsterer, U., Blood volume measurement - state-of-the-art. *Anaesthesist* **2001,** 50, (8), 562-568.

8. Andrews-Wilberforce, D.; Patonay, G., Investigation of near-infrared laser dye albumin complexes. *Spectrochimica Acta Part a-Molecular and Biomolecular Spectroscopy* **1990,** 46A, (8), 1153-1162.

9. Li, W. R.; Wang, H.; Yang, T. X.; Zhang, H. S., Direct spectrometric determination of proteins in body fluids using a near-infrared cyanine dye. *Analytical and Bioanalytical Chemistry* **2003,** 377, (2), 350-355.

10. Zheng, H.; Zhu, C. Q.; Li, D. H.; Chen, Q. Y.; Yang, H. H.; Chen, X. L.; Xu, J. G., A novel method for the determination of total protein in human serum by near infrared fluorescence recovery. *Fresenius J Anal Chem* **2000,** 368, (5), 511-5.

11. Sowell, J.; Parihar, R.; Patonay, G., Capillary electrophoresis-based immunoassay for insulin antibodies with near-infrared laser induced fluorescence detection. *J Chromatogr B Biomed Sci Appl* **2001,** 752, (1), 1-8.

12. Sowell, J.; Mason, J. C.; Strekowski, L.; Patonay, G., Binding constant determination of drugs toward subdomain IIIA of human serum albumin by near-infrared dye-displacement capillary electrophoresis. *Electrophoresis* **2001,** 22, (12), 2512-2517.

13. Sophianopoulos, A. J.; Lipowski, J.; Narayanan, N.; Patonay, G., Association of near-infrared dyes with bovine serum albumin. *Applied Spectroscopy* **1997,** 51, (10), 1511-1515.

14. Meadows, F.; Narayanan, N.; Patonay, G., Determination of protein-dye association by near infrared fluorescence-detected circular dichroism. *Talanta* **2000,** 50, 1149-1155.

15. Sugio, S.; Kashima, A.; Mochizuki, S.; Noda, M.; Kobayashi, K., Crystal structure of human serum albumin at 2.5 A resolution. *Protein Engineering* **1999,** 12, 439-446.

16. He, X. M.; Carter, D. C., Atomic structure and chemistry of human serum albumin. *Nature (London, United Kingdom)* **1992,** 358, 209-215.

17. Sudlow, G.; Birkett, D.; Wade, D., *Molecular Pharmacology* **1975,** 11, 824-832.

18. Sudlow, G.; Birkett, D.; Wade, D., *Molecular Pharmacology* **1976,** 12, 1052-1061.

19. Jisha, V. S.; Arun, K. T.; Hariharan, M.; Ramaiah, D., Site-selective binding and dual mode recognition of serum albumin by a squaraine dye. *Journal of the American Chemical Society* **2006,** 128, (18), 6024-6025.

20. Colyer, C. L., Noncovalent labeling of proteins in capillary electrophoresis with laser-induced fluorescence detection. *Cell Biochemistry and Biophysics* **2000,** 33, 323-337.

21. Nakazumi, H.; Ohta, T.; Etoh, H.; Uno, T.; Colyer, C. L.; Hyodo, Y.; Yagi, S., Near-infrared luminescent bis-squaraine dyes linked by a thiophene or pyrene spacer for noncovalent protein labeling. *Synthetic Metals* **2005,** 153, (1-3), 33-36.

22. Tarazi, L.; Narayanan, N.; Patonay, G., Investigation of the spectral properties of a squarylium near-infrared dye and its complexation with Fe(III) and Co(II) ions. *Microchemical Journal* **2000,** 64, (3), 247-256.

23. Kim, J. S.; Kodagahally, R.; Strekowski, L.; Patonay, G., A study of intramolecular H-complexes of novel bis(heptamethine cyanine) dyes. *Talanta* **2005,** 67, (5), 947-954.

24. Patonay, G.; Strekowski, L.; Kim, J. S.; Henary, M., The increasing role of NIR fluorescence spectroscopy in bioanalytical chemistry *NIR news* **2007,** 18, (3), 7-9.

25. Patonay, G.; Kim, J. S.; Kodagahally, R.; Strekowski, L., Spectroscopic study of a novel bis(heptamethine cyanine) dye and its interaction with human serum albumin. *Appl Spectrosc* **2005,** 59, (5), 682-90.

26. Ellis, A. L.; Mason, J. C.; Lee, H. W.; Strekowski, L.; Patonay, G.; Choi, H.; Yang, J. J., Design, synthesis, and characterization of a calcium-sensitive near infrared dye. *Talanta* **2002,** 56, (6), 1099-1107.

27. Tatikolov, A. S.; Costa, S. M. B., Complexation of polymethine dyes with human serum albumin: a spectroscopic study. *Biophysical Chemistry* **2004,** 107, (1), 33-49.

28. Zhang, Y. Z.; Du, H. Y.; Tang, Y. L.; Xu, G. Z.; Yan, W. P., Spectroscopic investigation on the interaction of J-aggregate with human serum albumin. *Biophysical Chemistry* **2007,** 128, (2-3), 197-203.

29. Wang, H.; Li, W. R.; Guo, X. F.; Zhang, H. S., Spectrophotometric determination of total protein in serum using a novel near-infrared cyanine dye, 5,5 '-dicarboxy-1,1 '-disulfobutyl-3,3,3 ',3 '-tetramethylindotricarbocyanine. *Analytical and Bioanalytical Chemistry* **2007,** 387, (8), 2857-2862.

30. Filyasova, A. I.; Kudelina, I. A.; Feofanov, A. V., A spectoscopic study of the interaction of tetrasulfonated aluminum phthalocyanine with human serum albumin. *Journal of Molecular Structure* **2001,** 565-566, 173-176.

31. Cassim, J.; Yang, J., A computerized calibration of the circular dichrometer. *Biochemistry* **1969,** 8, (5), 1947-1951.

32. Konno, T.; Meguro, H.; Murakami, T.; Hatano, M., A critical study on circular dichroism measurement in longer side of visible region. *Chemistry Letters* **1981,** 10, (7), 953-956.

33. Chen, G.; Yang, J., Two-Point Calibration of Circular Dichrometer with d-10-Camphorsulfonic Acid. *Analytical Letters* **1977,** 10, 1195-1207.

34. Beaven, G.; Chen, S.; d'Albis, A.; Gratzer, W., A spectroscopic study of the haemin--human-serum-albumin system. *European Journal of Biochemistry* **1974,** 41, (3), 539-546.

35. Scatchard, G., The attractions of proteins for small molecules and ions. *Ann. N. Y. Acad. Sci.* **1949,** 51, 660-672.

36. Healy, E. F., Quantitative determination of DNA-ligand binding using fluorescence spectroscopy. *Journal of Chemical Education* **2007,** 84, (8), 1304-1307.

37. Tarazi, L.; George, A.; Patonay, G.; Strekowski, L., Spectral characterization of a novel near-infrared cyanine dye: a study of its complexation with metal ions. *Talanta* **1998,** 46, (6), 1413-1424.

38. Patonay, G.; Antoine, M. D.; Devanathan, S.; Strekowski, L., Near-Infrared Probe for Determination of Solvent Hydrophobicity. *Applied Spectroscopy* **1991,** 45, (3), 457-461.

39. Casay, G. A.; Shealy, D. B.; Patonay, G., In *Topics in Fluorescence Spectroscopy*, Lakowicz, J. R., Ed. Plenum: New York, 1994.

40. Mishra, A.; Behera, R. K.; Behera, P. K.; Mishra, B. K.; Behera, G. B., Cyanines During the 1990s: A Review. *Chemical Reviews* **2000,** 100, (6), 1973-2011.

41. Hermel, H.; De Rossi, U., Examination of polypeptide beta-sheet structure in solutions and thin layers: determination of the concentration and the 'critical aggregation concentration' using a cyanine dye as sensor. *International Journal of Biological Macromolecules* **1997,** 21, (3), 263-70.

42. Hermel, H.; Holtje, H. D.; Bergemann, S.; De Rossi, U.; Kriwanek, J., Band-shifting through polypeptide beta-sheet structures in the cyanine UV-Vis spectrum. *Biochimica et Biophysica Acta* **1995,** 1252, (1), 79-86.

43. Zhang, Y. Z.; Xiang, J. F.; Tang, Y. L.; Xu, G. Z.; Yan, W. P., Chiral transformation of achiral J-aggregates of a cyanine dye templated by human serum albumin. *Chemphyschem* **2007,** 8, (2), 224-226.

44. Tatikolov, A. S.; Panova, I. G., A spectroscopic study on the interaction of polymethine dyes with collagens. *High Energy Chemistry* **2005,** 39, (4), 232-236.

45. Lobenstine, E. W.; Schaefer, W. C.; Turner, D. H., Fluorescence Detected Circular Dichroism of Proteins with Single Fluorescent Tryptophans. *Journal of the American Chemical Society* **1981,** 103, 4936-4940.

46. Thomas, M. P.; Patonay, G.; Warner, I. M., Selective Monitoring of Stern-Volmer Quenching of Chiral Molecules Via Fluorescence Detected Circular Dichroism. *Analytical Letters* **1987,** 20, (5), 717-730.

47. Thomas, M. P.; Patonay, G.; Warner, I. M., Fluorescence-Detected Circular Dichroism in Biochemical Analysis. In *Luminescence Techniques in Chemical and Biochemical Analysis*, Baeyens, W. R. G.; Keukeleire, D. D.; Korkidis, K., Eds. Marcel Kekker Inc: New York, 1991; pp 421-451.

48. Mason, J. C.; Patonay, G.; Strekowski, L., A new pH-sensitive near-infrared chromophore. *Heterocyclic Communications* **1997,** 3, (5), 409-411.

49. Tanaka, K.; Pescitelli, G.; Nakanishi, K.; Berova, N., Fluorescence detected exciton coupled circular dichroism: Development of new fluorescent reporter groups for structural studies. *Monatshefte Fur Chemie* **2005,** 136, (3), 367-395.

CHAPTER IV

Identifying Geometrically Selective NIR Sensors

Introduction

The deposition of amyloid fibrils is known to result in tissue damage and degeneration.[1] At least 16 types of human diseases have been associated with amyloid fibrils. Amyloid diseases are characterized by the abnormal self-assembly and deposition of proteins into insoluble aggregates.[2] Examples of amyloid diseases include Alzheimer's disease, Parkinson's disease, spongioform encephalopathies, and type II diabetes. Although nearly 20 different amyloidogenic precursors are currently known, the detailed mechanism of the fibril formation is still not fully understood. Amyloid, as well as prion, related diseases are often referred to as conformational diseases. Conformational diseases involve conformational changes leading to misfolded proteins forming β secondary structures. These β structures have a high propensity to aggregate and become resistant to proteolysis.[3] Studies involving conformational disease have contributed to the idea that biological function is mediated by changes in protein conformation. This principle has inspired the use of countless research in which the detection of protein secondary structures is the primary goal.

Amyloid Fibril Structure. The German physician Virchow first used the term "amyloid" in 1854, believing that the iodine-containing component was starch.[3] Normally soluble proteins or peptides can misfold and polymerize into amyloid fibrils.[1]

Many authors report in the literature proteins forming amyloid-like fibrils, yet not associated with any disease. For example, α-helical proteins such as myoglobin or apo-cytochrome *c* have formed fibrils under certain conditions.

In solution, amyloid fibrils cannot be observed, although pre-amyloidogenic conformation can be observed in crystalline form. Fibrils are often indefinite in length, unbranched, and repetitive in structure. Using electron microscopy at low resolution, all amyloid deposits can be characterized as bundles of straight, rigid fibrils ranging in width from 60 to 130 Å and in length from 1000 to 16000 Å. Fibrils are made up of cross-β structures which contain β strands running perpendicular to the long axis of the fibrils and *β*-sheets extending parallel to this axis. The structural hierarchy of amyloid fibrils is depicted in **Figure 4.1**. Every 115 or 250 Å, the β strands also form a β helical twist to change the direction of the strands. There are two major types of fibrils known. Type 1 fibrils are very thin and are formed from only one fibril. Type 2 fibrils are formed from two filaments intertwined, usually with a diameter from 80 to 130 Å. In addition to a fibrillar component, a nonfibrillar component of has also been observed including serum amyloid protein, heparin sulfate proteoglycans, and apolipoprotein E.

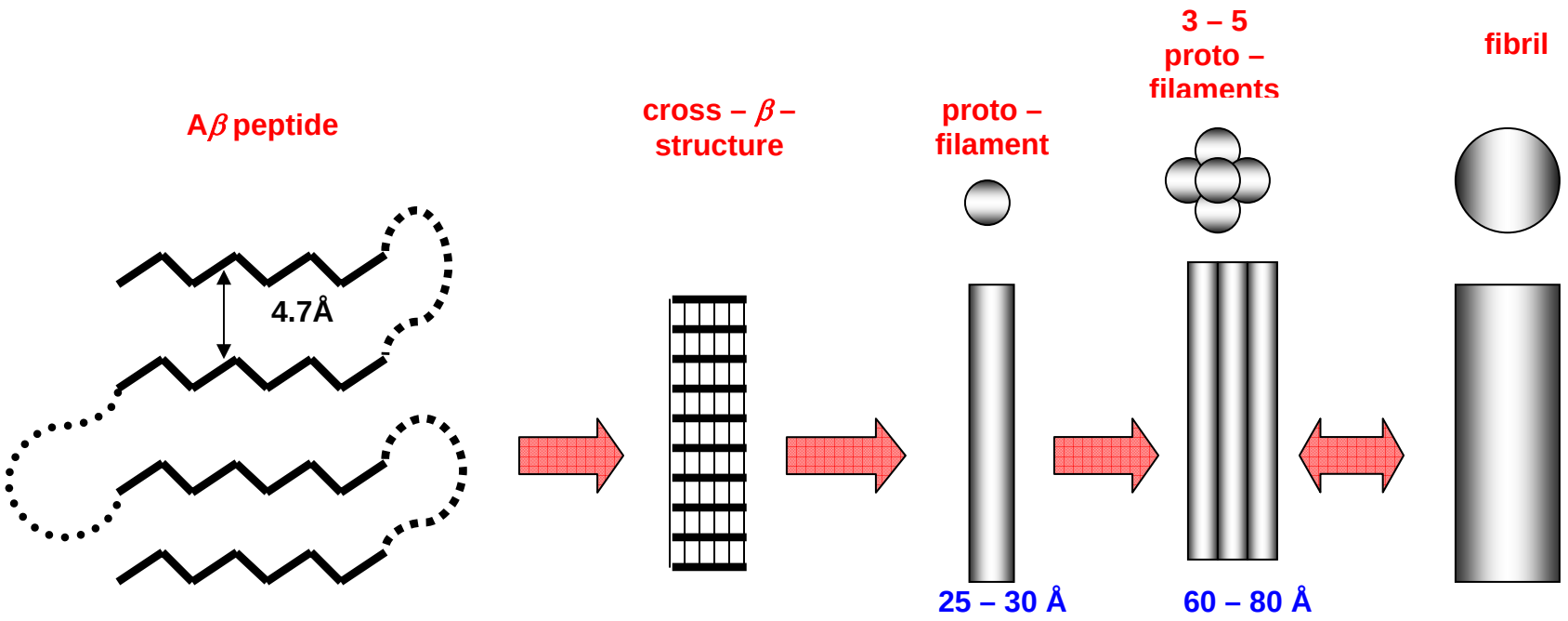

Figure 4.1. The structural hierarchy of amyloid fibrils which contain β-sheets oriented first parallel, then perpendicular to the axis of the fibril to form a cross-β structure. Several cross-β structures then make up the protofilament and several protofilaments make up the amyloid fibril visualized in electron microscopy.

Determining Congo Red Specificity to Amyloid Fibrils. One of the primary techniques for diagnosing amyloid fibrils *ex vivo*, is treatment with the histological dye Congo red (CR). In the presence of amyloid fibrils, CR exhibits a characteristic birefringence under polarized light.[3] There many drawbacks to using CR for amyloid identification. First, this assay must be carried out under extreme conditions such as 50-80% ethanol, high salt, and alkaline pH.[4] In addition, CR does not bind specifically to amyloid, and binding to collagen fibers or cytoskeletal proteins may result in false-positive observations. In lieu of the birefringence assay, filtration based assays using CR have been used. Amyloid samples are treated with CR and then passed through a 0.2 μm filter. The concentration of free CR dye remaining is then measured to determine the amount of CR bound to amyloid.[5] However, the filtration assays cannot detect CR bound to soluble monomers or oligomers not retained by the filter.

In an effort to determine the specificity of CR binding, Khurana and co-workers have used induced CD assays of CR in the presence of native proteins, partially folded protein conformations, and amyloid fibrils using protein from various structural classes.[4] The group wanted to determine if CR was an appropriate secondary structural probe for amyloid assays. Experiments were performed at low concentrations of fibrils because it is known that CR yields red precipitates with amyloids at high concentrations. Khurana et al report that amyloid fibrils have more binding sites available for CR than the native proteins. This work also determined that all classes of secondary structures bind to CR. Thus, CR binding is not restricted to only the predominantly β-sheet conformation of amyloid fibrils. Because this data conflicts with previously reported studies, Khurana and co-workers used FTIR to confirm that CR binding did not change the secondary

structure of the proteins examined in the study. Yet as expected, no secondary changes were observed in the proteins bound to CR. Although structural distinctions made from induced CR CD spectra differing in shape and intensity is promising, more work in this area is necessary. Khurana suggests binding sites for CR in individual proteins could be more related to local environment rather than the type of secondary structure.

Khurana also examined CR's usefulness as a probe of hydrophobic regions of partially folded and native proteins. Apomyoglobin was bound to CR in its native (pH 7), unfolded (pH 2 in the absence of salts), and partially folded intermediate (pH 4 and pH 2 in salt) states (Figure 4). Both native and partially folded conformations induce different CR CD bands. Thus, CR binding sites are present in the partially folded intermediates.

To further probe the mechanism of CR binding, CR was then bound to native β-lactoglobin. The protein concentration was varied from 0 to 20 μM in a constant CR concentration of 40 μM (Figure 5A). Ellipticity minima and maxima were then plotted against β-lactoglobin concentration (Figure 5B). Binding analysis determined that 1.52 ± 0.05 molecules of dye were bound to one β-lactoglobin molecule, in agreement with the literature. Khurana suggests that perhaps three protein molecules are intercalated with two CR molecules between them, resulting in the oligomerization of protein molecules. This hypothesis was further supported using cross-linking and nonreducing SDS-PAGE analysis. Khurana concluded that CR bridges two molecules by intercalating between hydrophobic surface patches with the appropriate electrostatic regions for the sulfonate

groups of CR. In an earlier study, Carter and Chou proposed this model through molecular modeling that CR intercalates between two insulin monomers at an interface formed by a pair of anti-parallel β-strands.[6] This model is illustrated in **Figure 4.2**.

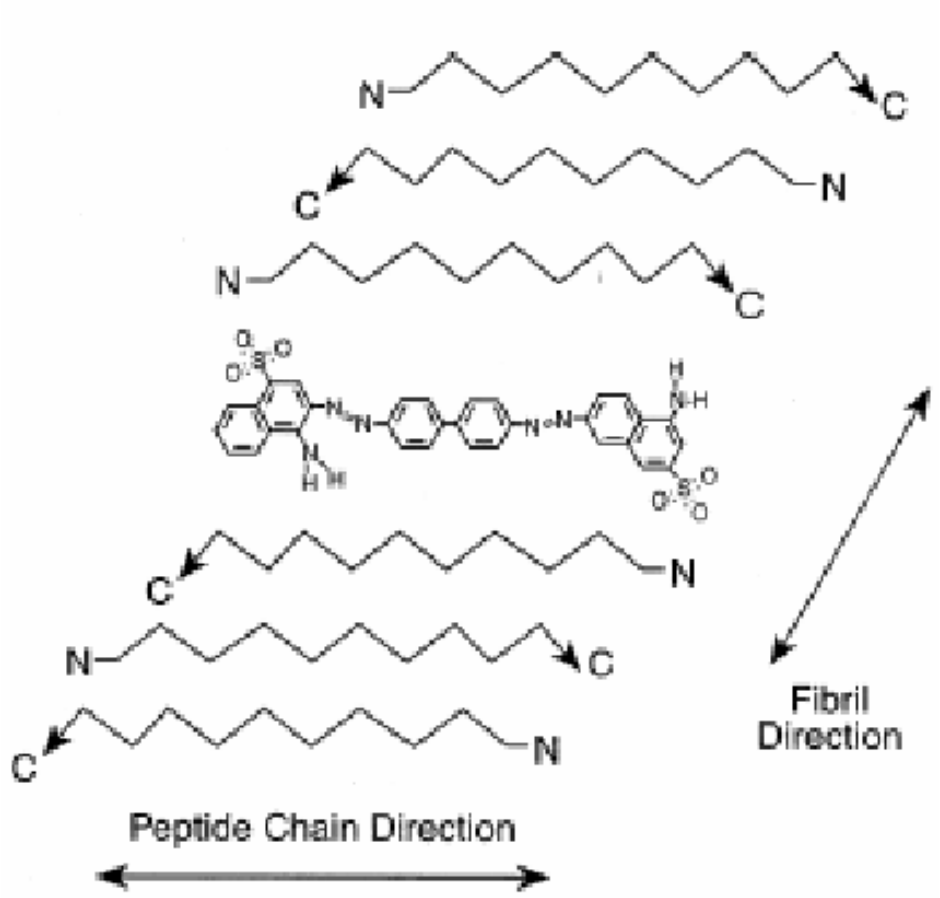

Figure 4.2. The model of amyloid binding to CR proposed by Carter and Chou. Picture reproduced from reference 6.

Section I

Project Aims

In the first part of this project, the research goals were aimed at observing the binding interactions NIR dyes with bovine insulin fibrils using induced CD and FDCD measurements of the symmetrical label. The precise binding modes of CR, as well as other anionic probes, bound to amyloid fibrils are not well understood. Chiroptical techniques are quite useful in the study of protein-ligand interactions. As with absorption and emission spectroscopy, information about the bound protein is obtained through changes in the label's spectra. However, induced CD for an achiral dye will only be achieved if the dye forms three-points of interaction with the biomolecule. Therefore, the dye will only exhibit CD bands when biomolecular interactions are strong, and most likely, specific in nature.

NIR dyes are an ideal alternative to visible dyes such as CR currently used clinically. NIR dye absorption and emission wavelengths are far removed from the autofluorescence of biomolecules, thereby minimizing analyte as well matrix interference. NIR labels also exhibit high molar absorptivities. This property means that lower dye concentrations can be used in analysis, thus preventing distortion of protein and polypeptide structures by the labels. Furthermore, the properties NIR probes can be uniquely tailored through modest structural modification. The particularly unique feature of the carbocyanine labels reported herein is the inherent planarity of heterocyclic rings, thus allowing the probe to intercalate between anti-parallel β-sheets.

Insulin

Insulin is a small globular protein (~5733 Daltons) composed of two polypeptide chains linked by two disulfide bonds. Although the action of insulin *in vivo* is initiated by the binding of monomer insulin to the receptor, the protein is stored in the pancreas within β granules where six molecules of insulin, complexed with zinc ions.[7] The oligomerization of insulin model proposed by Uversky et al is shown in **Figure 4.3**. Zinc ions are not involved in dimer formation but are involved in the association of tetramers to produce the hexameric complex.

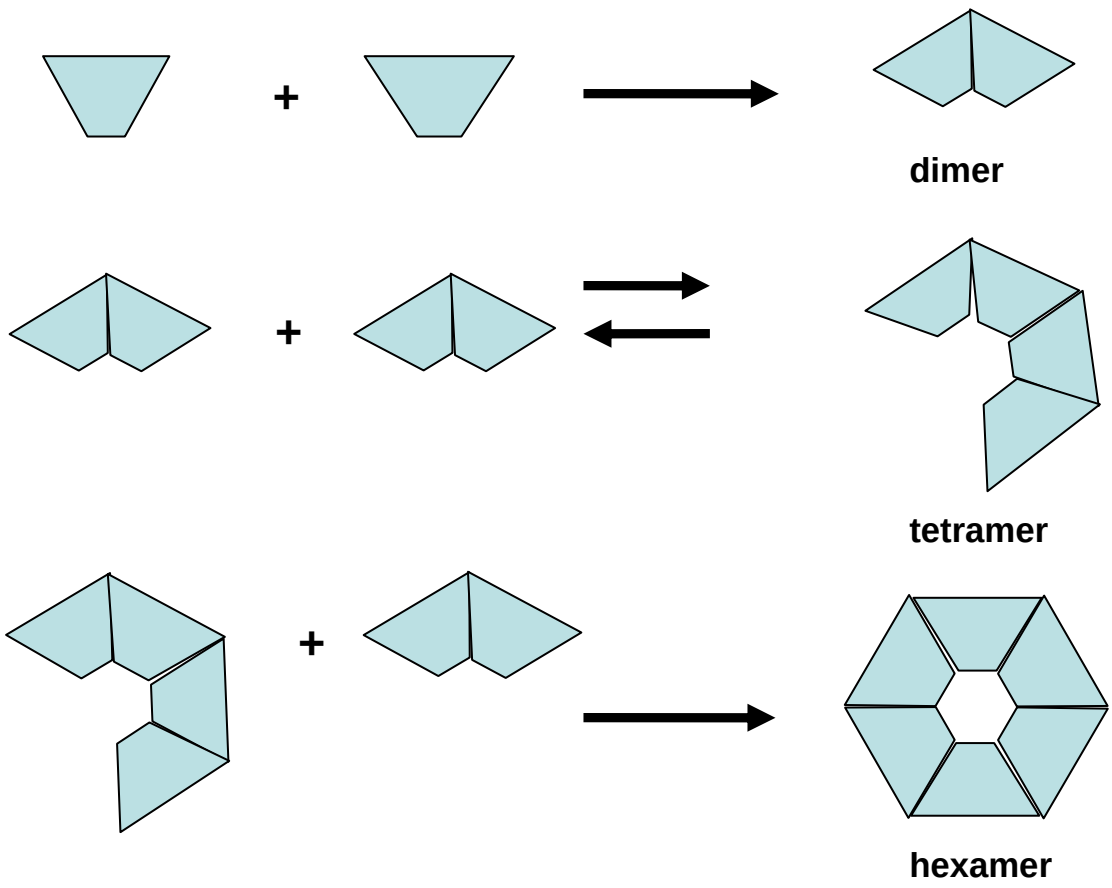

Figure 4.3. Model for the association of insulin revised from reference 7.

Experimental I

Removal of Zinc from Insulin. Bovine insulin was purchased from Sigma (St. Louis, MO) and was reported to contain only ~0.5% zinc (I5500). However, further purification steps were required to make the insulin completely zinc-free for monomer *in vitro* fibrillation techniques. Removal of zinc was performed after methods reported by Sluterman.[8] Since insulin has low solubility at neutral pH, a 10 mg/mL solution of insulin containing acetic acid was first prepared. Concentrations were confirmed by UV measurements at 276 nm (ε = 6080 L/mol). EDTA was then added at a concentration of 0.75 mg/mL. The solution pH was brought then brought back to pH 5.3-5.4 (i.e., the pI of insulin) so the protein precipitates out of solution. This preparation was then left at room temperature overnight. After low speed centrifugation, the supernatant was carefully pipetted off and the remaining solid was washed three times with water.

***In V itro* Fibril Formation.** A wide variety of insulin fibrillation techniques have been reported in the literature.[1, 2, 4, 9-17] For this particular project the method outlined by Burke and Rougvie was chosen for its simplicity and available resources.[12] A 1% solution of zinc-free insulin solution was prepared in distilled water. The pH of this solution was then adjusted to 2 with HCl. The sample was then placed in a sealed tube and heated in a waterbath to 80-100 °C until a clear gel is formed (approximately 10 minutes). The tube was then cooled and immersed in a dry ice-acetone bath. The sample was then thawed under running water and then reheated in the 80-100 °C water bath for 2 minutes. This cycle of heating and cooling was repeated until a firm gel is formed (approximately 3-7 times).

Congo Red Validation. The presence of fibrillar structures is typically validated by either transmission electron microscopy (TEM)[1, 9], thioflavin T fluorescence[10, 18], or the congo red method[19, 20] discussed forthwith. A 100 μM CR stock solution in 90% PBS buffer and 10% ethanol, to dissolve CR micelles. The stock solution was then filtered three times with Gelman filters containing 0.3 μm pores. The final CR concentration was determined by measuring CR absorbance at 498 nm ($\varepsilon = 5.93 \times 10^4$). While keeping the insulin concentration constant (11 μM), four suspensions of CR and fibrils were prepared containing 1, 3, 5, and 10 μM of CR. Samples were gently vortexed for 30 seconds and incubated for 30 minutes before analysis. When in the presence of fibrillar structures, CR will exhibit hyperchromicity and a spectral shift at its absorption maxima. In addition, isosbestic points should be observed around 349, 406, and 477 nm. A linear relationship between spectral differences at 540 nm and CR concentration are typically indicative of fibrils present. The linear relationship is reported in Equation 4.1:

Spectral difference = (26, 800) ([CR]) + 0.003 (4.1)

A representative difference spectra of the assay performed to validate that insulin fibrils were formed is shown in **Figure 4.4**. As seen in this difference spectra, the isosbestic points predicted at 349, 406, and 477 nm were not present. In addition, absorption maxima should be at 540 nm, with spectral changes which are linearly related to changes in CR concentration. However, the absorption maxima observed was actually observed at 549 nm. Thus, according to the assays performed, in vitro fibril formation of bovine insulin was not achieved. The CR assay may have been unsuccessful one of several reasons. First, simple operator error may have been a factor, although this is unlikely since the assay was performed several times. In addition, zinc atoms may not have been

completely removed by the method previously described. Also, insulin fibrils do not have a random conformation. Perhaps fibrillization was not achieved to due to errors made in the in vitro fibrillation process. Dozens of fibrillation methods are reported in the literature. In future work, these other methods should be explored and compared using the CR assay. Furthermore, the harshness of the zinc removal process may have denatured the protein. This idea was further examined in the following section using both near and far UV CD measurements.

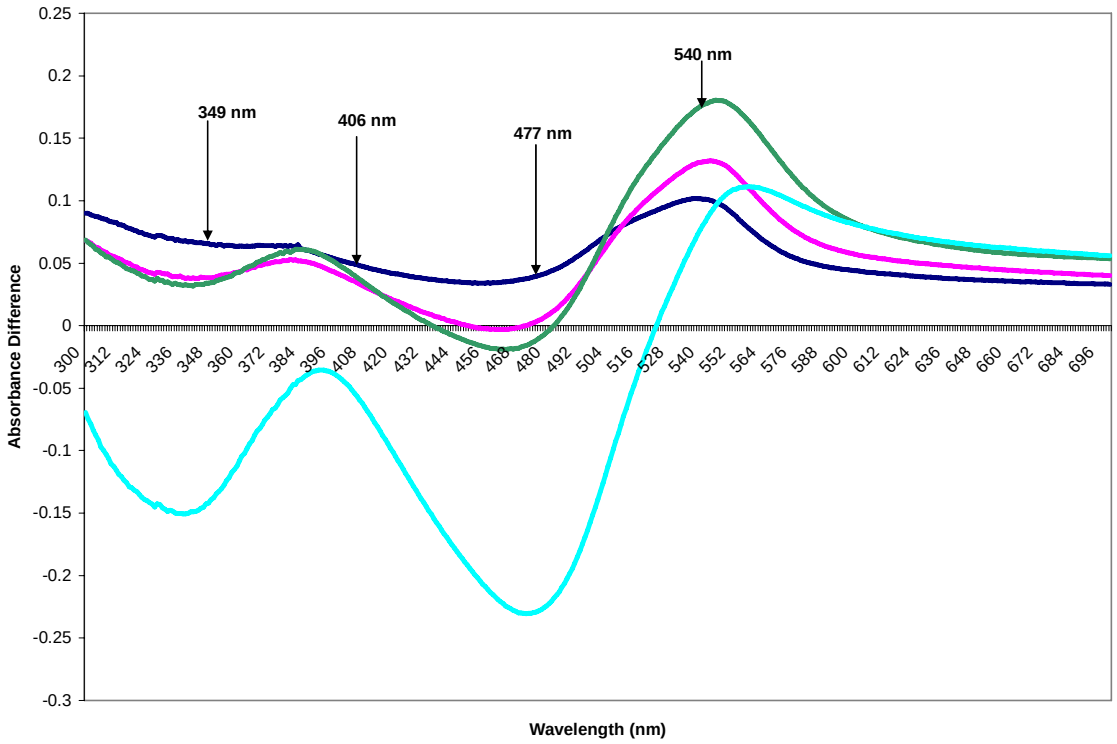

Figure 4.4. CR validation of insulin fibrils. UV-Vis difference spectrum of CR in the presence of insulin fibrils. In the presence of insulin fibrils, isosbestic points should be present at 349, 406, and 477 nm. A linear spectral difference at 540 nm will also be observed in the presence of insulin fibrils.

Near and Far UV CD of Insulin. In order to confirm that the insulin remained in its native conformation after zinc was removed, CD measurements were conducted in both the near and far regions for bovine insulin. As previously mentioned in Chapter 1, the peptide bond chromophore exhibits different electronic transitions for all three basic protein secondary structures. Melberg and Johnson[21] determined from far UV CD analysis that native insulin contains 57% α-helix, 1% β-strand, 18% β-turn, and 24% random coil. The secondary structure of the monomer shows a 10-15% increase in anti-parallel β-structure and a corresponding reduction in random coil structure. Burke and Rougvie[12] have reported that monomer insulin exhibits negative CD maxima at 208 and 222 nm as well as a negative CD band at 195 nm. Alternately, insulin fibrils will exhibit negative and positive CD bands at 217.5 nm and 193.5 nm, respectively. The far UV CD of the zinc-free insulin analyzed is shown in **Figure 4.5**. The sample concentrations were varied between 0.6 to 6 mM to improve the sensitivity of the measurements. The data was normalized with respect to pathlength and concentration and then reported in units of molar ellipticity. The CD maxima exhibited for this data were observed around 240 nm. This was quite a large spectral shift in comparison to results reported in the literature. Several CD secondary structure analysis software packages are available free on the world wide web such as DICHROWEB[22], *Cdtool*[23], *k2d*[24], CD Pro[25, 26]. The secondary structure of the data reported in **Figure 4.5** was further examined using CD Pro and *k2d* software. However, the determinations made using these software suites were inconclusive due to the extremely large errors encountered during software analysis. These observations point to possible operator error since values are so very different than

the data reported in the literature and no conclusions could be made from CD software analysis. Far UV CD can be quite challenging since these measurements require high concentrations in which cell pathlengths as low as 1 mm must be utilized. Issues with sample purity and consistency are often encountered with microscopic pathlengths. In additions, such cells are often difficult to clean and air bubbles are also concerns.

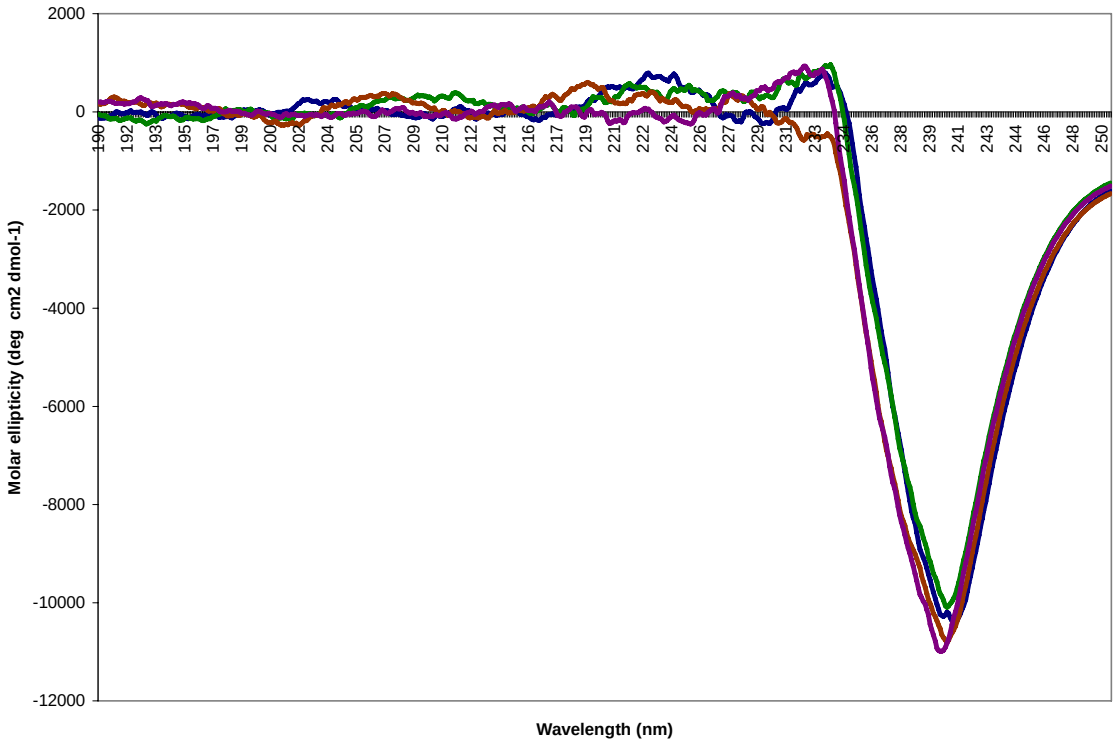

Figure 4.5. Far UV CD of native bovine insulin in the absence of zinc (monomer insulin). Measurements were performed using a 1 mm pathlength circular cell with a 0.6 to 6 mM samples. S/N = 5.

Fortunately, the problems faced in the far UV region can be overcome by examining near UV CD of insulin. By using near UV CD, the native conformation of zinc free insulin was confirmed at 275 nm. The near UV CD originates mostly from tyrosyl side chains, as this protein lacks tryptophan and contains four tyrosine and three phenylalanine residues.[7] When insulin monomers (zinc-free) are oriented in their native conformations, the CD bands at 275 nm will be between -165 to 210 deg cm^2 $dmol^{-1}$. The data shown in Figure 4.6 displays the characteristic near UV CD bands of monomer insulin in its native conformation. This data confirms that no protein denaturation occurred during the removal of zinc from the commercially acquired insulin.

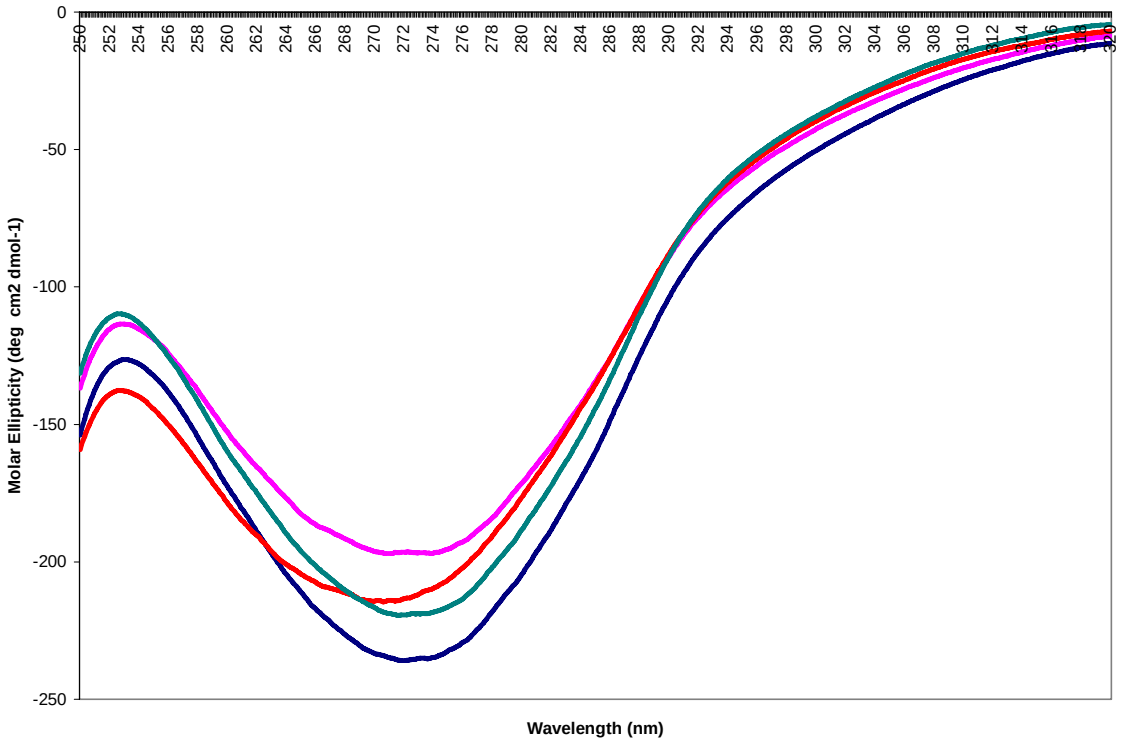

Figure 4.6. Near UV CD of zinc-free insulin (monomer). Measurements were performed using a 1 mm pathlength circular cell with a 0.6 to 6 mM samples. S/N = 5.

Summary

The research goals of the first part of the project were aimed at observing the binding interactions NIR dyes with bovine insulin fibrils using induced CD and FDCD measurements of the symmetrical labels. To this end, the zinc was removed from commercially obtained bovine insulin. Insulin fibrils were then prepared by an *in vitro* fibrillation technique. To confirm if the appropriate insulin fibril structure was indeed achieved, a CR assay was utilized. However, according to the CR assay, the in vitro fibrillation technique chosen was unsuccessful in producing insulin fibrils. Near UV CD confirmed that protein denaturation was not a possible source of error. The insulin fibril model for fibrils *in vivo* is rather a complex system. Moreover, obtaining fibrils commercially can be quite expensive. For this reason, this part of the study was set aside and project aims were directed toward a more simplistic and inexpensive model such as poly-L-lysine.

Section II

Poly-L-Lysine

For several decades, poly-L-lysine (PLL) has been commonly used as a model for protein secondary structure determination. Below the pKa of the residual ammonium substituents (pH 10.5), the polypeptide exhibits a randomly coiled conformation.[27] Above pH 10.5, PLL is observed in either the α-helix or β-sheet conformations, depending on conditions of pH, temperature, and ionic strength. Moreover, the homopolypeptide can take on an α-helical conformation in 100% methanol (i.e., neutral pH) while the ammonium substituents remain charged.[28] Thus, the versatility of this biopolymer has made it ideal for use in studies where secondary structure is closely

related to biofunction (i.e., DNA, enzymes, and biomemic sensing).[29] Charged α-helix PLL is of particular interest because of its potential use in host chemistry studies. It is well known that specificities of the biofunctions of enzymes are dependent on the three-dimensional structures constructed by the polypeptide secondary structure. Charged α-helix PLL allows for specific microenvironments for ionic molecular substances. The charged α-helix PLL allows for a more rigid and uniform enzyme-substrate compared to the more heterogeneous charged randomly coiled PLL conformation.

In most of the earlier induced CD studies, PLL in its charged randomly coiled state was bound to azo dyes such as methyl orange (MO) to produce CD bands within the region of dye aggregate absorption.[30-36] The chemical structure of MO is illustrated in **Figure 4.7**. When no PLL was present, MO did not readily aggregate with increasing concentration.[30] However, induced CD of MO using PLL exhibited an exciton coupled spectra corresponding to dimeric MO interacting with one residual ammonium substituent. It was proven that complex formation was due to both electrostatic interactions between the cationic ammonium groups of PLL and the anionic sulfonate group of the azo dye as well as van der Waals' interactions. Thus, the Davydov splitting (i.e., exciton coupling) observed at shorter wavelengths than monomer MO can be attributed to the dipole-dipole interactions of the dimeric MO molecules. Other studies involving induced CD of both MO and ethyl orange using PLL and its more hydrophobic poly (N^{ε}-alkyl-L-lysine) analogues showed that the absolute conformation of the dye-polypeptide complexes could be converted from S-chiral to R-chiral when more hydrophobic substituents are introduced.[31, 33] Furthermore, induced CD of MO was only observed when PLL was in its protonated state.[32]

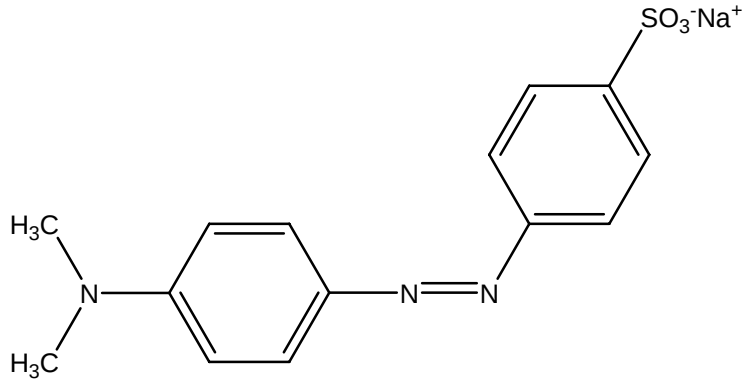

Methyl Orange

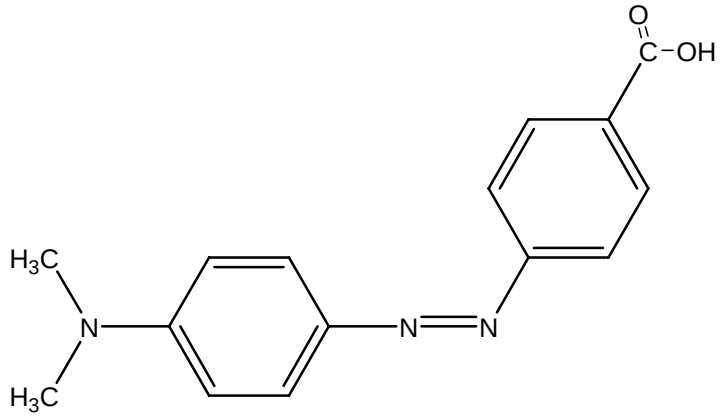

DAAC

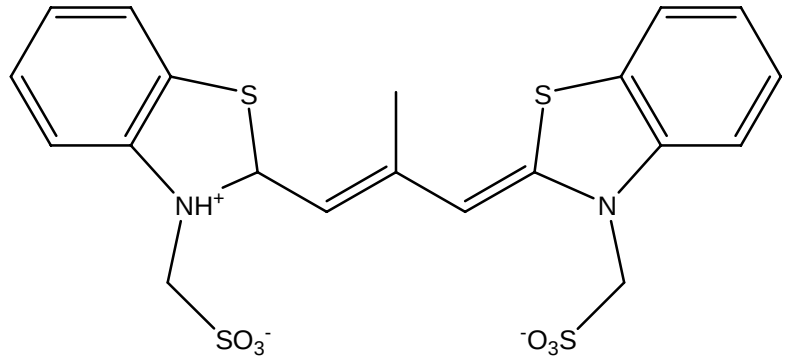

NK2012

Figure 4.7. Chemical structures of Methyl Orange, DAAC, and NK2012.

Other studies of azo dyes containing carboxylic acid substituents have been successful in using neutral PLL to induce CD.[37-39] The azo dye 4'-dimethyl amino azo benzene-4-carboxylic acid (DAAC) binds cooperatively to α-helix PLL at pH 11.5. The chemical structure of DAAC is depicted in **Figure 4.7**. The binding of DAAC resulted in the conformational transition of PLL from α-helix to β-sheet. The extended conformation of β-sheet PLL allowed for increased DAAC binding. It was confirmed that electrostatic interactions did not play an important role in DAAC-PLL binding. Thus, hydrophobic interactions between the hydrocarbon portion of DAAC and the uncharged alkyl side chain of PLL at pH 11.5. Because DAAC is not completely planar in solution, the α-helix conformation is most likely too rigid to accommodate the bulky DAAC molecule. Furthermore, the addition of dioxane destroyed the DAAC-PLL complex, confirming hydrophobic binding as the predominant interaction involved. Moreover, exciton splitting was again observed due to the interaction of two identical chromophores around PLL residues.

To date, there have been no NIR dyes used as protein secondary structural probes reported in the literature. Polymethine dyes are ideal for this application since their properties are readily controlled by structure and solvent environment. In addition, the self-association properties of cyanines can be exploited for structural sensing, since α-helical structures make model templates for chiral J-aggregates to form.[40-43] The trimethine cyanine dye NK2012 (**Figure 4.7**) has been reported to have extrinsic Cotton effects in the presence of charged α-helix PLL in methanol.[29, 44-47] As mentioned previously, the ε-ammonium groups of PLL remain charged within the α-helix conformation in 100% methanol. The chirality of the induced CD band of NK2012 has

been proven to be dependent on secondary structure. Exciton coupled NK2012 molecules bind with charged PLL to produce S-chiral and R-chiral dimers in water and methanol, respectively.[45] PLL is rather rigid and the residual ammonium groups assume identical positions as binding sites for the anionic dye to bind. While observing the induced CD band of NK2012, it has been proven that charged α-helix PLL showed geometrically selective binding for geometric isomers of dicarboxylic acids.[44] The chiral dimers can be dispersed into monomers by the addition N^{α}-benzyloxycarbonyl amino acid derivatives, further supporting the idea of geometrically selective binding.[47]

Project Aims

Although NK2012 has shown chiral selectivity with respect to secondary structure, trimethine dyes such as this one only excite in the visible region, where dyes are typically less sensitive, and more susceptible to matrix interference. With the simple addition of methines, dyes exhibiting properties in the more advantageous NIR region are constructed. For the second part of the project, NIR carbocyanine dyes were screened for their potential as protein secondary structural probes. Cyanine dyes are particularly advantageous for this application because their spectral properties are quite sensitive to solvent polarity. The dye's photochemical properties were evaluated using both absorption spectroscopy and induced absorption CD techniques in the NIR region.

Dye Screening Scheme

Approximately fifteen NIR dyes were furnished from KPS Technologies, LLC. The dyes were initially grouped according to the scheme outlined in **Figure 4.8**. In the first tier, dyes differ with respect to their polymethine character. As previously discussed in Chapter 2, polymethine character, and subsequently dye flexibility, governs the

photostability of carbocyanine dyes. As methine groups are added to the polymethine bridge, absorption and emission wavelengths will extend further into the NIR region. However, the addition of methine groups also leads to a larger, much more flexible dye. Dye flexibility is incongruent with dye stability; i.e., the rule of thumb dictates that increased flexibility in a chromophore leads to decreased photostability. This is particularly true with respect to fluorescence properties. To overcome the inherent instability of penta- and heptamethine dyes, groups such as the Patonay and the Strekowski groups have inserted cyclic structures into the polymethine bridge to increase dye rigidity and thereby enhance the dye's stability as well as other photophysical properties. Dyes containing either a typical polymethine bridge, a squaric, or croconic moiety were all evaluated. The chemical structures of all the dyes examined in this study are displayed in **Figures 4.9-10**.

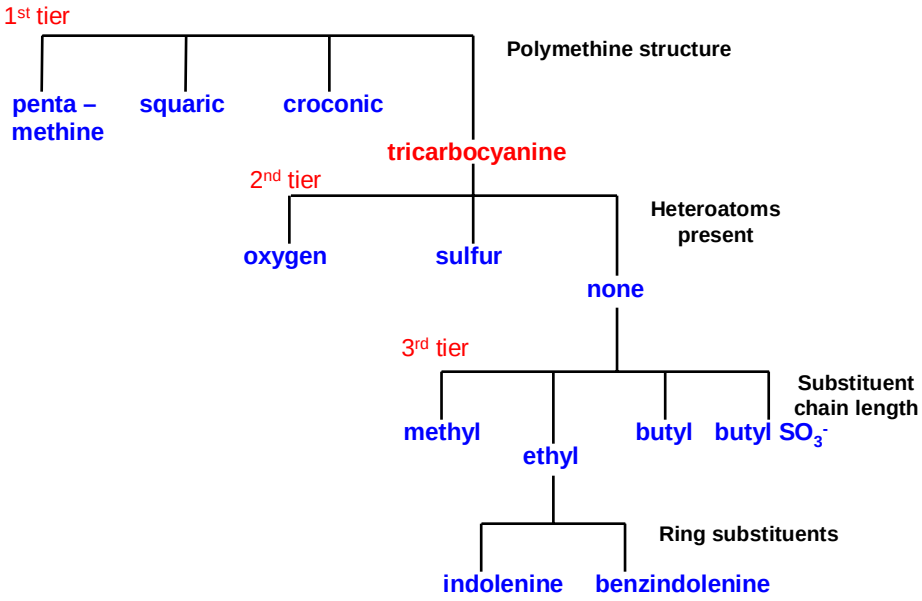

Figure 4.8. Dye analysis scheme. The labels were first organized according to their polymethine character. The presence of heteroatoms as well as the size of the dye substituents were also evaluated. The characteristic ring substituent was also examined in order to observe the contribution that hydrophobicity plays in secondary structure discrimination.

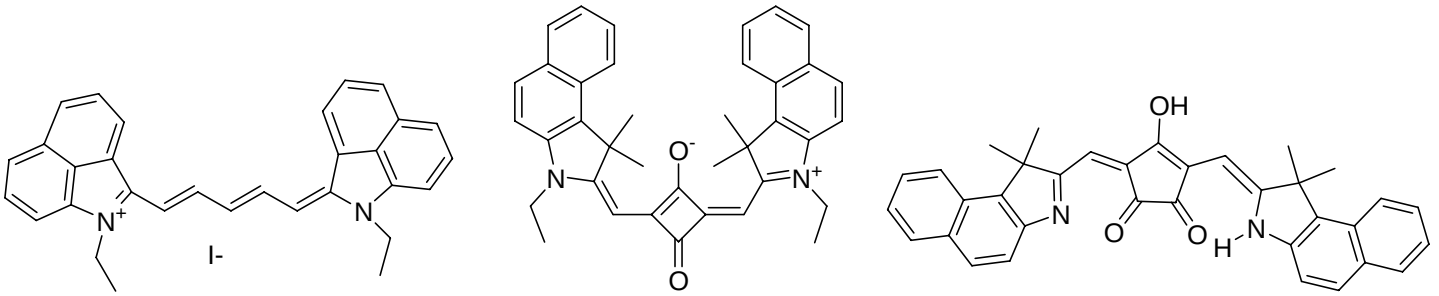

PD1 nn127 croconic I

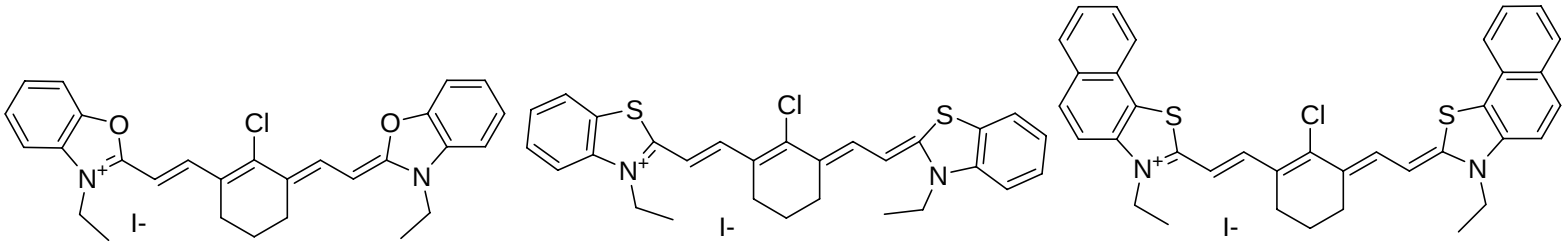

nn359 39B nn346

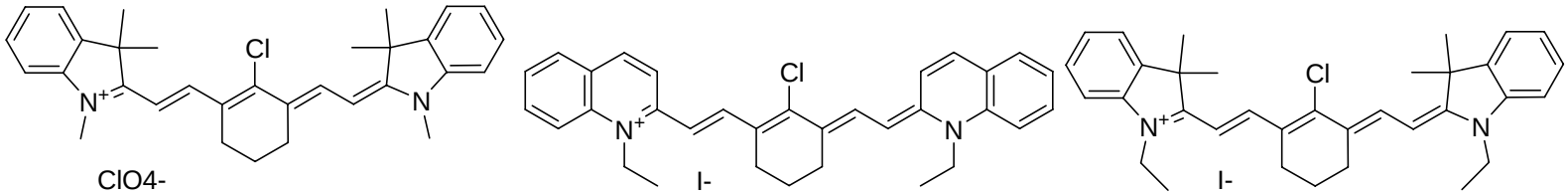

IR 786-perchlorate 48A 19

Figure 4.9. Chemical structures of the dyes screened for their polymethine character (e.g., squaric, croconic, crotonic) and the presence of heteroatoms.

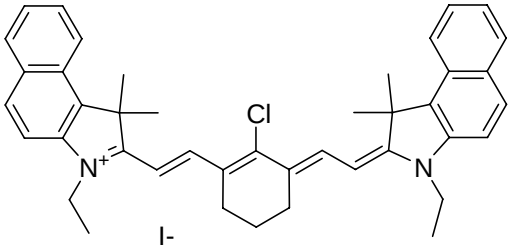

33C

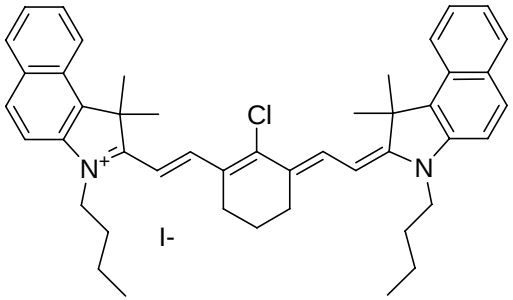

DB 820

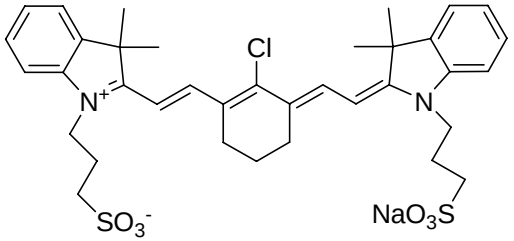

IR783

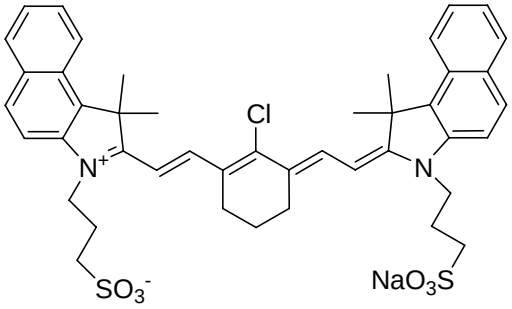

IR 820

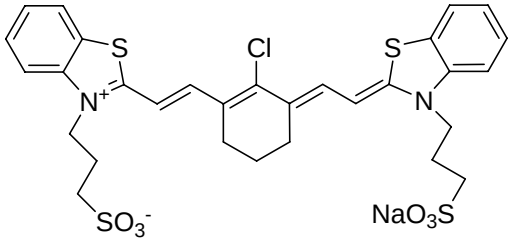

IR804

Figure 4.10. Chemical structures of dyes screened for length and charge of their substituents as well as the hydrophobic effect of an additional benzene rings.

In the second tier, crotonic (tricarbocyanine) dyes are grouped with respect to the presence or absence of heteroatoms such as oxygen or sulfur present at the 3 and 3' positions. Andrews-Wilberforce and Patonay previously reported that sulfur groups at these positions bind preferentially to BSA and HSA binding sites.[48] Furthermore, sulfur atoms are also present in the visible dye NK2012 and could perhaps contribute to it's specificity as well. The third tier examined dyes based solely on their substituent length and charge. Substituent length was considered an important feature in preferential binding since Carter and Chou[6] reported that CR intercalated between anti-parallel β-strands as sulfonate groups bound to alternate ends and alternate strands of amyloid fibrils (**Figure 4.2**). Therefore, the substituents should not be too long or too short for noncovalent binding. In addition, the Carter and Chou study also contributed to the argument that CR binding electrostatically, hence its inherent lack of specificity. Therefore, dyes containing butyl sulfonate groups were also examined. And finally, dyes with indolenine vs. benzindolenine groups were also compared. The hydrophobicity, and subsequent increased planarity, may allow for better dye intercalation.

Other Considerations. For use as a structural probe with the ability to differentiate between the α-helical character of native insulin and the cross β-structure of insulin fibrils, dye structure is most important. However, dyes were not used to target amino acid functional groups since the primary structure of both native and fibrillar insulin was identical. This idea is also true for the PLL models as well. A desirable probe should be quite planar in order to intercalate between the extended conformations of β-strands. Dye fit is also imperative in order to avoid nonspecific interactions of the dye to protein or polypeptide surfaces.

PC modeling and simulation® work was performed early on by Dr. Brian Crow and dyes containing 3, 3' dimethyl groups were found to lack the required planarity, and could potentially inhibit π-π interactions of intercalation. Dyes containing dimethyl substituents at these positions were not excluded, but were closely monitored for their ultimate utility in insulin fibril models.

Using absorption spectroscopy, stability and aggregation behavior of the dyes shown in **Figures 4.9-10** were first evaluated. The oxacyanine dye nn359 was discarded due to extreme instability in methanol. Molar absorptivity of nn359 in methanol decreased exponentially within 12 hours of dye dissolution. Croconic dye I could not be evaluated because the dye was insoluble in all solvents (e.g., phosphate buffer, PBS buffer, 100% methanol, 90% water/10%methanol) except DMSO. Visibly insoluble aggregates of croconic dye I were observed for all reagents mentioned. This observation is quite unique since the cyanine moiety typically allows for moderate solubility in aqueous solution. Some dyes were also excluded due to a lack of purity. This problem was encountered for dyes 39B and 48A.

Dyes were finally screened using absorption spectroscopy according to similar studies performed by Hermel and Rossi.[49] Spectral shifts of the dye's monomer or aggregate bands in the presence of either α- or β-PLL structures were considered indicative of structural sensitivity. Two carbocyanine NIR dyes were selected based on these criteria: PD1 and DBS804. The details of this data are discussed in the section to follow.

Experimental II

Instrumentation. Circular dichroism (CD) experiments were performed using a Jasco 710 spectropolarimeter (Easton, MD). The instrument was equipped with a 450 W Xenon Arc lamp, a 50 kHz piezo-elastic modulator, and a double prism monochromator. Fluorescence detected circular dichroism measurements were obtained using a long wavelength (600 – 1100 nm) Hamamatsu R375 photomultiplier tube (PMT) positioned perpendicular to the excitation beam. Far UV CD measurements were performed with a short wavelength (200 – 800 nm) Hamamatsu R375 PMT positioned directly in front of the excitation beam using a 0.01 cm pathlength circular cell. All NIR CD measurements were performed in rectangular quartz cells containing 1 cm path lengths. The instrument was calibrated in the UV region using (+)-camphorsulfonic acid (CSA) as described in the literature.[50] Prior to the measurement of polypeptide spectra, the CSA standard was scanned in a 1 cm quartz cell and the instrument's high tension (HT) voltage was adjusted to 190.4 ± 1 mdeg at 290.5 nm (**Figure 4.11**). Any subsequent far UV CD measurements for polypeptides were done in the 200 to 300 nm region. NIR CD measurements were performed only after the instrument was calibrated in the near infrared region (NIR). CD calibrations were performed as described by Konno using nickel sulfate.[51] The HT voltage was adjusted until molar CD values were approximately -101.2 ± at 718 nm and -100.7 ± 1 at 777 nm respectively (**Figure 4.12**). Absorption measurements were performed on the Perkin Elmer UV-Vis/NIR spectrophotometer (Norwalk, CT). The instrument was calibrated prior to measurement by using a quartz cell containing phosphate buffer as a blank. The blank was scanned in the 600 to 900 nm region with a 1 nm step resolution. Baselines were recorded as the optically inactive

fluorophores in CD cuvettes. Fluorescence measurements were performed on an ISS K2 Multifrequency Phase Fluorometer (Champaign, IL). The slit widths were 2 mm and the integration time was 3 sec. Step resolution between 0.2 and 0.5 nm/sec was used. All samples were excited with a commercial GaAlAs laser diode (Laser Max, Rochester, NY) at 690 nm, to avoid the potential inner filter effects of the high quantum yield of the dyes studied. All absorption and fluorescence measurements were taken with a 1 cm cuvette.

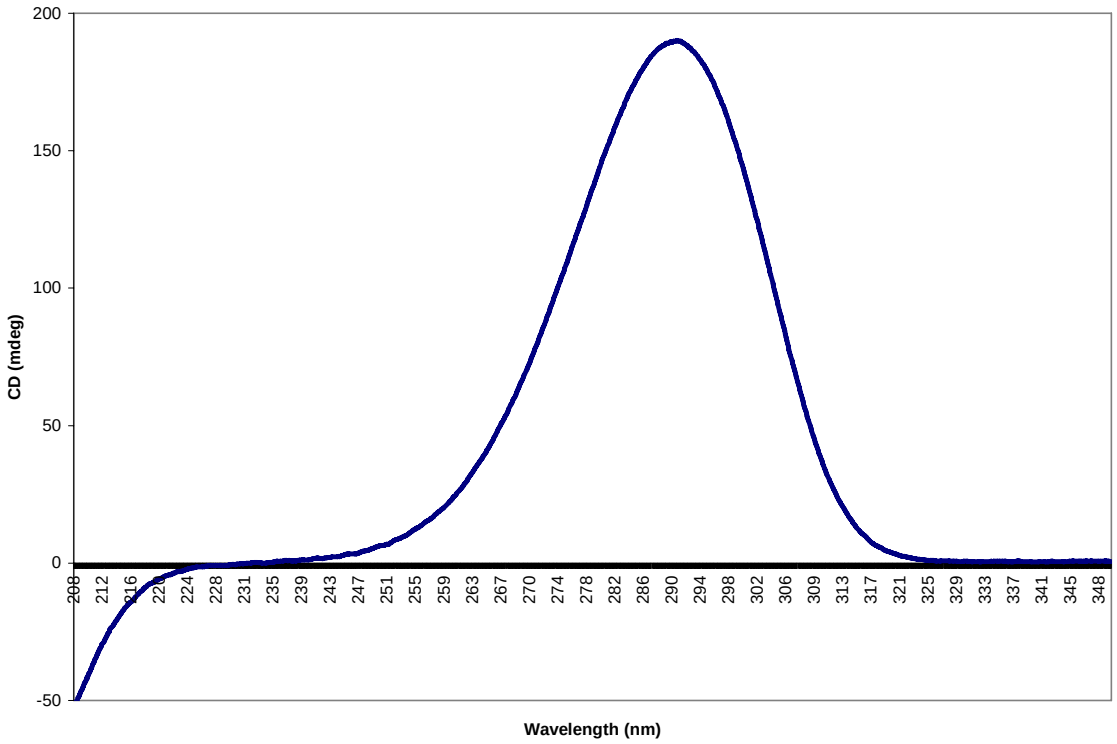

Figure 4.11. Calibration of the short wavelength PMT for far UV protein analysis using a 0.06% ammonium (+)-10-camphorsulfonate standard. Measurements were performed using a 1 cm pathlength rectangular cell. S/N = 5.

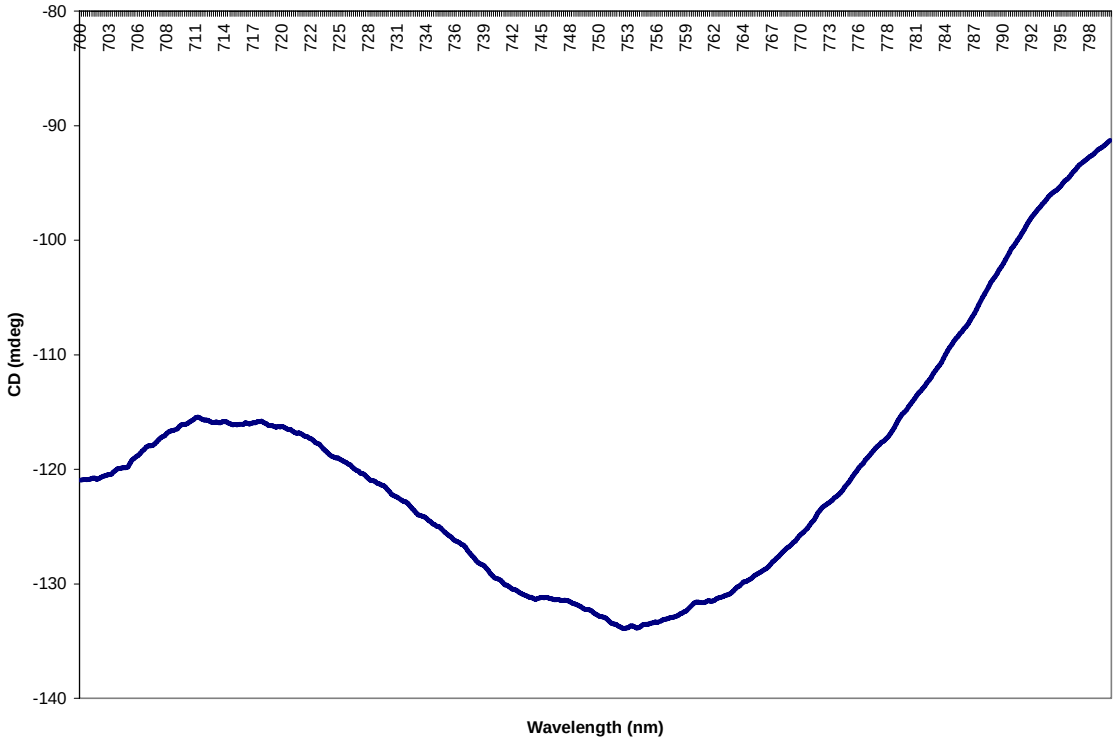

Figure 4.12. Calibration of the long wavelength PMT for use in the NIR region using a nickel tartrate standard. Measurements were performed using a 1 mm pathlength rectangular cell. S/N = 5.

Materials. Poly-L-lysine hydrobromide (PLL), MW = 61000, degree polymerization = 296, (+)-camphor sulfonic acid, nickel sulfate hexahydrate, and potassium sodium tartrate were purchased from Sigma. HPLC grade methanol was purchased from Fisher Scientific (Pittsburgh, PA). All other reagents were purchased from Sigma. Water was obtained from a Barnstead NANOpure Ultrapure Water System (Van Nuys, CA). Filtering was performed using Anotop® 25 Disposable Syringe Filters manufactured by Whatman (Clifton, NJ).

Biuret Assay. Since PLL is a polypeptide, conventional methods for determining its concentration such as molar absorptivity at 280 nm or a Coomassie blue assay cannot be utilized. Therefore, the biuret assay was employed instead. The biuret assay makes use of the principle that, under alkaline conditions, samples containing two or more peptide bonds form a purple complex with the copper salts in the reagent. Biuret reagent contains 2.25 g sodium potassium tartrate, 0.75 g copper sulfate x 5 H_2O, 1.25 g potassium iodide, all of which are dissolved in 0.2 M sodium hydroxide. The volume is then brought to 250 mL with distilled water. Standard samples of bovine serum albumin (BSA) from 1 to 10 mg/mL were also prepared. The PLL samples analyzed were also prepared to fall approximately within the range of the BSA standard curve. Standards and samples were both added to test tubes at 1 mL volumes. Next, 9 mL of biuret were added to each tube. Test tubes were vortexed and allowed to incubate for 20 minutes. Absorbance measurements were then recorded for the standards and samples at 550 nm.

Poly-L-Lysine Preparations. At neutral pH, PLL residues are arranged in the randomly coiled conformation. In addition, randomly coiled PLL is also charged below the ε-amine's pKa 10.5. Above the ε-amine pKa, PLL is uncharged and will exhibit an α-helix conformation from the intramolecular hydrogen bonds between carboxyl and amino groups. However, when α-PLL was heated above 50 °C, these hydrogen bonds are disrupted and the polypeptide will take on the extended conformation of β-PLL. After approximately 30 minutes of heating PLL, the samples were quickly cooled on ice to bring the samples back down to room temperature. At room temperature, hydrogen bonds were reformed to stabilize the β-PLL complex. The α- to β-PLL transition of PLL is illustrated in **Figure 4.13**. In 100% methanol, PLL not only exists in an α-helix, but the polypeptide residues are charged as well. In this study, PLL was dissolved in water to give a 2×10^{-5} M stock solution. Polypeptide concentration was confirmed by the biuret assay for peptide bonds.

Far UV CD of PLL. When the polypeptide secondary structures were prepared in solution, the conformations of each structure were then validated by far UV CD measurements (**Figure 4.14**). Samples were first diluted to 0.01% concentrations. Then using a 0.1 cm pathlength circular cell, CD measurements were determined from an accumulation of approximately 3 system scans (S/N=3) at a bandwidth of 0.5 nm. All samples (i.e., charged and uncharged α-helix, β-sheet, and random coil) were in good agreement with the mean residue ellipticities reported in the literature.[27]

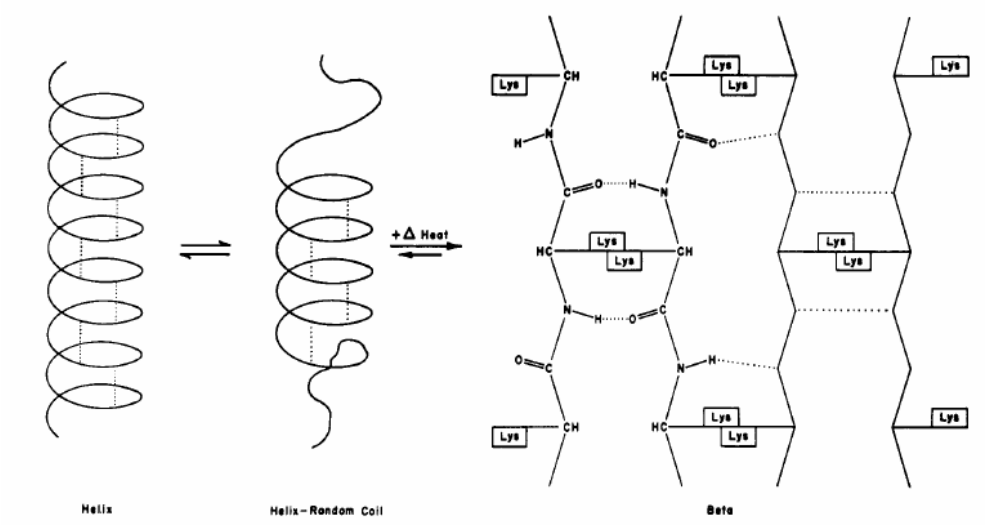

Figure 4.13. Structural transitions of uncharged α-PLL into the β-PLL conformation. Adapted from Davidson and Fasman, Biochemistry (1967) **6**, 1616. Under heated conditions, the hydrogen bonds of α-PLL will be disrupted and the polypeptide will reform as β-PLL.

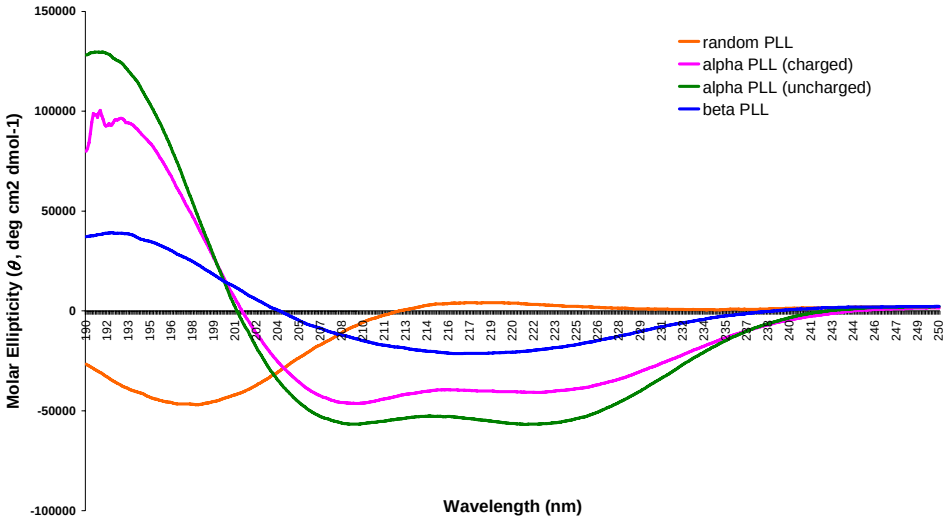

Figure 4.14. Far UV CD of 0.01% PLL samples. Prior to induced CD analysis, all models were validated according to values reported in the literature. Measurements were performed using a 0.1 cm pathlength circular cell and a 0.5 nm bandwidth. S/N = 3.

Dye Preparation. NIR dyes were first solubilized in minimum concentrations of methanol. Dyes were then further diluted to appropriate concentration with water. In most cases, the final total volume of methanol was not more than 3%. Polypeptide and dye solutions were prepared by using equal volumes of both. Dye and polypeptide solutions were prepared and allowed to incubate at room temperature for one hour in the dark. A 0.06% (w/v) stock solution of ammonium (+)-10-camphorsulfonate was prepared in water. Stock solutions of nickel (II) sulfate (solution A) and potassium sodium tartrate (solution B) were prepared in water at 0.240 M and 0.360 M concentrations, respectively. The nickel (II) sulfate solution was prepared by mixing equal volumes of solutions A and B immediately preceding NIR CD calibration.

Results and Discussion

PD1 in Poly-L-lysine

Dyes were screened using UV-Vis/NIR absorption spectroscopy according to techniques performed by Hermel and Rossi.[49] Spectral shifts of the dye's monomer or aggregate bands in the presence of either α- or β-PLL structures were considered indicative of a potential structural probe. The tier I (**Figure 4.8**) carbocyanine dye PD1 was the first dye observed to meet these criteria. As the chemical structure in **Figure 4.9** shows, PD1 is a pentamethine carbocyanine dye with a relatively flexible polymethine bridge and three heterocyclic fused rings on either side. Although the polymethine bridge of PD1 was assumed to lack the rigidity necessary for a photostable compound, PD1 was found to maintain its molar absorptivity in methanol for at least two weeks before degradation occurred. The fused ring moieties of PD1 make this dye particularly novel. A typical pentamethine dye containing indolenine ring moieties absorbs around 650 nm. However, the fused heterocyclic rings of PD1 allow this dye to absorb far into the near infrared region. The absorption spectra displayed in **Figure 4.15** shows the effects of solvent polarity on PD1. In 100% methanol, the monomer band is strongly exhibited at 854 nm. However, in 10% methanol/90% water, the PD1 monomer is minimized and various H-aggregates appear. Similar bands are observed in 90% phosphate buffer (PB). Additionally, when salt is added to PB (PBS), H-aggregate bands shift once more and a small J-aggregate appears as well. All experiments discussed hereafter are were performed in 90% water for the sake of simplicity and to avoid matrix interference during absorption CD measurements. The absorption spectra of PD1in 90% water at varying

dye concentrations is given in **Figure 4.16**. Even when dye concentration is increased 20-fold, the dye-aggregate to monomer band ratios appear to remain constant, implying that the H-aggregates form relatively stable complexes.

The criteria for dye screening are illustrated in **Figure 4.17**. In the presence of α-PLL, the monomer band of PD1 is shifted from 854 to 880 nm, exhibiting a 26 nm shift of the monomer band. In contrast, β-PLL exhibits a 33 nm shift of its monomer band from 854 to 887 nm. The β-PLL monomer band is quite distinctive as compared to the α-PLL monomer band, which suggests that PD1 may selectively bind to proteins from different secondary structural classes. In addition, PD1 exhibited similar bands in the visible region around 475 nm. These peaks are often observed for cyanine dyes in the presence of protein and were assigned the PLL-dye complex band. Moreover, a small J-aggregate band is also observed for α-PLL around 985 nm. This band was attributed to J-aggregation into a helical orientation, templated by the α-helix structure of the PLL. Another smaller band observed around 785 nm appeared unique to only β-PLL. This band is most likely the result of a spectral of the H-aggregate band observed at 730 nm for PD1 alone in 90% water. The relatively short aggregate band observed for PD1 alone in water at 700 nm also appears bathochromically shifted 35 and 25 nm for α- and β-PLL respectively.

PD1 in Ovalbumin

Heat denatured ovalbumin was also used as a β-sheet model. The absorbance spectra of PD1 in varying concentrations of the heat denatured protein are displayed in **Figure 4.18**. The monomer band of PD1 bound to ovalbumin displayed a monomer band similar to the one observed for the dye bound to β-PLL. This gives further credence the

dye's potential as a secondary structural probe. In addition, at low ovalbumin concentrations, PD1's the absorption bands observed around 675 nm are nearly identical to the bands observed at the same wavelengths in the presence of β-PLL. PD1 not only appears sensitive to protein secondary structure, but protein concentration as well. At low protein concentrations (~1 x 10^{-6} M), the monomer band exhibits no spectral shift. Yet, at higher protein concentrations (i.e., $\leq$ 1 x 10^{-6} M), a spectral shift of ~27 nm is observed. The spectral changes of PD1's monomer band in varying concentrations of heat denatured ovalbumin are summarized in **Table 4.1**. Since protein concentration is a major factor of protein aggregation. PD1 may have potential as a probe for protein aggregates. This feature makes this dye's potential use in amyloid fibril applications even more valid.

The spectral changes observed for PD1 determined that the dye may be useful as a structural probe. However, no CD bands were detected for PD1 bound to neither α- or β-PLL. In addition, PD1 samples containing ovalbumin were considered too turbid for CD analysis.

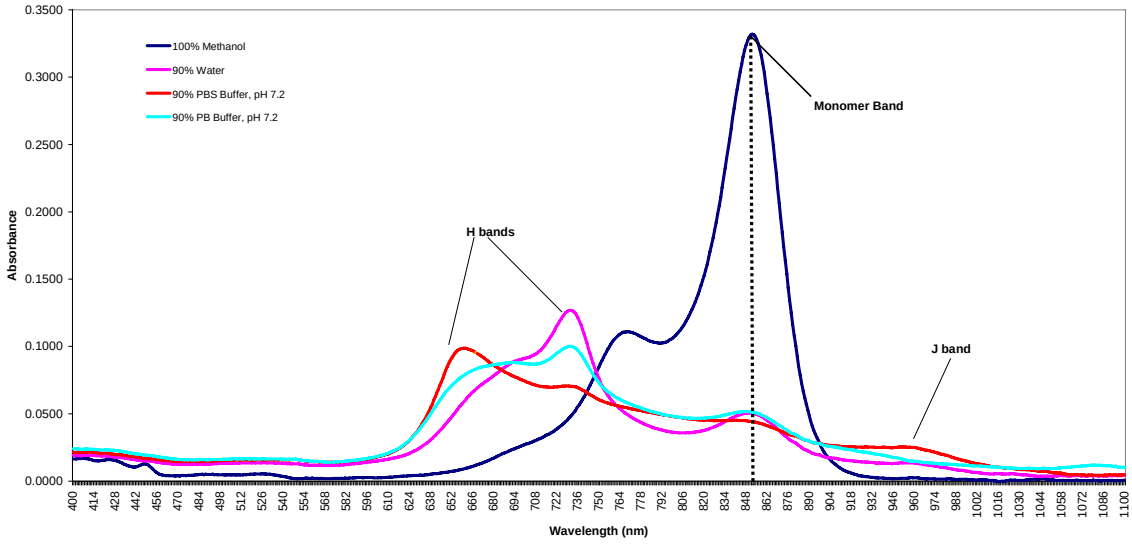

Figure 4.15. Solvent effects of PD1 in UV-Vis/NIR absorbance spectroscopy.

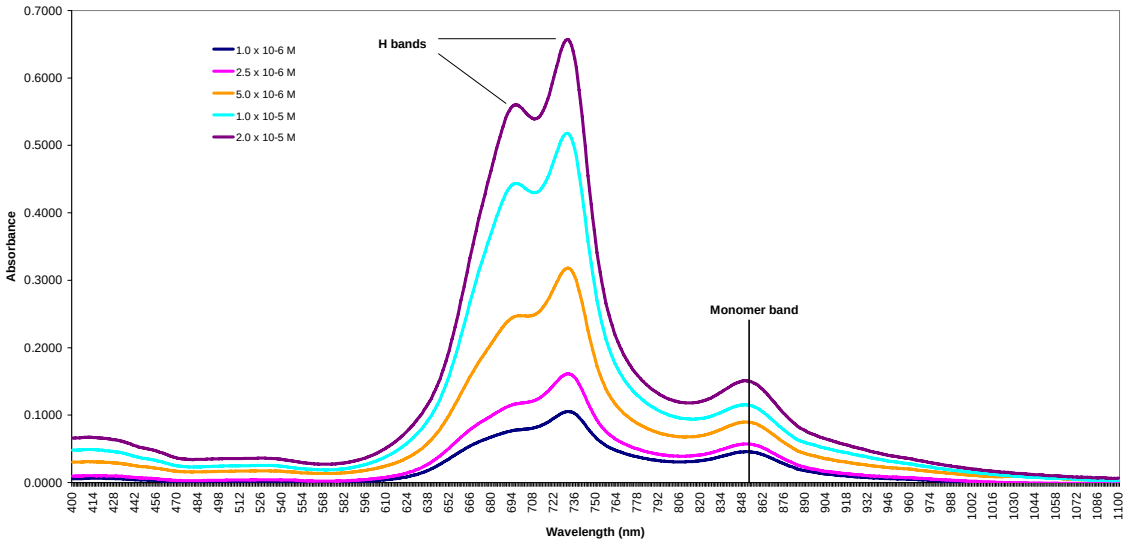

Figure 4.16. UV-Vis/NIR absorbance spectra of PD1 in 90% water/10% methanol in various dye concentrations.

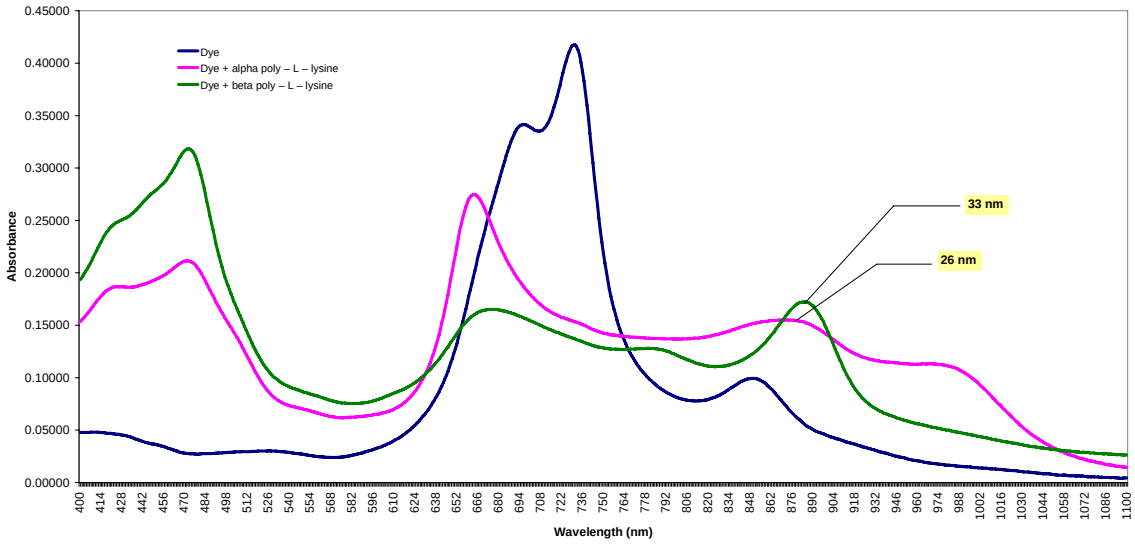

Figure 4.17. UV-Vis/NIR absorbance spectra PD1 bound to uncharged α- and β-PLL.

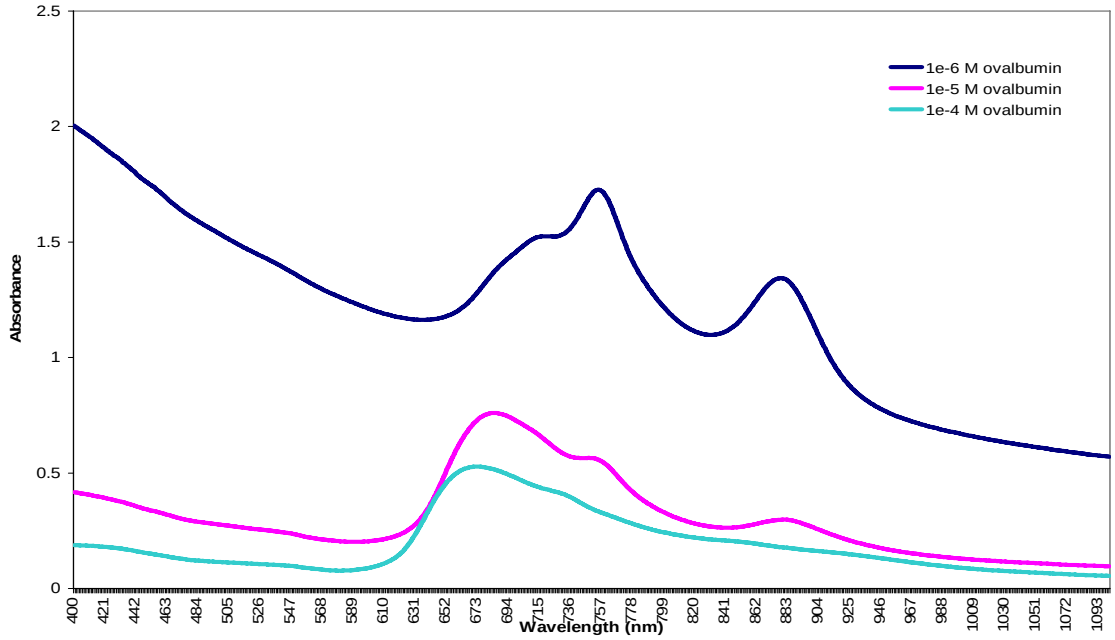

Figure 4.18. PD1 in varying concentrations of heat-denatured ovalbumin.

Table 4.1. Sensitivity of PD1 to protein concentration

ovalbumin concentration ($\times 10^{-5}$ M)	**Monomer shift (λ_{max}/nm)**
0.1	none
1	881
10	879

DBS804 in β-lactoglobin

The heptamethine carbocyanine DBS804 was also screened for its potential as a secondary structural probe. Cyanine dyes are quite sensitive to polar media, and have a high propensity for self-association in aqueous solution. The absorption spectra of DBS804 in water and methanol shown in **Figure 4.19** demonstrate the sensitivity of cyanines to solvent polarity. In methanol, an intense monomer band is observed at 800 nm. However, in 90% water, the monomer band of DBS 804 is minimized and various blue-shifted bands corresponding to dimeric and higher order H-aggregates are observed.

The globular protein β-lactoglobin, containing a high β-sheet content, was also used as a model for β-sheet sensing. The absorbance spectra of DBS804 in the presence of β-lactoglobin are shown in **Figure 4.20**. When bound to β-lactoglobin the DBS804 monomer band begins to reappear with increasing protein concentration. Furthermore, the monomer band also exhibits a hypsochromic shift of approximately 25 nm. The blue-shifted aggregates of DBS804 also appear to interact with the protein as well, where the more blue-shifted aggregate bands begin to disappear with increasing protein concentration. Therefore, the spectral changes of DBS804 in the presence of β-lactoglobin suggest that the dye may be useful as a protein secondary structural probe. The dye bound to different conformations of PLL were also analyzes to investigate this application.

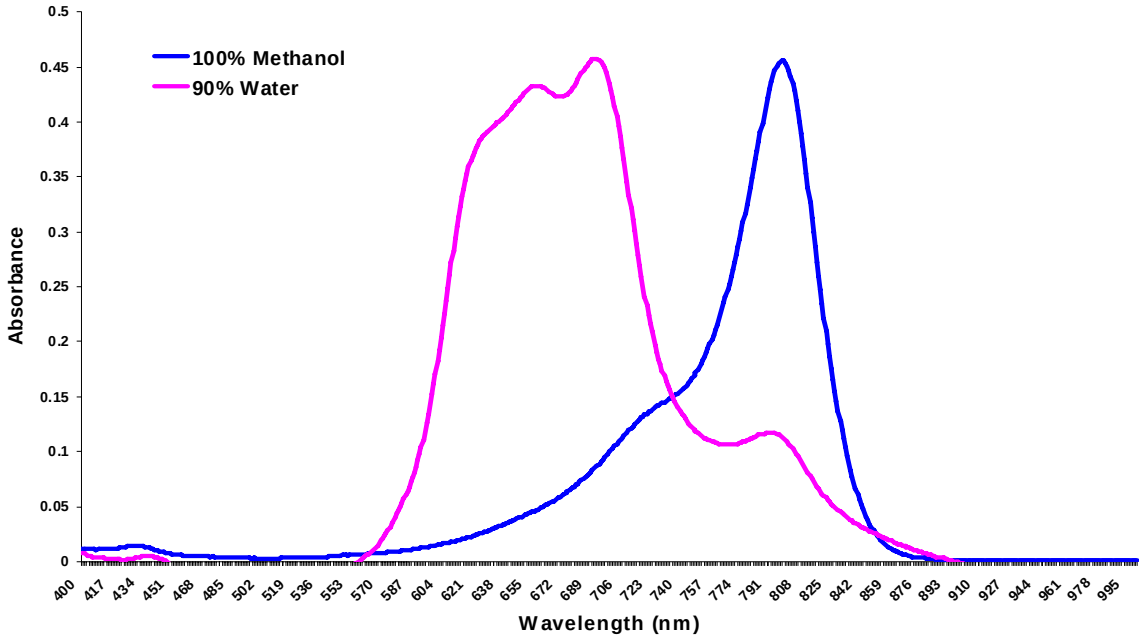

Figure 4.19. Normalized absorption spectra of DBS804 depicting dye solvent effects.

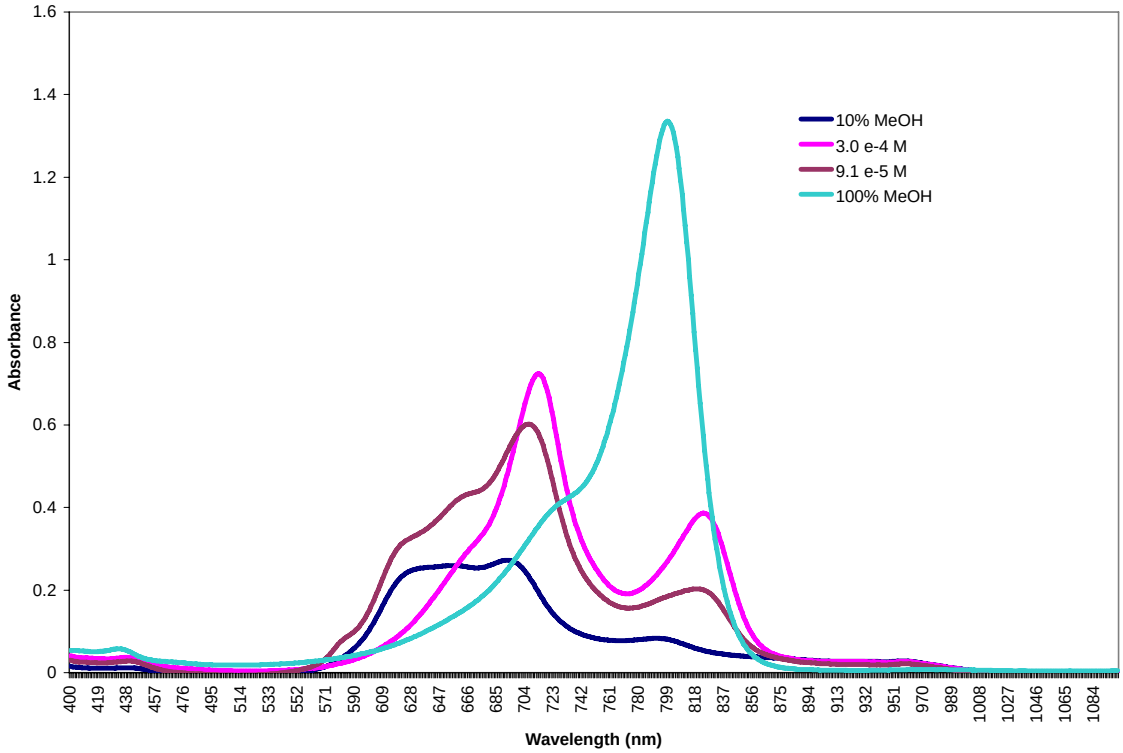

Figure 4.20. Absorbance spectra of DBS804 in the presence of varying concentrations of β-lactoglobin.

DBS804 in Uncharged PLL

The spectral differences of DBS804 bound to α- and β-PLL were also investigated. The absorption spectra of DBS804 bound to both α- and β-PLL in water at pH 11.5 is displayed in **Figure 4.21**. Since both PLL conformations contain uncharged residues, it is presumed that no electrostatic interactions occur between the polypeptides and the anionic dye. In aqueous solvent, DBS804 exhibits several H-aggregate bands. The aggregate band showing the highest molar absorptivity was observed around 700 nm. In the presence of both α- and β-PLL, this aggregate band displays a slight increase in absorbance. Most interestingly, the aggregate band observed around 700 nm appears as a plane of symmetry for both PLL samples in which aggregate bands appear blue-shifted with respect to the 700 nm band for α-PLL, whereas aggregates are red-shifted with respect to the 700 nm band for β-PLL. The intense bathochromically shifted band observed for α-PLL bound to DBS804 around 575 nm is particularly unique in nature, as it has been widely reported that H-aggregates typically exhibit lower absorption with respect to the monomer band. Furthermore, bands displaying such sharp intensity are usually characteristic of red-shifted J-aggregates.[52-56] A red-shifted band observed near the monomer band is also observed for DBS804 bound to β-PLL. The sharp peak observed at 575 nm was attributed to helical H-aggregate formation. A thiapentamethine dye has been previously reported in the literature showing similar H-bands templated by DNA helices.[57] The monomer band for the α-PLL bound dye is almost completely absent, whereas the DBS804 bound to β-PLL is present, although partially hidden by an apparent J-aggregation band. J-aggregate bands are commonly observed for cyanines in the presence of proteins, templated by helices contained in the biomolecules. When

closely examining the β-PLL conformation displayed in **Figure 4.13**, J-aggregation can be readily imagined. While lysyl substituents of parallel β-strands will have noncovalent interactions with each other, dye molecules can likewise interact with each other as well as these substituents. Only the β-PLL conformation exhibited the protein-dye complex in the far visible region, a spectral feature commonly observed for cyanines in the presence of proteins.

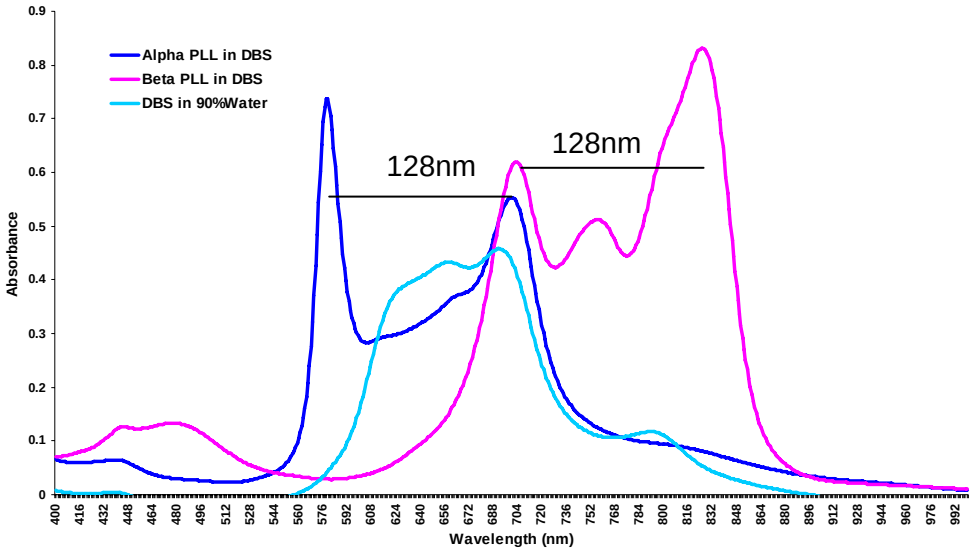

Figure 4.21. Absorption spectra of DBS804 bound to both uncharged α- and β-PLL.

From the very beginning of the DBS804 study, reproducibility was always an issue. In an effort to optimize the DBS804-PLL system, time dependence experiments were performed. The time dependence spectra of α-PLL in the presence of DBS804 is shown in **Figure 4.22**. Using a UV-Vis/NIR spectrometer, an α-PLL sample was subsequently analyzed after increasing five minutes of incubation inside the instrument. A protein-dye complex began to emerge over incubation time. A mantle observed at 920 nm remained unchanged over time. With the exception of time 0, the band observed at 830 nm had an increase in absorptivity with increasing incubation time.

The most important element of the time dependence experiment was the observation that, except for the complex observed around 475 nm, the aggregate band observed around 625 nm was the only band to exhibit a spectral change other than absorptivity. The DBS804 aggregate band observed around 625 nm also displayed induced CD. The time dependence spectra of the induced CD of DBS804 are shown in **Figure 4.23**. After 30 minutes of incubation in natural light, DBS804 bound to α-PLL exhibits an exciton split at 625 nm. In addition, DBS804 bound to both α-PLL and β-PLL exhibit weak bands around 830 nm. When the incubation time was extended to 1.5 hr., the intensity of the 625 nm band observed for α-PLL bound to DBS increased only slightly. Interestingly, after 1.5 hr incubation both α-PLL and β-PLL exhibited bands around 916 and 905 nm respectively. Furthermore, both samples exhibited visible color changes from bluish green to red.

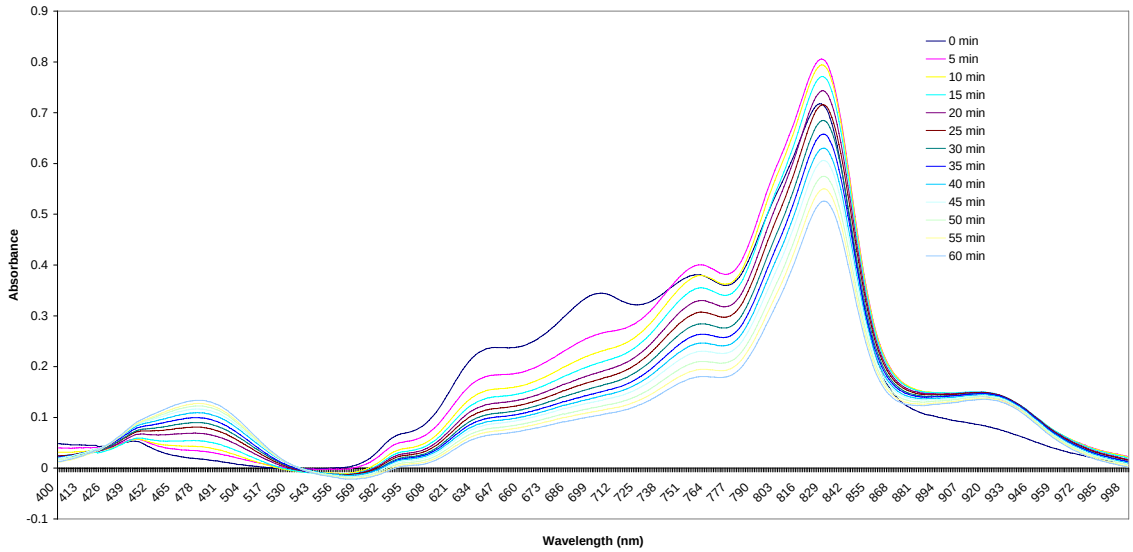

Figure 4.22. Time dependence spectra of α-PLL in the presence of DBS 804. The residue to dye ratio (R/D) for both samples was approximately 433 ([PLL] = 2.19 x 10^{-5} M and [dye] = 1.5 x 10^{-5} M).

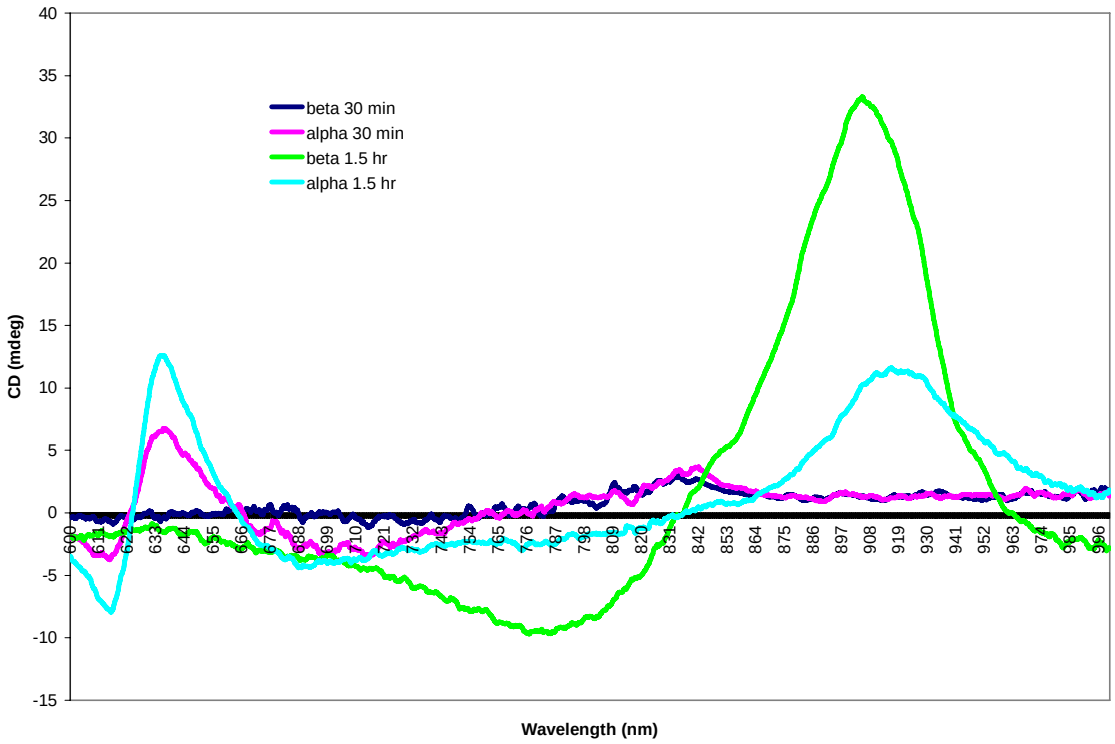

Figure 4.23. Time dependence of induced CD of DBS804 bound to both uncharged α- and β-PLL.

The data collected after 1.5 hr incubation was looked at rather cautiously, since several factors after the appearance of induced CD of DBS804 by PLL samples. First, meaningful CD bands are only observed when samples are incubated in natural light. When samples were incubated in the dark for 1.5 hr, only a noise level exciton split was observed around 800 nm (monomeric DBS804 band) for α-PLL bound dye. The visibly apparent color change as well as necessity for light incubation could point to photostability issues or dye degradation. As mentioned previously, the longer the conjugated π-system, the more susceptible cyanines are to instability, even with the presence of a ring structure within the polymethine bridge. However, the peaks observed above 900 nm may not be artifact since a small shoulder was observed in this region in time dependence experiment shown in **Figure 4.22**.

In addition to dye degradation, the stability of the PLL samples bound to DBS 804 in 10% methanol was also closely monitored. The far UV CD data reported in **Table 4.2** confirms that both α- and β-PLL samples maintained their structural conformations after 1.5 hr of incubation with DBS804 in 10% methanol. The far UV CD values reported in this table are in rather good agreement with measurements reported in the literature.[27]

Both initial and final pH determinations were made for samples incubated 1.5 hr. Before incubation, dye-polypeptide samples were displayed pH values between 11.5 and 11.5. However, after such a long incubation time, pH values dropped to between 10.5-10.7. Samples were first purged with nitrogen and then covered to minimize pH variability, but pH values were always lower after long incubation times. This fact could mean that CD bands observed after 1.5 hr are the result of electrostatic interactions of the

either partially charged or completely charged PLL structures. To confirm that electrostatic interactions were not responsible for the bands exhibited around 625 nm, the cationic thiaheptamethine dye nn356 was studied. The absorbance CD spectra for dye nn356 are shown in **Figure 4.24**. This dye displays a very intense H-aggregate absorption band around 650 nm in aqueous solvent (data not shown). The two extra benzene rings contained in the dye's structure compared to DBS804 structure make nn356 particularly sensitive to the hydrophobic effect. Yet, the induced CD band observed around 650 nm actually increases when the methanol concentration is increased from 1% to 10%. This observation is interesting since such small changes in solvent composition are typically undetectable. It is also important to note that H-aggregates nn346 appeared to bind to both α- and β-PLL indiscriminately. Whereas, even with a shorter incubation time of 0.5 hr, H-aggregates of DBS804 appear to bind discriminately to α-PLL and is detected by CD around 625 nm. This data suggests that DBS804 is potentially useful as a protein secondary structural probe.

Table 4.2. Secondary structure validation of PLL in 10% methanol and DBS804

Polypeptide	**λ_{max} (nm)**	**$[\theta]$ (M/deg cm^2 dmol^{-1})**
α poly – L – lysine	191.0	66,000
	208.5	-30,000
	221.5	-34,000
β poly – L – lysine	194.0	34,000
	215.0	-18,000

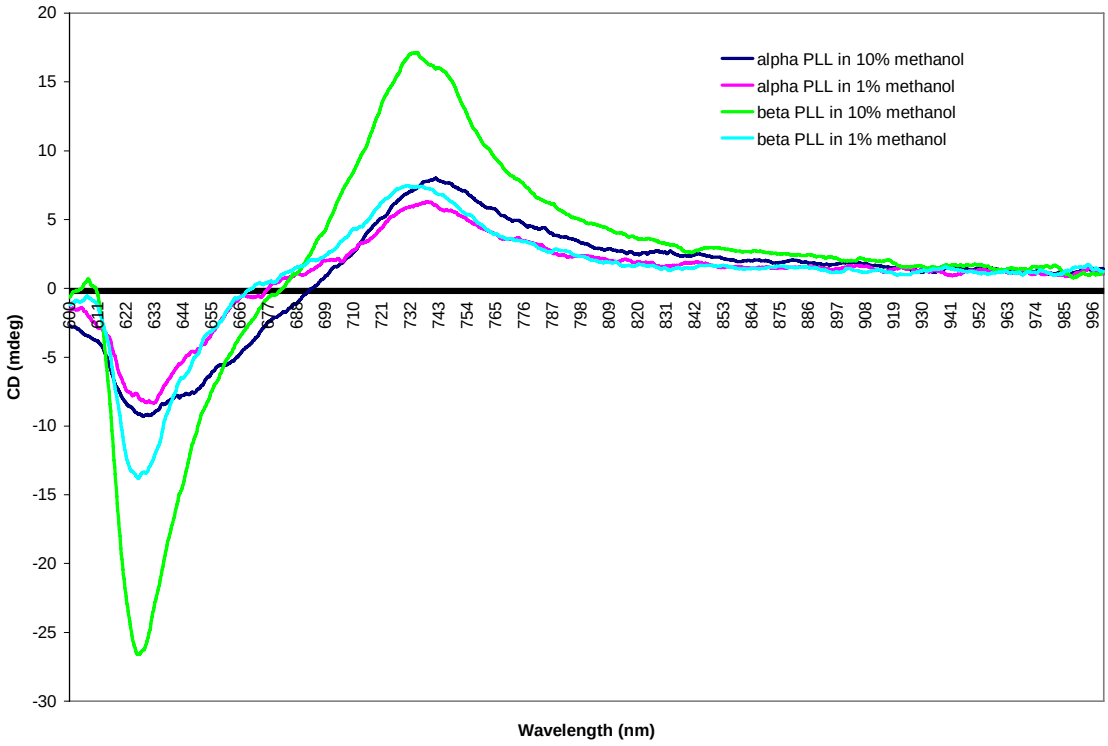

Figure 4.24. Induced CD spectra of nn356 bound to both α-PLL and β-PLL. The residue to dye ratio (R/D) for both samples was approximately 5 ([PLL] = 1.5 x 10^{-7} M and [dye] = 1.5 x 10^{-5} M).

DBS804 in Charged PLL

The spectral comparisons of both charged and uncharged α-PLL to monomeric DBS804 alone in methanol are shown in **Figure 4.25**. Charged α-PLL in methanol exhibits both a distinct monomer band and H-aggregate bands that are uncharacteristically large and broad in nature. The blue shifted bands are indicative of a strongly absorbing complex of charged α-PLL interacting electrostatically with the anionic DBS804 label, since dye self-association in methanol is not likely.

Although ideally CD measurements are typically performed within the absorbance range 0.5-0.8, CD analysis was performed on charged α-PLL. Induced CD measurements were performed on charged α-PLL at varying residue to dye (R/D) ratios, while the dye remained at a constant concentration of 2×10^{-5} M (**Figure 4.26**). A negative CD band was detected around 850 nm. However, the dye was not responsive to the change in R/D ratios. This was first attributed to the high dye concentrations at which experiments were performed. However, when induced CD of DBS804 bound to charged α-PLL was studied in varying concentrations (**Figure 4.27**), it was evident that higher concentrations of DBS804 are required even at very low residue to dye concentrations (R/D=5).

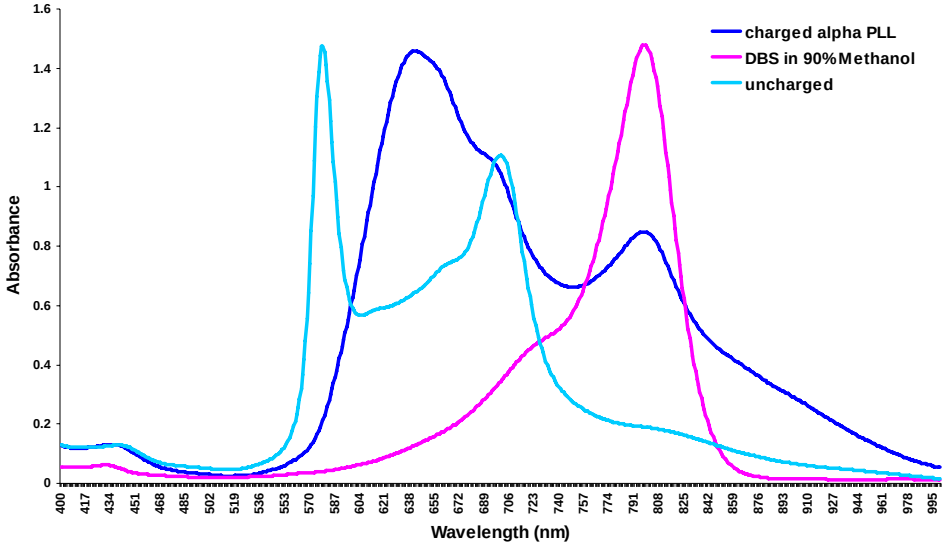

Figure 4.25. Absorption spectra of DBS804 at 20 μM concentration bound to uncharged α-PLL in water (pH = 11.5) and charged α-PLL in methanol at neutral pH.

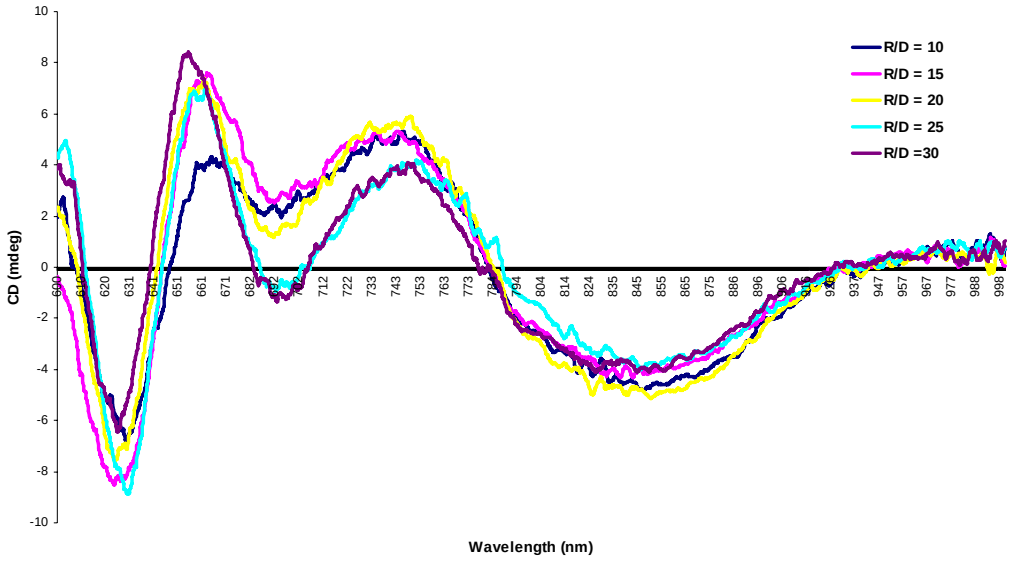

Figure 4.26. Induced CD DBS804 bound to charged α-PLL at varying residue to dye ratios. [Dye] = 20 μM.

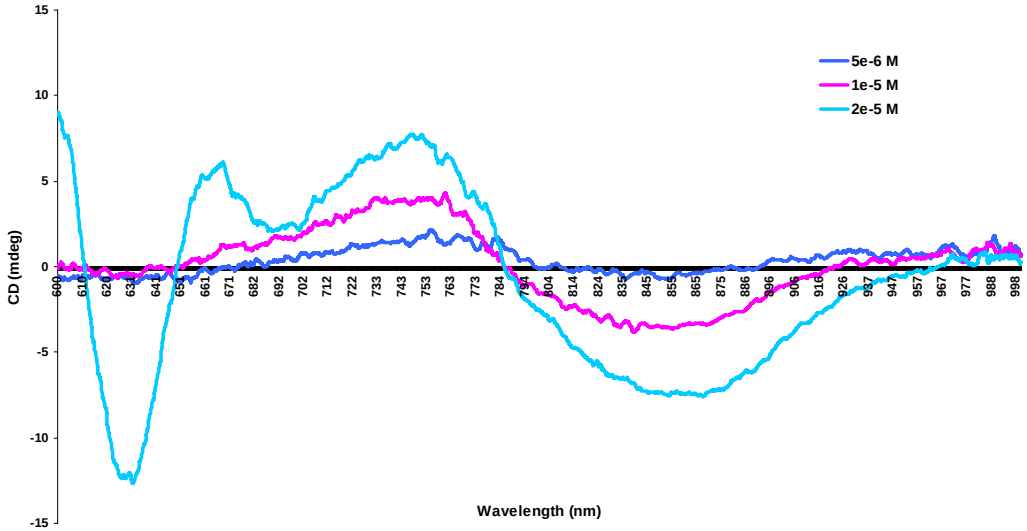

Figure 4.27. Induced CD illustrating the dye concentration dependence of DBS804 bound to charged α-PLL. R/D=5.

Conclusion

Studies involving conformational disease have frequently reported that biological function is mediated by changes in protein conformation. This belief has inspired the use of countless research in which the detection of protein secondary structures is the primary goal. Structural probes currently utilized for amyloid fibril detection such as CR and thioflavin T have been reported to lack the specificity needed for such work. For this reason, research involving β-sheet sensing has increasingly become an area of interest.

Herein, the potential of NIR dyes PD1, DBS804, and nn346 are discussed for application of protein secondary structural probes. The study first began with the intention of using amyloid fibrils produced in vitro using bovine insulin. However, attempts to validate the structure of the amyloid model were unsuccessful. Due to the complexity and expense of the insulin amyloid model, this experimental approach was set aside for a more simplistic, cheaper poly-L-lysine (PLL) model.

Before induced CD studies of NIR dyes bound to PLL structural models were performed, dye were screened thoroughly using UV-Vis/NIR spectroscopy methods. The specific criteria examined was adapted from Hermel and Rossi[49] in which the monomer as well as aggregate absorption bands were monitored for differential spectral shifts in the presence of either α-helix or β-sheet structures. Two NIR dyes were found to meet these criteria: the pentamethine dye PD1 and the thiaheptamethine dye DBS804.

Pentamethine and heptamethine dyes have been previously reported to exhibit different monomer shifts in both wavelength and intensity in the presence of α and β conformations.[49, 58, 59] In addition, these dyes have also been used to detect the % β content of polypeptide solutions.[59] The data reported in this chapter readily supports data

found in the literature. PD1 and DBS804 both appeared to be quite sensitive to the structural features of uncharged α- and β-PLL as well as the β-sheet models heat denatured ovalbumin and β-lactoglobin.

In this chapter, the spectral properties of DBS 804 bound to charged α-PLL in 100% methanol were also discussed. DBS 804 exhibited strong aggregation bands in the presence of charged α-PLL. This supports the hypothesis that the dye molecules could possibly be engaging in noncovalent self-association interactions (i.e., intermolecular H-aggregation) as well as interactions with the charged substituents of α-PLL simultaneously to form strong complexes.

Based on the data presented in this chapter, the planarity of PD1 made the dye's spectroscopic properties quite sensitive to protein secondary structure. Probe planarity was also a key feature in other studies in which azo dyes such as DAAC and MO were used. The presence of heteroatoms may also add to the structural rigidity as well as planarity of cyanine structural probes such as NK2012 and DBS804. Another key feature of both NK2012 and PD1 is their hydrophobicity and enhanced propensity to self-associate. The ordered, repeating organization of dye aggregates makes cyanines ideal for noncovalent interactions with the secondary structures of proteins and polypeptides whereby the biomolecules serve as a scaffold for the formation of supramolecular structures. Thus, the potential application of NIR dyes for use as secondary structural probes is quite promising.

References

1. Jimenez, J.; Guijarro, J.; Orlova, E.; Zurdo, J.; Dobson, C.; Sunde, M.; Saibil, H., Cryo-electron microscopy structure of an SH3 amyloid fibril and model of the molecular packing. *The EMBO Journal* **1999,** 18, 815-821.

2. Bouchard, M.; Zurdo, J.; Nettleton, E.; Dobson, C.; Robinson, C., Formation of insulin amyloid fibrils followed by FTIR simultaneously with CD and electron microscopy. *Protein Science* **2000,** 9, 1960-1967.

3. Zerovnik, E., Amyloid-fibril formation - Proposed mechanisms and relevance to conformational disease. *European Journal of Biochemistry* **2002,** 269, (14), 3362-3371.

4. Khurana, R.; Uversky, V. N.; Nielson, L.; Fink, A. L., Is Congo Red an Amyloid-specific Dye? *Journal of Biological Chemistry* **2001,** 276, (25), 22715-22721.

5. Klunk, W.; Pettegrew, J.; Abraham, D., Quantitative evaluation of congo red binding to amyloid-like proteins with a beta-pleated sheet conformation. *The Journal of Histochemistry and Cytochemistry* **1989,** 37, 1273-1281.

6. Carter, D.; Chou, K.-C., A model for structure-dependent binding of congo red to alzheimer beta-amyloid fibrils. *Neurobiology of Aging* **1998,** 19, (1), 37-40.

7. Uversky, V. N.; Garriques, L. N.; Millet, I. S.; Frokjaer, S.; Brange, J.; Doniach, S.; Fink, A. L., Prediction of the Association State of Insulin Using Spectral Parameters. *Journal of Pharmaceutical Sciences* **2003,** 92, (4), 847.

8. Sluterman, L. A., Electrophoretic behaviour in filter paper and molecular weight of insulin. *Biochimica et Biophysica Acta* **1955,** 17, 169-176.

9. Guijarro, J.; Sunde, M.; Jones, J.; Campbell, I.; Dobson, C., Amyloid fibril formation by an SH3 domain. *Proceedings in the National Academy of Science* **1998,** 95, (8), 4224-4228.

10. Bouma, B.; Kroon-Batenburg, L. M. J.; Wu, Y. P.; Brunjes, B.; Posthuma, G.; Kranenburg, O.; de Groot, P. G.; Voest, E. E.; Gebbink, M. F. B. G., Glycation induces formation of amyloid cross-beta structure in albumin. *Journal of Biological Chemistry* **2003,** 278, (43), 41810-41819.

11. Jimenez, J.; Nettleton, E.; Bouchard, M.; Robinson, C.; Dobson, C.; Saibil, H., The protofilament structure of insulin amyloid fibrils. *Proceedings in the National Academy of Science* **2002,** 99, (14), 9196-9201.

12. Burke, M.; Rougvie, M., Cross-protein structures. I. Insulin fibrils. *Biochemistry* **1972,** 11, (13), 2435-2439.

13. Khurana, R.; Ionescu-Zanetti, C.; Pope, M.; Li, J.; Nielson, L.; Ramirez-Alvarado, M.; Regan, L.; Fink, A. L.; Carter, S., A general model for amyloid fibril assembly based on morphological studies using atomic force microscopy. *Biophysical Chemistry* **2003,** 85, (2), 1135-1144.

14. Garriques, L. N.; Frokjaer, S.; Carpenter, J. F.; Brange, J., The effect of mutations on the structure of insulin fibrils studied by Fourier transform infrared (FTIR) spectroscopy and electron microscopy. *Journal of Pharmaceutical Sciences* **2002,** 91, (12), 2473-2480.

15. Nielson, L.; Frokjaer, S.; Carpenter, J. F.; Brange, J., Studies of the structure of insulin fibrils by Fourier transform (FTIR) spectroscopy and electron microscopy. *Journal of Pharmaceutical Sciences* **2001,** 90, (1), 29-37.

16. Murali, J.; Koteeswari, D.; Rifkind, J.; Jayakumar, R., Amyloid insulin interaction with erythrocytes. *Biochem Cell Biol* **2003,** 81, (1), 51-59.

17. Nielson, L.; Khurana, R.; Coats, A.; Frokjaer, S.; Brange, J.; Vyas, S.; Uversky, V. N.; Fink, A. L., Effect of environmental factors on the kinetics of insulin fibril formation: elucidation of the molecular mechanism. *Biochemistry* **2001,** 40, (20), 6036-6046.

18. LeVine III, H., Quantification of beta-sheet amyloid fibril structures with thioflavin T. *Methods in Enzymology* **1999,** 309, 274-284.

19. Klunk, W.; Jacob, R.; Mason, R., Quantifying amyloid by congo red spectral shift assay. *Methods in Enzymology* **1999,** 309, 285-305.

20. Klunk, W.; Pettegrew, J.; Abraham, D., Two simple methods for quantifying low-affinity dye-substrate binding. *The Journal of Histochemistry and Cytochemistry* **1989,** 37, (8), 1293-1297.

21. Melberg, S.; Johnson, W. J., Changes in secondary structure follow the dissociation of human insulin hexamers: a circular dichroism study. *Proteins* **1990,** 8, (3), 280-286.

22. Whitmore, L.; Wallace, B., DICHROWEB, an online server for protein secondary structure analyses from circular dichroism spectroscopic data. *Nucleic Acids Research* **2004,** 32, W668-W673.

23. Lees, J.; Smith, B.; Wien, F.; Miles, A.; Wallace, B., CD*tool* - an integrated software package for circular dichroism spectroscopic data processing, analysis, and archiving. *Analytical Biochemistry* **2004,** 332, 285-289.

24. Andrade, M.; Chacon, P.; Merelo, J.; Moran, F., Evaluation of secondary structure of proteins from UV circular dichroism using an unsupervised learning neural network. *Protein Engineering* **1993,** 6, 383-390.

25. Sreerama, N.; Venyaminov, S.; Woody, R., Estimation of protein secondary structure from circular dichroism spectra: inclusion of denatured proteins with native proteins in the analysis *Analytical Biochemistry* **2000,** 287, 243-251.

26. Sreerama, N.; Woody, R., Estimation of protein secondary structure from circular dichroism spectra: comparison of CONTIN, SELCON, and CDSSTR methods with an expanded reference set. *Analytical Biochemistry* **2000,** 287, 252-260.

27. Greenfield, N.; Fasman, G. D., Computed circular dichroism spectra for the evaluation of protein conformation. *Biochemistry* **1969,** 8, (10), 4108-16.

28. Joubert, F. J.; Lotan, N.; Scheraga, H. A., A nuclear magnetic resonance study of the helix-coil transition of poly-L-lysine in methanol-water solvents. *Physiological Chemistry and Physics* **1969,** 1, 348-354.

29. Ihara, H.; Matsumoto, A.; Shibata, M.; Hirayama, C., Host-guest chemistry [using alpha-helical poly (L-lysine)]. In *Polymeric Materials Encyclopedia*, Salamone, J. C., Ed. CRC Press: New York, 1996; Vol. 5, pp 3067-3074.

30. Hatano, M.; Yoneyama, M.; Sato, Y.; Kawamura, Y., Induced optical activity in poly-L-lysine-methyl orange system. *Biopolymers* **1973,** 12, (10), 2423-6.

31. Yamamoto, H., Chiral configuration in the complexes of poly (N-alkyl-L-lysine)s with alkylamino azo dyes. *Makromolecular Chemistry* **1983,** 184, 1479-1487.

32. Yamamoto, H.; Nakazawa, A.; Hayakawa, T., Induced optical activity in the complex of poly-L-lysine with azo dyes. *Journal of Polymer Science: Polymer Letters Edition* **1983,** 21, 131-138.

33. Yamamoto, H.; Nakazawa, A., Absolute configuration of polypeptide and dye complexes by an application of the exciton chirality method. *Chemistry Letters* **1983,** 12, (1), 47-50.

34. Yamamoto, H.; Nakazawa, A.; Hayakawa, T.; Mitshuishi, M., Some factors influencing the magnitude of the induced circular dichroism of poly (L-lysine) hydrobromide and azo dye complexes. *Polymer Journal* **1984,** 16, 791-793.

35. Yamamoto, H., Induced circular dichroism and structure of the complexes of poly (L-ornithine) and poly (L-diaminobutyric acid) with azo dyes. *International Journal of Biological Macromolecules* **1986,** 8, 130-136.

36. Yamamoto, H.; Nishida, A.; Inouye, K., Effect of light irradiation in the chiral complex of poly (L-lysine) with methyl orange. *Polymer Photochemistry* **1986,** 7, 349-358.

37. Scaria, P. V., Atreyi, Rao, M. V. R., Helix to Beta conformational transition of poly(L-lysine) on dye binding. *Biopolymers* **1986,** 25, (12), 2349-2358.

38. Scaria, P. V.; Atreyi, M.; Rao, M. V. R., Induced circular dichroism of poly (L-lysine)-dye complexes in aqueous solutions. *International Journal of Biological Macromolecules* **1988,** 10, 60-62.

39. Ratna, M. A.; Atreyi, M.; Rao, M. V. R., Interaction of two fragments of Cibacron Blue F3GA having anthraquinone chromophores with basic polypeptides. *International Journal of Biological Macromolecules* **1992,** 14, 201-209.

40. Zhang, Y.; Du, H.; Tang, Y.; Xu, G.; Yan, W., Spectroscopic investigation on the interaction of J-aggregate with human serum albumin. *Biophysical Chemistry* **2007,** 128, 197-203.

41. Zhang, Y. Z.; Xiang, J. F.; Tang, Y. L.; Xu, G. Z.; Yan, W. P., Chiral transformation of achiral J-aggregates of a cyanine dye templated by human serum albumin. *Chemphyschem* **2007,** 8, (2), 224-226.

42. Tatikolov, A. S.; Costa, S. M. B., Complexation of polymethine dyes with human serum albumin: a spectroscopic study. *Biophysical Chemistry* **2004,** 107, (1), 33-49.

43. Panova, I. G.; Sharova, N. P.; Dmitrieva, S. B.; Poltavtseva, R. A.; Sukhikh, G. T.; Tatikolov, A. S., Use of a cyanine dye as a probe for albumin and collagen in the extracellular matrix. *Analytical Biochemistry* **2007,** 361, (2), 183-189.

44. Ihara, H.; Matsumoto, A.; Shibata, M.; Goda, H.; Hirayama, C., Geometrically selective recognition using alpha-helical poly (L-lysine). *Materials Science and Engineering* **1994,** C2, L1-L3.

45. Shibata, M.; Ihara, H.; Hirayama, C., Unique Property of Cyanine Dyes on Charged Poly(L-Lysine). *Polymer* **1993,** 34, (5), 1106-1108.

46. Ihara, H.; Shibata, M.; Hirayama, C., Molecular recognition using cyanine-alpha-helical poly (L-lysine) complexes in methanol. *Chemistry Letters* **1992,** 21, 1731-1734.

47. Arimura, T.; Shibata, M.; Ihara, H.; Hirayama, C., Evaluation of Selective Binding Ability in Chiral Supramolecules Using Induced Chirality. *Analytical Sciences* **1993,** 9, (3), 401-403.

48. Andrews-Wilberforce, D.; Patonay, G., Investigation of near-infrared laser dye albumin complexes. *Spectrochimica Acta Part a-Molecular and Biomolecular Spectroscopy* **1990,** 46A, (8), 1153-1162.

49. Hermel, H.; Holtje, H. D.; Bergemann, S.; De Rossi, U.; Kriwanek, J., Band-shifting through polypeptide beta-sheet structures in the cyanine UV-Vis spectrum. *Biochimica et Biophysica Acta* **1995,** 1252, (1), 79-86.

50. Cassim, J.; Yang, J., A computerized calibration of the circular dichrometer. *Biochemistry* **1969,** 8, (5), 1947-1951.

51. Konno, T.; Meguro, H.; Murakami, T.; Hatano, M., A critical study on circular dichroism measurement in longer side of visible region. *Chemistry Letters* **1981,** 10, (7), 953-956.

52. Herz, A., Aggregation of sensitizing dyes in solution and their adsorption onto silver halides. *Advances in Colloid and Interface Science* **1977,** 8, (4), 237-298.

53. Mishra, A.; Behera, R. K.; Behera, P. K.; Mishra, B. K.; Behera, G. B., Cyanines During the 1990s: A Review. *Chemical Reviews* **2000,** 100, (6), 1973-2011.

54. Zhang, Y. Z.; Xiang, J. F.; Tang, Y. L.; Xu, G. Z.; Yan, W. P., Aggregation behaviour of two thiacarbocyanine dyes in aqueous solution. *Dyes and Pigments* **2008,** 76, (1), 88-93.

55. Slanova, T. D.; Gorner, H.; Chibisov, A. K., J-Aggregation of Anionic Ethyl meso-Thiacarbocyanine Dyes Induced by Binding to Proteins. *J.Phys.Chem B* **2007,** 111, 10023-10031.

56. Egorov, V. V., Nature of the optical transition in polymethine dyes and J-aggregates. *Journal of Chemical Physics* **2002,** 116, (7), 3090-3103.

57. Chowdhury, A.; Wachsmann-Hogiu, S.; Bangal, P.; Raheem, I.; Peteanu, L., Characterization of chiral H and J aggregates of cyanine dyes formed by DNA templating using stark and fluorescence spectroscopies. *J.Phys.Chem B* **2001,** 105, (48), 12196-12201.

58. Hermel, H.; De Rossi, U., Polypeptide B-sheet detection by cyanine dyes. *Progress in colloid & polymer science* **1995,** 98, 212-214.

59. Hermel, H.; De Rossi, U., Examination of polypeptide beta-sheet structure in solutions and thin layers: determination of the concentration and the 'critical aggregation concentration' using a cyanine dye as sensor. *International Journal of Biological Macromolecules* **1997,** 21, (3), 263-70.

CHAPTER V

Conclusions

Optical spectroscopy is a widely used tool for the study of biological systems, owing to the many advantages compared with other analytical methods. Unlike IR spectroscopy, absorption and luminescence techniques do not require thin layer samples for analysis. And in absorption spectroscopy, transparent as well as highly turbid, light scattering samples can be measured. Furthermore, when luminescence techniques are used, minute sample concentrations reported as low as concentrations down to 10^{-18} moles are detectable.[1] In general, optical spectroscopy methods are both nondestructive and noninvasive. For this reason, radioactive markers for the investigation of biochemical and molecular-biological processes are increasingly being replaced by fluorescent labels instead.

Circular dichroism (CD) is a powerful chiroptical technique that has been mainly used since the early 1960s to determine the absolute configuration of both natural and synthetic compounds.[2] It is only recently that CD measurements have been used in the pharmaceutical industry, despite the fact that chiral drugs drastically outnumber achiral ones. In order for a compound to be CD active, it must display some measurable absorbance within the same region studied. This requisite confers a high degree of selectivity to the technique, thereby allowing a CD-active drug to be analyzed in complicated mixtures such as human serum. Using CD techniques within the absorption bands of β-lactam antibiotics, Gortazar et al proved the validity of using CD to determine drugs levels in human serum.[2]

In biological applications, spectrophotometry is often used in the UV-Vis (185-700 nm) region of the electromagnetic spectrum. However, in this region analysis is susceptible to a great deal of background interference. Thus, near infrared (NIR) labels have been increasingly used since analysis in this region is far removed from the absorption spectrum of most biological materials. Nanoparticle-based optical contrast agents such as quantum dots (QDs) have been studied extensively for their utility over the conventional use of organic dyes such as NIR labels.[3-5] However, many of the advantages observed with QDs are also reported using NIR labels as well. Both QDs and NIR dyes exhibit high molar absorptivity. And as with QDs, the properties and spectral region of NIR dyes are readily controlled through structural modifications. In addition, both labels can be used in the more advantageous NIR spectral region of the electromagnetic spectrum. However, since the properties of QDs are so dependent on size and chemical make-up, their experimental use is quite susceptible to assay heterogeneity. Yet, NIR are quite susceptible to photobleaching and can be unstable over the long timescale of some bioimaging techniques. But problem has been overcome by simply attaching the NIR labels to biomolecules such as albumin[4], poly aspartate[6] and poly-L-lysine[7] through both covalent and noncovalent interactions. The stabilization of the NIR dyes by the biomolecules is achieved by the inhibition of dye self-association.

This dissertation presented research in which various optical spectroscopy methods were used to observe and understand the biomolecular noncovalent interactions of NIR carbocyanines with albumin and poly-L-lysine. In Chapter 3, intramolecular and intermolecular self-associations were reported for three bis-cyanine dyes containing di-, tri-, and tetra(ethylene glycol) spacers, corresponding to the generic names OxoDye 1,

OxoDye 2, and OxoDye 3 respectively. ChemDraw® Ultra 8.0 Software was first utilized to predict the orientation of the bis-cyanines in solution. In the case of OxoDye 1, the benzene rings of the two monomeric subunits will only partially overlap, and the two benzene rings do not form π-π interactions due to the steric hindrance of the di(ethylene glycol) spacer. Yet, the tri(ethylene glycol) linker in OxoDye 2 allowed for a complete overlap of the benzene rings, to form π-π interactions which should exhibit intra-molecular H-aggregation bands. And the tetra(ethylene glycol) spacer of OxoDye3 displays no aggregation since the energy minimization of this long linker allows for no chromophoric overlap. In contrast with the BHmC simulations in which the whole chromophoric units of the BHmCs interact with each other, the poly(ethylene glycol) only allows for partial interactions of the chromophores. These assumptions were all confirmed by absorption, emission, and fluorescence detected circular dichroism (FDCD).

Blue-shifted bands relative to the monomeric band were detected for both IR783 and OxoDye2 alone in 10 mM phosphate buffer in the near infrared region, corresponding to both intramolecular (OxoDye2) and intermolecular H-aggregates (IR783 and OxoDye2). In addition, no fluorescence was detected for these bands. In the presence of HSA, the aggregate bands of IR 783 dissipated. The intermolecular H-aggregation bands exhibited by OxoDye2 also decreased with increasing HSA concentration, and a very distinct intramolecular dimer H-band also appeared as well. Thus, monomeric IR 783 and bis-cyanine dimers both interact with HSA binding sites.

In aqueous buffer, OxoDyes 1 and 3 exhibited no aggregation bands most likely due to the steric hindrance of the poly(ethylene glycol) linkers. Both exhibited fluorescence alone in aqueous. However, when a noncovalent complex between HSA and OxoDye 1 forms, monomeric as well as H-aggregate bands are observed. In addition, OxoDye1 exhibited increased in absorptivity and fluorescence with increasing protein concentration. Monomeric subunits bound to HSA appeared to be the primary binding modality for OxoDye3.

Although all four dyes exhibited enhanced fluorescence in the presence of HSA, OxoDyes1 and 3 were considered suitable for noncovalent labeling, since their inherent fluorescence could potentially make it difficult to distinguish between protein bound dye and unbound dye in solution.

The high sensitivity of luminescence techniques combined with high selectivity of chiroptical techniques was utilized in the fluorescence detected circular dichroism (FDCD) measurements reported. This valuable analytical technique reports on the specific interactions of the achiral NIR dyes bound in an asymmetric environment, in this case, protein binding sites. Induced FDCD of protein bound NIR labels was detected for all four labels. In order for induced CD to occur, the achiral chromophore must have at least three points of contact with its chiral inducer (i.e., the protein) thereby, owing to the inherent selectivity of the chiroptical technique.

Using fluorescence data, binding constants were determined to be between 1 and 7 x 10^5 M^{-1} for the bis-heptamethine dyes and the monomeric analogue. However, additional calculations must be conducted to verify that the appropriate binding equation was used. Furthermore, Scatchard and Hill analysis using FDCD measurements could potentially be useful in validating binding association values.

The β-sheet structure is one of the fundamental secondary structures of proteins.[8] It greatly stabilizes protein domains by forming an array of several parallel peptide backbone pieces five to fifteen amino acids long, interconnected solely by multiple hydrogen bonds. The amino acids which are commonly found in the β-sheets of globular proteins are typically hydrophobic in nature and therefore susceptible to the hydrophobic effect which would cause these structures to aggregate when exposed to aqueous media. Therefore, beta structures are often buried deep inside the core of most globular proteins. The active centers of many enzymes contain a β-sheet fragment which binds to a target peptide. In addition, the identical domains of enzymes such as HIV-I protease form a fours-stranded β-sheets. Thus, β-sheet structures are important recognition modes for delivering the critical functionality of many enzymes. In Chapter 4, the potential of NIR dyes PD1, DBS804, and nn346 were investigated for their utility as protein secondary structural probes. Before induced CD studies of NIR dyes bound to PLL structural models were performed, dye were screened thoroughly using UV-Vis/NIR spectroscopy methods. The specific criteria examined was adapted from Hermel and Rossi[9] in which the monomer as well as aggregate absorption bands were monitored for differential spectral shifts in the presence of either α-helix or β-sheet structures. Two NIR dyes were found to meet these criteria: the pentamethine dye PD1 and the thiaheptamethine dye

DBS804. In addition, both appeared to be quite sensitive to the structural features of uncharged α- and β-PLL as well as the β-sheet models heat denatured ovalbumin and β-lactoglobin. The spectral properties of DBS 804 bound to charged α-PLL in 100% methanol were also discussed. DBS 804 exhibited strong aggregation bands in the presence of charged α-PLL. This supports the hypothesis that the dye molecules could possibly be engaging in noncovalent self-association interactions (i.e., intermolecular H-aggregation) as well as interactions with the charged substituents of α-PLL simultaneously to form strong complexes.

References

1. Schmidt, W., *Optical Spectroscopy in Chemistry and Life Sciences: An Introduction*. Wiley-VCH: KGaA, 2005.

2. Gortazar, P.; Roen, A.; Vazquez, J., Determination of Drug Levels in Human Serum by Circular Dichroism. *Chirality* **1998,** 10, 507-512.

3. Sharma, P.; Brown, S.; Walter, G.; Santra, S.; Moudgil, B., Nanoparticles for bioimaging. *Advances in Colloid and Interface Science* **2006,** 123-126, 471-485.

4. Ohnishi, S.; Lomnes, S. J.; Laurence, R. G.; Gogbashian, A.; Mariani, G.; Frangioni, J. V., Organic alternatives to quantum dots for intraoperative near-infrared fluorescent sentinel lymph node mapping. *Mol Imaging* **2005,** 4, (3), 172-81.

5. Lakowicz, J. R., *Principles of Fluorescence Spectroscopy*. 3rd ed.; Springer Science: New York, 2006.

6. Rajagopalan, R.; Uetrecht, P.; Bugaj, J. E.; Achilefu, S. A.; Dorshow, R. B., Stabilization of the optical tracer agent indocyanine green using noncovalent interactions. *Photochemistry and Photobiology* **2000,** 71, (3), 347-350.

7. Place, I.; Perlstein, J.; Penner, T. L.; Whitten, D. G., Stabilization of the aggregation of cyanine dyes at the molecular and nanoscopic level. *Langmuir* **2000,** 16, (23), 9042-9048.

8. Schrader, T.; Wehner, M.; Rzepecki, P., Artificial receptors for the stabilization of beta-sheet structures. In *Highlights in Bioorganic Chemistry*, Schmuck, C.; Wennemers, H., Eds. Wiley-VCH: KGaA, 2004.

9. Hermel, H.; Holtje, H. D.; Bergemann, S.; De Rossi, U.; Kriwanek, J., Band-shifting through polypeptide beta-sheet structures in the cyanine UV-Vis spectrum. *Biochimica et Biophysica Acta* **1995,** 1252, (1), 79-86.